Final Report

for

NASA Grant NAG2-523 (SUNY 431-3159A)

Studies of the Chemistry of the Nightside Ionosphere

of Venus

for the period 1 July 1988 to 30 November 1990

J. L. Fox, Principal Investigator

Institute for Terrestrial and Planetary Atmospheres and

Department of Mechanical Engineering

State University of New York at Stony Brook

Stony Brook, NY 11794

January, 1991

1

During the tenure of this grant, we have been looking into the chemistry of the nightside ionosphere of Venus with a view toward elucidating the relative roles of electron precipitation and plasma transport as sources of the nightside ionosphere. Secondary goals have included determining the densities of minor species on the nightside, and verifying the relative normalization of the Pioneer Venus orbiter ion mass spectrometer (OIMS) and orbiter neutral mass spectrometer (ONMS) in the photochemical equilibrium region. Our studies have involved a combination of numerical modeling and analysis of the Pioneer Venus UADS data base, specifically data from the OIMS, ONMS and electron temperature probe (OETP). We have set up a one-dimensional model of the Venus nightside ionosphere, in which downward fluxes of atomic ions are introduced at the upper boundary to simulate transport of ions from the dayside. Our model shows that the densities of mass-28 ions (CO^+ + N_2^+) resulting from an influx of atomic ions from the dayside are quite small, due to the high ionization potentials of CO and N_2 that make chemical production difficult. A look at the data reveals that the actual densities of mass-28 ions are quite variable, from values near 10 to more than 10^4 cm^{-3}. We suggest the excess mass-28 ions are produced by electron precipitation and that the presence of high densities of mass-28 ions is a signature of "auroral" precipitation. Details are given in the attached reprint of an article published in GRL in September, 1990 by H. A. Taylor and myself entitled "A signature of auroral precipitation in the nightside ionosphere of Venus".

Also attached are two other articles supported partially under this grant. The first, a chapter of the book *Dissociative recombination: experiment, theory and applications* is entitled "Dissociative recombination in aeronomy". The chapter contains a discussion of the atomic oxygen green line in the nightglow of Venus,

which is produced mainly by dissociative recombination of O_2^+. In this work, the O_2^+ is assumed to be produced by reaction of O^+ transported from the dayside with CO_2. In fact, the presence of electron precipitation will increase the emission in the green line in two ways: by increasing the density of O_2^+ and by direct production of $O(^1D)$ from electron impact on atomic oxygen.

The second is a review article that Steve Bougher and I have written entitled "Structure, luminosity and dynamics of the Venus thermosphere", to be published in Space Science Reviews soon. This manuscript, while officially a review article, contains original calculations of production rates of excited states for models based on Pioneer Venus data, that I needed to do for completeness. Tables 2, 3, 5, 6, 7, and 11 contain original, unpublished calculations.

A SIGNATURE OF AURORAL PRECIPITATION IN THE NIGHTSIDE IONOSPHERE OF VENUS

J. L. Fox

Institute for Terrestrial and Planetary Atmospheres
State University of New York at Stony Brook

H. A. Taylor, Jr.

Taylor Enterprises, Beaver River, Nova Scotia

Abstract. We show here that the densities of mass-28 ions measured by the Pioneer Venus Orbiter ion mass spectrometer (OIMS) on the nightside of Venus are highly variable and show little correlation with the values of the O^+ densities. We have determined the total production rates of mass-28 ions in the chemical equilibrium region and find that this production rate cannot be explained by known chemical production reactions. We propose that the "excess" production is due to precipitation of electrons into the nightside thermosphere.

Introduction

The source of the Venus nightside ionosphere has been disputed since the first radio occultation measurements of the nightside electron density profile by Mariner 5 [Kliore et al., 1967]. Since then, the viable mechanisms have been reduced to two: transport of atomic ions, mostly O^+, from the dayside and precipitation of energetic electrons that have been observed in the Venus umbra. Models appropriate to high solar activity have shown that plasma transport is the dominant maintenance mechanism, since it alone can produce the observed densities of O^+, with electron precipitation playing a possible secondary role in enhancing the lower O_2^+ peak [Spenner et al., 1981; Cravens et al., 1983]. Gringauz et al. [1977] maintain that precipitation of electrons alone is sufficient to produce the main ion peak, as measured by the Venera 9 and 10 radio occultation experiments at solar minimum.

We have been investigating the chemistry of the nightside ionosphere, with a view toward elucidating the relative roles of electron precipitation and plasma transport in its maintenance. Model calculations based on ion transport as the source of the nightside ionosphere showed that the reaction

$$O_2^+ + N \rightarrow NO^+ + O \qquad (1)$$
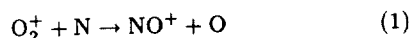
was the major source of NO^+ in the chemical equilibrium region. Analysis of data from eight Pioneer Venus (PV) orbits chosen for low periapsis and the availability of data showed that the NO^+ densities could be modeled with reaction (1) as the sole source for some orbits, but for others it was completely inadequate. A close look at those orbits showed that they were all characterized by high densities of mass-28 ions ($N_2^+ + CO^+$). This deviation is easily ex-

plained since N_2^+ reacts rapidly with O to produce NO^+

$$N_2^+ + O \rightarrow NO^+ + N. \qquad (2)$$
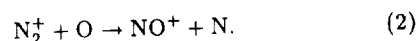
Because of the high ionization potentials of both N_2 and CO, the chemical sources are limited. Yet a survey of early Pioneer Venus orbits with periapsis below 165 km reveals a large variability in the maximum densities of mass-28 ions with values ranging from about 10 cm^{-3} to about 10^4cm^{-3}. Taylor et al. [1982] had earlier remarked that the occasional large densities of NO^+ and O_2^+ measured by the OIMS appeared to require a source in addition to ion transport; they suggested that the densities were enhanced by particle precipitation, but the mechanism of the source was not resolved. We propose that the excess NO^+ is produced from N_2^+ created by particle precipitation, and that high densities of mass-28 ions in the nightside ionosphere are an *in situ* signature of precipitation of electrons into the nightside atmosphere.

In the discussion that follows, we identify the sources and sinks of mass-28 ions in the chemical equilibrium region, that below approximately 165-170 km. There the ion production and loss rates are equal, so the magnitude of the source can be estimated because the total loss rate can be computed fairly accurately. From the loss rate and the known chemical sources, the "excess" production rate, that we ascribe here to particle precipitation, is determined.

Sources of N_2^+ and CO^+

Reactions, references and rate coefficients used in this work are summarized in Table 1, and the reactions numbers cited below refer to the numbers in that table. Because of the high ionization potential of N_2 (15.58 eV), only a few charge transfer reactions of atmospheric species are energetically capable of producing N_2^+, including charge transfer from He^+, O^{++} and $O^+(^2D)$ (reactions 3–5). Reaction (3) is potentially important, since nighttime He^+ densities are larger than daytime values, peaking in the the pre-dawn sector [Taylor et al., 1980]. Densities of O^{++} were measured by the PV OIMS, but are often above the noise level of the instrument only above the chemical equilibrium region. In addition, the products of reaction (4) are unknown; the large exothermicity suggests that the dissociative channel probably dominates. Charge transfer from $O^+(^2D)$ to N_2, reaction (5), is a major source of N_2^+ in the dayside ionosphere [Fox, 1982], and the importance of this reaction depends on whether the metastable $O^+(^2D)$ ion could survive transport from the dayside. A detailed analysis would be required to model the role of reaction (5) in producing the observed
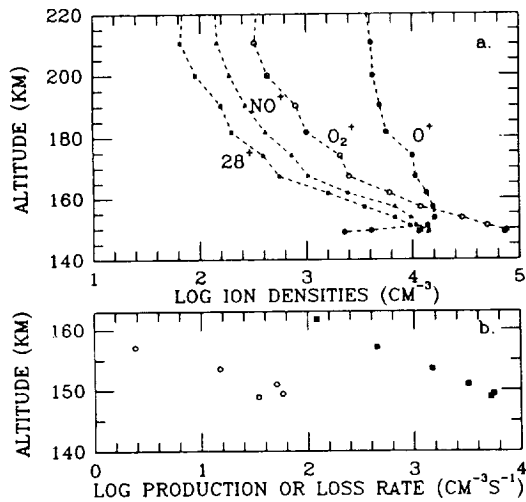
Fig. 2. Same as for Fig. 1, but for Orbit 529 (inbound). In Fig. 2b, the total production rate and excess production rate are essentially superimposed.

$cm^{-3}s^{-1}$. For orbit 505, the maximum auroral production rate is about a factor of 40 less than for orbit 529, although the production rates due to chemical reactions are about the same for the two orbits.

Other evidence for the precipitation of electrons into the nightside thermosphere exists. Fluxes of suprathermal electrons have been measured above the atmosphere in the Venus umbra by the PV retarding potential analyzer (ORPA) [e.g. Knudsen and Miller, 1985] as well as by the plasma analyzers on the Soviet Venera 9 and 10 spacecraft [e.g. Gringauz et al., 1977]. Continuous but highly variable emissions of atomic oxygen at 1304 and 1356 Å have been observed in images of the nightside of Venus by the PV orbiter ultraviolet spectrometer (OUVS) [Phillips et al., 1986]. Fox and Stewart [1990] have proposed that these emissions are caused by the precipitation of soft electrons into the nightside atmosphere.
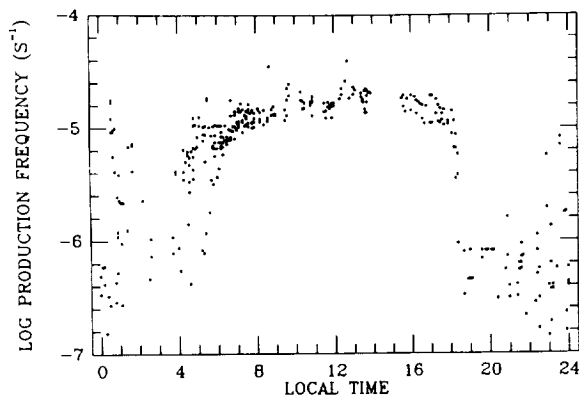

Fig. 3. Production frequency of mass-28 ions in excess of that that can be accounted for by chemical reactions at the mass-28 ion peak as a function of local time for all orbits of the first 600 for which sufficient data are available.

Figure 3 shows the excess production "frequency" of mass-28 ions at the mass-28 ion peak for all orbits among the first 600 that meet the following criteria: periapsis al-

titude below 165 km, and data at the mass-28 ion peak for the densities of O^+, O_2^+, He^+, CO_2, O, and N_2. In this calculation, only the reactions of He^+ (reactions 3 and 6) were included as chemical sources of mass-28 ions, since experience with individual orbits showed the other sources to be unimportant. The electron temperature was assumed to be about 1000 K for all the data points. Errors resulting from this assumption should be small, since the electron temperature dependence of the dissociative recombination coefficient is weak, and dissociative recombination is not the major loss mechanism. In order to reduce the effects of variability due to changes in the neutral atmosphere and in the altitude of periapsis, the excess production "frequency" was obtained by dividing the rate by the factor $3[N_2] + 0.1[CO_2]$. The first term in the factor represents ionization of N_2 and CO, and was chosen because the CO density is about twice the N_2 density on the nightside above the homopause [Hedin et al., 1983]. The second term represents the contribution of dissociative ionization of CO_2; the factor 0.10 is the high energy ratio of the electron impact cross sections for production of CO^+ from CO_2 and CO. On the dayside, the excess production is due to direct ionization and chemical reaction other than reactions (3) and (6). The production frequency appears large on the dayside also because CO is more abundant relative to N_2 there [Hedin et al., 1983]. The variability on the dayside is small, because all the data were taken near solar maximum, but some scatter remains from the variation of periapsis altitude. The large variability in the source on the nightside, ranging over more than two orders of magnitude, itself suggests particle precipitation as the source mechanism. Some excess production appears to be present in nearly all the orbits. This is consistent with the morphology of the 1304 Å aurora [Phillips et al., 1986], which is nearly always visible on the nightside, but exhibits large spatial and temporal variations.
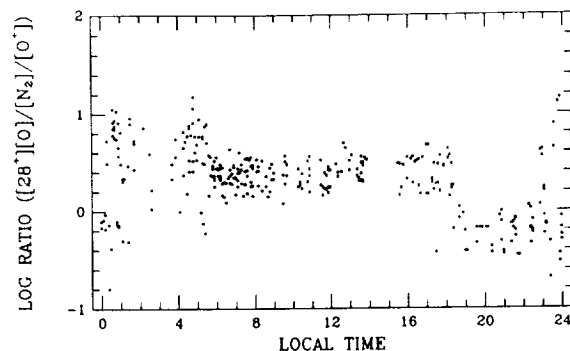

Fig. 4. Ratio of $[28^+][O]/[N_2]$ at the mass-28 ion peak to the density of O^+ at its peak, as a function of local time for the first 600 orbits. The variability on the nightside is substantially greater than the variability on the dayside.

Since models have shown that the measured O^+ densities can only be accounted for by transport from the dayside, and if mass-28 ions are mostly produced by auroral processes, the relative values of the maximum mass-28 ion and O^+ densities would be indicative of the relative importance of ion transport and particle precipitation in the nightside ionosphere. Figure 4 is a plot of the ratio of the peak mass-28 ion density (divided by $[N_2]/[O]$) to the peak O^+ density as a function of local time for all orbits

DISSOCIATIVE RECOMBINATION IN AERONOMY

J. L. Fox

Institute for Atmospheric Sciences
and
Department of Mechanical Engineering
State University of New York at Stony Brook
Stony Brook, NY 11794

ABSTRACT

The importance of dissociative recombination in planetary aeronomy is summarized and two examples are discussed. The first is the role of dissociative recombination of N_2^+ in the escape of nitrogen from Mars. A previous model is updated to reflect new experimental data on the electronic states of N produced in this process. Second, the intensity of the atomic oxygen green line on the nightside of Venus is modeled. Use is made of theoretical rate coefficients for production of $O(^1S)$ in dissociative recombination from different vibrational levels of O_2^+.

1. INTRODUCTION

Dissociative recombination (DR) is an important elementary process in planetary upper atmospheres for several reasons. Its obvious importance is to the ionization structure: it provides a loss mechanism for molecular ions that is unavailable to atomic ions. Consequently molecular ions have shorter chemical lifetimes at high altitudes than atomic ions. The relative importance of dissociative recombination compared to ion-neutral reactions depends on the availability of the latter. Ion-neutral reactions tend to transform ions into other ions whose parent neutrals have lower ionization potentials. This is strictly true for charge transfer reactions and is practically true for other ion-neutral reactions because the dissociation energies of atmospheric molecules tend not to differ as much as ionization potentials. Generally, for ions derived from parent neutrals with low ionization potentials, dissociative recombination may be the major loss process over a wide range of altitudes. For those derived from neutrals with high ionization potentials, dissociative recombination may dominate at sufficiently high altitudes. In the terrestrial ionosphere, for example, the most important molecular ions are N_2^+, O_2^+ and NO^+. For N_2^+, whose parent N_2 has a relatively high ionization potential of 15.58 eV, DR is the most important loss mechanism only above 250 km.

Immediately below that altitude, the major loss process is reaction with O:

$$N_2^+ + O \rightarrow NO^+ + N. \qquad (R1)$$

O_2 has an intermediate ionization potential of 12.15 eV, and DR controls the loss of O_2^+ over a larger altitude range, beginning at about 190 km. The reaction

$$O_2^+ + N \rightarrow NO^+ + O \qquad (R2)$$

is the most important loss mechanism immediately below that altitude. NO has the lowest ionization potential of any of the major atmospheric species and consequently DR of NO^+ is the only loss mechanism available over the entire ionosphere.

Dissociative recombination may be an important source of airglow emissions, if the fragments are produced in excited states with short radiative lifetimes. In $O(^1S)$ in dissociative recombination from different vibrational levels of O_2^+. DR of CO_2^+,

$$CO_2^+ + e \rightarrow CO + O \qquad (R3)$$

55% of the CO molecules are produced in the excited $CO(a^3\Pi)$ state.[1] $CO(a^3\Pi)$ is a metastable state with a lifetime of about 8 ms[2,3]; it radiates to the ground $^1\Sigma$ state producing emission in the well-known Cameron Band System. The Cameron Bands are the brightest features in the ultra-violet dayglows of Venus and Mars. On Venus, approximately 5 kR of 20 kR total integrated intensity is due to DR of CO_2^+.[4] (One kiloRayleigh (kR) is an apparent column emission rate of 10^9 photons $cm^{-2}s^{-1}$.) In DR of O_2^+, the O atoms may be produced in various combinations of the electronic states ^3P, ^1D, and ^1S. $O(^1D)$ radiates to the ground state producing the 6300 Å "red line" and $O(^1S)$ to $O(^1D)$ producing the 5577 Å "green line". This source is important in the dayglows and nightglows of all the terrestrial planets and in terrestrial auroras. It is relatively more important in the nightglow, due to the absence of sources involving the direct interaction of solar radiation or photoelectrons with atmospheric gases.

The fragments produced in dissociative recombination may be important chemically. For example, ionization of N_2 followed by dissociative recombination of N_2^+ is a net source of odd nitrogen, an important family of species that are interconverted more rapidly than they are created or destroyed. The fragments may also be formed in metastable excited states whose chemistry is different from that of ground state species. For example, in DR of N_2^+ ($v = 0$), the yield of $N(^2D)$

has recently been measured by Queffelec et al. to be about 1.85.[5] $N(^2D)$ may radiate to the ground $N(^4S)$ state, producing emission at 5200 Å, but the transition probability is small, about $1.06 \times 10^{-5}\,s^{-1}$.[6] It is probable that the atom will be chemically destroyed before radiating. In the terrestrial atmosphere, the reaction

$$N(^2D) + O_2 \rightarrow NO + O \qquad (R4)$$

is an important source of NO,[7,8] as is the reaction

$$N(^2D) + CO_2 \rightarrow NO + CO \qquad (R5)$$

on Venus and Mars.[9,10] Reactions of ground state N atoms with O_2 and CO_2 are much slower than reactions (R4) and (R5).[11,12,13,14] Constantinides et al.[15] have shown that the reaction

$$N(^2D) + O^+ \rightarrow N^+ + O, \qquad (R6)$$

which is endothermic for ground state N atoms, is the most important source of N^+ above 250 km in the terrestrial ionosphere.

That the fragments produced in dissociative recombination may have large kinetic energies has several important consequences for planetary atmospheres. First, DR may be an important heat source for the neutral atmosphere. On Earth, most of the heating due to exothermic reactions is from dissociative recombination reactions.[16] On Venus, DR of O_2^+ is the dominant heat source above 135 km.[17] If the fragments are produced at a sufficiently high altitude and with sufficient kinetic energy, they may escape from the planet. (See the review by Hunten[18] for a description of thermal and non-thermal escape processes.) A common approximation, is that above the *exobase*, where the mean free path is equal to a scale height, the atmosphere is assumed to be collisionless . Then all atoms traveling upward with velocities greater than the escape velocity actually escape. For thermal escape, this approximation has been shown to produce essentially no error.[19] The cut-off velocity, v_{esc}, is that for which the kinetic energy, $\frac{1}{2}mv^2$, is equal to the gravitational potential energy, mgr, where r is the distance of the exobase from the center of the planet. On Mars, the escape velocity is about 5 km/s, corresponding to an escape energy of 0.125 eV per amu. DR of O_2^+, CO+ and N_2^+ are sufficiently exothermic in at least some channels to produce escaping O, C and N atoms. On Venus and Earth the escape energies exceed 0.5 eV per amu and none of the dissociative recombination processes are exothermic enough

to produce escaping atoms. On Venus, dissociative recombination is implicated in an indirect way in the escape of H through the sequence[20]

$$O_2^+ + e \rightarrow O^* + O^* \qquad (R7)$$

followed by the transfer of energy in a collision of the translationally hot O* with an H atom:

$$O^* + H \rightarrow O^* + H^*. \qquad (R8)$$
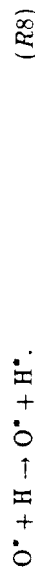
Cooper et al.[21] have computed the fraction of H atoms that come away from (R8) with energy greater than the escape energy as 6.9 and 8.5% at 200 and 300 K, respectively.

Even if the atoms released above the exobase have insufficient energy to escape, they may travel to high altitudes producing a "corona" of hot atoms surrounding the planet. The hot O coronas of the terrestrial planets are produced mainly by the dissociative recombination of O_2^+ at the exobase. The hot O corona of the Earth has been discussed Yee et al.[22] Such a corona was predicted for Venus and Mars by Wallis[23] and distributions of hot O have been computed by Nagy et al.,[24] Paxton,[25] and Nagy and Cravens.[26] The hot C corona around Venus has been studied by analysis of the limb profiles of the atomic carbon emission multiplets at 1561 and 1657 Å measured by the Pioneer Venus Orbiter (PVO) Ultraviolet Spectrometer.[25] These features are produced at high altitudes by fluorescent scattering of sunlight by atomic carbon. The hot C is produced partly in dissociative recombination of CO+, but mostly by (R7) followed by

$$O^* + C \rightarrow O + C^*, \qquad (R9)$$

a process that Paxton refers to as "sputtering", but which is more accurately termed "knock-on".[18]

In the remainder of this article, two problems in planetary aeronomy in which dissociative recombination plays a major role will be described in detail. The first is the escape of nitrogen from Mars. In modeling this phenomenon, knowledge of the kinetic energies and therefore, indirectly, the electronic states of the N atoms produced in DR of N_2^+ is important. Second, the production of the atomic oxygen green line in the nightglow of Venus is discussed. Here the production rates of $O(^1S)$ from dissociative recombination of O_2^+ in different vibrational levels is required.

2. THE ESCAPE OF NITROGEN FROM MARS

The mass spectrometer on the Viking spacecraft measured an anomalous ^{15}N:^{14}N ratio of about 0.0060 in the Martian atmosphere; the value in the terrestrial atmosphere is 0.00368.[27,28] This isotope enhancement of a factor of 1.62 over the terrestrial value is presumably due to preferential escape of ^{14}N. The thermosphere of Mars is composed mostly of CO_2, with smaller amounts of N_2, O, CO, Ar, O_2 and NO. The model thermosphere used here is essentially the same as that used by Fox and Dalgarno[29] and the calculations described here are an updating of that model. At the *turbopause* (about 120 km), the mixing ratio of N_2 is about 2.5%.[30] Diffusion largely controls the distribution of species above the turbopause, so the mixing ratios of heavier species decrease with altitude and those of lighter species increase. Thus between the turbopause and the exobase at about 200 km, the ratio, f of $^{15}N^{14}N$:$^{14}N_2$ decreases. The exact value of the ratio at the exobase, f_c depends on the ratio at the turbopause, f_o, which is assumed equal to that in the bulk atmosphere, and on the value of the eddy diffusion coefficient, a measure of the strength of mixing in the thermosphere. McElroy et al.[31] computed the deficiency factor $R = f_c/f_o$ and reported a value of about 0.82. If we call $\phi(t)$ the $^{14}N_2$ flux at time t, $\mathcal{N}_{14}$ the column density of $^{14}N_2$ and $\mathcal{N}_{15}$ the column density of $^{15}N^{14}N$ then

$$\frac{d\mathcal{N}_{14}}{dt} = -\phi(t) \quad (1)$$

and

$$\frac{d\mathcal{N}_{15}}{dt} = -f_c\phi(t) = -Rf\phi. \quad (2)$$
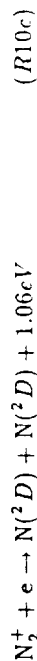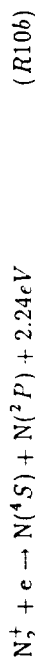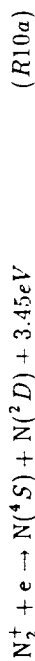
Combining (1) and (2) we obtain an equation for the isotope ratio f:[27]

$$\frac{df}{dt} = \frac{\phi f(1-R)}{\mathcal{N}_{14}}. \quad (3)$$

The isotope enhancement produced by escape operating over a time t before the present can be obtained by integrating equation (3) backward in time. The effects on the escape rate of changes in the composition of the atmosphere and in the heights of the exobase and turbopause are taken into account as described by Fox and Dalgarno.[29]

The steady state ion densities are computed by solving the continuity equations including photochemistry and ambipolar diffusion and the results are shown in Fig. 1. Also shown are the O_2^+ and CO_2^+ densities derived from the Viking I Retarding Potential Analyzer and reported by Hanson et al.[32] The atomic oxygen density was not measured by the mass spectrometers and has been adjusted to fit the O_2^+ and CO_2^+ densities at the ion peak. A mixing ratio of 2% at about 130 km is derived. The N_2^+ density peaks above the exobase at approximately 215 km where it attains a value of about 180 cm^{-3}. The total rate of N_2^+ DR above the exobase is about 2×10^6 cm^{-2} s^{-1}, but not all channels are sufficiently exothermic for escape to occur. Dissociative recombination may produce N atoms in three channels:

$$N_2^+ + e \rightarrow N(^4S) + N(^2D) + 3.45 eV \quad (R10a)$$

$$N_2^+ + e \rightarrow N(^4S) + N(^2P) + 2.24 eV \quad (R10b)$$

$$N_2^+ + e \rightarrow N(^2D) + N(^2D) + 1.06 eV \quad (R10c)$$

Because the N escape energy is 1.74 eV, escape is possible only when the reaction proceeds via (R10a). If a statistical distribution of products is assumed, the fraction of dissociative recombinations proceeding by (R10a) is about 0.24. With this assumption, DR is the dominant N escape mechanism.[29,33] The measurements of Queffelec et al.[5] have shown, however, that the predominant channel is (R10c) and that the yield of $N(^4S)$ is less than 0.10. We therefore assume that an upper limit to the fraction of dissociative recombinations proceeding according to (R10a) is 0.10.

For most escape mechanisms, preferential escape of ^{14}N is assumed to occur only because the ratio $^{15}N^{14}N$:$^{14}N_2$ is reduced at the exobase compared to that in the bulk atmosphere. The process of dissociative recombination via channel (R10a) itself, however, discriminates against ^{15}N. The escape energy of ^{14}N is about half the exothermicity of (R10a), but the escape energy of ^{15}N is 1.86 eV, much more than half the energy released. Wallis[23] computed the escape probabilities for both atoms and found that ^{14}N is about twice as likely to escape as ^{15}N. The exothermicities shown for (R10a-c) apply to DR of N_2^+ ions in the ground vibrational state. For vibrationally excited ions, the exothermicity is larger and the isotope discrimination due to the mechanism itself disappears! In order to model the evolution of the isotope ratio, it is necessary to determine the fraction of dissociative recombinations that occur from vibrationally excited states. Therefore we need to know the vibrational distribution of N_2^+ at the exobase and the rate

Table 1. The vibrational distribution of N_2^+ at the Martian exobase, 200 km.

v	Fraction
0	0.56
1	0.21
2	0.107
3	0.058
4	0.035
5	0.028

coefficients for dissociative recombination from individual vibrational levels. The latter are not available, although evidence suggests that the rate coefficient increases with increasing vibrational level.[34] We adopt the rate coefficient reported by Zipf[34] of $2.2 \times 10^{-7}(300/T_e)^{0.39}$ cm^{3}s^{-1} for dissociative recombination from all the vibrational levels ($v = 0 - 5$) included in the calculation. The model of Fox and Dalgarno[29] for the vibrational distribution of N_2^+ at the exobase on Mars has been updated (c.f. Fox and Dalgarno[35]) and the distribution presented in Table 1 was computed. The vibrational distribution at the exobase is essentially controlled by fluorescent scattering of sunlight in the Meinel and First Negative Band systems, which can be represented by

$$N_2^+(X^2\Sigma_g^+, v) + h\nu \rightarrow N_2^+(A^2\Pi_u, B^2\Sigma_u^+, v') \qquad (R11)$$

followed by

$$N_2^+(A, B, v') \rightarrow N_2^+(X, v'') \qquad (R12)$$

The fraction of N_2^+ ions in vibrationally excited levels is found to be about 44%, so the isotope discrimination operates only 56% of the time.

The ^{14}N escape fluxes from all sources are presented in Table 2. Values for both high and low solar activity were computed and averaged to obtain the escape fluxes used in the calculation. The values for photodissociation, photodissociative ionization, and photoelectron impact ionization are unchanged from those of Fox and Dalgarno.[29] The products of the reaction

$$O^{++} + N_2 \rightarrow N + N^+ + O^+ \qquad (R13)$$

are unknown, but exothermicity is large, about 10.9 eV, and it is assumed that an energetic N atom is produced in every reaction. The reaction

$$N_2^+ + O \rightarrow NO^+ + N \qquad (R1)$$

produces an N atom in the ^2D state at least 90% of the time.[36] In that case the exothermicity is not sufficient to allow escape of the N atom produced. We assume initially that 10% of the reactions (R1) produce a ground state N atom. With these assumptions, dissociative recombination is still the largest source of escaping N atoms, but photodissociation and reaction (R1) are comparable. The differential escape of ^{15}N and ^{14}N due to DR from the ground vibrational level,
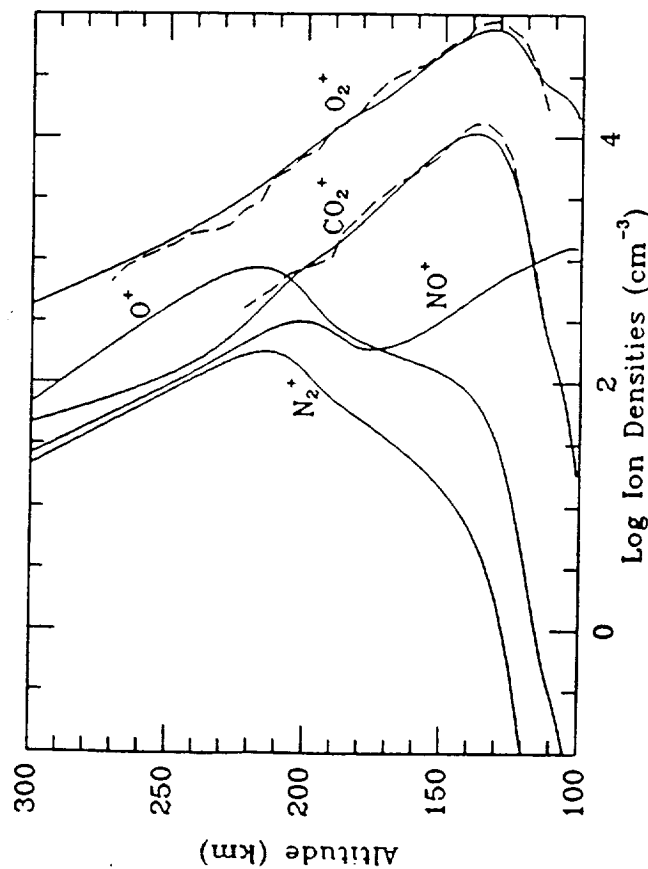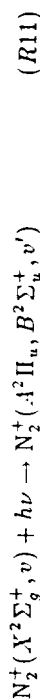

Fig. 1. Altitude profiles of the steady state ion densities for low solar activity. The solar zenith angle is 60°. The dashed lines are Viking 1 data from Hanson et al. (Ref. 32).

Table 2. ^{14}N Escape Fluxes (10^4 cm^{-2} s^{-1})

Process	Solar Activity		
	Low	High	Average
N$_2$ + hν → N + N	5.9	14	10
N$_2$ + hν → N$^+$ + N + e	1.7	6.0	3.9
N$_2$ + e → N$^+$ + N + 2e	1.4	4.8	3.1
N$_2^+$ + O → NO$^+$ + N	6.1	17	11
O^{++} + N$_2$ → N$^+$ + N + O$^+$	0.6	1.7	1.1
N$_2^+$ + e → N + N	4.0	22	13
TOTAL	20	66	42

however, causes this mechanism to produce a much larger isotope enhancement than the other mechanisms.

Using the average escape fluxes shown in Table 2 and integrating equations (1) and (3) backward in time over the age of the solar system, 4.6×10^9 years (1.45×10^{17}s), we find an initial column density of 8.5×10^{22} N$_2$ molecules cm^{-2}, about 14 times that found in the present atmosphere. The resulting isotope enhancement is shown in Fig. 2. The isotope enhancement for the escape processes operating over 4.6×10^9 years is 2.0, somewhat larger than the measured value. An isotope enhancement of 1.62 is reached in 7.5×10^{16}s (2.4×10^9 years). The escape fluxes due to reaction (R1) and to dissociative recombination are actually upper limits, so we tested the sensitivity of the model to the assumed yields by reducing both fluxes by half. The resulting initial N$_2$ column density is reduced by one-third and the predicted isotope enhancement is 1.71. The difference between the measured and the model isotope enhancements is probably within the uncertainties in the model. The magnitude of the solar flux, for example, in the early solar system was undoubtedly different from the current values, but arguments have been presented for both larger[37,38] and smaller values.[39] The isotope enhancement predicted for a statistical distribution of product states in (R10) was much larger, about 2.51.[29]

It was necessary then to invoke a mechanism to reduce the escape fluxes in the past, such as a denser CO$_2$ atmosphere, surviving over a period exceeding 2×10^9 years. Such an atmosphere has been predicted (e.g. Cess et al.[40], Pollack et al.[41]) to be consistent with an earlier presence of liquid water on the surface. While it is no longer necessary, a dense CO$_2$ atmosphere is not excluded by the current model, as long as it was lost early in the history of the solar system.

3. THE GREEN LINE OF ATOMIC OXYGEN ON THE NIGHTSIDE OF VENUS

Ultra-violet emission features of atomic oxygen at 1304 and 1356 Å have been seen on the nightside of Venus by the PVO Ultraviolet Spectrometer.[42] Fox and Stewart[43] have suggested that the emissions are due to the precipitation of soft electrons into the nightside atmosphere. Suprathermal electrons have been detected outside the atmosphere by the PVO Retarding Potential Analyzer[44] and by the plasma analyzers on the Soviet spacecraft Veneras 9 and 10.[45] The PVO measurements suggest that the electron energy spectrum approximates a Maxwellian distribution with a characteristic energy of about 14 eV. Impact of such electrons
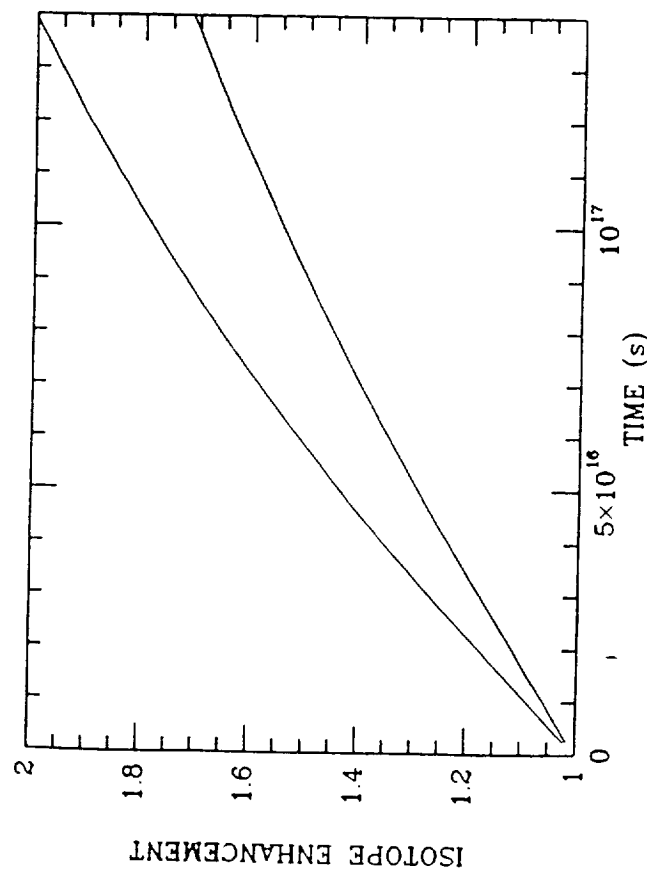
Fig. 2. Evolution of the isotope enhancement, the ratio ^{15}N:^{14}N relative to the terrestrial value. The upper curve was calculated assuming fluxes due to (R1) and (R10) equal to their upper limits, as explained in the text. The lower curve is for both fluxes reduced by half.

of DR to be substantial, although not necessarily a maximum. We have modeled this ionosphere by introducing a flux of O^+ of $1.0 \times 10^8 \, cm^{-2} s^{-1}$ at the top of our model thermosphere. Fluxes of other atomic ions, including C^+, N^+ and O^{++} were assumed proportional to their densities at high altitudes on the nightside as measured by the PVO Ion Mass Spectrometer.[60] Altitude profiles of the major ions in the resulting ionosphere are shown in Fig. 3. The effect of drag on the upward diffusion of molecular ions by the downward flux of O^+ is included in an approximate way by reducing the diffusion coefficients of the molecular ions by a factor of 10. This factor was chosen to reproduce the approximate shape of the measured O_2^+ profiles presented by Taylor et al.[60] The maximum O_2^+ density in our model is about $2.4 \times 10^4 \, cm^{-3}$.

Fig. 3. Computed profiles for the major ion densities in the nightside ionosphere of Venus. The model was constructed by introducing a flux of O^+ of $1.0 \times 10^8 \, cm^{-2} s^{-1}$ at the top of the neutral atmosphere.

should also excite atomic oxygen to the ^1S and ^1D states, producing emission at 5577 and 6300 Å. The Venera 9 and 10 fly-by spacecraft carried visible spectrophotometers, but no 5577 Å emission was measured on the nightside of Venus and an upper limit of 10 R has been placed on its intensity[46] (Krasnopol'sky, private communication, 1985). This upper limit places another constraint on models for the auroral production mechanism. In order to evaluate the constraint, it is necessary to predict the rate of production of the green line from other sources. Dissociative recombination of O_2^+ (R7) is probably the most important source in the nightglow. The production of $O(^1S)$ in (R7) has been shown to depend on the vibrational quantum number of O_2^+. Abreu et al.[47] showed that the 5577 Å emission in the terrestrial nightglow depends on the ratio of the electron density to atomic oxygen density, a measure of the extent of vibrational excitation of O_2^+.[48] Guberman[49,50] has performed ab initio calculations of the rate coefficients for the production of $O(^1S)$ and $O(^1D)$ in DR from the lower vibrational levels of O_2^+. He has shown in particular that the rate coefficient for production of $O(^1S)$ is a strong function of vibrational level, increasing almost 2 orders of magnitude from $v = 0$ to $v = 2$. We have constructed a model of the nightside ionosphere of Venus, including a model of the vibrational distribution of O_2^+, and we have used Guberman's rate coefficients to predict the intensities of the red and green lines in the Venus nightglow.

The thermosphere of Venus is similar to that of Mars, and consists mostly of CO_2 at low altitudes, with small amounts of N_2, CO and O. The neutral densities we have used are taken from the model of Hedin et al.[51] for 165° solar zenith angle and $F_{10.7} = 200$. This model is based on measurements of the PVO Neutral Mass Spectrometer.[52] The nightside ionosphere is maintained largely by transport of atomic ions, primarily O^+, from the dayside ionosphere.[53,54] Cravens et al.[55] constructed a quasi-two-dimensional model that showed that the observed O^+ horizontal velocities from the dayside are sufficient to maintain the nightside ionosphere. Spenner et al.[56] showed that a flux of O^+ ions of $1 - 2 \times 10^8 \, cm^{-2} s^{-1}$ over the nightside is sufficient to maintain the observed mean ion densities. The nightside ionosphere is, however, highly variable and almost always exhibits some degree of disturbance.[57,58] Sometimes the ionosphere disappears completely, leaving only a few scattered patches of plasma.[59] Our model ionosphere is designed to represent "full-up" relatively undisturbed conditions, when we expect the rate

Vibrationally excited $O_2^+(v)$ is produced on the nightside mainly in the reaction

$$O^+ + CO_2 \rightarrow O_2^+(v \leq 5) + CO. \quad (R14)$$

The rate coefficient for this reaction is large, about $9.4 \times 10^{-10} cm^3 s^{-1}$.[61] In the dayside ionosphere, the major source of O_2^+ is

$$CO_2^+ + O \rightarrow O_2^+(v \leq 6) + CO, \quad (R15)$$

which has a rate coefficient $k = 1.64 \times 10^{-10} cm^3 s^{-1}$.[62] The nascent vibrational distribution produced in these reactions is unknown, so the energetically accessible vibrational levels are assumed to be populated equally. Since the distribution assumed for the production reactions is similar, and fluorescent scattering is not important for O_2^+, we expect the steady state vibrational distribution on the nightside to be similar to that computed for the dayside.[63] Loss of O_2^+ is mostly by DR, reaction (R7), but in the lower ionosphere reactions with N

$$O_2^+ + N \rightarrow NO^+ + O \quad (R16)$$

and NO

$$O_2^+ + NO \rightarrow NO^+ + O_2 \quad (R17)$$

are also important.

In addition to the net sources and sinks of O_2^+, there are mechanisms that interchange vibrational levels with no net production or loss. Quenching of vibrational excitation is one such mechanism. In the lower ionosphere, the most important quencher is CO_2:

$$O_2^+(v) + CO_2 \rightarrow O_2^+(v-1) + CO_2. \quad (R18)$$

The rate coefficient for this reaction is surprisingly large, about $1-2 \times 10^{-10} cm^3 s^{-1}$. The rate coefficients for this and other quenching reactions have been taken from the measurements of Böhringer et al.[64] The rate coefficient for quenching by atomic oxygen

$$O_2^+(v) + O \rightarrow O_2^+(v-1) + O \quad (R19)$$

is unknown, but is probably large. We assume first a rate coefficient of $1 \times 10^{-10} cm^3 s^{-1}$, but we test the sensitivity of the model to this rate coefficient by

repeating the calculations with a nearly gas kinetic value of $6 \times 10^{-10} cm^3 s^{-1}$. Collisional excitation

$$O_2^+(v) + O \rightarrow O_2^+(v+1) + O \quad (R20)$$
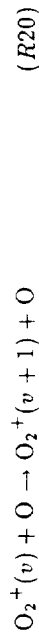
is the reverse of quenching and the rate coefficient is related to that for quenching by detailed balance, that is, $k_{20} = k_{19} \times e^{-\Delta E/kT}$, where ΔE is the energy difference between the vibrational levels.

We have solved the continuity equations for O_2^+, taking into account vibrational levels $v = 0-60$ of the ground electronic state, as was done for the dayside.[63] Fig. 4 shows the fractions of O_2^+ in the first four vibrational levels as a function of altitude from 130 km to 200 km. The calculation of the
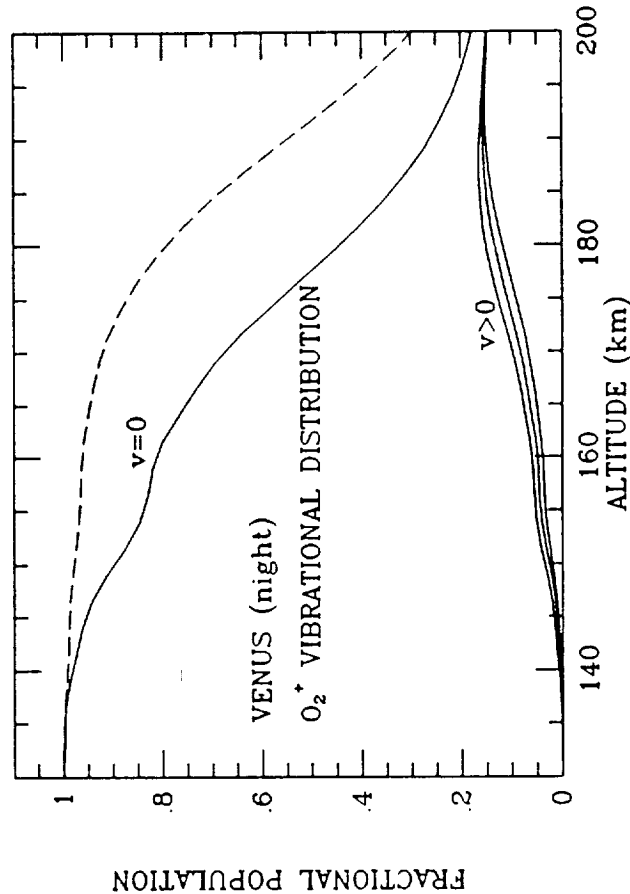
Fig. 4. Fractions of O_2^+ ions in vibrational states $v = 0-3$ as a function of altitude calculated with a photochemical steady state model, with an assumed value for k_{19} of $1 \times 10^{-10} cm^3 s^{-1}$. The curves labeled $v > 0$ are, from top to bottom, $v = 1$, $v = 2$ and $v = 3$. The dashed line is the fraction in $v = 0$ for $k_{19} = 6 \times 10^{-10} cm^3 s^{-1}$.

Fig. 6. Altitude profiles of the volume emission rates of the red and green lines of atomic O. Solid lines are computed assuming $k_{19} = 1 \times 10^{-10} cm^3 s^{-1}$. The dashed line is for $k_{19} = 6 \times 10^{-10} cm^3 s^{-1}$.

The vibrational distributions are combined with the rate coefficients from Guberman[49,50] and the total DR rate coefficient from Alge et al.[66] to give the yields for $O(^1S)$ and $O(^1D)$. For dissociative recombination from vibrational levels for which no information is available, the rate coefficient is assumed to be equal to that for the highest level for which data are available. Altitude profiles of the yields and the volume emission rates are shown in Figs. 5 and 6, respectively. The $O(^1S)$ yield varies from much less than 1% to about 8% at high altitudes. Fig. 6 shows that most of the emission arises between 140 and 160 km where the ^1S yield is in the range 1 – 2%. The dashed lines show the yields and volume emission rates for the assumption of the larger value for k_{19}. The integrated overhead intensities are 1.2R for the green line and 46R for the red line. If O_2^+ is quenched by O at the larger rate, the integrated green line intensity is reduced to

steady state ion densities includes transport by ambipolar diffusion, but the calculation of the vibrational distribution assumes photochemical equilibrium. Consequently, the distributions shown in Fig. 4 are probably valid only below about 170 km. The ions at higher altitudes are produced largely by transport from below. The dashed line shows the fraction in $v = 0$ for the larger rate coefficient for (R19), $k_{19} = 6 \times 10^{-10} cm^3 s^{-1}$. It should be noted here that the number of vibrational quanta lost in (R19) is unknown and may be more than the assumed value of 1, because the reaction can occur by atom-interchange,[48] but the rate coefficient and the average number of vibrational quanta lost cannot be varied independently in a meaningful way.

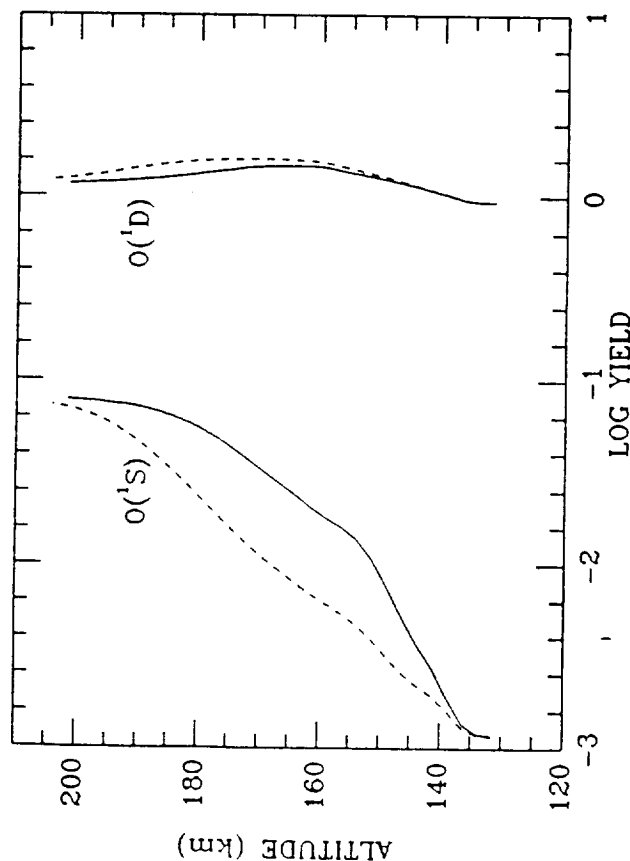Fig. 5. Altitude profiles of the yields of $O(^1S)$ and $O(^1D)$ produced in dissociative recombination of $O_2^+(v)$. Solid lines are computed assuming $k_{19} = ... \times 10^{-10} cm^3 s^{-1}$. Dashed lines are for $k_{19} = 6 \times 10^{-10} cm^3 s^{-1}$.

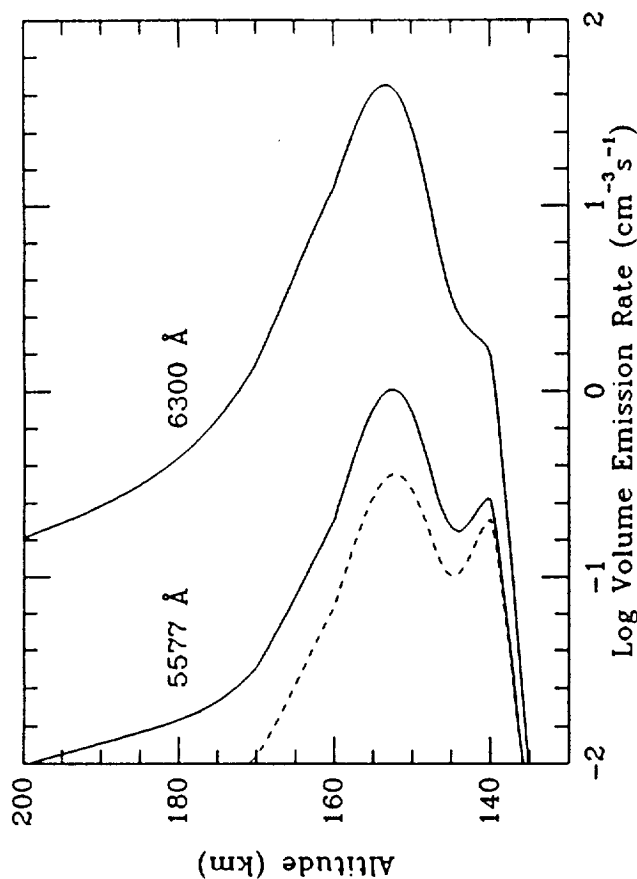0.5 R. Since the maximum electron density is somewhat larger than the average nightside value[58] the upper limit for auroral production is probably close the the measured upper limit. Had we adopted a yield of, say, 10% for the production of $O(^1S)$, independent of vibrational level of O_2^+, as has been done often in the past, close to 10 R would be predicted from dissociative recombination alone. A flux of soft electrons of sufficient magnitude to produce the observed 1304 and 1356 Å intensities produces 4 to 7 R of 5577 Å emission.[43] The results of this study of the green line show that the auroral model remains viable.

Acknowledgements

REFERENCES

1. Wauchop, T. S. and H. P. Broida, Lifetime and quenching of $CO(a^3\Pi)$ produced by recombination of CO_2 ions in a helium afterglow. *J. Chem. Phys.*, 56, 330 (1972).

2. James, T. C., Transition moments, Franck-Condon factors, and lifetimes of forbidden transitions. Calculation of the intensity of the Cameron system of CO, *J. Chem. Phys.* 55, 4118 (1971).

3. Lawrence, G. M., Quenching and radiation rates of $CO(a^3\Pi)$, *Chem. Phys. Lett.* 9, 575 (1971).

4. Fox, J. L. and A Dalgarno, Ionization, luminosity and heating of the upper atmosphere of Venus, *J. Geophys. Res.* 86, 629 (1981).

5. Queffelec, J. L., B. R. Rowe, M. Morlais, J. C. Gonet and F. Vallee, The dissociative recombination of $N_2^+(v=0,1)$ as a source of metastable atoms in planetary atmospheres, *Planet. Space Sci.* 33, 263 (1985).

6. Garstang, R. H., Transition probabilities of auroral lines, in *The Airglow and Aurorae*, ed. by E. B. Armstrong and A. Dalgarno, p. 324, Pergamon, New York (1956).

7. Cravens, T. E, J. C. Gérard, A. I. Stewart and D. W. Rusch, The latitudinal gradient of nitric oxide in the thermosphere. *J. Geophys. Res.* 84, 2675 (1979).

8. McCoy, R. P., Thermospheric odd nitrogen 1. NO, $N(^4S)$ and $O(^3P)$ densities from rocket measurements of the NO δ and γ bands and the O_2 Herzberg 1 bands. *J. Geophys. Res.* 88, 3197 (1983).

9. Rusch, D. W. and T. E. Cravens, A model of the neutral and ion chemistry in the daytime thermosphere of Venus. *Geophys. Res. Lett.* 6, 791 (1979).

10. Fox, J. L., The chemistry of metastable species in the Venusian ionosphere, *Icarus* 61, 248, (1982).

11. Lin, C. L. and F. Kaufman. Reactions of metastable nitrogen atoms, *J. Chem. Phys.* 55, 3760 (1971).

12. Baulch, D. L., D. D. Drysdale, D. G. Horne and A. C. Lloyd, *Evaluated Kinetic Data for High Temperature Reactions. II. Homogeneous Gas Phase Reactions of the H_2-N_2-O_2 System*, Butterworths, London (1973).

13. Brown, R. and C. A. Winkler, The chemical behavior of active nitrogen. *Angew. Chem. intern. Edit.* 9, 181 (1970).

14. Piper, L. G., M. E. Donahue and W. T. Rawlins, Rate coefficients for $N(^2D)$

reactions J. Phys. Chem. 91, 3883 (1987).

15. Constantinides, E. R., J. H. Black, A. Dalgarno and J. H. Hoffman, The Photochemistry of N^+ ions. Geophys. Res. Lett. 6, 569 (1979).

16. Torr, M. R., P. G. Richards and D. G. Torr, A new determination of the ultraviolet heating efficiency of the thermosphere. J. Geophys. Res. 85, 6819 (1980).

17. Fox, J. L., Heating efficiencies in the thermosphere of Venus reconsidered, Planet. Space Sci. 36, 27 (1988).

18. Hunten, D. M., Thermal and non-thermal escape mechanisms for terrestrial bodies, Planet. Space Sci. 30, 773 (1982).

19. Chamberlain, J. W., Planetary coronae and atmospheric evaporation, Planet. Space Sci. 11, 901 (1963).

20. McElroy, M. B., M. J. Prather and J. M. Rodriguez, Escape of hydrogen from Venus, Science, 215, 614 (1982).

21. Cooper, D. L., J. H. Yee, and A. Dalgarno, Energy transfer in oxygen-hydrogen collisions, Planet. Space Sci. 32, 825 (1984).

22. Yee, J. H., J. W. Meriwether, P. B. Hays, Detection of a corona of fast oxygen atoms during solar maximum, J. Geophys. Res. 85, 3396 (1980).

23. Wallis, M. K., Exospheric density and escape fluxes of atomic isotopes on Venus and Mars, Planet. Space Sci. 26, 949 (1978).

24. Nagy, A. F., T. E. Cravens, J.-H. Yee and A. I. F. Stewart, Hot atoms in the upper atmosphere of Venus, Geophys. Res. Lett. 8, 629 (1981).

25. Paxton, L. J., Atomic carbon in the Venus thermosphere: observations and theory, PhD thesis, University of Colorado (1983).

26. Nagy, A. F. and T. E. Cravens, Hot oxygen atoms in the upper atmospheres of Venus and Mars, Geophys. Res. Lett. 15, 933 (1988).

27. Nier, A. O., M. B. McElroy and Y. L. Yung, Isotopic composition of the Martian atmosphere. Science 194, 68, (1976).

28. Nier, A. O. and M. B. McElroy, Composition and structure of Mars upper atmosphere: Results from the neutral mass spectrometers on Viking 1 and 2, J. Geophys. Res., 82, 4341 (1977).

29. Fox, J. L. and A. Dalgarno, The escape of nitrogen from Mars, J. Geophys. Res., 88, 9027 (1983).

30. Nier, A. O., W. B. Hanson, A. Seiff and M. B. McElroy, Composition and structure of the Martian atmosphere: Preliminary results from Viking I. Science 193, 786 (1976).

31. McElroy, M. B., T. Y. Kong and Y. L. Yung, Photochemistry and evolution of Mars atmosphere: a Viking perspective, J. Geophys. Res. 82, 4379 (1977).

32. Hanson, W. B., S. Sanatani and D. R. Zuccaro, The Martian ionosphere as observed by the retarding potential analyzers, J. Geophys. Res. 82, 4351 (1977).

33. Fox, J. L. and A. Dalgarno, The production of nitrogen atoms on Mars and their escape, Planet. Space Sci. 28, 41 (1980).

34. Zipf, E. C., The dissociative recombination of vibrationally excited N_2^+ ions. Geophys. Res. Lett. 7, 645 (1980).

35. Fox, J. L. and A. Dalgarno, The vibrational distribution of N_2^+ in the terrestrial ionosphere, J. Geophys. Res. 90, 7557 (1985).

36. Frederick, J. E., and D. W. Rusch, On the chemistry of metastable atomic nitrogen in the F region deduced from simultaneous satellite measurements of the 5200-A airglow and atmospheric composition, J. Geophys. Res. 82, 3509 (1977).

37. Canuto, V. M., J. S. Levine, T. R. Augustson and C. L. Imhoff, UV radiation from the young sun and oxygen and ozone levels in the prebiological palaeoatmosphere, Nature 296, 816 (1982).

38. Zahnle, K. J. and J. C. G. Walker, The evolution of solar ultraviolet luminosity, Rev. Geophys. Space Phys. 20, 280 (1982).

39. Newman, M. J. and R. T. Rood, Implications of solar evolution for the Earth's early atmosphere, Science 198, 1035 (1977).

40. Cess, R. D., V. Ramanathan and T. Owen, The Martian paleoclimate and enhanced atmospheric carbon dioxide, Icarus 41, 159 (1980).

41. Pollack, J. B., F. J. Kasting, S. M. Richardson and K. Poliakoff, The case for a wet, warm climate on early Mars, Icarus 71, 201 (1987).

42. Phillips, J. L., A. I. F. Stewart and J. G. Luhmann, The Venus ultraviolet aurora: observations at 130.4 nm, Geophys. Res. Lett. 13, 1047 (1986).

43. Fox, J. L. and A. I. F. Stewart, The Venus ultraviolet aurora: a soft electron source, in preparation (1988).

44. Knudsen, W. C. and K. L. Miller, Pioneer Venus superthermal electron flux measurements in the Venus umbra, J. Geophys. Res. 90, 2695 (1985).

45. Gringauz, K. I., M. I. Verigin, T. K. Breus, and T. Gombosi, The interaction of electrons in the optical umbra of Venus with the planetary atmosphere—The origin of the nighttime ionosphere. *J. Geophys. Res.* 84, 2123 (1979).

46. Krasnopolsky, V. A., Excitation of oxygen emissions in the night airglow of the terrestrial planets, *Planet. Space Sci.* 29, 925 (1981).

47. Abreu, V. J., R. W. Eastes, J. H. Yee, S. C. Solomon and S. Chakrabarti, Ultraviolet nightglow production near the magnetic equator by neutral particle precipitation, *J. Geophys. Res.* 91, 11,365 (1986).

48. Bates, D. R. and E. C. Zipf, The $O(^1S)$ quantum yield of O_2^+ dissociative recombination, *Planet. Space Sci.* 28, 1081 (1980).

49. Guberman, S. L., The production of $O(^1D)$ from dissociative recombination of O_2^+, *Planet. Space. Sci.* 36, 47 (1988).

50. Guberman, S. L., The production of $O(^1S)$ in dissociative recombination of O_2^+, *Nature*, 327, 408 (1987).

51. Hedin, A. E., H. B. Niemann, W. T. Kasprzak and A. Seiff, Global empirical model of the Venus thermosphere, *J. Geophys. Res.* 88, 73 (1983).

52. Niemann, H. B., W. T. Kasprzak, A. E. Hedin, D. M. Hunten and N. W. Spencer, Mass spectrometric measurements of the neutral gas composition of the thermosphere and exosphere of Venus, *J. Geophys. Res.* 85, 7817 (1980).

53. Knudsen, W. C., K. Spenner, K. L. Miller and V. Novak, Transport of ionospheric O^+ ions across the Venus terminator and implications, *J. Geophys. Res.* 85, 7803 (1980).

54. Knudsen, W. C., K. Spenner, and K. L. Miller, Antisolar acceleration of ionospheric plasma across the Venus terminator. *Geophys. Res. Lett.* 8, 241 (1981).

55. Cravens, T. E., S. L. Crawford, A. F. Nagy and T. I. Gombosi, A two-dimensional model of the ionosphere of Venus, *J. Geophys. Res.* 88, 5595 (1983).

56. Spenner, K., W. C. Knudsen, R. C. Whitten, P. F. Michelson, K. L. Miller and V. Novak, On the maintenance of the Venus nightside ionosphere: electron precipitation and plasma transport, *J. Geophys. Res.* 86, 9170 (1981).

57. Taylor, H. A., R. E. Hartle, H. B. Niemann, L. H. Brace, R. E. Daniell, S. J. Bauer and A. J. Kliore, Observed composition of the ionosphere of Venus: implications for the ionization peak and the maintenance of the nightside iono-

sphere, *Icarus* 51, 283 (1982).

58. Knudsen, W. C., K. L. Miller and K. Spenner, Median density profiles of the major ions in the central nightside Venus ionosphere. *J. Geophys. Res.* 91, 11,936 (1986).

59. Cravens, T. E., L. H. Brace, H. A. Taylor, C. T. Russell, W. L. Knudsen, K. L. Miller, A. Barnes, J. D. Mihalov, F. L. Scarf, S. J. Quenon and A. F. Nagy, Disappearing ionospheres on the nightside of Venus. *Icarus* 51, 271 (1982).

60. Taylor, H. A., H. C. Brinton, S. J. Bauer, R. E. Hartle, P. A. Cloutier and R. E. Daniell, Global observations of the composition and dynamics of the ionosphere of Venus: implications for the solar wind interaction. *J. Geophys. Res.* 85, 7765 (1980).

61. Smith, D., N. G. Adams and T. M. Miller, A laboratory study of the reactions of N^+, N_2^+, N_3^+, N_4^+, O^+, O_2^+ and NO^+ with several molecules at 300 K, *J. Chem. Phys.* 69, 308 (1978).

62. Fehsenfeld, F. C., D. B. Dunkin and E. E. Ferguson, Rate constants for the reaction of CO_2^+ with O, O_2 and NO; N_2^+ with O and NO; and O_2^+ with NO. *Planet. Space Sci.* 18, 1267 (1970).

63. Fox, J. L., The O_2^+ vibrational distribution in the Venusian ionosphere, *Adv. Space Res.* 5, 165 (1985).

64. Böhringer, H., M. Durup-Ferguson, E. E. Ferguson and D. W. Fahey, Collisional vibrational quenching of $O_2^+(v)$ and other molecular ions in planetary atmospheres, *Planet. Space Sci.*, 31, 483 (1983).

65. Fox, J. L., The O_2^+ vibrational distribution in the dayside ionosphere, *Planet. Space Sci.* 34, 1252 (1986).

66. Alge, E., N. G. Adams and D. Smith, Measurements of the dissociative recombination coefficients of O_2^+, NO^+ and NH_4^+ in the temperature range 200 – 600 K. *J. Phys. B.* 16, 1433 (1983).

PROOFS

STRUCTURE, LUMINOSITY, AND DYNAMICS OF THE VENUS THERMOSPHERE

J. L. FOX

*Institute for Terrestrial and Planetary Atmospheres and Department of Mechanical Engineering,
State University of New York at Stony Brook, Stony Brook, NY 11974, U.S.A.*

and

S. W. BOUGHER

Lunar and Planetary Laboratory, University of Arizona, Tucson, AZ 85721, U.S.A.

Abstract. We review here observations and models related to the chemical and thermal structures, airglow and auroral emissions and dynamics of the Venus thermosphere, and compare empirical models of the neutral densities based in large part on *in situ* measurements obtained by the Pioneer Venus spacecraft. Observations of the intensities of emissions are important as a diagnostic tool for understanding the chemical and physical processes taking place in the Venus thermosphere. Measurements, ground-based and from rockets, satellites, and spacecraft, and model predictions of atomic, molecular and ionic emissions, are presented and the most important sources are elucidated. Coronas of hot hydrogen and hot oxygen have been observed to surround the terrestrial planets. We discuss the observations of and production mechanisms for the extended exospheres and models for the escape of lighter species from the atmosphere. Over the last decade and a half, models have attempted to explain the unexpectedly cold temperatures in the Venus thermosphere; recently considerable progress has been made, although some controversies remain. We review the history of these models and discuss the heating and cooling mechanisms that are presently considered to be the most important in determining the thermal structure. Finally, we discuss major aspects of the circulation and dynamics of the thermosphere: the sub-solar to anti-solar circularion, superrotation, and turbulent processes.

1. Introduction

CO_2 was first identified as a constituent of the Venus atmosphere by Adams and Dunham (1932), who, in their search for evidence of O_2 and H_2O in ground-based infrared spectra observed these CO_2 bands at 7820, 7883, and 8689 Å. Over the following forty years, spectral resolution in the infrared improved and allowed the abundances of HCl, HF, and CO in the atmosphere to be determined (e.g., Connes *et al.*, 1967, 1968, 1969). A review of this early period in Venus spectroscopy has been presented by Young (1972) and more recently by von Zahn *et al.* (1983). That the atmosphere is composed mostly of CO_2 was suggested by Connes *et al.* (1967), Belton *et al.* (1968), and by Moroz (1968), but confirmation was not obtained in the first *in situ* measurements were performed in 1967 by instruments on the Soviet Venera 4 entry probe (Vinogradov *et al.*, 1968). The experiments were simple: the pressure of a sample of atmospheric gas was determined before and after adsorption by a chemical absorber. A description of the instruments on Venera 4, and on two similar spacecrafts that were launched two years later, Veneras 5 and 6, have been presented by Vinogradov (1971). The major constituents and their mixing ratios (used hereafter to mean fraction of

particles by number) in the lower atmosphere were reported by Kuz'min (1970, 1971) as $95 \pm 2\%$ CO_2, 2-5% N_2, 0.1-1% H_2O and less than 0.4% O_2.

Up to the homopause, the composition of the thermosphere of a planet is nearly the same as that of the bulk atmosphere, at least with respect to the major constituents that are not affected by photochemistry; above the homopause photolysis of the molecular constituents and diffusive separation in the gravitational field causes lighter constituents to become increasingly abundant. Exploration of the thermosphere of Venus began in October 1967 when two spacecrafts, the U.S. fluby Mariner 5 and the Soviet Venera 4 carried ultraviolet photometers to Venus. Both instruments were designed to detect resonance emission features of H at 1216 Å and of O at 1304 Å, from which column densities and altitude profiles of the H and O densities could be derived. No signal was reported at 1304 Å by either teh Mariner 5 photometer (Barth *et al.*, 1967) or the Venera 4 instrument, which observed the atmosphere in darkness below about 350 km (Kurt *et al.*, 1968). Both detected strong Lα emission. The Venera Lα intensities were used to derive a nightside density profile of H atoms from 1 to about 4 Venus radii. From the scale height of the H densities and the upper limit on the O densities Kurt *et al.* (1968) deduced, more or less correctly, that 'the Venus nightside atmosphere is cold . . . and undergoes a sharp transition to interplanetary space'. The Mariner 5 Lα channel detected emission that was characterized by an abrupt increase in scale height as the minimum distance of the photometer line-of-sight to the center of the planet exceeded about 9000 km (Barth *et al.*, 1967; Barth, 1968). From the scale height, the ratio of the temperature to the mass of the species responsible for the of the inner component was derived to be about 350 K amu^{-1}. Exospheric temperatures as low as 350 K were considered unlikely, based partly on model calculations (McElroy, 1969) that were reinforced by prejudices arising from the analogy with Earth, where the solar fluxes are a factor of two lower and the average exospheric temperature is about 1000 K. Therefore, species heavier than H, including D and H_2 were considered also as the source of the low altitude component, the latter assumed to produce emission from photodissociative excitation rather than resonance scattering (e.g., Barth, 1968; Donahue, 1968; Wallace, 1969; McElroy and Hunten, 1969). Later work showed that the actual exospheric temperature was even lower than the 'unlikely' value of 350 K (Anderson, 1975). The measurement of the outer, larger scale height component was the first detection of the hot hydrogen corona, although it was not immediately identified as such.

That the thermospheric abundance of O was low was suggested by the non-detection of 1304 Å emission and by profiles of the electron density in the daytime ionosphere that were obtained from the radio occultation experiment on Mariner 5 (Kliore *et al.*, 1967). The electron density profile, shown in Figure 1, exhibited a single maximum that was interpreted as an F_1 peak, a Chapman layer consisting of a molecular in (initially believed to be CO_2^+) produced by photoionization and photoelectron impact ionization and destroyed by dissociative recombination. The absence of a distinguishable O$^+$ (F_2) peak above the F_1 layer was interpreted as implying that the mixing ratio of atomic O in the Veznus thermosphere was smallk (Stewart, 1968; McElroy, 1969; Kumar and Hunten, 1974).
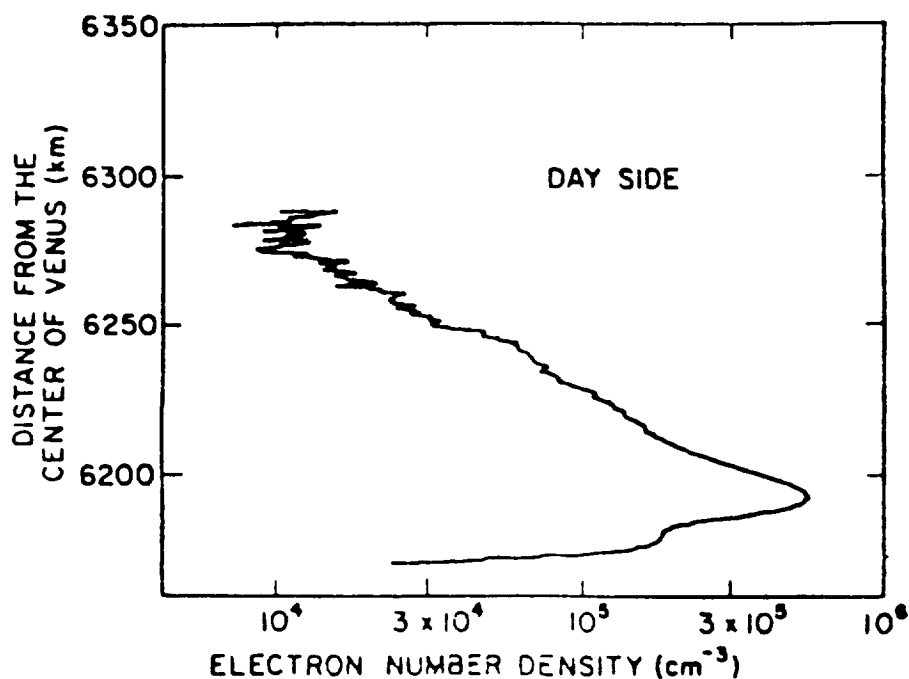
Fig. 1. Electron density profile as measured by the radio occultation experiment on Mariner 5. Taken from Kliore et al. (1967).

Mariner 10 flew by Venus in February 1974, carrying an objective grating spectrometer with channel electron multipliers at the wavelengths of 9 atomic and molecular emission features between 200 and 1700 Å, two zero-order channels and a background channel at 430 Å (Broadfoot et al., 1977). The spectral features that the Mariner 10 instrument was designed to detect are listed in Table I. Strong emissions were detected in the positions of the helium, hydrogen, oxygen, CO, and carbon features in the spectrum (Broadfoot et al., 1974).

In October 1975, the Soviet spacecraft Veneras 9 and 10 were inserted into orbit about Venus. The spacecraft were equipped with hydrogen and deuterium absorption cells in front of an NO counter to study the hydrogen corona, and visible spectrometers to record nightglow emission features in the 3000 to 8000 Å wavelength range (Keldysh, 1977; Krasnopol'sky, 1983). Four band systems of O_2 were detected in the Venus nightglow with maximum volume emission rates appearing near 100 km. Upper limits were placed on other species and processes from the absence of emission features at 5577 Å (the atomic oxygen green line), 5893 Å (the sodium D-line doublet) and 3914 Å (the (0, 0) N_2^+ first negative band) (Krasnopol'sky, 1978, 1979). Unfortunately, the sensitivity of the detectors decreased by a factor of 5 after the first month of operations, so the number of orbits yielding useful data was limited.

In December 1978 ten separate space probes arrived at Venus, including the Pioneer Venus (PV) Orbiter and Multiprobe, which included the Bus and four probes that were

TABLE I

Features detected by the photometers on Mariner 10 and Veneras 11 and 12

Species	Wavelength (Å)	Mariner 10	Venera 11	Venera 12
He⁺	304	no	yes	yes
He	584	yes	yes	yes
Ne	740	no	no	no
O⁺	834	n/a [a]	yes	n/a
Ar	869	no	n/a	no
Ar	1048	no	no	no
H	1216	yes	yes	yes
O	1304	yes	yes	yes
C	1657	yes	yes	yes
CO	1480–1500	yes	yes	yes

[a] No detector at that wavelength.

released prior to entry into the Venus atmosphere, and the Soviet Veneras 11 and 12 flyby spacecraft and landers. The composition of the atmosphere below the clouds was measured by a mass spectrometer (LNMS) (e.g., Hoffman et al., 1980a) and gas chromatograph (LGC) (e.g., Oyama et al., 1980) on the Pioneer Venus sounder probe, neutral mass spectrometers on the Venera 11 and 12 landers (e.g., Istomin et al., 1979; Grechnev et al., 1980) and a gas chromatograph on the Venera 12 lander (Gel'man et al., 1979). A comparison of the results of these measurements has been presented by Hoffman et al. (1980b). CO_2 and N_2 are found to make up 99.9% of the atmosphere. The range of values of the N_2 mixing ratio was 2.5 to 4.5%. Von Zahn et al. (1983) have reviewed the available measurements of N_2 in the bulk atmosphere and recommend an abundance of 3.5 ± 0.8%; that value has also been adopted by the Venus International Reference Atmosphere (von Zahn and Moroz, 1986) (see Section 2.2).

The Venera 11 and 12 flybys carried UV spectrophotometers with detectors at 9 wavelengths with bandpasses about 12 Å wide and zero-order channel that provided an integral of the intensity over the wavelength region from 300 to 1700 Å. The wavelengths of and species responsible for the emission features that the instruments were designed to detect are also listed in Table I. The Venera instruments were similar to, but more sensitive than, the Mariner 10 instrument (Bertaux et al., 1981; Krasnopol'sky, 1986a). Unlike the Mariner 10 instrument, however, during the flyby the slits were not oriented parallel to the limb and consequently the spatial resolution was insufficient to derive altitude profiles of the intensities; except for Lα and the He 584 Å emission, only surface brightnesses were reported (Kurt et al., 1979, 1983; Bertaux et al., 1981). The resonance emissions of Ar and Ne were not detected, but the first observations of the O⁺ and He⁺ emission features at 834 and 304 Å, respectively, were reported.

The Pioneer Venus bus and orbiter carried a number of instruments that have provided information about the structure and composition of the thermosphere. A magnetic sector neutral mass spectrometer (BNMS) aboard the bus measured neutral densities from about 650 km to below the homopause, near 128 km (e.g., von Zahn,

1977; von Zahn *et al.*, 1980). The orbiter payload included a quadrupole neutral mass spectrometer (ONMS) to measure thermospheric densities of CO_2, O, CO, N_2, N, and He (e.g., Niemann *et al.*, 1979, 1980a, b), and an atmospheric drag experiment (OAD) to measure the total mass density profile (e.g., Keating, 1977; Keating *et al.*, 1980). The orbiter ultraviolet spectrometer (OUVS) was designed to measure intensities of airglow emission features of neutral atmospheric atoms, molecules, and ions. A complete description of the OUVS has been presented by Stewart (1980). Briefly, the instrument consists of 250-mm *f*/5 Cassegrainian telescope, an Ebert–Fasie monochromator of 125 mm focal length, and two photomultipliers, sensitive in the ranges 1100 to 1800 Å and 1600 to 3300 Å. The OUVS instrument can be commanded to scan the spectrum, or the wavelength may be fixed. Images of the planet at a fixed wavelength may be obtained from successive scans of the disk that are made as the spinning spacecraft approaches the planet from apoapsis. When the spacecraft is near periapsis altitude profiles of the emissions may be obtained. Among the features that the OUVS has detected are the γ and δ bands in the NO nightglow, the 1304, 1356, and 2972 Å features of O, H Lα, the 1561 and 1657 Å features of C, and the CO fourth positive bands in the dayglow, and the 1304 and 1356 Å auroral emission features.

We present here a brief history of investigations into and our current understanding of the structure, emission features, and dynamics of the Venus thermosphere. In Section 2, we present a description of the basic structure of the thermosphere, including the exospheric temperature and chemical composition, mostly as determined by Pioneer Venus *in situ* measurements. We compare empirical models of the major thermospheric constituents. In aurora, both Earth-bsed and from American and Soviet spacecraft. Measurements and models of emission features of the species, O, CO, N_2, O_2, C, NO, and He and their ions are described. Discussion of emission features of atomic hydrogen is deferred until Section 4, where we describe the hot atom coronas and atmospheric escape. Section 5 contains a detailed discussion of the thermal structure and heating and cooling mechanisms, mostly as given by models. The last part of the paper, Section 6, describes the circulation and dynamics of the thermosphere.

2. Basic Thermospheric Structure

2.1. EXOSPHERIC TEMPERATURE

The prejudice that Venus exospheric temperatures, T_∞, should not be too much smaller than terrestrial values, persisted until about 15 years ago, in spite of early indications that the temperatures were lower. The scale height of the H profile derived from Venera 4 Lα intensities close the the planet implied temperatures on the Venus nightside near 100 K, but a specific value was not presented by Kurt *et al.* (1968), who merely remarked that the nightside atmosphere was cold. Stewart (1968) first suggested the interpretation that the two-scale height Lα profile measured by Mariner 5 was H atoms at two different temperatures, which would imply that the temperature of the inner component on the dayside was about 350 K. Over the next few years, further measurements and models

ruled out H_2 and D at higher temperatures as sources of the emissions (see Section 4 for further details). The higher temperatures, near 700 K, computed by McElroy (1969) could be accommodated only if CO_2^+ was considered to be the major ion. Fehsenfeld *et al.* (1970) showed that in the presence of a small admixture of O, CO_2^+ is converted rapidly to O_2^+ through the reaction

$$CO_2^+ + O \rightarrow O_2^+ + CO.$$ (1)

Kumar and Hunten (1974) showed that a model ionosphere with an exospheric temperature of 350 K and O_2^+ as the major ion fit the Mariner 5 electron density profiles. Mariner 10 measurements of the He corona gave a T_∞ of about 375 $\pm$ 105 K (Kumar and Broadfoot, 1975). Anderson (1976) reanalyzed the Mariner 5 Lα data and reported for the inner component a dayside temperature of 275 K and a nightside temperature of 150 K. These low values were later confirmed by the Pioneer Venus *in situ* measurements. A value of T_∞ of 275 $\pm$ 15 K was derived from the He densities measured by the Bus Neutral Mass Spectrometer at 08:30 local time, 37.9° S latitude (von Zahn *et al.*, 1980). Keating *et al.* (1980) constructed an empirical model from the OAD data obtained in the early PV orbits; dayside values of T_∞ were about 280–300 K. Airglow emission profiles measured by the OUVS were consistent with an exospheric temperature of about 275 K (Stewart *et al.*, 1979). Hedin *et al.* (1983) derived a global average temperature of 228 K from ONMS data taken between December 1978 and August 1980 for a narrow latitude range of a few degrees around 16° N. Variations with solar activity during this limited time period were observed to be only 10% of the change seen in the terrestrial thermosphere. The variation in the exospheric temperatures with solar flux in the model of Hedin *et al.* (1983) is 0.14 K per unit $F_{10.7}$, the 10.7 cm solar flux in units of 10^{-22} W m^{-2} Hz^{-1} at 1 AU.

The temperature at the lower boundary of the thermosphere, near 100 km, takes on values near 175 K and, unlike the exospheric temperature, varies little with solar zenith angle (Seiff *et al.*, 1980). The thermospheric temperature structure will be discussed in detail in Section 5.

2.2. MODELS OF THE VENUS THERMOSPHERE

Information about the composition and structure of the thermosphere of Venus, obtained largley from *in situ* measurements, have been summarized in several empirical models. Von Zahn *et al.* (1980) presented a model of the morningside atmosphere (hereafter the BNMS model) that is based mostly on measurements of densities of CO_2, He, N_2, and CO made by the BNMS. The 10.7 cm solar flux index ($F_{10.7}$) was about 189 at the time of the bus entry. The densities of O in the model were derived from the ratio O/CO_2 of 3 reported at 167 km by Niemann *et al.* (1980b) from ONMS measurements. The mass densities measured by the BNMS agree fairly well with those measured by the OAD and merge smoothly near 130 km with densities measured by the accelerometers on the entry probes (Seiff *et al.*, 1980). Altitude profiles of the major constituents in the model are shown in Figure 2. The exospheric temperature is 275 K and the temperature at 100 km, the lower boundary of the model, is 178 K.
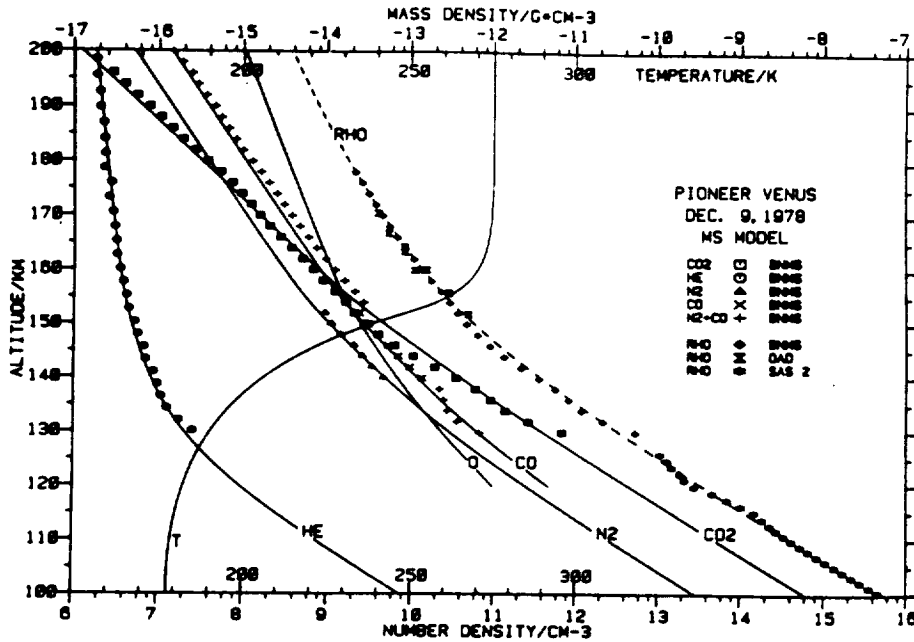
Fig. 2. Number densities of He, N_2, CO, N_2 + CO, and CO_2 measured by the BNMS versus altitude, interpolated to integer altitudes. Also shown are mass densities measured by the large probe accelerometer from 100 to 126 km, those derived from the BNMS between 130 and 180 km, and those from orbiter drag data (OAD) between 150 and 170 km. The lines represent number densities, mass density and temperature from the BNMS model. Taken from von Zahn *et al.* (1980).

The density profiles of He, CO, and N_2 were used by von Zahn *et al.* (1980) to derive an expression for the eddy diffusion coefficient K (in units of $cm^2 s^{-1}$):

$$K = \frac{A}{n^{1/2}} ,$$

(2)

where n is the total number density in cm^{-2}. The constant A was determined to be within a factor of 2 of 1.4×10^{13}. The molecular diffusion coefficient D has a steeper altitude dependence, since it is proportional to n^{-1}. K and D are equal at the homopause, which for N_2 is near 136 km. The molecular diffusion coefficient for He is larger than that of N_2 and the He homopause is located lower, near 130 km. Extrapolating the mixing ratios to the lower atmosphere, the composition of the lower atmosphere is derived to be about 95.5% CO_2, 4.5% N_2, and 12 ppm He. The mixing ratio of He is very sensitive to the uncertainty in the eddy diffusion coefficient and is good to only about a factor of three. The probably uncertainty in the N_2 mixing ratio is about 25%.

Hedin *et al.* (1983) presented a global empirical model of the Venus thermosphere (hereafter referred to as the VTS3 model) based on measurements of CO_2, O, CO, N_2, He, and N made by the Pioneer Venus ONMS. The VTS3 model incorporates

variations in the densities with latitude, local time and solar activity based on three diurnal cycles of observations. The altitude rnage of the orbiter measurements is from about 142 to 250 km, but data from the entry probe accelerometers (Seiff *et al.*, 1980), the BNMS (von Zahn *et al.*, 1980), and theoretical considerations were used to extend the model to 100 km. Dissociation of CO_2 is the primary source of O and CO in the lower thermosphere; the production is balanced by three-body recombination

$$O + O + CO_2 \rightarrow O_2 + CO_2 \qquad (3)$$

below 110 km (Massie *et al.*, 1983). Thus the mixing ratio of CO should be equal, to a first approximation to the sum of the mixing ratio of O plus twice that of O_2. In the VTS3 model, the mixing ratios of O and CO are assumed to be equal at 100 km, since photochemical considerations indicate that the mixing ratio of O_2 is small (Yung and DeMore, 1982). Data from the PV sounder probes, shown in Figure 3 compared to the ONMS model densities, indicate that latitude and local time variations of the mass densities near 100 km are small (Seiff *et al.*, 1980), so pressure gradients at the lower boundary in the model are constrained to be minimal. The mass densities measured by the ONMS are about 60% less than those given by the simpler PV OAD, the accelerometers on the probes and the BNMS. Ionospheric models also indicate that the ONMS densities are low (e.g., Cravens *et al.*, 1981). It has been suggested that the gas flow into the ONMS ion source at satellite velocities may deviate frm that assumed in the data reduction, but efforts to quantify the effect experimentally have been successful (Hedin *et al.*, 1983). The model densities presented by Hedin *et al.* (1983) have, however, been normalized by a factor of 1.63 to bring them into agreement with the dag data. Since the nightside temperatures are much lower than the dayside, the midnight densities above 100 km are less than the noon densities, and above the homopause, diffusive separation is more effective, cuasing the nighttime mixing ratios of lighter constituents at a given altitude to be larger. For example, in the model for $F_{10.7} = 200$ at the equator, the mixng ratio of O at 135 km is 7.3% at noon and 17% at midnight; atomic oxygen becomes the dominant component above 155 km at noon and above 140 km at midnight. The noon and midnight models are shown in Figure 4. The variability of the neutral densities is found to be larger on the nightside than on the dayside: the standard deviations are 15–23% on the dayside and 50–60% on the nightside (Hedin *et al.*, 1983; Keating *et al.*, 1985). Although the VTS3 model is based on observations near high solar activity, a full rnage of solar activity variations has been incorporated into the model using the 10.7 cm flux at 1 AU ($F_{10.7}$) as a parameter. Thus, the low solar activity models should be considered somewhat speculative. It is interesting to note, however, that Kim *et al.* (1989) found that the solar cycle minimum electron density profiles measured by the PVO radio occultation experiment (ORO) are well reproduced by photochemical equilibrium models that employ the VTS3 model, but efforts to reproduce the solar cycle maximum ORO profiels suggest that the VTS3 densiteis are too low below 135–140 km.

The BNMS model can be compared to the model for conditions appropriate to the PV Bus entry: 39°, $F_{10.7} = 189$ and 08 : 30 local time. The CO_2 densities at 100 km in the BNMS model are smaller by about 15% compared to the VTS3 model, but the
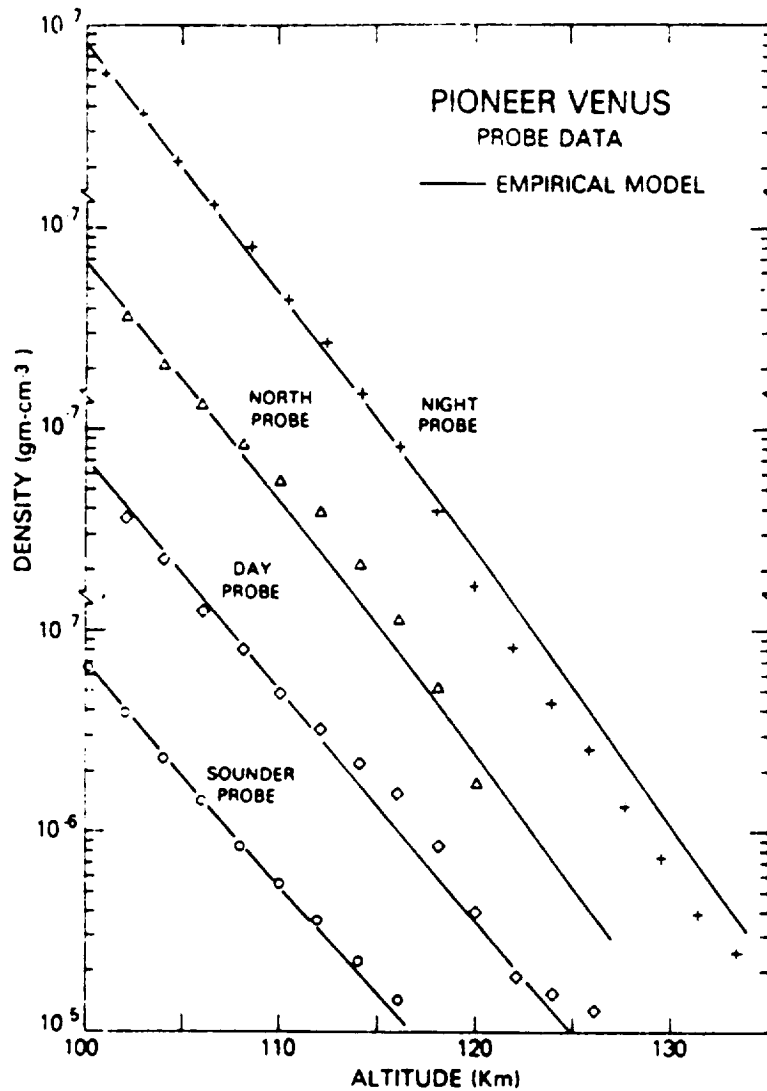
Fig. 3. Total mass densities from the sounder probes as a function of altitude. Corresponding density profiles from the VTS3 empirical model are shown as solid lines. Taken from Hedin *et al.* (1983).

thermospheric temperature are higher below and lower above 145 km. The CO_2 densities at about 160 km are 15% larger in the BNMS model. The mixing ratio of O at 135 km is 7.9% in the VTS3 model and 7.0% in the BNMS model, the near equality indicating only that the BNMS values are based on ONMS data. The mixing ratios of N_2 at 135 km are similar: 6.3 and 8.3% for the BNMS and VTS3 models, respectively, but the CO mixing ratios differ by nearly a factor of three: 14.7% (BNMS) and 5.7% (VTS3). The He densities in the two models are equal to within 10%, but the mixing ratio is smaller by about 30% in the BNMS model.
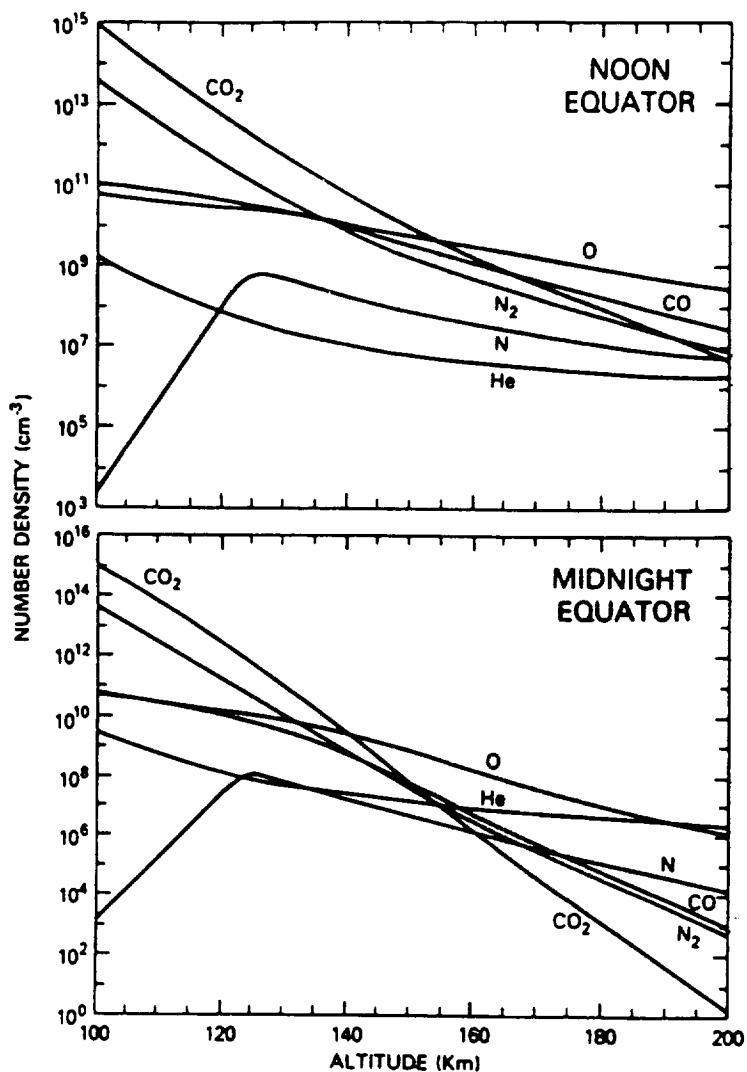
Fig. 4. VTS3 model densities as a function of altitude at noon and midnight at 0° latitude. Taken from Hedin *et al.* (1983).

Massie *et al.* (1983) constructed daytime (08 : 00 and 16 : 00 hr local time) and midnight models of the densities of CO_2, O, CO, N_2, He, and O_2 in Venus thermosphere over the altitude range 100 to 180 km by solving the one-dimensional continuity equation constrained by the PV in *in situ* measured neutral densities. No morning-evening asymmetry was included, although a bulge is observed in the light constituents near the morning terminator (see Section 4). The downward fluxes of N and O near midnight were inferred from the observed NO and O_2 nightglow intensities (see Section 3), and the nightside density profiles of N and O were constrained to fit the measurements. Massie *et al.* preferred the BNMS measurements of CO_2 and N_2, which were about 1.8

and 2.4 times the non-normalized values ONMS values, and the ONMS measurements of O and CO. Alternative values of O and CO that were 1.6 times the ONMS values were also given. The densities of O_2 in their dayside model are computed from the continuity equation assuming that the major production reaction is three-body recombination (Equation (3)) and loss is by photodissociation and three-body recombination of O and O_2:

$$O + O_2 + M \rightarrow O_3 + M . \tag{4}$$

At the lower boundary, the mixing ratio of O_2 was set equal to 1×10^{-3}, that computed by Yung and DeMore (1982) from mesospheric chemistry. The dayside and nightside models of Massie *et al.* with non-normalized values for O and CO densities are shown in Figures 5(a) and 5(b).

A comprehensive model of thermospheric composition, part of the Venus International Reference Atmosphere (VIRA), has been constructed by Keating *et al.* (1985) based on information available through 1985. The thermosphere is divided into two regions, the lower region includes altitudes from 100 to 150 km and the upper region
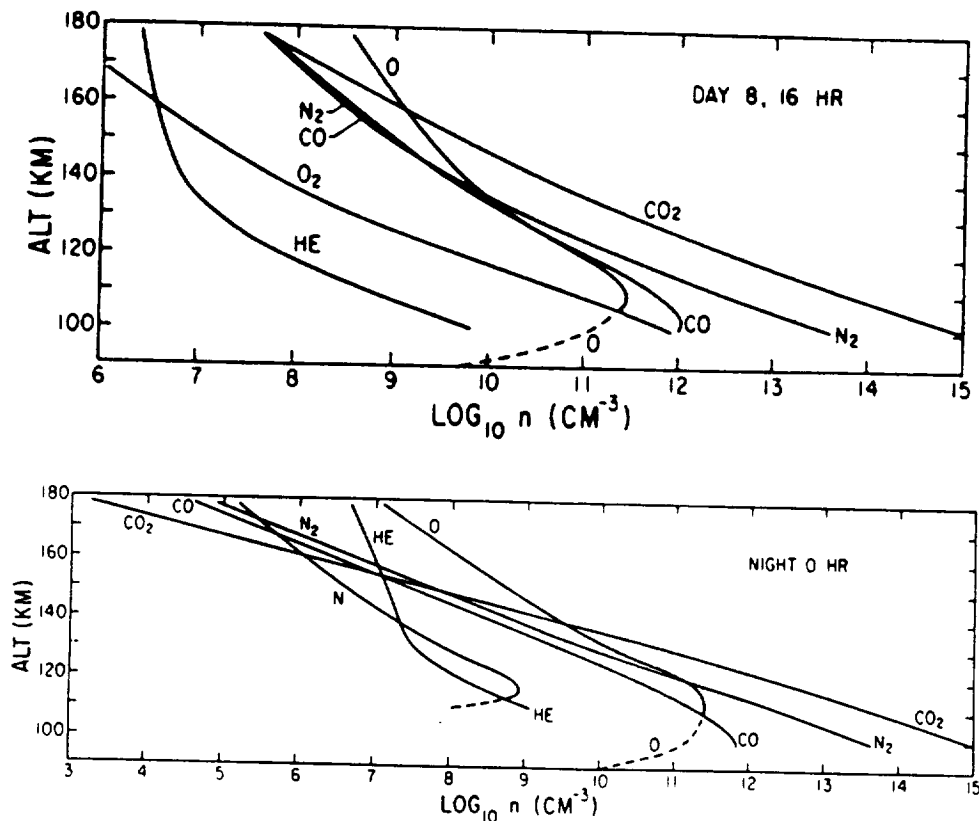
Fig. 5. (a) Neutral number densities from the dayside (08:00 and 16:00 hours local time) model of Massie *et al.* (1983). (b) Neutral densities from the midnight model of Massie *et al.* (1983).

is that above 150 km. The models for noon and midnight are shown in Figures 6(a–d). Diffusive equilibrium is assumed for all species in the upper region; the composition is based on the measurements of the ONMS, normalized to the OAD data. The normalization factors used in the VIRA models, 1.83 for CO_2 and 1.58 for O, are slightly
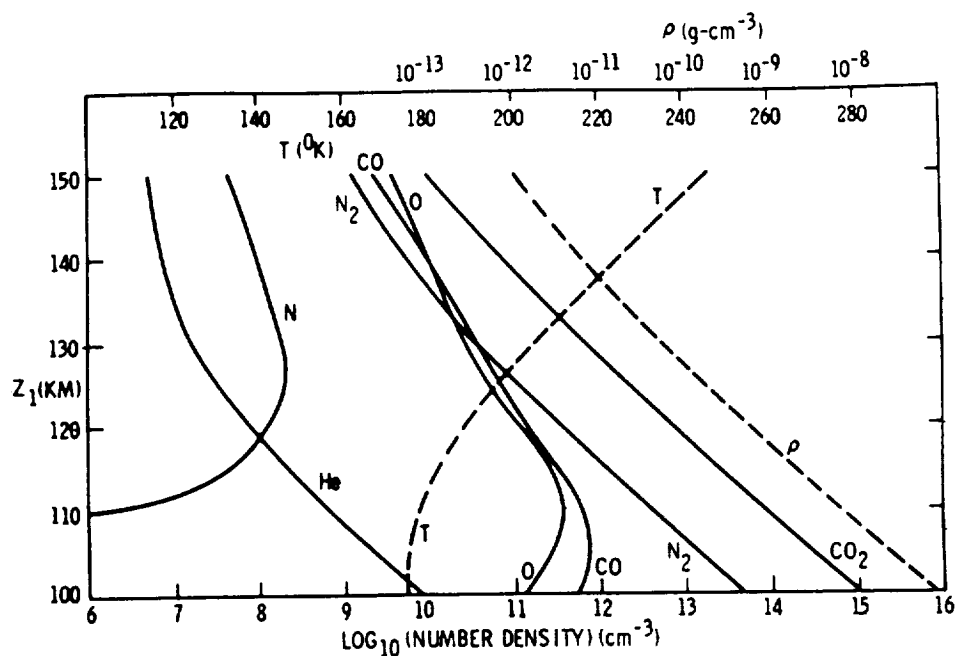
Fig. 6a.
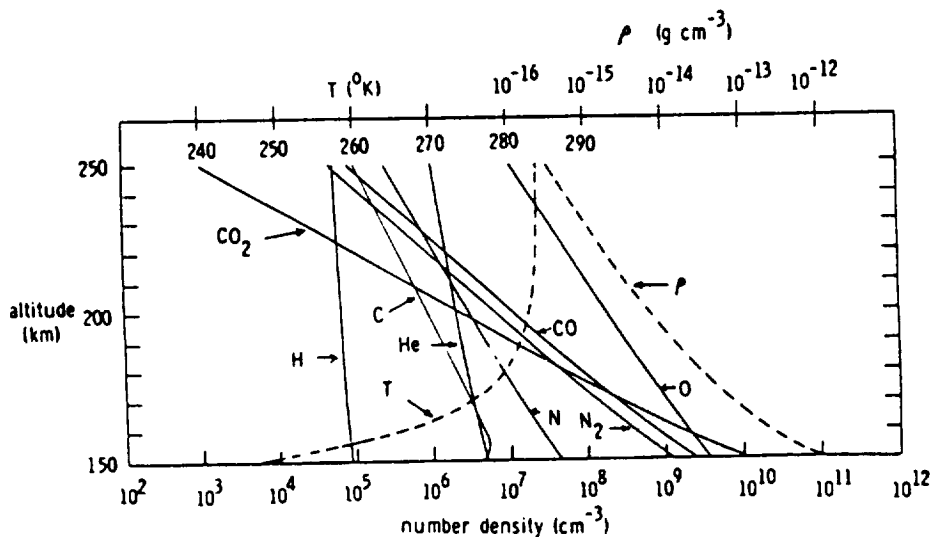
Fig. 6b.
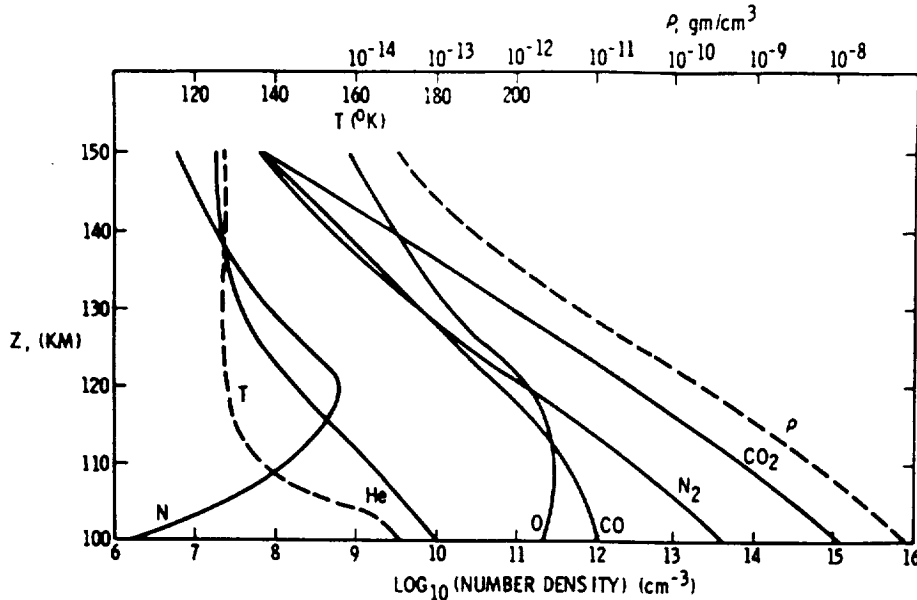
Fig. 6c.
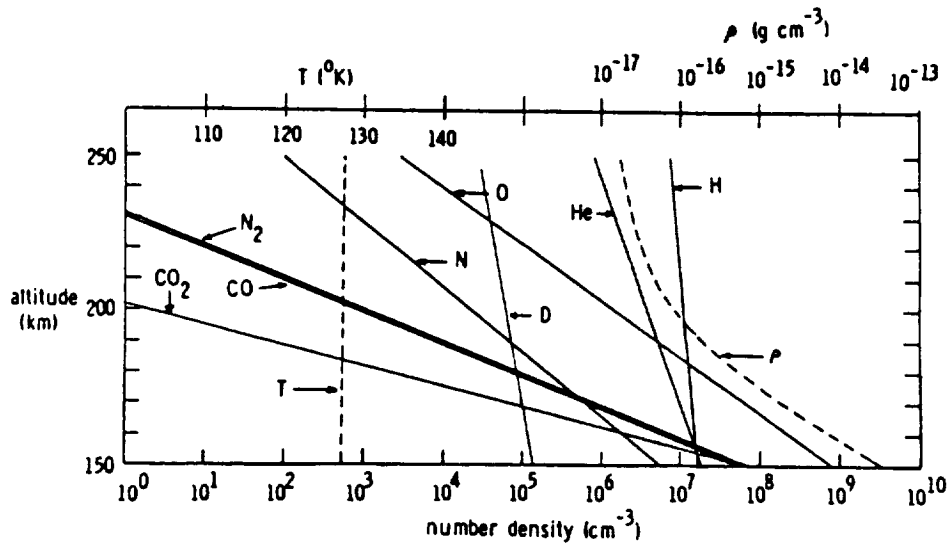
Fig. 6d.

Fig. 6. Neutral number densities as a function of altitude (z) from the VIRA model. (a) Dayside 100 to 150 km. (b) Dayside 150 to 250 km. (c) Nightside 100 to 150 km. (d) Nightside 150 to 250 km. Taken from Keating *et al.* (1985).

different from the factor 1.63 used for all species in the VTS3 model. Normalization factor for CO and N_2 could not be derived and were arbitrarily assumed to be the same as for O.

The VIRA models nominally apply to moderately high solar activity $F_{10.7} = 150$, but Keating et al. (1985) give an empirical expression for the change in the temperature and in the log of the number densities of CO_2, N_2, CO, O, He, and N as a function of $F_{10.7}$ and the 81 day mean value of $F_{10.7}$. The expressions are based on the VTS3 model and on the drag data, but they are simpler than those used in the VTS3 model. The use of the 10.7 cm solar flux as an index of ultraviolet fluxes and thermospheric densities and emissions is widespread, but not firmly grounded. For example, Tobiska et al. (1988) show that upper thermospheric heating in the terrestrial atmosphere is dominated by absorption of chromospheric emissions, whereas $F_{10.7}$ correlates better with transition region and cool coronal emissions.

The VIRA model can be compared to the VTS3 model appropriate to $16°$ N latitude and $F_{10.7} = 150$. The total number densities at noon and 135 km are comparable, but the O and CO mixing ratios are about 5% in the VTS3 model and somewhat larger, about 6% in the VIRA model. The VTS3 model for high solar activity ($F_{10.7} = 200$), however, has larger mixing ratios of about 7% for O and CO at 135 km. Possibly the solar activity variations in the O abundance assumed in the VTS3 model are larger than those implied by the VIRA model, although there have been no in in situ measurements at low solar activity. In the VIRA model, the O density profile exhibits a maximum near 110 km, as the photochemical model of Massie et al. (1983) shows, whereas the O densities continue to increase with decreasing altitude in the VTS3 model. In situ measurements of O are not available below the altitude of minimum periapsis of the PV Orbiter, near 140 km, and the theoretical profiles of O are preferred below 140 km. At midnight, the mixing ratios of O and CO at 135 km are 26 and 8%, respectively, in the VIRA model compared to 17 and 5%, respectively, in the VTS3 model. Both models give N_2 mixing ratios near 100 km of about 4%, but because of different assumptions about the temperatures and eddy diffusion coefficients, at 135 km the noon mixing ratio of N_2 is 7.3% in the VTS3 model and 5.3% in the VIRA model; at midnight, the N_2 mixing ratio is 9.8% in the VTS3 model and 8.6% in the VIRA model.

3. Emission Features

3.1. INTRODUCTION

Atmospheric emission features are usually categorized as dayglow, nightglow, or aurora. Dayglow emissions are produced by the direct interaction of solar radiation or photoelectrons with atmospheric gases, and by prompt chemiluminescent reactions. Nightglow is luminosity produced by chemiluminescent reactions of species that are produced during the day or transported from the dayside. Auroral emissions are usually considered to be those that are produced by impact of particles other than photoelectrons. Although Venus does not have an intrinsic magnetic field, ultraviolet emission features attributed to particle impact have been detected on the nightside of the planet in images from the PV orbiter ultraviolet spectrometer (Phillips et al., 1986; see Section 3.2).

The sources of dayglow emission features include photoionization and excitation

$$X + h\nu \rightarrow X^{+*} + e, \qquad (5)$$

electron impact excitation

$$X + e \rightarrow X^* + e, \qquad (6)$$
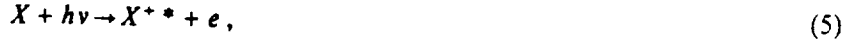
and electron impact ionization and excitation

$$X + e \rightarrow X^{+*} + 2e, \qquad (7)$$

In the foregoing expressions, X is either an atomic or molecular species, and the asterisk (*) represent an excited state of the species that can decay to a lower state with the emission of radiation. In addition, dayglow emission features attributable to fragments or fragment ions of a molecular species AB may be produced by photodissociative excitation

$$AB + h\nu \rightarrow A + B^*, \qquad (8)$$

electron impact dissociative excitation

$$AB + e \rightarrow A + B^*, \qquad (9)$$

photodissociative ionization and excitation

$$AV + h\nu \rightarrow A + B^{+*} + e \qquad (10)$$

and electron impact dissociative ionization and excitation

$$AB + e \rightarrow A + B^{+*} + 2e. \qquad (11)$$

Excited species that may emit to the ground state by a dipole-allowed transition can be produced by resonance scattering of solar photons by an atomic species X

$$X + h\nu \rightarrow X^* \rightarrow X + h\nu \qquad (12)$$

and fluorescent scattering by a molecular species AB

$$AB(v) + h\nu \rightarrow AB^*(v') \rightarrow AB(v'') + h\nu'. \qquad (13)$$
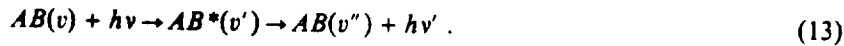
The probability of an atom resonantly scattering a solar photon per unit time is called the g factor, which is related to the oscillator strength f by the expression

$$g = (\pi F)\,\frac{\pi e^2}{mc^2}\,\lambda^2 f, \qquad (14)$$

where πF is the photon flux in units of photons cm^{-2} s^{-1} Å^{-1} and λ is the wavelength. In these units, the constant $\pi e^2/mc^2$ has the value 8.829×10^{-13} cm. For fluorescent scattering in a molecular band system, it is convenient to define an excitation rate $q_{v'}$ that is the probability per unit time of producing the excited state in the vibrational level

v' by absorption of a photon

$$q_{v'} = (\pi F)\lambda^2 \frac{\pi e^2}{mc^2} f_{0, v'} \tag{15a}$$

or

$$q_{v'} = (\pi F) \frac{\omega'}{\omega''} \frac{\lambda^4}{8\pi c} A_{v' 0} , \tag{15b}$$

where ω' and ω'' are the statistical weights of the upper and lower states and $A_{v' 0}$ is the absolute transition probability of the transition from vibrational level v' of the upper state to $v = 0$ of the ground state. The g factor for production of emission in the (v', v'') band is then given by

$$g_{v' v''} = q_{v'} \frac{A_{v' v''}}{\sum_v A_{v' v}} . \tag{16}$$

A pedagogical discussion of atmospheric emissions and their measurement can be found in Barth (1969).

3.2. ATOMIC OXYGEN EMISSIONS

The atomic oxygen emissions at 1304 and 1356 Å arise from the transitions

$$O(^3S^0) \rightarrow O(^3P) + h\nu(1302, 1304, 1306 \text{ Å}) \tag{17}$$

and

$$O(^5S^0) \rightarrow O(^3P) + h\nu(1356, 1358 \text{ Å}) , \tag{18}$$
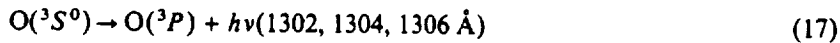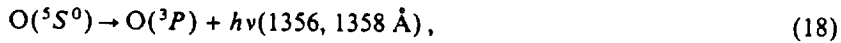
respectively. The $O(^3S^0)$ state is connected to the ground state by a dipole-allowed transition with an oscillator strength of 0.048 (Doering et al., 1985) so resonance scattering of solar radiation is an important source of the emission in the dayglow. Other sources include electron impact excitation of O, and electron-impact and photo-dissociative excitation of CO and CO_2. The sources of the 1356 Å emission are the same, except that, since the transition from the ground state of O to the $^5S^0$ state is spin forbidden, resonance scattering is not important.

Mariner 5 and Venera 4 searched for the 1304 Å resonance triplet of O, under the assumption that photodissociation of CO_2 and diffusive separation should cause O to become the major constituent of the atmosphere at high altitudes. The 1304 Å intensity is a measure of the integrated O density above the altitude of CO_2 absorption, although because the emission is optically thick, a radiative transfer model is necessary to interpret the measured brightness. No emission was initially reported for the Mariner 5 spectrophotometer (Barth et al., 1967) or the Venera 4 instrument (Kurt et al., 1968). Venera 4 observed the atmosphere below 300 km in shadow. Strickland (1973) suggested that the thickness of the airglow layer was not within the resolution of the

Mariner 5 instrument. According to von Zahn *et al.* (1983), the three channels of the Mariner 5 spectrophotometer were allowed to go off scale as they swept across the bright disk of the planet, and the oxygen channels did not recover before the bright limb had been crossed. Several years later, a reanalysis of the Mariner 5 airglow data by Anderson (1975) revealed the presence of the 1304 Å triplet in the region of the terminator with an intensity of 670 R. By scaling to the subsolar point by analogy with terrestrial data, a nadir intensity of 11 kR was inferred and an O mixing ratio of 10% O was derived.

In 1967 Moos *et al.* (1969) detected emission from Venus near 1300 Å using a low-resolution rocket-borne spectrometer. Moos and Rottman (1971) later measured the FUV spectrum (1200–1900 Å) of Venus using a moderate resolution spectrometer and reported preliminary values for the intensities of the O emissions. The psectrum is shown here in Figure 7. Rottman and Moos (1973) refined the analysis and reported
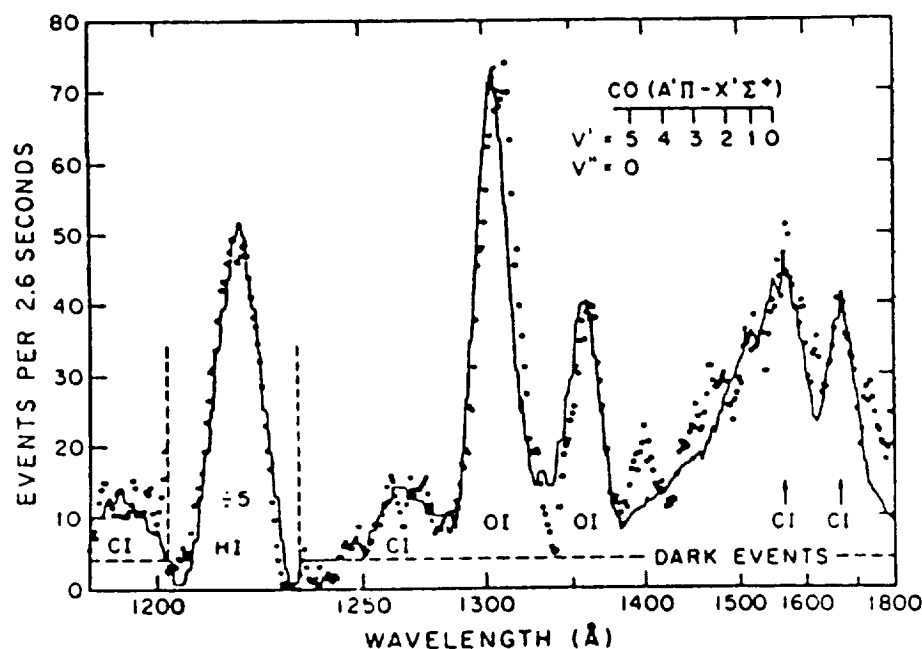
Fig. 7. Rocket spectrum of Venus (points) compared with a best-fit synthetic spectrum. The 'mystery' feature at 1400 Å was identified by Durrance *et al.* (1980) as the (14, 5) CO fourth positive band. From Rottman and Moos (1973).

disk intensities of 5.5 ± 0.5 and 2.7 ± 0.5 kR for the 1304 and 1356 Å emissions, respectively. They estimated a mixing ratio for O of 10% at a CO_2 column density of 4×10^{16} cm^{-2}, the CO_2 column density above the altitude of absorption reported by Strickland *et al.* (1972) for Mars. Their production compares well to values found from Pioneer Venus *in situ* measurements. For example, in the VIRA dayside model, the O/CO_2 ratio is 13% at a column density of 4×10^{16} cm^{-2}. The agreement is, however,

largely fortuitous. The analysis of Rottman and Moos was based on the Venus model of Strickland (1973), except for the cross sections for electron impact excitation of O, which were adopted from Zipf and Stone (1971). These cross sections have recently been shown to be too large, by a factor of about 7 for the 1304 Å emission and a factor of 2 for the 1356 Å emission (Stone and Zipf, 1974; Zipf and Erdman, 1985; Zipf, 1986). Rottman and Moos found electron impact excitation to be the major source of both of the emissions. Strickland (1973) computed intensities for the emissions using a model atmosphere of McElroy (1969) with an exospheric temperature of 700 K. He could not reconcile the 1304 Å intensity for the ratio of 1304 to 1356 Å intensity of about 2 with the model even with several tens of percent O, based on excitation parameters (g values for resonance scattering and 'effective' g values for electron impact excitation) derived from analyses of terrestrial airglow and Mariner 6, 7, and 9 airglow from Mars (Strickland *et al.*, 1972). Strickland's (1973) assumed impact excitation rate for the 1304 Å emission was a factor of 3 to 4 less than that derived from the cross section reported by Zipf and Stone (1971), but only about a factor of 2 larger than the currently accepted value. Strickland suggested, among other possibilities, that another source of emission might be present in the 1356 Å signal. Durrance *et al.* (1981) later showed that the (14, 4) CO fourth positive band contaminates the 1356 Å signal.

The Mariner 10 spectrophotometer also detected strong emission at 1304 Å (Broadfoot *et al.*, 1974); the brightness was 17 kR, about 3 times the Moos and Rottman (1971) rocket values and an order of magnitude larger than the values reported from Mariners 6 and 7 for Mars (Strickland *et al.*, 1972). Although the O abundance was difficult to model accurately, the conclusion that the atmosphere of Venus contained more O than that of Mars was inescapable.

In 1978, the Venera 11 and 12 spectrophotometers measured disk brightness at 1304 Å of 6.4 kR, from which they inferred an atomic oxygen column density of $1.9 \times 10^{12} \text{ cm}^{-2}$. They also concluded that electron impact on O must be an important source of $O(^3S^0)$, since the intensity was not flat across the disk. The importance of electron impact can be evaluated by reference to Table II, where we present computed excitation rates of various excited states of atmospheric species produced in electron-impact processes for a model appropriate to high and low solar activity based on the neutral VTS3 models computed by Fox (unpublished calculations; cf. Fox, 1982). Table III shows the production rates due to photoprocesses for the same models. The integrated electron-impact excitation rate of $O(^3S^0)$ for the high solar activity model is only $3.4 \times 10^8 \text{ cm}^{-2} \text{ s}^{-1}$, but the apparent emission rate will be enhanced by radiative transfer.

Stewart *et al.* (1979) reported the first measurements of the UV airglow from the Pioneer Venus OUVS, including the oxygen emission lines; the noted that the 1356 Å emission was limb brightened and ascribed this effect to the production of energetic $O(^5S^0)$ atoms in dissociative excitation of CO. Cross sections are not available for production of $O(^5S^0)$ in electron impact or photodissociative excitation of CO. Table III shows that electron impact and photodissociative excitation of CO_2 are negligible sources of the 1304 Å emission. In their study of the CO fourth positive band

TABLE II

Integrated column production rates for excited electronic species due to electron impact for model Venus thermospheres based on Pioneer Venus data. The high solar activity (High SA) model is that of Hedin *et al.* (1983) for $F_{10.7} = 200$ and the low solar activity (Low SA) model for $F_{10.7} = 74$. The solar fluxes are the SC No. 21REFW and F79050N spectra of Hinteregger (private communication; see also Torr *et al.*, 1979) for the low and high solar activity models, respectively.

Species	Source	Column production rate $(10^6 \text{ cm}^{-2} \text{ s}^{-1})$	
		High SA	Low SA
$CO(a^3\Pi)$	CO_2	2.1(4)	7.0(3)
	CO	1.1(4)	2.1(3)
$CO(A^1\Pi)$	CO_2	5.5(2)	1.8(2)
	CO	4.0(3)	7.5(2)
$CO_2^+(A^2\Pi_u)$	CO_2	3.7(3)	1.2(3)
$CO_2^+(B^2\Sigma_u^+)$	CO_2	2.2(3)	7.2(2)
$CO^+(A^2\Pi)$	CO	1.1(3)	2.0(2)
$CO^+(B^2\Sigma^+)$	CO	3.5(2)	6.5(1)
$O(^1D)$	O	1.4(4)	2.1(3)
$O(^1S)$	CO_2	6.2(3)	2.1(3)
	O	1.1(3)	1.7(2)
$O(^3S^0)$	CO_2	4.0(1)	1.3(1)
	O	3.0(2)	4.6(1)
	CO	2.0(0)	4.0(-1)
$O(^5S^0)$	CO_2	4.0(1)	1.3(1)
	O	8.8(2)	1.4(2)
$N_2^+(A^2\Pi_u)$	N_2	2.6(2)	7.9(1)
$N_2^+(B^2\Sigma_u^+)$	N_2	8.8(1)	2.7(1)

system, Durrance *et al.* (1981) found that the limb brightening at 1356 Å is the result of contamination of the 1356 Å emission by the (14, 4) CO fourth positive band at 1352 Å.

Meier *et al.* (1983) modeled the atomic oxygen emissions using a Monte-Carlo technique for solution of the radiation transport equations. They found that the incorporation of partial frequency redistribution also enhanced the predicted limb brightening. Their model calculations reproduced the measurements if the O densities from the BNMS model were reduced by about 40%, but their analysis was based on cross sections for electron impact production of emission at 1304 and 1356 Å reported by Stone and Zipf (1974) that were later reduced by a factor of 2.8 (Zipf and Erdman, 1985; Zipf, 1986). A model of the terrestrial dayglow oxygen emissions (Meier *et al.*, 1985) suggested that the Stone and Zipf cross sections should be scaled down by 40%. A reanalysis of the Pioneer Venus data using the renormalized cross sections showed good agreement between the O densities necessary to explain the measured emission and the BNMS model densities (Paxton and Meier, 1986).

Remote sensing can be a reliable method of determining thermospheric densities, as

TABLE III

Column production rates of some excited electronic states of species in the Venus thermosphere due to photodissociative excitation or photoionization and excitation. The models used are as described in Table II.

Species	Source	Column production rate $(10^6 \text{ cm}^{-2} \text{ s}^{-1})$	
		High SA	Low SA
$CO(a^3\Pi)$	CO_2	1.8(4)	7.9(3)
$CO(A^1\Pi)$	CO_2	7.8(2)	3.1(2)
$CO_2^+(A^2\Pi_u)$	CO_2	9.0(3)	3.6(3)
$CO_2^+(B^2\Sigma_u^+)$	CO_2	1.0(4)	4.1(3)
$CO^+(A^2\Pi)$	CO	3.4(3)	7.4(2)
$CO^+(B^2\Sigma^+)$	CO	1.3(3)	2.5(2)
$O(^1D)$	CO_2	1.6(6)	6.5(5)
$O(^1S)$	CO_2	2.1(5)	7.6(4)
$O(^3S^0)$	CO_2	1.2(1)	6.1(0)
$N_2^+(A^2\Pi_u)$	N_2	2.0(3)	7.8(2)
$N_2^+(B^2\Sigma_u^+)$	N_2	4.1(2)	1.5(2)

Meier and Anderson (1983) have suggested, but in practice, the use of 1304 and 1356 Å intensities to infer atomic oxygen densities both in the terrestrial atmosphere and in planetary atmospheres has been plagued by uncertainties. The major sources of error in models are in the electrons impact cross sections and in the solar fluxes, although, if limb scans of an optically thick emission are available, the altitude distribution of the scatterer can be obtained from the shape of the intensity profile independent of the solar flux or the calibration of the instrument (e.g., Anderson et al., 1987). In this case, the solar flux can be derived from the intensity of the emission. The accepted values for the electron impact cross section have changed by nearly a factor of 3 in recent years, although there is now substantial agreement between the excitation cross sections measured using electron energy loss methods (Vaughan and Doering, 1986; Doering and Vaughan, 1986; Gulcicek and Doering, 1988; Doering and Gulcicek, 1989) and the renormalized emission cross sections. There is also a wide range in the values of the solar photon fluxes used in or derived form resonance scattering calculations, even allowing for solar activity variations. Both the rocket flights of Moos and Rottman (1971) and the initial PV OUVS measurements were during period of high solar activity. Strickland (1973) required a photon flux integrated over the multiplet of $5 \times 10^9 \text{ cm}^{-2} \text{ s}^{-1}$, whereas the calculations of Meier et al. (1983) were consistent with a total flux of $1.4 \times 10^{10} \text{ cm}^{-2} \text{ s}^{-1}$. Link et al. (1988) required a 1304 Å irradiance of $7 \times 10^9 \text{ cm}^{-2} \text{ s}^{-1}$ to explain the terrestial dayglow experiments at high solar activity. Experimental measurements of the total photon flux in the 1300 to 1310 Å range, of which the 1304 Å triplet accounts for about 85–90% (Mount and Rottman, 1981), also vary widely. At high solar activity, reported values range from $9.5 \times 10^9 \text{ cm}^{-2} \text{ s}^{-1}$ from the F79050N spectrum of Hinteregger (private communication; see also Torr et al.,

1979) to 1.54×10^{10} from rocket measurements (Mount and Rottman, 1981); at low solar activity from 4.8×10^9 from the SC No. 21REFW spectrum of Hinteregger to $7.1-7.3 \times 10^9$ (Mount and Rottman, 1983, 1985) to $1.21 \times 10^{10} \, cm^{-2} \, s^{-1}$ from the Solar UV Spectral Irradiance Monitor (SUSIM) data (Van Hoosier *et al.*, 1987). There are, however, independent reasons to believe that the Hinteregger fluxes are too low. Ogawa and Judge (1986) used a rocket-borne Ne ionization chamber to measure the integrated solar flux between 50 and 575 Å, with an estimated error of 7.3%. Their results indicate that the Hinteregger fluxes in this wavelength region are low by a factor of 2 at low solar activity and by 30% at high solar activity. Given the uncertainties in the parameters used in modeling the oxygen emissions, densities derived from these measurements should probably not be considered reliable to better than a factor of 2.

Emissions at 1304 and 1356 Å have been detected by the Pioneer Venus OUVS in images of the nightside of Venus. The emissions appear in bright patches that vary in size and intensity; the sheer spatial and temporal variability of the emissions suggests that they are produced by particle impact. The morphology of the aurora has been described by Phillips *et al.* (1986). Figure 8 hows a series of brightness images recorded
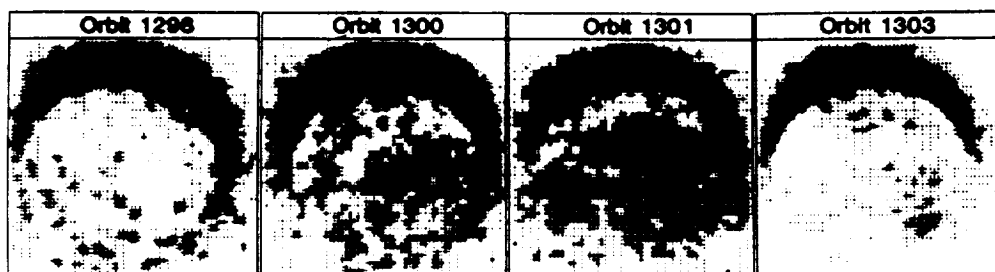
Fig. 8. Series of brightness images from the PV OUVS for the orbital sequence of June 25–July 1, 1982 with apoapsis near midnight. Note expansion and intensification of emissions to fill the nightside in orbit 1301. Missing orbits were not imaged at 1304 Å. From Phillips *et al.* (1986).

by the OUVS for our nearly contiguous orbits. The intensity of the 1304 Å emission is usually about 10 R, but values near 100 R have been recorded; the 1304/1356 ratio is about 6. Fox and Stewart (1990) have presented evidence that the emissions are produced by impact of very soft ($\sim$ a few eV) electrons. More energetic electrons would penetrate too deeply and produce high intensities of the Cameron bands of CO, which are not observed, and ion densities that exceed observed values. Both radiative recombination of O^+ and precipitation of O^+, the sources in the terrestrial equatorial nightglow, are ruled out for Venus because the 1304 and 1356 Å emissions are produced with comparable intensities by these mechanisms and because the predicted intensities due to radiative recombination are less than 10^{-3} R (Julienne *et al.*, 1974; Abreu *et al.*, 1986). In addition, soft electrons have been observed in the Venus wake by both the PV orbiter retarding potential analyzer (ORPA) (e.g., Knudsen and Miller, 1985) and the plasma analyzers on board Veneras 9 and 10 (e.g., Gringauz *et al.*, 1979). Fox and

Stewart have modeled the intensities that would be produced by precipitation of electrons with the same energy spectrum and fluxes as the downward traveling portion of the ORPA spectrum. The total fluxes required were determined to be between 8 and 28% of the ORPA values.

The energies of the electrons producing the aurora are constrained to be low so that they lose their energy in the upper thermosphere where O is the dominant constituent of the atmosphere. If the electrons penetrate down to the part of the atmosphere where CO_2 is the most important constituent (below about 140 km) unobserved emissions, such as the CO Cameron bands, would be observed with large intensities and the O emissions would be excited less efficiently, producing a larger ratio of ionization to excitation for a given 1304 Å intensity. An alternative explanation has been proposed by J. Grebowsky (private communication). He has suggested that the same effect would be realized if the depth of penetration of the electrons were limited by the presence of a horizontal magnetic field in the nightside ionosphere, rather than by their energy.

The excitation of ground state oxygen atoms by electron impact, photodissociation and electron-impact dissociation of CO_2 and CO, and dissociative recombination of O_2^+ can produce O atoms in the ^1S and ^1D states, which can either be quenched or decay by the emission of photons. $O(^1D)$ produces the atomic oxygen 'red line' in the process

$$O(^1D) \to O(^3P) + h\nu(6300 \text{ Å}). \tag{19}$$

Ninety-five percent of $O(^1S)$ decays on $O(^1D)$ producing the atomic oxygen 'green line':

$$O(^1S) \to O(^1D) + h\nu\left(5577 \text{ Å}\right). \tag{20}$$

Only 5% decays to the ground state producing an ultraviolet photon of wavelength 2972 Å

$$O(^1S) \to O(^3P) + h\nu(2972 \text{ Å}). \tag{21}$$

Dayglow intensities of 730 kR, 48 kR, and 2.4 kR were predicted for the 6300, 5577, and 2972 Å emissions, respectively by Fox (1978) and Fox and Dalgarno (1981) in a low solar activity pre-Pioneer Venus model. The major source of both $O(^1D)$ and $O(^1S)$ is photodissociative excitation of CO_2. Since pre-Pioneer Venus models differed from current models mostly in the mixing ratios of O and CO, the intensities should not be highly model-dependent. $O(^1D)$ is strongly quenched by CO_2, so most of the $O(^1D)$ produced does not radiate. The rate coefficient for quenching of $O(^1S)$ by CO_2

$$O(^1S) + CO_2 + O(^1D) + CO_2 \tag{22}$$

is $3.3 \times 10^{-11} \exp(-1320/T) \text{ cm}^3 \text{ s}^{-1}$ (Atkinson and Wedge, 1972) and the quenching altitude, where the lifetime against collisional deactivation is approximately equal to the radiative lifetime, is about 100 km. The altitude profile for production of $O(^1S)$, shown in Figure 9 is characterized by two peaks, the upper one due mainly to absorption of solar photons in the 1100–1140 Å range and the lower peak, near 115 km is due to photodissociation of CO_2 by Lα.

LeCompte *et al.* (1989) have reported intensities of the 2972 Å emission measured by
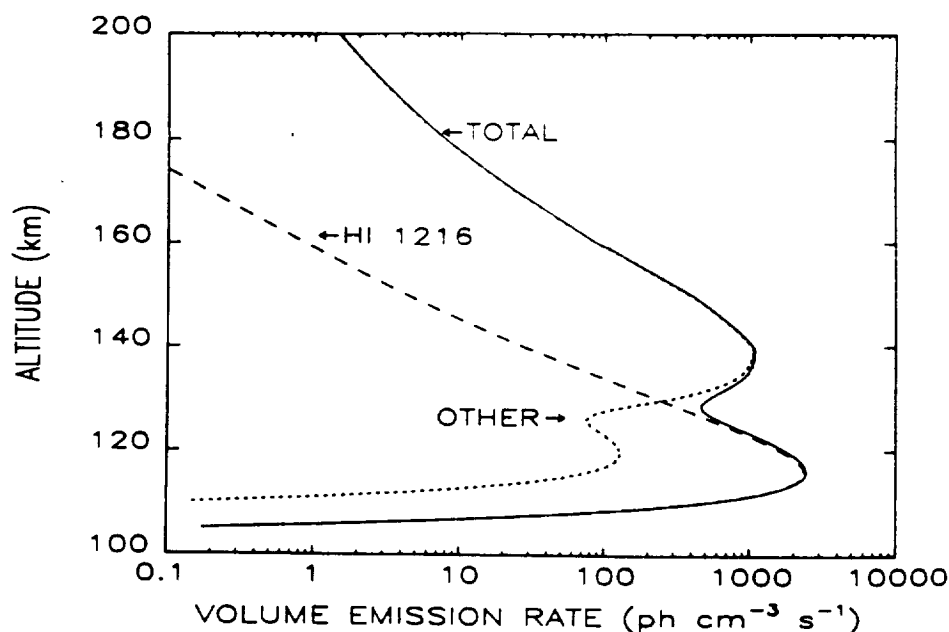
Fig. 9.   Volume production rate of 2972 Å emission from photodissociation of CO_2 by Lα (dashed line), from the rest of the solar spectrum (dotted line) and total (solid line). From LeCompte *et al.* (1989).

the Pioneer Venus OUVS. The zenith intensity reported for orbit 187, for which high solar activity was appropriate, is 7.0 kR, compared to 2.4 kR predicted by the low solar activity model of Fox and Dalgarno (1981). LeCompte *et al.* analyzed limb profiles from two orbits. They showed that photodissociation is the major source of $O(^2S)$ below 175 km. Above that altitude, dissociative recombination of O_2^+ and a contribution from the CI 2967 Å ($^5S \rightarrow {}^3P$) emission dominate the production profile. Fairly good agreement was obtained between the measurements and the model at high altitudes, although the model intensity deviates from the measurements at altitudes below 130 km. They suggested that the difference arises from oscillations in the temperature profile that result from the passage of gravity waves. Gravity waves have been shown that affect terrestrial airglow emissions (e.g., Porter *et al.*, 1974; Taylor *et al.*, 1987). Emission from $O(^1S)$ is sensitive to temperature because the rate coefficient for quenching of $O(^1S)$ by CO_2 (reaction 22) depends exponentially on temperature. Oscillatory structures appear in the temperature profiles inferred from neutral densities measured by several PV instruments, including the BNMS (von Zahn *et al.*, 1980), the ONMS (Kasprzak *et al.*, 1988), and by the accelerometers on the probes (Seiff *et al.*, 1980). The temperature profile that LeCompte *et al.* use for their standard model is the VTS3 model of Hedin *et al.* (1983), which is not based on (ONMS) measurements below 140 km. It has been suggested that the temperatures below 140 km in the VTS3 model are too low (Keating *et al.*, 1985; see also Section 2). LeCompte *et al.* tested a constant (positive) offset in the temperature profile from the VTS3 model, but did not consider a temperature profile in which the deviation increases as altitude decreases. Their assertion that the temperature profile

must return to the VTS3 profile at the lower boundary is not entirely convincing. As they admit, LeCompte *et al.* test deviations of the VTS3 temperature profile without changing the neutral densities in a consistent way. More important, the model intensity profile is normalized to the measurements at low altitudes, where the source of the signal is mostly Rayleight scattering. At 05 km the 2972 Å volume production rate vanishes, so the sensitivity of the model to the quenching coefficient and, hence, to the temperature near that altitude is small.

Visible spectrometers on Venera 9 and 10 searched for emissions on the nightside at 6300 and 5577 Å, but found none. Upper limits have been placed on the intensities of the green and red lines of 10 and 20–25 R, respectively (Krasnopol'sky, 1981, 1986, and private communication, 1988). In the nightglow, the emissions are produced mostly in dissociative recombination of O_2^+. Fox (1990a) has combined a model for the vibrational distribution of O_2^+ on the nightside with rate coefficients computed by Guberman (1987, 1988) for production of $O(^1D)$ and $O(^1S)$ in dissociative recombination of $O_2^+(v)$ from different vibrational levels, v. Altitude profiles of the volume emission rates are shown in Figure 10. The integrated overhead intensities are 1–2 R for the green line and about 46 R for the red line. The intensity of the green line is sensitive to the vibrational distribution of O_2^+, but the yield of $O(^1D)$ and, therefore, the emission rate of the red
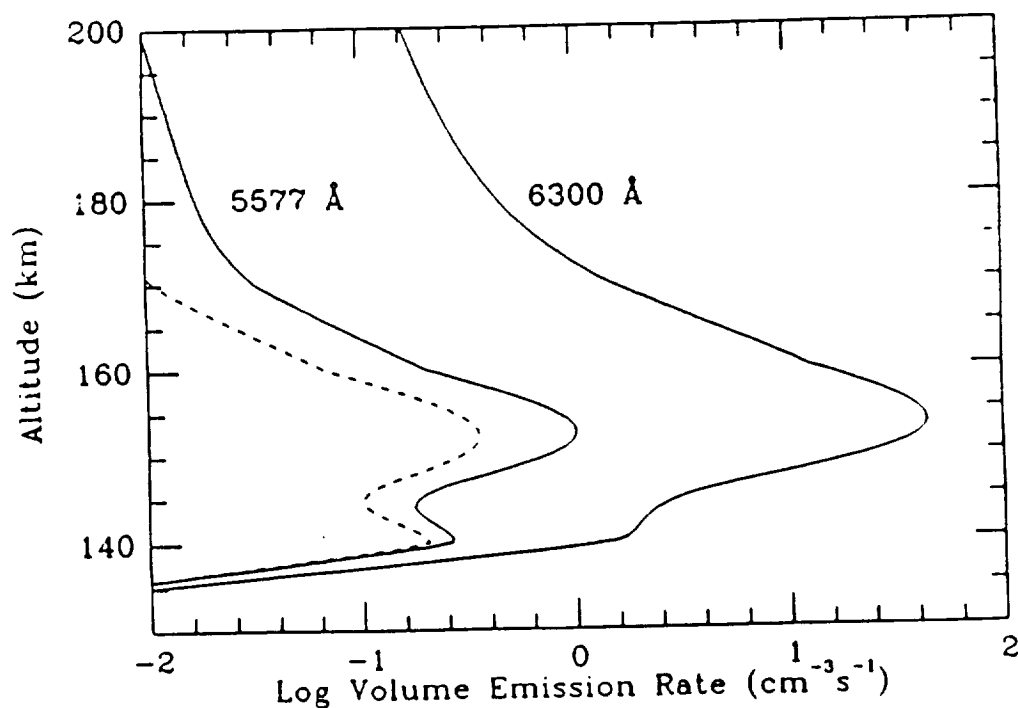

Fig. 10. Altitude profiles of the volume emission rates of the red and green lines of atomic oxygen in the Venus nightglow. Solid lines are computed assuming $k_{43} = 1 \times 10^{-10}$ cm^3 s^{-1}. The dashed line is for $k_{43} = 6 \times 10^{-10}$ cm^3 s^{-1}. From Fox (1990a).

line is less sensitive to the vibrational distribution. The predicted intensity of the red line exceeds the Venera upper limit for the particular model ionosphere chosen. The night-side ionosphere, at least at times of high solar activity, is produced mainly by transport of O^+ from the dayside (Knudsen et al., 1980; Spenner et al., 1981; Cravens et al., 1983), although it has been suggested that at times of low solar activity, electron impact is the most important ion source (Gringauz et al., 1979; Breus et al., 1985; Knudsen, 1988). The nightside ionosphere is highly variable, sometiems disappearing nearly completely (Cravens et al., 1982). The model ionosphere of Fox (1990a) corresponds to undisturbed, relatively 'gull-up' conditions for a moderate downward flux of O^+ of $1 \times 10^8 \, cm^{-2} \, s^{-1}$ and may not be representative of any single measurement.

3.3. O^+ EMISSIONS

$O^+(^2D)$ and $O^+(^2P)$ are metastable states of O^+ that lie 3.32 and 5.02, respectively, above the ground state of O^+. Radiation of $O^+(^2D)$ produces a doublet at 3726 and 3728 Å. $O^+(^2P)$ may radiate to the $O^+(^2D)$ state producing a doublet at 6319 and 7329 Å, or to the ground $O^+(^2S)$ state producing an emission feature at 2470 Å. These states are produced in the atmosphere of Venus mainly in photoionization and electron impact ionization of O. The yields of $O^+(^2D)$ and $O^+(^2P)$ are about 37 and 31%, respectively, in photoionization and 42 and 22%, respectively, n electron impact ionization of O (see Kirby et al., 1979; Burnett and Rountree, 1979). Emission from $O^+(^2D)$ in dipole forbidden and consequently its radiative lifetime is long, about 2.4×10^4 s (Seaton and Osterbrock, 1957). Most of the loss of $O^+(^2D)$ is via chemical reactions and the importance of this species is, therefore, in its effect on the ion chemistry. For example, charge transfer reactions of $O^+(^2D)$ have been shown to be important for the production of N_2^+, CO^+, and N^+ (Fox, 1982).

No measurements of intensities of the emission from $O^+(^2D)$ and $O^+(^2P)$ have been reported. Altitude profiles of the volume emission rates computed for a Pioneer Venus high solar activity model by Fox (1982) are shown Figure 11. The integrated overhead intensities are given here in Table IV.

The O^+ emission triplet at 834 Å arises from the dipole allowed transition $2s2p^4 \, ^4P \to 2s^2p^3 \, ^4S^0$, so resonance scattering of solar radiation by O^+ is a potential

TABLE IV

Integrated overhead intensities (volume production rates integrated over the layer) of emissions arising from metastable states of O^+ and N (adapted from Fox, 1982)

Transition	Wavelength (Å)	Intensity (R)
$O^+(^2P) \to O^+(^2D) + h\nu$	7319, 7329	720
$O^+(^2P) \to O^+(^4S) + h\nu$	2470	200
$O^+(^2D) \to O^+(^4S) + h\nu$	3726, 3728	4.3
$N(^2D) \to N(^4S) + h\nu$	5200	16
$N(^2P) \to N(^2D) + h\nu$	10,400	2.5
$N(^2P) \to N(^4S) + h\nu$	3466	160
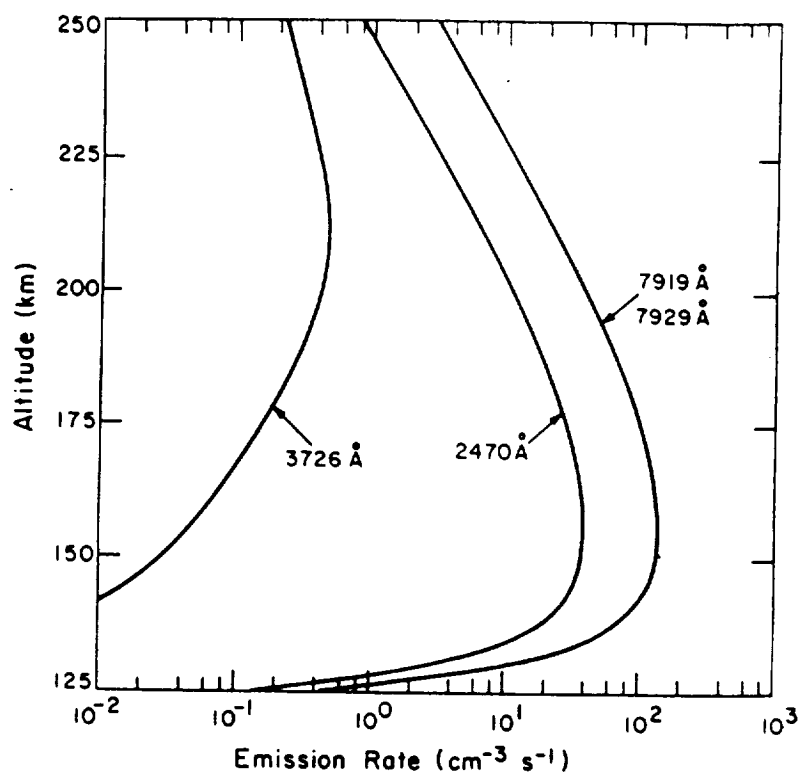
Fig. 11. Volume emissions rates of the transitions $O^+(^2D) \to O^+(^4S)$, $O^+(^2P) \to O^+(^2D)$ and $O^+(^2P) \to O^+(^4S)$ at 3726, 7319–7329, and 2470 Å. From Fox (1982a).

source, as are electron impact and photoionization of $O(^3P)$. The first measurements of the intensity of the O^+ emission line at 834 Å were made by Venera 11 in December 1978. Bertaux et al. (1981) reported a maximum brightness on the disk of 156 R, with fluctuations of less than 20% across the disk. They interpreted their measurements as showing that resonance scattering of solar radiation is not important, as has also been found for the Earth. In the terrestrial ionosphere photionization of O produces a low altitude source that is reonantly scattered by the F2 region O^+ ions at higher altitudes (e.g., Carlson and Judge, 1973; Feldman et al., 1981; Klumar et al., 1983b). Presumably the same is true for Venus also.

3.4. ATOMIC C AND C^+ EMISSIONS

From their low-resolution rocket spectrum of Venus, Moos et al. (1969) reported the existence of a signal longward of 1500 Å that they attributed tentatively to braodband fluorescence with an intensity of 10–100 kR. Marmo and Engleman (1970) proposed that the signal could be explained by the presence of 14 kR of emission in the 1657 Å resonance line of atomic carbon. Although the suggestion was influenced by the erroneous belief that the thermosphere was largely decomposed under the influence of

solar ultraviolet radiation (see Section 3.11), the conclusion was at least partially correct. Rottman and Moos (1973) reported the first positive detection of emission lines of C in the Venus ultraviolet spectrum obtained by their rocket-borne FUV spectrometer (see Figure 7). The reported intensities were 2.4 ± 1.2 kR and 4.0 ± 1.5 kR for the 1561 and 1657 Å emissions, respectively. The Mariner 10 UV spectrohotometer also detected strong emission at 1657 Å, with a measured brightness of 30 kR (Broadfoot et al., 1974). The Venera 11 and 12 EUV spectrophotometers recorded a signal at 1657 Å, but the maximum brightness on the disk (10–15 kR) was close to the background level (Kurt et al., 1979; Bertaux et al., 1981). The resolution of the Venera instrument was insufficient to exclude some emission in the fourth positive bands of CO, but Bertaux et al. (1981) estimated that 85% of the signal could be assigned to the CI line. Spectra recorded by the Pioneer Venus OUVS also showed features at 1561 and 1657 Å and limb profiles have been reported by Paxton (1985). A typical limb profile for the 1657 Å emission is shown in Figure 12.
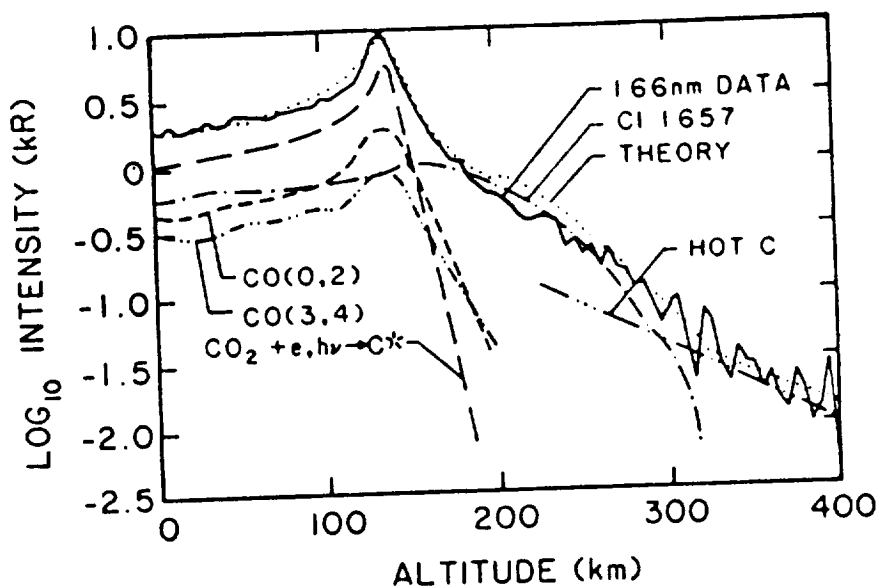
Fig. 12.   Comparison of calculated limb intensity and PV OUVS 1657 Å limb observations. The modeled sources include the resonant scattering of solar photons by atomic carbon, the CO fourth positive bands and electron and photon impact excitation of CO_2. Taken from Paxton (1985).

Possible sources for the CI emission include resonance scattering by atomic carbon, electron impact excitation of atomic carbon and photodissociative- and electron-impact dissociative excitation of CO_2 and CO. Fox and Dalgarno (1981) modeled the intensities due to electron impact dissociative excitation of CO_2 and showed that those sources could not explain the intensities. In order to determine the source due to resonance scattering, densities of C must be known, but because of the production of C from fractionation of CO_2 (Niemann et al., 1980), the densities were below the detection

threshold of the mass spectrometers on Pioneer Venus. McElroy and McConnell (1971) modeled the atomic carbon in the Venus atmosphere, but were unable to explain the large intensities using a model atmosphere with a thermospheric CO mixing ratio equal to the measured abundance above the clouds, 4.5×10^{-5} (Connes *et al.*, 1968). Pioneer Venus *in situ* measurement showed that thermospheric mixing ratios are much larger than those in the mesosphere (see Section 2). The first successful models of the atomic carbon densities based on Pioneer Venus neutral models were constructed by Krasnopol'sky (1982b) and by Fox (1982b). These models showed that the major source of atomic carbon in the Venus thermosphere is photodissociation of CO. The most important sink is reaction with O_2 (McElroy and McConnell, 1971):

$$C + O_2 \rightarrow CO + O, \tag{23}$$

which proceeds with a rate coefficient of $3.3 \times 10^{-11} \, cm^3 \, s^{-1}$ (Braun *et al.*, 1969). There are, however, no measurements of the densities of O_2 in the Venus thermosphere. For treated the O_2 mixing ratio, f_{O_2}, as a free parameter and computed the atomic carbon density profiles shown in Figure 13. The profiles exhibit maximum C densities at 145–155 km of 5×10^6 and 3×10^7 for O_2 mixing ratios of 3×10^{-3} and 1×10^{-4}, respectively. Fox also showed that photoionization of C is the major source of C^+ and used the measured C^+ densities (Taylor *et al.*, 1980) to infer that the mixing ratios of

Fig. 13.   Computed number densities of neutral atomic carbon as a function of altitude for O_2/CO_2 mixing ratio was adopted by the Venus International Reference Atmosphere (Keating *et al.*, 1985). Taken from Fox (1982b).

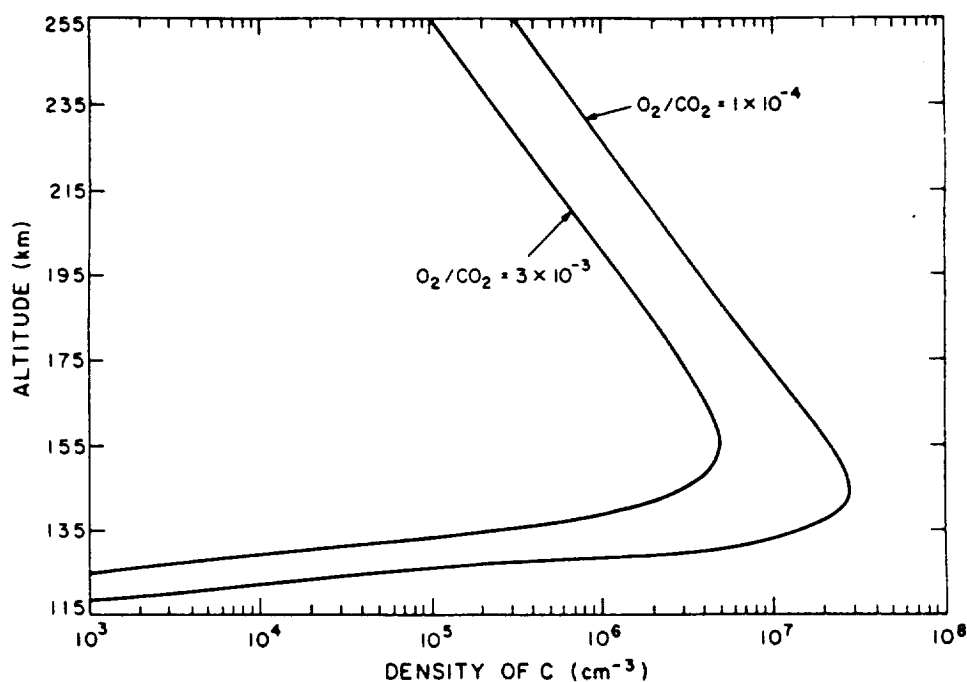O_2 must be closer to the lower value. Krasnopol'sky (1982b) computed C densities using an O_2 mixing ratio of 2×10^{-3}, based on the mesospheric photochemical model of Krasnopol'sky and Parshev (1981) and obtained similar C densities to those in the larger f_{O_2} model of Fox.

Paxton (1985) modeled CI limb intensities at 1657 and 1561 Å made by the PV OUVS, including the contamination of the signal by several CO fourth positive bands. Figure 12 shows a comparison of the measured and computed limb intensities of the 1657 Å emission due to various sources. He reported CO_2 unattenuated photodissociative excitation frequencies of 2×10^{-10} and 4×10^{-10} s^{-1} for the 1561 and 1657 Å lines, respectively; for photodissociation excitation of CO the correspnding unattenuated frequencies were 1.8×10^{-9} and 2.7×10^{-9} s^{-1}. Resonance scattering of solar radiation was found to be the most important source of the emissions. Paxton used a radiation transport model to compute the resonance scatering intensities and to derive the atomic carbon densities. The best fit to the emission rates was obtained for a C density profile similar to the lower density profile of Fox (1982b), for which the O_2/C_2 mixing ratio was 3×10^{-3}. Thus a discrepancy exists between the C profiles derived from the C^+ densities and those derived from the CI airglow. Paxton has suggested that the problem is with the ion chemistry. It is also possible that the rate coefficients on which the atomic carbon models are based are inaccurate. In any case, the CO photodissociation rates computed in the models above were based, in part, on low-resolution photoabsorption cross sections in the wavelength region longward of the ionization threshold at 885 Å measured by Cook et al. (1965). Recent evidence has shown that the absorption in this wavelength regin is due to discrete absorption into predissociating states rather than continuum absorption (Yoshino et al., 1988; Letzelter et al., 1987). Fox and Black (1989) constructed high-resolution photodissociation cross sections for rotational temperatures appropriate to the Venus thermosphere from a line list compiled by van Dishoeck and Black (1988) from information communicated privately to them by Stark, Smith, Yoshino, and Parkinson. They showed that the CO photodissociation rate, and the corresponding C production rate, are reduced by a factor of two over the values obtained using the low-resolution cross sections. This may have important consequences for the chemistry of atomic carbon in the Venus thermosphere that remain for future work to determine.

3.5. CO AND CO$^+$ EMISSIONS

CO was first identified in the atmosphere of Venus from gorund-based infrared observations of the first overtone band at 2.35 μm by Sinton (1963) and by Moroz (1964). Connes et al. (1968) observed several rotational lines in the CO fundamental ($v = 1 \rightarrow 0$) vibration-rotation band and derived a mixing ratio above the cloud tops of 4.5×10^{-5}. Young (1972) applied new information about the line widths to revise that value to 5.5×10^{-5}. In situ measurements were carried out only below the clouds by the PV sounder probe gas chromatograph (LGC), which measured CO mixing ratios of 20–32 ppm from 52 to 22 km (Oayama et al., 1980) and by the gas chromatograph on Venera 12, which measured an abundance of 28 ppm (Gel'man et al., 1979).

The first microwave detection of CO in the Venus atmosphere was that of Kakar *et al.* (1976), who observed the 0.26 cm ($J = 0 \rightarrow 1$) pure rotational transition of CO. Microwave measurements are potentially more sensitive to lower pressures and therefore to higher altitudes than infrared measurements. Kakar *et al.*, as well as Schloerb *et al.* (1980) and Wilson *et al.* (1981) observed a strong diurnal variation in the intensities, and concluded that the CO mixing ratio decreases by a factor of 10 from day to night in the range of total pressure 2–100 mb (about 65–85 km). Clancy and Muhleman (1985a) found that the CO abundance between 80 and 90 km peaks near 08 : 30 local time, but above 95 km, the peak was found to occur near the anti-solar point. The magnitude of the diurnal variation is a factor of 2–4 for both altitude ranges. Between 100 and 105 km, the derived mixing ratios are in the range 4×10^{-4} to 1×10^{-3} at night and 2×10^{-4} to 5×10^{-4} during the daytime.

In situ measurements of thermospheric CO by the PV ONMS and BNMS show that the mixing ratio at 140 km is much larger than the microwave measurements indcate at 90 km (Niemann *et al.*, 1980b; von Zahn *et al.*, 1980; see Section 2). The thermospheric model of Massie *et al.* (1983) predicts larger CO densities at the lower boundary than the measurements of Wilson (1981) or Clancy and Muhleman (1985a) indicate, but given the uncertainties the agreement is adequate. That the model does not show the observed diurnal variation in the CO densities may be the results of its one-dimensional nature. Clancy and Muhleman (1985b) have suggested that the high altitude diurnal variation is a result of the sub-solar to anti-solar circulation, the return flow of which is in the upper mesosphere.

The fourth positive band system of CO is the most intense band system in the 1200 to 1800 Å region of the dayglow spectrum of Venus. It arises from the dipole allowed transition

$$CO(A^1\Pi; v') \rightarrow CO(X^1\Sigma; v'') + h\nu. \tag{24}$$

Potential sources include photodissociative excitation or electron impact dissociation of CO_2:

$$CO_2 + (e, h\nu; E > 13.5 \text{ eV}) \rightarrow CO(A^1\Pi; v') + O + (e,), \tag{25}$$

electron impact excitation of CO:

$$CO(X^1\Sigma; v'') + e(E > 8.02 \text{ eV}) \rightarrow CO(A^1\Pi; , v') + e, \tag{26}$$

dissociative recombination of CO_2^+

$$CO_2^+ + e \rightarrow CO(A^1\Pi; v') + O, \tag{27}$$

and fluorescent scattering by ground state CO,

$$CO(X^1\Sigma; v) + h\nu \rightarrow CO(A^1\Pi; v') \rightarrow CO(X^1\Sigma, v'') + h\nu'. \tag{28}$$
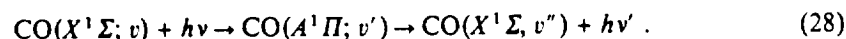
The branching ratio for production of $CO(A^1\Pi)$ in dissociative recombination of CO_2^+ (reaction 27) is about 5% (Gutcheck and Zipf, 1973).

The observed signal longward of 1400 Å in the rocket spectrum reported by Rottman

and Moos (1973) was interpreted as being due to the atomic carbon features and to the CO fourth positive band system. The total intensity of the band system was determined by fitting a synthetic spectrum to the measurement (see Figure 7). Except for an unidentified feature at 1400 Å (later identified by Durrance et al. (1980), see below) a good fit to the measured spectrum was obtained and a brightness of 25 ± 5 kR was reported. The process(es) responsible for the observed emission could not be unequivocably determined, but the source due to fluorescent scattering was judged to dominate the production, and a CO mixing ratio of 10% at a CO_2 column of $4 \times 10^{16} \, cm^{-2}$ was inferred. The PV ONMS later confirmed the implication that the atmosphere of Venus contains larger amounts of CO than the atmosphere of Mars. The VTS3 model for $F_{10.7} = 200$ and 12:00 hr local time exhibits a CO mixing ratio of 12% at 137.5 km, the altitude at which the CO_2 column density is about $4 \times 10^{16} \, cm^{-2}$.

The Mariner 10 EUV spectrophotometer recorded a brightness at 1480 Å of 55 kR that was attributed to emission in the CO fourth positive bands (Broadfoot et al., 1974). The spectrophotometers on Venera 11 and 12 also recorded the intensity at 1500 Å (see Table I). Significantly smaller disk brightnesses of 2.1 and 2.7 kR for Venera 11 and 12, respectively, were reported (Bertaux et al., 1981). The disagreement with the Mariner 10 data was attributed by Bertaux et al. (1981) to contamination of the airglow signal by Rayleigh scattering.

Durrance et al. (1980) presented observations of the Venus dayglow from 1250 to 1430 Å made by the PV OUVS and Durrance et al. (1981) measured the Venus dayglow spectrum from 1280 to 1380 Å at high (0.4 Å) resolution with the International Ultraviolet Explorer (IUE) satellite. The strongest features in this region of the spectrum, other than the atomic oxygen emission at 1304 and 1356 Å, were shown to be due to the $(14, v'')$ progression of the fourth positive band system excited by fluorescent scattering of solar Lα. As ponted out by Kassal (1976), this source is larger than fluorescent scattering in all the rest of the fourth positive bands for CO column densities larger than $1 \times 10^{17} \, cm^{-2}$. The overlap of the rotational lines of the $(14, 0)$ fourth positive band with the solar Lα line are shown in Figure 14. The unidentified feature at 1400 Å in the rocket spectrum of Rottman and Moos (1973) (see Figure 7) was identified by Durrance et al. (1980) as the $(14, 5)$ fourth positive band.

The CO_2 absorption cross section is about $8 \times 10^{-20} \, cm^2$ at 1216 Å (Nakata et al., 1965); consequently solar Lα penetrates to a column density of about 1.25×10^{19}, or to about 110 km. The CO_2 cross sections in the region of the CO emissions, 1250 to 1400 Å, are in the range $2-9 \times 10^{-19} \, cm^2$, so the emission bands will be absorbed if they are produced below about 120 km. Because the $(14, 5)$ bands at 1400 Å is unblended and produced almost entirely by fluorescent scattering, measurement of the intensity of this feature could provide a valuable remote sensing technique for determining CO abundances in the Venus thermosphere (Durrance et al., 1980).

Durrance (1981) presented spectra with a resolution of 4 Å recorded by a sounding rocket telescope and spectrometer and constructed synthetic spectra using high-resolution solar fluxes. He showed that the $(14, 3)$ and $(14, 4)$ bands contaminate the O emission features at 1304 and 1356 Å; potentially 67% of the 1356 Å feature was
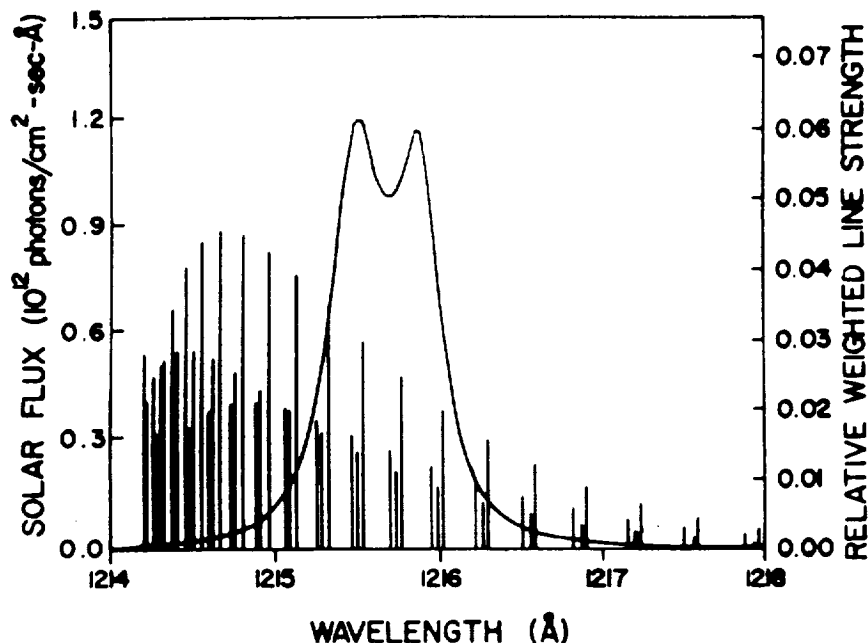
Fig. 14. The rotational lines of the (14, 0) CO⁺ fourth positive band showing the overlap with the solar Lα line. Taken from Durrance *et al.* (1980).

estimated as arising from CO, thus bringing the ratio of 1304/1356 Å intensities to about 8, in agreement with the terrestrial value. Fox and Dalgarno (1981) presented altitude profiles of the sources of the CO fourth positive band system from a pre-Pioneer Venus model shown here as Figure 15. Ninety percent of the observed intensity of the band system is due to fluorescent scattering, with the other four sources about equally to the observed intensity. The computed integrated overhead volume emission rate is about 20 kR.

The Cameron band system of CO appears in the 1800 to 2600 Å region of the spectrum. It arises from the dipole forbidden transition

$$CO(a^3\Pi; v') \rightarrow CO(X^1\Sigma; v'') + h\nu.$$ (29)

The $CO(a^3\Pi)$ state is metastable with a relatively short lifetime of about 8 ms (Johnson, 1972; Lawrence, 1971). The potential sources are the same as those for the fourth positive band system, except for fluorescent scattering. The Cameron band system is the brightest feature in the Martian ultraviolet airglow measured by the UV spectrometers on Mariners 6, 7, and 9 (e.g., Stewart *et al.*, 1972; Barth *et al.*, 1971). The PV OUVS longer wavelength channel measured spectra in the region of the Cameron bands, but no observations or analyses have been reported. Table V gives intensities predicted by a pre-Pioneer Venus model of Fox and Dalgarno (1981) and unpublished calculations for a model based on Pioneer Venus data. The source due to dissociative recombination
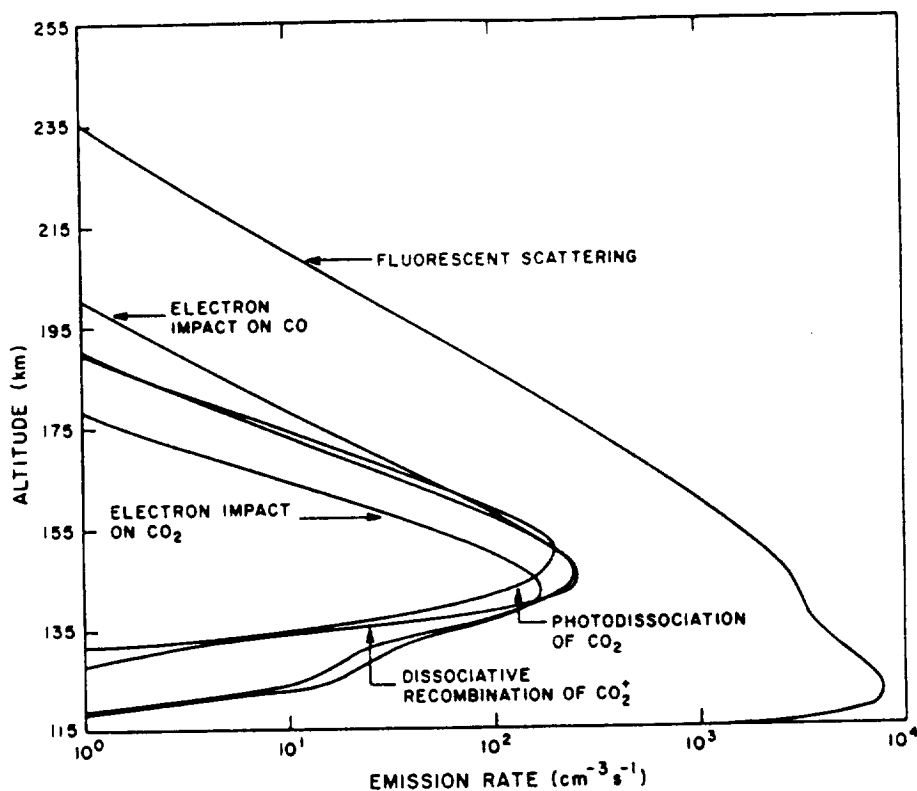
Fig. 15. Altitude profiles of the sources of the CO fourth positive band system. Fluorescent scattering of $L\alpha$ in the $v' = 14$ progression is responsible for 90% of the intensity. The shoulder above the peak in the fluorescent scattering source is due to absorption of shorter wavelength photons. Taken from Fox and Dalgarno (1981).

TABLE V

Computed Cameron band overhead integrated intensities due to different sources for high solar activity (high SA) and low solar activity (low SA) models

Source	Intensities (kR)	
	Low SA[a]	High SA[b]
$CO_2 + h\nu$	6.7	20.8
$e + CO_2$	6.7	20.9
$e + CO$	1.3	11.1
$CO_2^+ + e$	5.1	4.5
Total	20	57

[a] From Fox and Dalgarno (1981) (pre-Pioneer Venus model).
[b] Pioneer Venus model, based on neutral densities from Hedin et al. (1983) (cf. Fox, 1982, 1985).

of CO_2^+ is overestimated in the pre-Pioneer Venus model because the atomic oxygen densities were too low and consequently, the densities of CO_2^+ are too large.

The source due to electron impact excitation of CO_2 is uncertain, because the normalization of the cross section is a matter of some controversy. Excitation functions have been measured by several workers but reported values for the maximum value of the cross section range from 3×10^{-17} to 3×10^{-16} cm^2 (Freund, 1971; Ajello, 1971; Wells et al., 1972; Erdman and Zipf, 1983). Conway (1981) constructed a synthetic spectrum of the Martian dayglow from 1800 to 2800 Å, and by comparing the model and measured intensities, found that a cross section with a maximum value of 7×10^{-17} cm^2 was consistent with the data. Taking into account new information about the lifetime of the $CO(a^3\Pi)$ state, Erdman and Zipf (1983), however, reported that laboratory data indicated a maximum value of the cross section closer to 2.4×10^{-16} cm^2, more than three times the Conway value. The electron-impact excitation rates in Tables II aand V are based on the cross sections of Conway. Analysis of the Pioneer Venus Cameron band data, if they are obtainable, might contribute to a resolution of this issue.

The CO$^+$ comet tail and first negative bands arise from the transitions: $A^2\Pi \rightarrow X^2\Sigma^+$ and $B^2\Sigma \rightarrow X^2\Sigma^+$, respectively. The thresholds for production of the A and B states are 2.53 and 5.65 eV, respectively (Herzberg, 1950). Therefore, the comet tail bands appear in the visible spectrum and the first negative bands in the ultraviolet. Potential production mechanisms include photoionization and electron impact ionization of CO, photodissociative and electron impact dissociative ionization of CO_2, and fluorescent scattering of solar radiation by ground state CO$^+$. No emissions have been observed that are attributable to either band system. Paxton (1988) has proposed that observations of these band systems by instruments on future spacecraft could help to determine the fraction of the mass-28 ion densities (which were measured by the PV OIMS (e.g., Taylor et al., 1980)) that is due to CO$^+$, rather than to N_2^+. He has predicted a nadir intensity of the (0, 0) first negative band at 2191 Å of 615 R; for the (3, 0) comet tail band at 4011 Å, the predicted nadir intensity is 45 kR. Tables II and III show that for high solar activity the predicted integrated overhead intensities due to photoionization and electron impact ionization of CO alone are 4.5 kR and 1.6 kR for the comet tail and first negative band systems, respectively.

3.6. CO_2^+ EMISSIONS

The Fox–Duffendack–Barker ($A^2\Pi_u \rightarrow X^2\Pi_g$) band system consists of several narrow bands between 2800 and 5000 Å. The ultraviolet doublet at 2883 and 2896 Å is produced by the (0, 0, 0)–(0, 0, 0) transition between the $B^2\Sigma_u^+$ state and the $X^2\Pi_g$ ground state. Both band systems are produced by photoionization and electron impact ionization of CO_2 and by fluorescent scattering of sunlight. They appear as prominent emissions in the Mariner 6, 7, and 9 UV spectra of Mars (Barth et al., 1971, 1972) and should be present in Venus spectra as well. No intensities have, however, been reported from the Pioneer Venus OUVS.

Intensities of both CO_2^+ band systems were predicted by Dalgarno and Degges

(1971). They computed g values for fluorescent scattering at Venus of 4.9×10^{-2} and 5.2×10^{-3} for the $A \rightarrow X$ and $B \rightarrow X$ band systems, respectively. The total sub-solar zenith intensities were 107 kR and 31 kR, with 87 and 9 kR from fluorescent scattering for the Fox–Duffendack–Barker band system and the ultraviolet doublet, respectively. The contribution from fluorescent scattering was overestimated because at that time CO_2^+ was assumed to be the major ion.

The low solar activity model of Fox and Dalgarno (1981) predicted a total intensity of 15 kR for the Fox–Duffendack–Barker band system and 9.2 kR for the ultraviolet doublet. The most important source of both emissions is photoionization of CO_2. The branching ratios in photoionization are uncertain, since photoelectron spectroscopy and fluorescence measurements imply different values (Samson and Gardner, 1973; Wauchop and Broida, 1972; Lee and Judge, 1972; Leach et al., 1978a). It has been suggested that a mixing of the A and B states occurs before emission, so that about 50% of the ionization into the B state leads to emission in the A state (Samson and Gardner, 1973; Leach et al., 1978b). The predicted intensities based on the fluorescence branching ratios are 19 kR for the Fox–Duffendack–Barker bands and 5.4 kR for the ultraviolet doublet. Revised calculations based on a Pioneer Venus model for high solar activity are shown in Table VI. The integrated overhead intensity of the Fox–Duffendack–

TABLE VI

Computed integrated volume emission rates of CO_2^+ features in the Venus dayglow for a model (high solar activity) based on Pioneer Venus data

Source	Intensity (kR)	
	$A^2\Pi_u \rightarrow X^2\Pi_g$	$B^2\Sigma_u^+ \rightarrow X^2\Pi_g$
Photoionization of CO_2	9.0 (14.1[a])	10.2 (5.1[a])
Electron impact ionization of CO_2	3.7	2.2
Fluorescent scattering	4.7	0.25
Total	17.4 (23[a])	12.6 (7.5[a])

[a] Computed assuming a 50% crossover of B to A before radiating.

Barker band system is 17.4 kR, with 12.7 kR from electron impact ionization and photoionizeation and 4.7 kR from fluorescent scattering. For the ultraviolet doublet the predicted intensity from photoionization and electron impact ionization is 12.4 kR and that from fluorescent scattering is negligible, only 0.25 kR, for a total integrated overhead intensity of 12.6 kR. If a 50% crossover from B to A occurs before radiating, the total intensities of the $B \rightarrow X$ and $A \rightarrow X$ band systems would be 7.5 and 23 kR, respectively.

3.7. He AND He⁺ EMISSIONS

The He abundance in the lower atmosphere has not been measured directly. The large probe mass spectrometer (LNMS) had the capability of measuring He densities, but the

mixing ratio indicated (f_{He}) by the LNMS data, about 450 ppm, was considered
unreliable because of contamination by the $He-N_2$ mixture used to fill the probe to
detect leaks (Hoffman et al., 1980a; Donahue and Pollack, 1983). Thus bulk atmosphere
mixing ratios have been obtained only by extrapolation from upper atmospheric values
obtained from measurements by the PV BNMS and ONMS instruments and from
airglow analyses. Because the mass of He is much less than the average molecular
weight, this procedure is extremely sensitive to assumptions about the profiles of eddy
diffusion coefficients and temperatures. The eddy diffusion coefficients presented by
von Zahn et al. (1980) were based on a fit to the He profile measured by the BNMS
above 130 km (see Section 2). The He homopause was lcoated at 130 km, the lower
boundary of the measurements. The morningside model gives a value for f_{He} at this
altitude of about 50 ppm. An extrapolation to 100 km yields a mixing ratio of about
12 ppm. The VTS3 model is based on largely ONMS measurements, but the He profile
below 130 km is based on BNMS values. Nonetheless, Hedin et al. (1983) found the
altitude of the He homopause to be lower, about 125 km, and the lower atmosphere
mixing ratio to be correspondingly lower; values of 1–2 ppm are obtained at the lower
boundaries of the noon and midnight models. Massie et al. (1983) tested the sensitivity
of their model to the value of the coefficient A in the numerator of the von Zahn et al.
(1980) expression for the eddy diffusion coefficient (Equation (1)); they found that
changing the value from 0.8 to 2.0 changed f_{He} for the lower atmosphere from 2 to
9 ppm. For the value $A = 1.4 \times 10^{13}$ preferred by von Zahn et al., they derived a helium
mixing ratio of 5 ppm.

Thermospheric He densities above 140 km given by the VTS3, BNMS, and VIRA
models are, however, in fairly good agreement. He densities at 150 km for solar zenith
angles less than about 60° are $4-5 \times 10^6$ cm^{-3}. ONMS data show a strong diurnal
variation in the He densities that is out of phase with the heavier constituents, with larger
densities at night than during the day and a distinct bulge in the He densities in the dawn
sector (Hedin et al., 1983). Figure 16 shows the densities of species included in the VTS3
model at 100 and 150 km as a function of hour angle. The VIRA model for 04 : 00 hr
local time shows a density at 150 km of 1.2×10^8 cm^{-3}; closer to midnight the density
is less, about 7×10^7 cm^{-3}.

He resonance radiation at 584 Å was detected by the both the Mariner 10 and
Venera 11 and 12 spectrophotometers (Broadfoot et al., 1974; Bertaux et al., 1981). A
maximum limb intensity of 600 R was measured by Mariner 10. The Mariner 10 bright
limb profile from 200 to 800 km was analyzed by Kumar and Broadfoot (1975). They
used a radiative transfer model that assumed spperical-symmetry and complete
frequency redistribution to fit the shape of the limb profile. The exospheric temperature
and the g factor were taken to be free parameters. The 'best fit' exospheric temperature
was 375 ± 105 K. Takacz et al. (1980) claim that a reanalysis of the data suggests that
a temperature of 270 K is a better fit to the data. A look at Figure 17, taken from Kumar
and Broadfoot (1975), does seem to suggest, with the full benefit of hindsight, that a
lower exospheric temperature would be an equally good fit. The line center solar flux
derived from the best fit g factor was 2×10^{10} cm^{-2} s^{-1} Å^{-1} at 1 AU. A He density
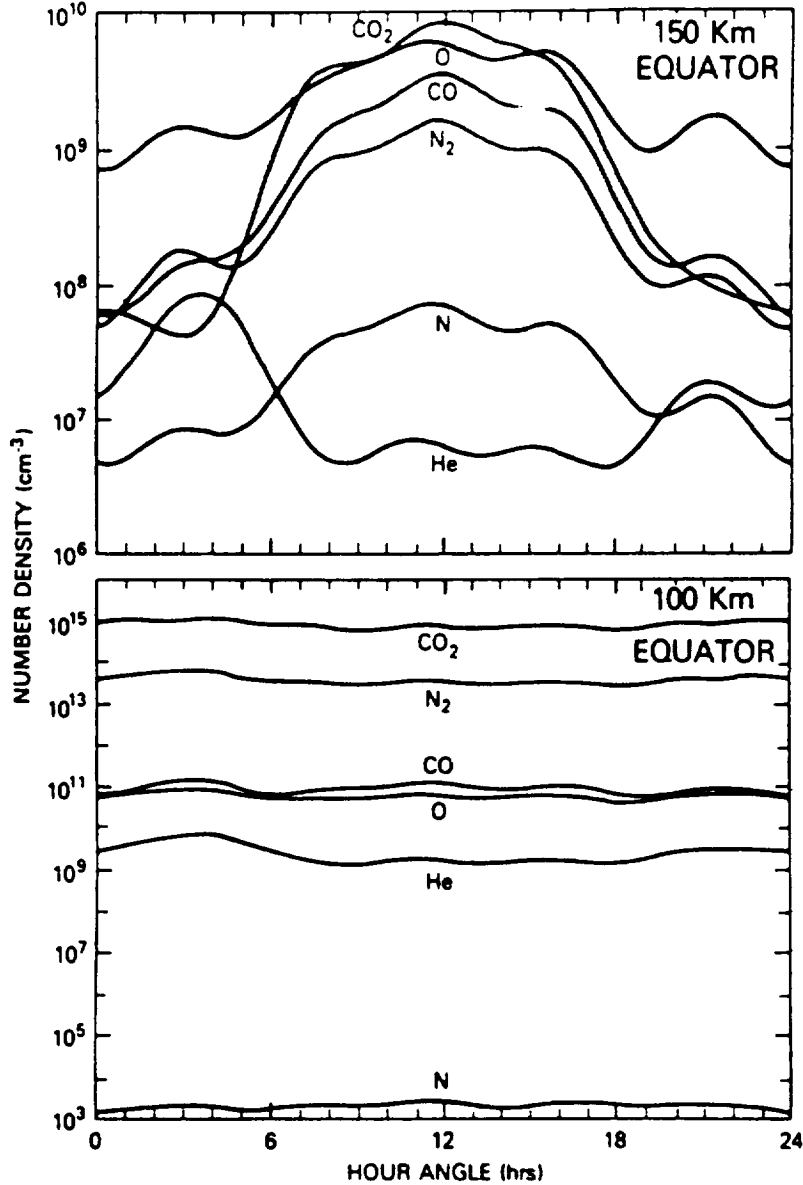
Fig. 16. Neutral number densities as a function of local time at 100 and 150 km, 0° latitude from the VTS3 model. Note that the daytime/nighttime ratio increases with increasing mass of the species. For helium (and hydrogen) the densities are larger on the nightside and peak in the predawn sector, forming the 'helium (or hydrogen) bulge'. Taken from Hedin *et al.* (1983).

of 2×10^6 cm^{-3} was derived at the assumed homopause (145 km), where the density of CO_2 was assumed to be 2×10^{11} cm^{-3}. Von Zahn *et al.* (1983) comment that if the lower (and more accurate, according to our present knowledge) temperature is assumed, the He abundance is almost exactly that determined by PV. We find that the column
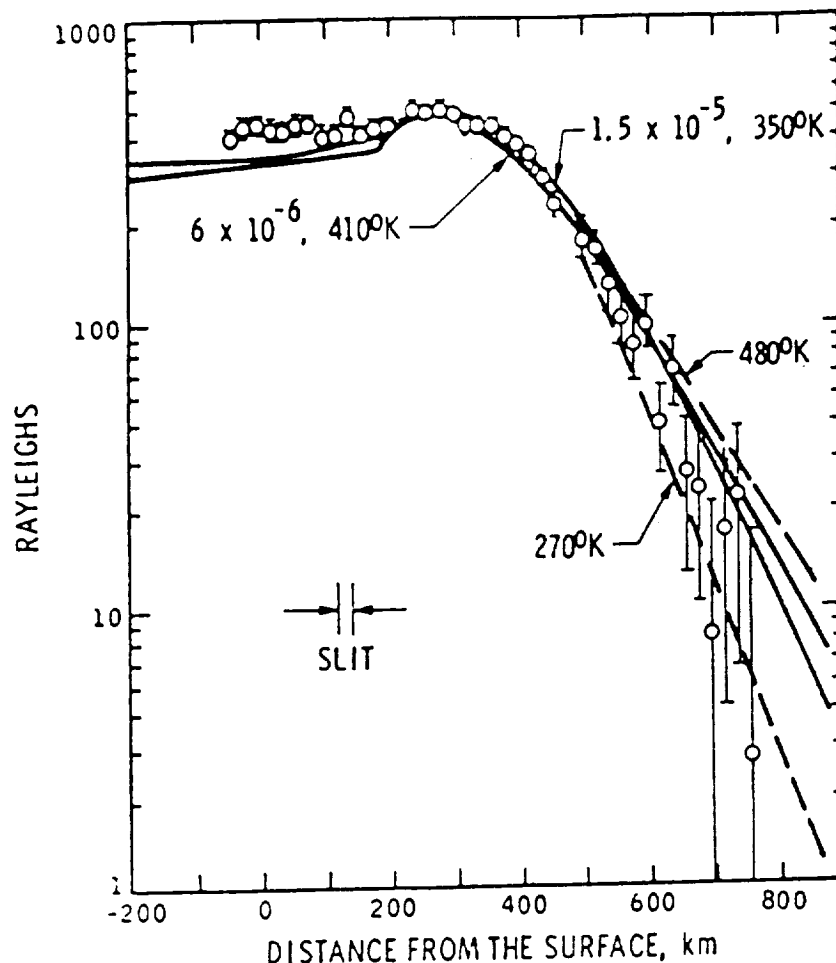
Fig. 17. Mariner 10 584 Å brightness as a function of distance from the limb. The points were derived by subtracting the background noise level. The dashed lines represent altitude variations based on a single scattering model. The solid lines are the result of radiative transfer calculations including multiple scattering. The calculations are normalized to the peak observed brightness. From Kumar and Broadfoot (1975).

density above 145 km, the presumed CO_2 absorption altitude, deduced from the Mariner 10 measurements is about 2×10^{13} cm^{-2}, whereas the coresponding value for the BNMS model is about 2.9×10^{13} cm^{-2}. Because the exospheric temperature is lower than Kumar and Broadfoot assumed, the CO_2 absorption altitude is, however, lower in Pioneer Venus models. The CO_2 absorption cross section at 584 Å is about 2.3×10^{-17} cm^{-2}, so the absorption altitude is about 140 km in the VIRA dayside model and 136 km in the BNMS model. The He column density above 136 km in the BNMS model is about 3.7×10^{13} cm^{-2}.

The He 584 Å disk brightnesses measured by Venera 11 and 12 were presented by Bertaux *et al.* (1981). The maximum intensity on the disk was 270–280 R. Several

analyses of the Venera data have appeared. Kurt *et al.* (1983) modeled the intensity across the disk, using the He optical depth as a free parameter. The best fit He optical depth, in the range 2–4, is independent of the solar flux and the instrument calibration. The derived He column density above the CO_2 absorption altitude, taken to be 140 km, is about $1.9-2.1 \times 10^{13}$ cm^{-3}, almost a factor of two less than the value from the Pioneer Venus models. Bertaux *et al.* (1985) presented a summary of similar results; a helium optical depth of 2.5, corresponding to a density of 1.6×10^6 cm^{-3} at 150 km, was required to fit the intensity profile across the disk. The implied column density is smaller than the PV value. Chassefiere *et al.* (1986) revised the required optical depth to 3.5 ± 1.5, for a number density at 150 km of 2.2×10^6 cm^{-2}. They suggest that the discrepancy with the Mariner 10 data may be due to poor absolute claibration of the Mariner instrument. Krasnopol'sky (1983a) has suggested that the Mariner 10 instrument had a more serious problem with stray light than the Venera instruments had. Although the hydrogen densities derived from Mariner 5 and 10 Lx data are a factor of 2 larger than the values derived from PV OUVS data (Paxton *et al.*, 1985, 1988) and from the *in situ* PV OIMS H$^+$ densities (Brinton *et al.*, 1980), Paxton *et al.* (1985) showed that the fault lay with the use of an isothermal spherically-symmetric radiative transport scheme. They also suggested that fly-by observations do not provide enough constraints to determine the distribution of scatterers. This may be the case for the He 584 Å data also. Indeed, given the large solar zenith angle variation of He densities, especially the existence of the pre-dawn bulge, one would expect a spherically-symmetric radiative transfer model, as all of the above models are including that of Kumar and Broadfoot (1975), to be a poor approximation. Furthermore, the analysis of Kurt *et al.* (1983) is isothermal and assumes a temperature in the scattering region of 300–400 K, whereas the dayside temperature varies from about 200 K near 140 km to about 275 above 180 km.

The solar fluxes at the 584 Å line center that are assumed or derived are different even for similar solar activities, illustrating the inadequacy of the analyses and/or a calibration problem with the instruments. Bertaux *et al.* (1981) determined a value from the Hinteregger 79050N solar fluxes, although there is some evidence that the Hinteregger fluxes are too low, by up to a factor of 30% at high solar activity (Ogawa and Judge, 1986; see Section 3.3). If so, the problem would be exacerbated, because a larger solar flux implies smaller He densities. Furthermore, Hinteregger presents the photon fluxes in the lines as integrated values and it is necessary to assume a lineshape to derive the line center fluxes; Bertaux *et al.* (1981) state merely that an appropriate line shape was assumed, but give no details. Doschek *et al.* (1974) found the shape of the 584 Å line to be approximately Gaussian with a slightly flattened core. Ogawa *et al.* (1984) report a value for the full width at half maximum of about 0.1 Å from a rocket measurement, in good agreement with previously measured values. For a Gaussian shape with a width of 0.1 Å, the line center solar flux implied by the Hinteregger integrated flux would be about 4.9×10^{10} cm^{-2} s^{-1} Å^{-1}. Other analyses fit the shape of the intensity profile and derive a value for the solar flux at line center that reflects the uncertain calibration of the instrument. Kurt *et al.* (1983) derive a value of 3.3×10^{10} cm^{-2} s^{-1} Å^{-1}, which

they state (incorrectly) agrees with the fluxes reported by Hinteregger. Bertaux *et al.* (1985) give a line center photon flux of $8.6 \times 10^9 \, cm^{-2} \, s^{-1} \, Å^{-1}$ for the best fit of the BNMS model to their disk data, and report that a column density about a third of the BNMS data gives a better fit to the shape of the intensity data. The value required by Kumar and Broadfoot (1975), at a time of lower solar activity, was $2 \times 10^{10} \, m^{-2} \, s^{-1} \, Å^{-1}$. The solar activity variation determined frm the (high solar activity) F79050N and the (low solar activity) SC No. 21REFW solar spectra of Hinteregger is a factor of about 3, although if the Hinteregger fluxes are low by a factor of 2 at low solar activity and by 30% at high solar activity (Ogawa and Judge, 1986), the solar activity variation is reduced to a factor of 2.

The He^+ line at 304 Å was not detected by Mariner 10, although one of the channels was designed to detect emissions at that wavelength. It was, however, measured by Venera 11 and 12, due to the greater sensitivity of the spectrophotometer. Bertaux *et al.* (1981) computed a column density of He^+ of $2 \times 10^{11} \, cm^{-2}$, which is larger by an order of magnitude than the column density of about $2 \times 10^{10} \, cm^{-2}$ implied by the PV OIMS measurements.

3.8. N_2 AND N_2^+ EMISSIONS

No emission arising from the band systems of N_2 has been detected in the Venus dayglow, even thought N_2 comprises 3–4% of the atmosphere. The intensities of the most important bands of the major band systems, including the Vegard–Kaplan $(A^3\Sigma_u^+ \rightarrow X^1\Sigma_g^+)$, the first positive $(B^3\Pi_g \rightarrow A^3\Sigma_u^+)$, the reverse first positive $(A^3\Sigma_u^+ \rightarrow B^3\Pi_g)$, the $W^3\Delta_u \rightarrow B^3\Pi_g$, the second positive $(C^3\Pi_u \rightarrow B^3\Pi_g)$, and the Lyman–Birge–Hopfield $(a^1\Pi_g \rightarrow X^1\Sigma_g^+)$ band systems were predicted by Fox and Dalgarno (1981). These bands, the upper states of which are connected to the ground state by dipole forbidden transitions, are produced only by photoelectron impact excitation of ground state N_2 in the dayglows of the terrestrial planets. The Vegard–Kaplan, second positive and Lyman–Birge–Hopfield bands emit in the ultraviolet. The (1, 9) Vegard–Kaplan band at 3199 Å, which falls between the (2, 0) and (3, 0) bands of the Fox–Duffendack–Barker band system, and which may have been observed in the Martian dayglow spectrum (Fox and Dalgarno, 1979), was predicted to have an intensity of 77 R and should be detectable. The (3, 0) Lyman–Birge–Hopfield band at 1354 Å may contaminate the signal at the O 1356 Å feature; the predicted intensity at 1354 Å was 25 R for low solar activity model of Fox and Dalgarno (1981). Calculations based on the O 1356 Å emission cross sections of Stone and Zipf (1974) indicated that the 1354 Å intensity would contribute little to the observed 1356 Å signal. Revised calculations, using the renormalized 1356 Å electron impact emission cross sections of Zipf and Erdman (1985) give a lower integrated intenseity for the 1356 Å emission of about 150 R at low solar activity (see Table II). Hence, the (3, 0) Lyman–Birge–Hopfield band may contribute about 15% of the observed intensity.

The N_2^+ Meinel $(A^2\Pi_u \rightarrow X^2\Sigma_g^+)$ and first negative $(B^2\Sigma_g^+ \rightarrow X^2\Sigma_g^+)$ band systems can be produced by photoionization and electron impact ionization of N_2, by fluorescent scattering of solar radiation, and by electron induced fluorescence (Degen, 1981). The

latter source is negligible in the dayglow. The Meinel band system occurs in the infra-red; the most intense band in the first negative band system is the (0, 0) band at 3914 Å. No emission at that wavelength was recorded by the visible spectrometers on Venera 9 and 10. An upper limit of 45 R has been placed on the overhead integrated intensity at 3914 Å (Krasnopol'sky, 1978).

Fox and Dalgarno (1981) predicted the intensities of the Meinel and first negative bands due only to photoionization and electron impact ionization. Paxton (1988) has suggested that intensities of the N_2^+ first negative bands could be used to determine the fraction of the mass-28 ion densities due to N_2^+. He has predicted an overhead intensity for the 3914 Å band of 17 kR, using the neutral Hedin model appropriate to the conditions of Pioneer Venus orbit 185, but this prediction must be in error. Fox and Dalgarno (1983, 1985) have computed the vibrational distribution of N_2^+ in the terrestrial and Martian atmospheres, where vibrationally excited N_2^+ is produced mainly in fluorescent scattering of solar radiation in the first negative and Meinel band systems. The same model has been adapted for the ionosphere of Venus (cf. Fox, 1982a) and the emission rates in the N_2^+ band systems computed. The results are presented in Table VII. The integrated overhead intensity of the entire first negative band system is

TABLE VII

Computed overhead integrated intensities of the Meinel $(A \to X)$ and first negative $(B \to X)$ band systems of N_2^+ for a high solar activity $(F_{10.7} = 200)$ Hedin model

Source	Intensities (kR)	
	Meinel	First negative
Photoionization	2.0	0.41
Electron impact	0.26	0.00088
Fluorescent scattering	1.7	1.4
Total	4.0	1.8

only 1.8 kR. The integrated overhead intensity of the 3914 Å band is 790 R; for the (1, 0) Meinel band the predicted intensity is 910 R. Fluorescent scattering is the major source of both band systems; only about a quarter of the emission of the 3914 Å is from photoionization and electron-impact ionization.

3.9. N EMISSIONS

The $N(^2D)$ and $N(^2P)$ states of atomic nitrogen are metastable, with radiative lifetimes of about 10^5 and 12 s, respectively. They are produced in photodissociation and electron impact dissociation of N_2 and in dissociative recombination of N_2^+. The transition $N(^2D) \to N(^4S) + h\nu$ produces a photon of wavelength 5200 Å; the transition of $N(^2P)$ to the $N(^2D)$ state leads to emission at 10400 Å; the transition to the ground $N(^4S)$ state leads to emission at 3466 Å. Like $O^+(^2D)$ and $O^+(^2P)$, the importance of these

metastable states lies in their effect on thermospheric and ionospheric chemistry, rather than in strong emission rates (Fox, 1982a). No measurements of the emissions have been reported, but the intensities have been modeled for a high solar activity Pioneer Venus model by Fox (1982a). The computed integrated overhead intensities are given in Table IV.

3.10. NO NIGHTGLOW

The ultraviolet night airglow was first mapped by the PV OUVS during the first diurnal period of the mission (Stewart and Barth, 1979; Stewart et al., 1980; Gerard et al., 1981). The airglow was detected and identified as the gamma and delta bands of nitric oxide (Feldman et al., 1979; see also Stewart and Barth, 1979) excited by the radiative recombination of N and O atoms. Since no emissions suggestive of a nightside source of N and O atoms were present, it was proposed that the airglow was the result of these atoms being transported from their source on the dayside to the nightside where recombination occurs. Thus the morphology and brightness of the airglow can provide a sensitive tracer of the thermospheric circulation. Other PV measurements, particularly the hydrogen and helium nightside bulges (Taylor et al., 1984; Hedin et al., 1983) (see Figure 16), substantiate this concept of a strong day-to-night Venus thermospheric circulation (Mayr et al., 1980). Modelling efforts have been very successful in validating the proposed transport mechanism yielding the NO nightglow distribution and intensity. However, chemical questions remain regarding the dayside N-atom production available for transport to the nightside (Bougher et al., 1990a).

Planet-wide observations by the OUVS at solar maximum initially showed that the NO(0, 1) δ-band airglow typicaly exhibits a bright spot reaching 2.8 kR near 02 : 00 local time just south of the equator (Stewart et al., 1980). This statisticaly averaged peak brightness is roughly four times the dark disk average vertical emission of 780 R as calculated for 25-orbits sampled early in the PV mission (Stewart et al., 1980). The intensities reported by Stewart et al. (1980) have been revised as described by Bougher et al. (1990a). Briefly, recent recalibration of the OUVS instrument has yielded an improved sensitivity for this early PV period, 52.5 counts s^{-1} kR^{-1}. An improved algorithm was also developed that conserved photon counts, revealing a factor of two errors in previous NO nightglow data processing. Finally, the calculation of the Stewart et al. (1980) dark disk airglow intensity omitted a latitudinal weighting factor for area; its incorporation further reduced the observed dark disk intensity. The updated nightglow dark-disk average and peak intensities are now 400–460 ± 120 R and 1.9 ± 0.6 kR, respectively, for the 1978–1980 OUVS observational period. Individual orbit nightglow patches were seen to vary significantly in intensity and location on time-scales of an Earth day or less (Bougher, 1980; Stewart et al., 1980; Bougher et al., 1990a). The mean altitude distribution of the NO airglow was determined from limb profiles obtained near periapsis, with a 5 km vertical resolution. The altitude of the peak emission was found to be 115 ± 2 km (Gerard et al., 1981).

The OUVS sensitivity was shown to degrade substantialy after orbit insertion (December 1978). Subsequent monitoring of the nightglow beyond the first three diurnal

periods (1979–1981) incorporated this effect. The PV spacecraft periapsis altitude was too high during 1984–1986 for the OUVS to obtain meaningful limb profiles of the solar minimum nightglow. However, several measurements during this period from apoapsis showed an average nightside bright patch intensity roughly a factor of three smaller than observed previously during 1979–1981. A substantial solar cycle variation in the night-glow emission is thus confirmed (Stewart, 1989, private communication).

The No nightglow is particularly valuable in constraining the Venus thermospheric circulation in the absence of measured winds (Bougher, 1980; Stewart *et al.*, 1980; Bougher *et al.*, 1990a). The verage brightness distribution map of Stewart *et al.* (1980) (revised in Bougher *et al.* (1990a)) can be viewed as an approximate map of the downward flux of N-atoms being supplied from the dayside. Correspondingly, the intensity of the resulting nightside emission is proportional to the dayside column production of N-atoms; i.e., dayside average net column production must balance the nightside average column destruction of ground state N-atoms. Since the NO emission occurs well below the nightside homopause, vertical transport other than molecular diffusion must be important, either due to eddy mixing and/or large-scale winds. In addition, the local time position of the average peak emission (and bright patch intensity) provides evidence for asymmetries in the otherwise mean sub-solar-to-anti-solar ther-mospheric circulation (Stewart *et al.*, 1980; Bougher *et al.*, 1990a). Superimposed retro-grade zonal winds having a period of 4–6 days are also inferred from measured helium densities (Mayr *et al.*, 1980; Mengel *et al.*, 1989).

The basics of the Venus dayside odd-nitrogen chemistry are summarized in Figure 18. The major processes are little different from those operating on the Earth. CO_2, in fact, plays a similar role on Venus as O_2 does in the lower thermosphere of the Earth; i.e., both species react rapidly with $N(^2D)$ but not with $N(^4S)$. The initial steps leading to the production of odd-nitrogen through N_2 bond-breaking are accomplished through the same processes. The principal sources are (1) the dissociation of N_2 by electron impact, (2) the dissociative ionization of N_2 by electrons, and (3) the predissociation of N_2 by 80–100 nm photons. An effective branching ratio ($f = 0.5$) is typically chosen for the partitioning of $N(^2D)$ and $N(^4S)$ atoms that are produced (Cleary, 1986). The sequential reactions $N(^2D) + CO_2$ producing NO followed by NO + $N(^4S)$ yielding N_2 are by far the most important in reducing the total dayside production of excited and ground state N-atoms to the net available for nightside transport. The reaction producing NO^+ followed by its dissociative recombination serve to redistribute the forms of atomic-N. A standard value of $g = 0.75$ for branching to $N(^2D)$ is usually chosen (Kley *et al.*, 1977). In addition, partial recovery of $N(^4S)$ atoms is obtained by quenching of $N(^2D)$ by O and CO above the $N(^4S)$ peak. The precise value of the $N(^2D) + O$ quenching coefficient is very important for understanding the terrestrial odd-nitrogen chemistry (cf. Fesen *et al.*, 1989).

A preliminary study of the neutral and ion odd nitrogen chemistry was made by Rusch and Cravens (1979) soon after the first Pioneer Venus results were available. Their model predicted that ground state $N(^4S)$ atoms were the major neutral odd nitrogen species, with a peak concentration of about 2×10^7 cm^{-3} near 130 km. The integrated
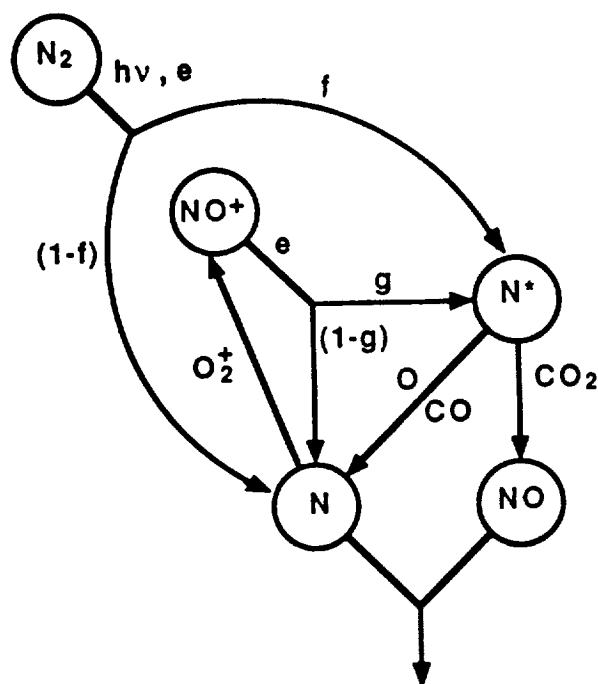
Fig. 18. Simplified Venus dayside odd-nitrogen chemical scheme. Taken from Bougher et al. (1989).

column production of atomic nitrogen produced in their model (for 70° SZA) was $4.5 \times 10^9 \, \text{cm}^{-2} \, \text{s}^{-1}$. Fox (1982) predicted a slightly larger maximum $N(^4S)$ density of $4 \times 10^7 \, \text{cm}^{-3}$. Later mapping studies and the nightside chemical-diffusive modeling of Stewart et al. (1980) showed that the originally reported dark disk nightglow intensity (780 R) required a downward flux of N-atoms of $1 \times 10^{10} \, \text{cm}^{-2} \, \text{s}^{-1}$. This flux should be reduced by a factor of nearly two due to the recent downward revision of the intensities reported by Stewart et al. (1980). No correlation was found between the nightglow brightness and the 10.7 cm solar fluxes for the observational period. The nightside vertical diffusion model, and additional limb profile studies (Gerard et al., 1981), furthermore, placed the peak volume emission rate altitude at 115 km using eddy diffusion of the same order as that used by von Zahn et al. (1980) for maintaining observed dayside densities. Thus, a determination of the altitude of the emission was found to be a sensitive indicator of the required nightside eddy diffusion profile (Stewart et al., 1980). Either global dynamics and/or small-scale mixing could be the underlying mechanism responsible. An adequate supply of dayside N-atoms appeared to be available for sustaining the observed nightglow.

This conclusion was challenged by Krasnopol'sky (1983), who concluded, based on a simplified dayside atomic-N model, that virtually all the dayside produced N-atoms would be required on the nightside to account for the NO nightglow. His dayside total column production of both ground state ($N(^4S)$) and excited ($N(^2D)$) atoms was

$1.1 \times 10^{10} \, \mathrm{cm}^{-2} \mathrm{s}^{-1}$. Virtually all of the $N(^2D)$ would have to be quenched to $N(^4S)$ rather than be converted to NO to sustain the required dayside to nightside flux. Presumably, this problem has been resolved with the reduction in the observed emission intensities.

Gerard *et al.* (1988) re-examined this problem using a 1-D photochemical-diffusive model that calculated $N(^4S)$, $N(^2D)$, and NO at selected SZA over the dayside. The daytime ionosphere and odd-nitrogen chemistry were coupled to obtain $N(^4S)$ profiles and local time distributions for comparison with PV measurements obtained with the neutral mass spectrometer (Kasprzak *et al.*, 1980; Hedin *et al.*, 1983). The average amount of total N-atoms produced on the dayside was estimated at $1.3 \times 10^{10} \, \mathrm{cm}^{-2} \mathrm{s}^{-1}$. A maximum $N(^4S)$ concentration of about $8 \times 10^7 \, \mathrm{cm}^{-2}$ was calculated at 124 km near LT = 17 : 00. Calculated $N(^4S)$ concentrations near 150 km were substantially less than those given by the empirical model of Hedin *et al.* (1983) (see Figure 19). However, a reasonable agreement with the original PV densities (Kasprzak *et al.*, 1980) was obtained. Approximately 50% of the dayside source was required for nightward transport to maintain the originally reported NO nightglow
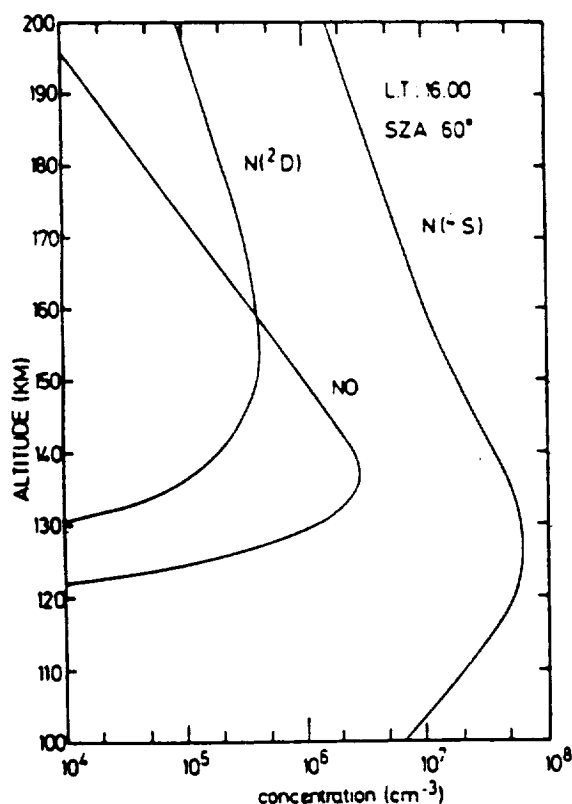

Fig. 19. Vertical distribution of $N(^4S)$, $N(^2D)$, and NO number densities as a function of altitude calculated at the equator for a local time of 16:00. Taken from Gerard *et al.* (1988).

J. L. FOX AND S. W. BOUGHER

intensities; the fraction would be smaller for the revised intensities. This estimate reflects a higher branching ratio for the (0, 1)–δ band resulting from NO recombination (0.32, after McCoy (1983)), which produces a required N-flux of $7 \times 10^9 \, \text{cm}^{-2} \, \text{s}^{-1}$. The model showed little sensitivity to the value of the efficiency of the $N(^2D)$ production by N_2 dissociation ($f = 0.5$ to 0.7); also, the calculated $N(^4S)$ was found to be rather insenstive to the $N(^2D)$–O quenching coefficient for values less than $2 \times 10^{-12} \, \text{cm}^3 \, \text{s}^{-1}$. This is so because the reaction of $N(^2D)$ with CO_2 yielding NO dominates all other N-atom destruction at the peak of the $N(^4S)$ density.

A comprehensive treatment of this flux problem requires the use of a three-dimensional model coupling the hydrodynamical flow with photochemical production and loss of odd-nitrogen. The results of the Gerard et al. (1988) detailed photochemical model were subsequently used in a 3-D Venus thermospheric general circulation model (VTGCM) to parameterize the sources and sinks of atomic nitrogen in the Venus dayside thermosphere (Bougher et al., 1990a). The VTGCM (see Section 6.2), an adaptation of the terrestrial NCAR TGCM, calculates global distributions of CO_2, CO, and O consistent with the 3-D model by day–night temperature contrasts and corresponding large-scale winds. Calculations of the observed nightglow distribution and intensity provide a further means to validate the basic model circulation and thermospheric structure. The model N-atoms produced are transported to the nightside by the VTGCM circulation and destroyed primarily by radiative recombination with O atoms, and mutual destruction with NO. NO, $N(^4S)$, and $N(^2D)$ are incorporated as minor species having no impact on the VTGCM major species, temperatures, or winds. NO and $N(^2D)$ are treated assuming photochemical equilibrium, while $N(^4S)$ was subject to diffusion and large-scale transport, in addition to chemistry.

Results for solar maximum conditions indicate that the recently revised dark-disk average NO(0, 1) δ-band intensity at 198.0 nm ($400-460 \pm 120 \, \text{R}$), based ons statistically averaged PV OUVS measurements, can be reproduced with minor modifications in chemical rate coefficients and global mean eddy diffusion. The calculated average dayside production of total N-atoms is about $9.4 \times 10^9 \, \text{cm}^{-2} \, \text{s}^{-1}$; chemical losses resulting from NO production and subsequent $N(^4S)$ destruction reduce this total production by a factor of 2 to 4. The nightward hemispheric flux of N-atoms required to yield 340 to 580 R of dark-disk average airglow is $\sim 2.5-3 \times 10^9 \, \text{cm}^{-2} \, \text{s}^{-1}$, which is roughly 30% of the total dayside N-atoms produced. This is realized for VTGCM cases using standard rate coefficients and branching ratios (Gerard et al., 1988), or slightly reduced NO production through a lower limit $N(^2D) + CO_2$ rate coefficient ($3 \times 10^{-13} \, \text{cm}^3 \, \text{s}^{-1}$) (Piper et al., 1987). A similar nightglow intensity could be simulated for somewhat weaker NO production coupled with enhanced global mean eddy diffusion ($K_t \leq 2 \times 10^7 \, \text{cm}^2 \, \text{s}^{-1}$). A large $N(^2D) + O$ quenching coefficient, of the magnitude measured by Jusinski et al. (1988), is not required for adequate dayside $N(^4S)$ production yielding observed nightglow intensities. The VTGCM peak intensity of 1.2 kR, calculated at LT = 01 : 00–03 : 00 near the equator, is in good agreement with PV OUVS observations (see Figure 20(a)). The altitude of the nightside peak emission layer (113 km) is also in agreement with PV OUVS data, and occurs where chemical
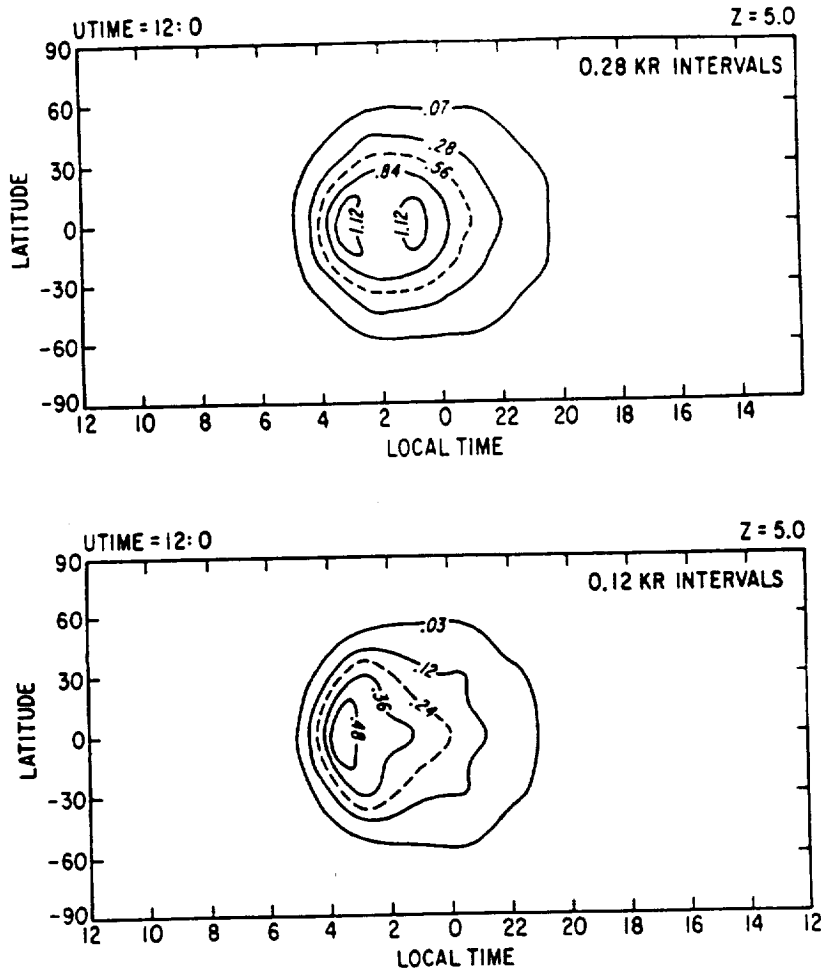
Fig. 20. VTGCM NO(0, 1) δ-band vertical intensity distributions: (a) a solar maximum simulation, corresponding to OUVS data of 1978–1981, and (b) a solar minimum simulation, appropriate to the 1984–1986 period. The vertical intensity distribution corresponds to the vertically integrated volume emission rate. Taken from Bougher et al. (1989).

transport (global wind plus eddy diffusion) lifetimes are comparable. Use of enhanced global mean eddy diffusion ($K \sim 2 \times 10^7 \, cm^2 \, s^{-1}$) also yields atomic O and N densities that are consistent with observed PV values. Peak N densities of 6.5 to 9.2 × $10^7 \, cm^{-3}$ are obtained at LT = 17:00 at about 130 km. The simultaneous production of observed dayside N-densities, corresponding to Hedin et al. (1983) values, and observed NO nightglow intensities requires a slightly slower wind system (terminator horizontal winds $\sim 150 \, m \, s^{-1}$) than currently simulated by the VTGCM.

Corresponding solar minimum calculations predict that the NO nightglow intensities should be very sensitive to the net dayside production of N-atoms. The factor of two decrease in the N_2 bond-breaking rate combined with the reduced VTGCM solar-driven

winds causes a reduction of nearly a factor of 3 in the dark-disk intensities. Figure 20(b) illustrates the VTGCM nightglow integrated vertical intensity distribution for solar minimum conditions; comparison can be made with Figure 20(a). This solar cycle variation is similar to that observed by the PV OUVS.

These VTGCM calculations confirm that the transport mechanism originally proposed is correct. Since this airglow is a good tracer of the thermospheric circulation, it provides a means to study remotely the variation of the Venus winds. The nightglow also provides a sensitive constraint on the magnitude and distribution of the global winds in the absence of available measurements, much like helium (Mengel et al., 1989). Furthermore, the Venus odd-nitrogen chemistry, since it is similar to that of the Earth, is also adversely impacted by the use of the large $N(^2D) + O$ quenching rate measured by Jusinski et al. (1988). It cannot be used for Venus and yield good dayside N-profiles plus NO nightglow intensities resembling Pioneer Venus observations. On Earth, present-day odd-nitrogen chemical schemes (e.g., Roble et al., 1987; Fesen et al., 1989) and observed $N(^2D)$ 520 nm airglow (Frederick and Rusch, 1977) cannot be reconciled with this large quenching rate. If $N(^2D) + O_2$ is the only important terrestrial NO source in the lower thermosphere, then the $N(^2D)$ production rate must be increased to compensate for the large quenching rate. Recent measurements of this rate coefficient, however, have yielded values near 1×10^{-12} cm^3 s^{-1}, a factor of 20 less than the Jusinski et al. (1988) rate (Piper, 1989; Miller et al., 1988). Further (Venus) progress requires future simultaneous measurements of $N(^2D)$, $N(^4S)$, and NO in the Venus lower thermosphere (Gerard et al., 1988). NO densities can also be derived from Venus nightside ion chemistry for comparison to VTGCM model values.

3.2. O_2 EMISSIONS

The first measurements of O_2 densities in the Venus atmosphere are those from the PV sounder probe gas chromatograph. Mixing ratios of 44 and 16 ppm were measured at 52 and 42 km; it appears that the mixing ratio decreases with altitude (Oyama et al., 1980). The gas chromatography experiments on Venera 13 and 14 measured an O_2 mixing ratio of 18 ppm for the altitude range 35 to 58 km (Mukhin et al., 1983). The PV sounder probe mass spectrometer determined an upper limit to the mixing ratio below the cloud tops of about 30 ppm (Hoffman et al., 1980a).

Above the cloud tops only upper limits have been measured. A ground-based search for absorption in the oxygen 'A band', the (0, 0) transition of the infrared atmospheric band system of $O_2(b^1\Sigma_g^+ \rightarrow X^3\Sigma_g^-)$, allowed Traub and Carleton (1974) to place an upper limit on the column abundance of O_2 of 1×10^{-6}; Trauger and Lunine (1983) reduced this number fo 3×10^{-7}.

Explaining these small O_2 mixing ratios in the mesosphere has been a major goal of mesospheric photochemical modeling. Oxygen atoms produced in the photolysis of CO_2

$$CO_2 + hv \rightarrow CO + O \qquad (30)$$

recombine very slowly by the process

$$CO + O + M \rightarrow CO_2 + M . \qquad (31)$$

At 300 K, the rate coefficient for reaction (31) is about $4.5 \times 10^{-36} \, \text{cm}^6 \, \text{s}^{-1}$, but the rate coefficient for the recombination of O atoms via

$$O + O + M \rightarrow O_2 + M \tag{32}$$
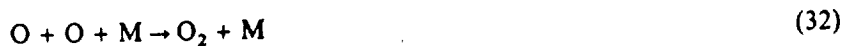
is much larger, about $1 \times 10^{-32} \, \text{cm}^6 \, \text{s}^{-1}$ (Baulch et al., 1980). Photolysis of CO_2 would cause the entire thermosphere to dissociate in a few weeks without effective recombination processes. The near-absence of O_2 in the mesosphere indicates that some probably catalytic process occurring in the Venus atmosphere acts to reform CO_2 from the O produced in reaction (30) or from the O_2 formed in reaction (2). On Mars, odd hydrogen compounds are implicated in the recombination of O and CO. A simple example of an odd-hydrogen catalytic cycle that effects recombination is

$$H + O_2 + M \rightarrow HO_2 + M, \tag{32a}$$

$$HO_2 + O \rightarrow OH + O_2, \tag{32b}$$

$$CO + OH \rightarrow CO_2 + H, \tag{32c}$$

with a net reaction of

$$CO + O \rightarrow CO_2 \tag{32d}$$

(Hunten and McElroy, 1970). On Venus, an extreme dearth of water vapor in the upper mesosphere precludes the presence of sufficiently large quantities of odd-hydrogen compounds. Compounds of chlorine have, however, been known to be present since HCl was identified in ground-based infrared spectra by Connes et al. (1967). The photochemical models of Sze and McElroy (1975), Krasnopol'sky and Parshev (1981, 1983), and Yung and DeMore (1982) rely largely on catalytic cycles in volving Cl compounds, such as

$$ClCO + O_2 + M \rightarrow ClCO_3 + M, \tag{33a}$$

$$ClCO_3 + O \rightarrow Cl + CO_2 + O_2, \tag{33b}$$

$$Cl + CO + M \rightarrow ClCO + M, \tag{33c}$$

with a net reaction of

$$CO + O \rightarrow CO_2, \tag{33d}$$
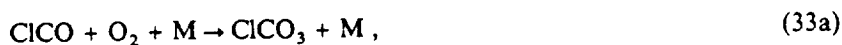
to effectively recombine CO and O.

The model of Krasnopol'sky and Parshev (1981, 1983), which is presented here in Figure 21, shows that O_2 forms a layer 15 km thick near 90 km. The thermospheric density of O_2 is consistent with a mixing ratio of 2×10^{-3} at 135 km. The upper boundary of the model of Yung and DeMore (1982) is at 110 km, where the mixing ratio of O_2 is about 1×10^{-3}. The model of Krasnopol'sky and Parshev has been critized by DeMore and Yung (1982) as including as a major step in destruction of O_2 the reaction:

$$ClCO + O_2 \rightarrow CO_2 + ClO. \tag{34}$$
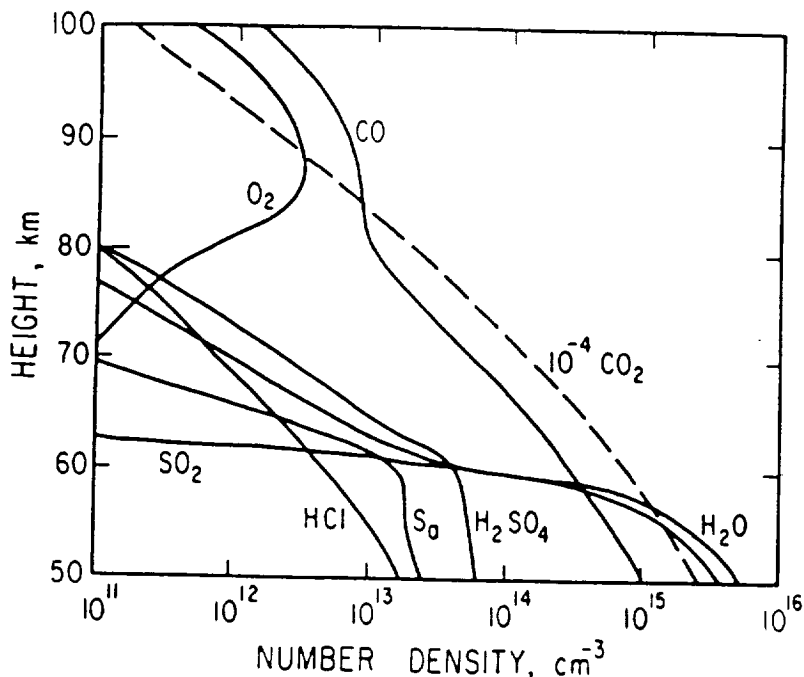
Fig. 21. Computed altitude profiles of the number densities of some neutral species in the Venus atmosphere. The CO_2 profile (dashed line) is a factor of 10^4 larger than shown. From Krasnopol'sky and Tomashova (1980).

Laboratory studies have shown the reaction above does not occur, the ClCO and O_2 combining preferentially in the three-body recombination reaction (33d). Krasnopol'sky and Parshev (1983) have criticized the model of Yung and DeMore for using a constant H_2O mixing ratio of 1×10^{-6} throughout the region above the clouds, when observations show that immediately above the clouds the mixing ratio is close to 200 times that value.

The chlorine and sulfur cycles have been found to be interconnected. DeMore *et al.* (1985) investigated the reaction of chlorine with SO_2 both with and without O_2 and they also discussed the implications for the Yung and DeMore (1982) model. A new reservoir species for chlorine, SO_2Cl_2 (sulfuryl chloride) was proposed, potentially increasing the total abundance of chlorine compounds in the mesosphere. Chlorine was found to catalyze the oxidation of SO_2 to H_2SO_4, thus providing another catalytic cycle for destruction of O_2.

All mesospheric models must explain the dayglow and nightglow intensities of 1.5 and 1.2 MR observed for the 1.27 μm infrared atmospheric band, from ground-based measurements of Connes *et al.* (1979). This band, which is the most intense feature in the Venus airglow, arises from the transition

$$O_2(a^1\Delta_g; v' = 0) \rightarrow O_2(^3\Sigma_g^-; v'' = 0) + h\nu(1\ 7\ \mu m).\qquad(35)$$
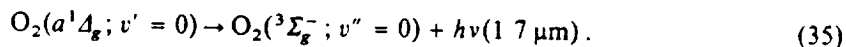
The intensity of this feature is presumably not indicative of the ambient density of ground state O_2, but rather of its formation rate by recombination of oxygen atoms. In the dayglow, $O_2(a^1\Delta_g)$ can also be produced by photolysis of ozone, but the near equality of the intensities of the day and night airglows shows that this source is minor for Venus. The model of Yung and DeMore (1982) required that the yield of $O_2(a^1\Delta_g)$ be 30% in reaction (2) and 67% in the reactions:

$$HO_2 + O \rightarrow OH + O_2, \tag{36}$$

$$Cl + O_3 \rightarrow Cl + O_2, \tag{37}$$

$$ClO + O \rightarrow Cl + O_2. \tag{38}$$

Subsequently, the yields of $O_2(a^1\Delta_g)$ and $O_2(b^1\Sigma_g^+)$ have been measured for the reactions above and several other postulated odd-chlorine reactions and the values have been found to be very small, gnerall less than 4% (Choo and Leu, 1985; Leu and Yung, 1987). Ali et al. (1986) have measured the rate for direct production of the $a^1\Delta_g$ state in reaction (2) and found that the yield is only about 7%, but that in the presence of O_2, the yield increases, indicating that the state is formed efficiently by energy transfer from a higher state. This conclusion is supported by an analysis of the oxygen bands in the terrestrial nightglow performed by Bates (1988b). Bates showed that the emission efficiency of the band systems originating in the $A^3\Sigma_g^+$, $A'^3\Delta_u$, and $c^1\Sigma_u^-$ states is small, indicating that the states are quenched efficiently, probably to the $a^1\Delta_g^+$ and $b^1\Sigma_g^+$ states, producing emission in the atmospheric and infrared atmospheric bands. In order to account for the emission rates at 1.27 μm in the terrestrial nightglow it is necessary to assume a large efficiency (~ 0.75) for the sum of direct recombination of O-atoms and energy transfer from higher states, and an additional, as yet unidentified source (e.g., McDade et al., 1987; Lopez-Moreno et al., 1988; Lopez-Gonzales et al., 1989).

Leu and Chung (1987) show that the total rate of CO_2 photolysis on Venus is about 8×10^{12} cm^{-2} s^{-1}, so the maximum emission rate of 1.27 μm emission would be 4 MR, if all the recombination reactions proceeded with a quantum yield of 1.0. The measured yields above imply an intensity of 0.05 MR of 1.27 μm emission from the chlorine reactions, whereas the observed value is 1.2–1.5 MR. Leu and Yung argue, therefore, that the 1.27 μ emission cannot arise from recombination of O atoms formed in photolysis of CO_2, and suggest an alternative source of O-atoms: photolysis of SO_2 introduced into the upper mesosphere by intermittent injections from the region near the cloud tops. The discrepancy for Venus is, however, rather more severe than the terrestrial nightglow problem, and seems to require a reconsideration of the basic theory of production of the 1.27 μm emission.

Massie et al. (1983) modeled the thermospheric densities of O_2, but at the lower boundary of the model, 100 km, the O_2 mixing ratio was constrained to the value indicated in the model of Yung and DeMore (1982). In the thermosphere, between 100 and 110 km photolysis of CO_2 is balanced by reaction (2). The computed mixing ratio of O_2 at 135 km is about 1×10^{-3}.

Thermospheric O_2 densities theoretically can be determined from the chemistry of

atomic C. The major loss process for C in the thermospheres of Venus and Mars is the reaction

$$C + O_2 \rightarrow CO + O \tag{23}$$

(McElroy and McConnell, 1971; Krasnopol'sky, 1982; Fox, 1982b). Although no measurements of C densities are available, since the predicted densities were just below the sensitivity of the PV ONMS, the PV orbiter ion-mass spectrometer measured densities of C^+ (e.g., Taylor et al., 1980). Fox (1982b) used the measured C^+ densities to constrain the O_2 mixing ratio; values of 10^{-4} or less were derived. Paxton (1983) used the intensities of atomic carbon emissions measured by the PV OUVS (see Section 3.4) to constrain the O_2 densities, and he derived an O_2 mixing ratio of 3×10^{-3}. As pointed out in Section 3.4, all of the models above are based on outdated photochemistry, and should be revised.

An outstanding success of the Soviet Venera 9 and 10 missions was the measurement of the visible nightglow of Venus in October 1975. The strongest features in the nightglow spectrum, shown in Figure 22, were identified by Lawrence et al. (1977) as the $v' = 0$
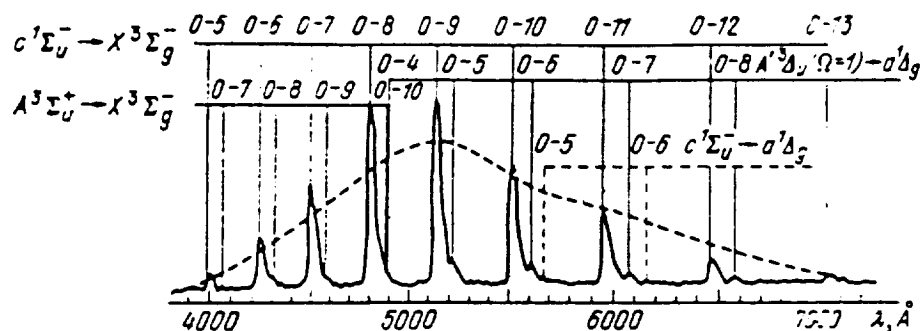
Fig. 22.   Visible night airglow spectrum measured by Venera 9 and 10. The dashed line is the instrument sensitivity. Taken from Krasnopol'sky and Tomashova (1980).

progression of the $O_2(c^1\Sigma_u^+ \rightarrow X^3\Sigma_g^-)$ Herzberg II band system; an average intensity of 2.7 kR was assigned to the band system (Krasnopol'sky, 1981). Three more band systems of O_2 were later identified in the Venus spectrum: the Herzberg I $(A^3\Sigma_u^+ \rightarrow X^3\Sigma_g^-)$ bands, the Chamberlain $(A'^3\Delta_u \rightarrow a^1\Delta_g)$ bands and the Slanger $(c^1\Sigma_u^- \rightarrow a^1\Delta_b)$ bands. The measured intensities of the Herzberg I and the Chamberlain bands were 140 and 200 R, respectively. All of these band systems are formed in recombination of atomic oxygen produced by photolysis of CO_2 on the dayside of the planet and transported to the nightside (Lawrence et al., 1977; Slanger, 1978). The maximum of the airglow layer is located near 100 km, the altitude of the maximum O density, and is about 15 km thick. Variations of about 10 km in the altitude of the maximum were observed. The emission shows a maximum at about 8–28° S latitude; diurnal variations of the nightglow intensities, shown in Figures 23, exhibit a maximum about 00 : 30 loca time, consistent with transport of O produced on the dayside by CO_2
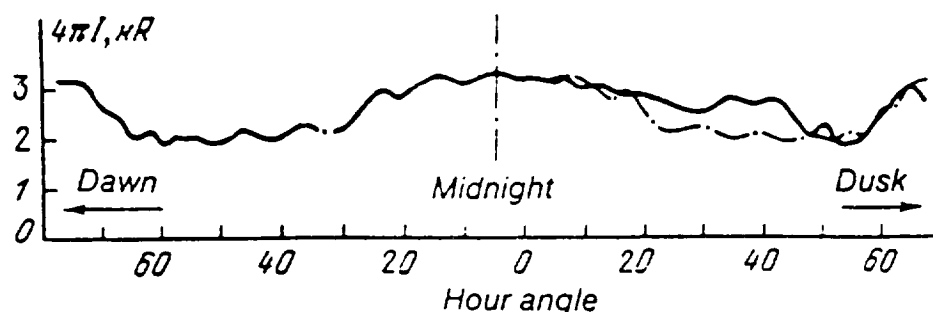
Fig. 23. Diurnal variation of the visible night airglow as measured by Venera 9 and 10. The dashed line is the symmetric continuation of the left part of the curve. From Krasnopol'sky and Tomashova (1980).

photolysis across the terminator and subsidence at the anti-solar point. A constraint similar to that placed on the Venus solar minimum thermospheric structure and circulation by the measured NO nightglow emissions is given by using the Herzberg II nightglow observations of the Venera 9 and 10 instruments. The VTGCM could be used to examine this visible airglow, provided that total temperature is incorporated explicitly and that its model lower boundary is extended from 105 to ~90 km (Bouger et al., 1988b, 1989). Such a study could yield information about the thermospheric circulation in the vicinity of 100 km.

Subsequent to the identification of the Herzberg II bands in the Venus nightglow, the band system was identified in the terrestrial nightglow, where the major molecular features are the Herzberg I bands (Slanger and Huestis, 1981). The dominance of different band systems in the terrestrial and Venus nightglows has led to many laboratory and modeling studies in an attempt to explain the differences. Slanger (1978) and Kenner et al. (1979) showed that the presence of CO_2 enhances emission in the Herzberg II bands, possibly due to its higher efficiency as a third body. Krasnopol'sky et al. (1976) proposed that the non-appearance of the Herzberg II bands in the Martian nightglow, as measured by the Mars 5 space probe, suggests that they are suppressed by efficient quenching by O_2. Subsequently, the rate coefficient for quenching of the $O_2(c^1\Sigma_u^-; v = 0)$ state by O_2 has been measured by Kenner and Ogryzlo (1983); the reported value is 3×10^{-14} cm^3 s^{-1}, whereas that for quenching by O is a factor of 200 larger. From studies of the dependences of the band systems on [O], [O_2], and [M], Kenner et al. (1979) found that the ratio of the intensity of the Herzberg II bands to that of the Herzberg I bands is proportional to [M]/[O]. They suggested that the Herzberg II bands dominate on Venus because the maximum O recombination takes place in a region of higher total density and lower atomic oxygen density. Although this would imply an even greater dominance of the Herzberg II bands on Mars, where the total density in the region of maximum O recombination is about 10 times that in the Venus atmosphere and 10^3 times that in the terrestrial atmosphere (Krasnopol'sky, 1981), it is possible that quenching renders the total emission rate small. Indeed, from calculations of the transition probabilities of the O_2 band systems (Bates, 1988a; values corrected in Bates, 1989), Bates (1988b) has shown that the efficiency of emission

relative to quenching in both the Herzberg I and II band systems in the terrestrial nightglow is on the order of 1–4%.

From an analysis of terrestrial and Venusian airglow profiles, Krasnopol'sky (1986b) proposed that the weakly bound $^5\Pi_g$ state, produced efficiently in three-body recombination of O atoms, is a common precursor for the five metastable states of $O_2(A, A', c, a, b)$, the lower states being produced by quenching or energy transfer to another O_2 molecule. This suggestion was based on calculations of the efficiency of production of various states of O_2 by Wraight (1982) and Smith (1984) that showed that the $^5\Pi_g$ state is produced with about a 66% efficiency. Bates (1988b) proposed that the fraction be reduced to 50% to account for the smaller potential well depth of the $^5\Pi_g$ state, about 0.14 eV as computed by Partridge et al. (1990, private communication to Bates), compared to the value 0.23 eV adopted by Wraight from the calculations of Saxon and Liu (1977). He proposed the fractions of associations into the seven lowest electronic states of O_2 shown in Table VIII. The efficiency of production of the A state

TABLE VIII

Fraction of direct associations (reaction 39) into various states of O_2. (From Bates, 1988b.)

State	Fraction
$X^3\Sigma_g^-$	0.12
$a^1\Delta_g$	0.07
$b^1\Sigma_g^+$	0.03
$c^1\Sigma_u^-$	0.04
$A'^3\Delta_u$	0.18
$A^3\Sigma_u^+$	0.06
$^5\Pi_g$	0.50

is only about 6%, 50% larger than that of the c state. Bates showed that at temperatures near 200 K redissociation of the $^5\Pi_g$ state is efficient and much larger than the potential rate for energy transfer to any of the lower states. Furthermore, because of this redissociation, the measured value of the three-body recombination rate coefficient underestimates the actual recombination rate. Temperatures are slightly lower in the Venus atmosphere near 100 km, however, so redissociation may not be as important there, and the dissociation energy itself is still somewhat uncertain.

The excited states of O_2 are relevant also for production of $O(^1S)$ and subsequent radiation in the atomic oxygen 'green line' at 5577 Å in the terrestrial nightglow. It is generally agreed that the production of $O(^1S)$ proceeds by the two-step mechanism proposed by Barth (1964):

$$O + O + M \rightarrow O_2^* + M,$$
(39)

$$O_2^* + O \rightarrow O_2 + O(^1S),$$
(40)

rather than the single step mechanism proposed by Chapman (1931). Bates (1981) has reviewed the development of the theory for production of the green line in the terrestrial atmosphere. The identity of O_2^* in reactions (39) and (40), the 'Barth precursor', is uncertain. The A, A', and $^5\Pi_g$ states and the c state for $v > 0$ are sufficiently energetic. No green line emission was detected by the visible spectrometers on Veneras 9 and 10, and an upper limit of 10 R has been placed on its intensity (Krasnopol'sky, 1981, 1986b). This suggests that the precursor is not present in the Venus atmosphere. The A state was ruled out based on the large required rate coefficient for quenching by O and its altitude profile (e.g., Slanger, 1978; Thomas, 1981; Llewellyn et al., 1980). Krasnopol'sky (1981) showed that, if the A' state were the precursor, the green line emission would be two orders of magnitude larger than the observed value, but that the identification of the vibrationally excited c state as the precursor did not contradict any available data. Indeed, the Herzberg IIn system in the terrestrial nightglow consists of bands originating in vibrational levels with $v = 4, 5$, and 6, whereas only bands originating in $v = 0$ have been observed on Venus. With this assumption, Krasnopol'sky derived a rate coefficient of 2.5×10^{-10} cm^3 s^{-1} for the quenching of the c state by O:

$$O_2(c^1\Sigma_u^-) + O \rightarrow O_2 + O(^1S), \tag{41a}$$

a value of 5.9×10^{-10} cm^3 s^{-1} was measured by Kenner and Ogryzlo (1983) for the reaction

$$O_2(c^1\Sigma_u^-) + O \rightarrow \text{products} . \tag{41b}$$

It is probable, however, that the rate coefficients for energy transfer and quenching depend upon the vibrational level of the O_2, but the vibrational distributions in the atmosphere and sometimes in the laboratory, are uncertain. Moreover, Krasnopol'sky's 1981 analysis preceded the calculations of Wraight (1982) and Smith (1984) and was based on a statistical distribution of states of O_2 formed in the three'body recombination. He has recently reconsidered the problem and has concluded that the $^5\Pi_g$ state is a more likely precursor, but this analysis assumes a larger well depth for the state than current calculations indicate and no significant redissociation (Krasnopol'sky, 1986b).

Combining measured intensities of the band systems (Greer et al., 1986; Slanger and Huestis, 1981) with computed transition probabilities (Bates, 1988a, 1989), Bates (1988c) has estimated the average rate coefficients for energy transfer, reaction (40), that would be necessary for each of the potential states to be the precursor in the terrestrial atmosphere and compared the requirements to measurements made on oxygen-argon afterglows by Slanger and Black (1976). Only the $c^1\Sigma_u^-$ and $^5\Pi_g$ states are not eliminated by this procedure, information on the reverse process

$$O(^1S) + O_2(X^3\Sigma_g^-) \rightarrow O(^3P) + O_2(c^1\Sigma_u^-), \tag{42}$$
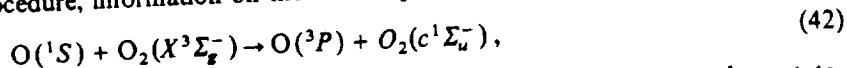
was used to further constrain the rate coefficient for energy transfer from the c state. The densities of $O_2(c; v = 0)$ present in the Venus atmosphere can be determined from the observed emission in the Herzberg II system, but no information is available about vibrationally excited states. From the Venus nightglow data, Bates also derived upper

limits for the transfer rate coefficients for the A state, which is marginally consistent, and for the A' state, which is inconsistent, with the terrestrial required rate coefficients. He does note, however, that the rate coefficients may vary with vibrational quantum number, so the constraints ar not rigid. The upper limit on the energy transfer rate coefficients for the $^5\Pi_g$ state from Venus data is inconsistent with terrestrial requirement, but there is no positive evidence in its favor.

3.12. O_2^+ EMISSIONS

The O_2^+ second negative band system arises from the transition $O_2^+(A^2\Pi_u \rightarrow X^2\Pi_g)$. The $O_2^+(A^2\Pi_u)$ state is produced in the Venus ionosphere mostly in fluorescent scattering of solar radiation by ground state O_2^+, since the ambient densities of O_2 in the Venus thermosphere are too low for photoionization and electron impact ionization to be significant sources. In order to determine the role of fluorescent scattering in producing vibrationally excited O_2^+, Fox (1985) computed the intensities of the bands in the second negative and first negative ($b^4\Sigma_g^- \rightarrow a^4\Pi_u$) band systems. The second negative bands are weak and spread over a large wavelength range. The intensities in 50 Å intervals are shown in Figure 24 for two assumptions about the (unknown) rate coefficient for the vibrational quenching of $O_2^+(X^2\Pi_g; v)$ by O:

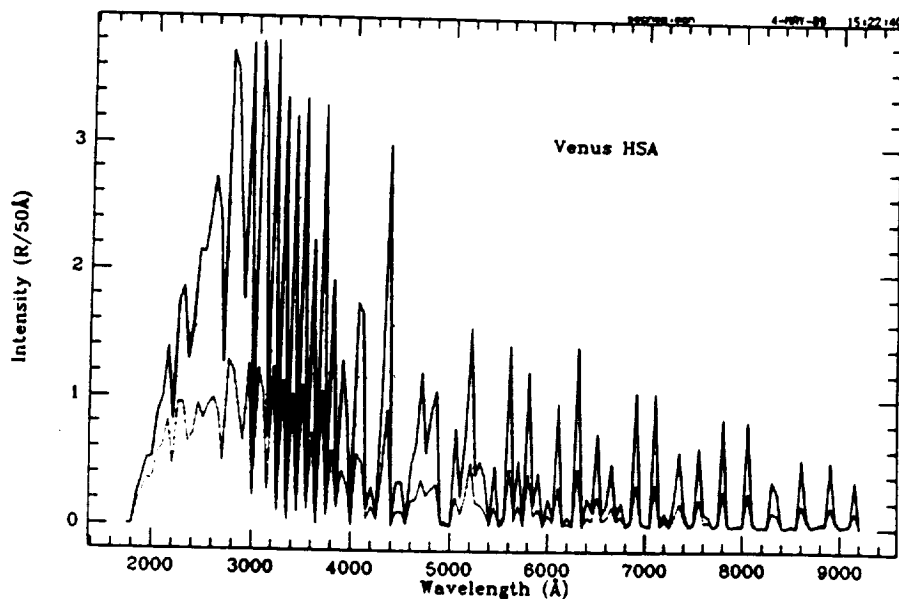$$O_2^+(v) + O \rightarrow O_2^+(v-1) + O . \tag{43}$$

Fig. 24. Computed intensities of the second negative band system, for a high solar activity (HSA) model, summed in 50 Å intervals. The solid line is for $k_{43} = 1 \times 10^{-10} \, cm^3 \, s^{-1}$. The dotted line is for $k_{43} = 6 \times 10^{-10} \, cm^3 \, s^{-1}$.

The integrated overhead intensity of the second negative band system for a rate coefficient of $1 \times 10^{-10}\, cm^3\, s^{-1}$ is 230 R. If the rate coefficient is near $6 \times 10^{-10}\, cm^3\, s^{-1}$, the intensity is reduced to 43 R. The first negative band system is very weak on Venus due to the near absence of O_2; the computed intensities are 0.75–1.5 R.

4. Hot Atom Cornas and Escape

4.1. INTRODUCTION

"This ingenious application of the properties of molecules to planetary despoiling of the weak, is due to an Irish gentleman whose name for the moment escapes me; and facts appear to support it."

PERCIVAL LOWELL (1984)

The idea of the escape of atoms from planetary atmospheres, the Moon and the Sun was first put forward in a paper read to the Royal Society by J. J. Waterston in 1845 (Chamberlain, 1963; Jeans, 1925). Because the paper contained 'certain inaccuracies' (Jeans, 1925), only an abstract was published (Waterston, 1846). The manuscript itself did not appear until 1892, when Lord Rayleigh had it published for historical interest (Waterston, 1892). The intervening development of the kinetic theory of gases and the Maxwell distribution law allowed the fundamental idea of evaporation of the energetic tail of the thermal distribution to be introduced (Stoney, 1898); the theory was later refined by Sir James Jeans (1925), whose name the thermal escape process now bears.

The idea of a planetary corona was first introduced by Stoney (1868). He remarked that at sufficient heights, atomic collisions would be so rare that most of the atoms traveling upward would follow ballistic orbits, eventually falling back to the denser parts of the atmosphere. The altitude above which collisions cease to be important is called the exobase or critical levle and the region of the atmosphere above the exobase is the exosphere. A comprehensive theory of the exosphere and atmospheric evaporation has been presented by Chamberlain (1963) and a pedagogical treatment of the subject can be found in Chamberlain and Hunten (1987). Other non-thermal escape processes have subsequently been found to be more important than thermal (Jeans) escape for the terrestrial planets (e.g., Liu and Donahue, 1974a, b; Hunten, 1982). Excellent reviews of thermal and non-thermal escape processes have been presented by Hunten and Donahue (1976) for the escape of hydrogen from the terrestrial planets, and by Hunten (1982) for the coronas and escape of species from all the terrestrial bodies in the sola system.

The exobase is mathematically defined as the altitude where the mean free path l is equal to the atmospheric scale height. The mean free path is defined by the expression $l = (n\sigma)^{-1}$, where n is the total number density and σ is the collision cross section. The probability that a particle, moving upward from the exobase with sufficient velocity will actually escape without suffering another collision is e^{-1}. The condition $l = H$, therefore, reduces to $nH\sigma = 1$ or, equivalently, to $N = \sigma^{-1}$, where N is the column density. Since

a typical collision cross section is about $3 \times 10^{-15}\,\text{cm}^{-2}$, in practice the exobase is located near the altitude above which the column density is about $3.3 \times 10^{14}\,\text{cm}^{-3}$. For the high solar activity ($F_{10.7} = 200$) VTS3 model the exobase altitude is near 210 km at noon and 154 km at midnight. The VIRA model for $16°$ N and $F_{10.7} = 150$ places the exobase near 201 km at noon and 161 km at $22:00$ hr local time. In the BNMS model, which applies to $08:30$ hr local time, the exobase is near 191 km. In the region of the pre-dawn bulge in the densities of H and He, the column density of H_2 is important in determining the altitude of the exobase (Kumar *et al.*, 1983).

Whether the trajectory of a particle traveling upward from the exobase is ballistic (bound) or escaping (free) is determined by the total energy E, which is the sum of its kinetic and potential energies:

$$E = \frac{1}{2}mv^2 + \int_{\infty}^{r_c} \frac{mGH}{r^2}\,dr,\qquad(44)$$

where m and v are the mass and velocity of the particle, G is the gravitational constant, M is the mass of the planet, and r is the distance from the center of the planet; the subscript c refers to the critical level or exobase. Expression (44) reduces to

$$E = \tfrac{1}{2}mv^2 - mg_c r_c,\qquad(45)$$

where g_c is the gravitational acceleration at the exobase. If the total energy is negative, the particle is bound; if the total energy is positive the particle may escape. The escape velocity, v_{esc}, is then defined by the condition $v_{esc} = (2gr)^{1/2}$. For Venus, the escape velocity is about $10.2\,\text{km s}^{-1}$.

In the Jeans escape process, particles with velocities greater than the escape velocity in the high-energy tail of the Maxwellian distribution may escape if they are oriented in the upward hemisphere (above the horizon). The escape flux, ϕ_J is given by

$$\phi_J = \frac{n_c u}{2\sqrt{\pi}}\,(1 + \lambda_c)\exp(-\lambda_c),\qquad(46)$$

where

$$\lambda = \frac{GMm}{rkT} = \frac{mgr}{kT}.\qquad(47)$$

λ is the gravitational potential energy in units of kT and u is the modal velocity of a gas in thermal equilibrium at temperature T,

$$u = (2kT/m)^{1/2}.\qquad(48)$$

Sometimes a correction factor is applied to the expression for the escape flux to account for the suppression of the tail of the distribution due to the escape of the energetic particles (Chamberlain, 1963; see also Hunten, 1982). Application of Equation (46) to

the escape of H from Venus, for the VIRA model with an exobase near 200 km, gives a value for λ of about 11 and a thermal escape flux of about 22 H atoms $cm^{-2} s^{-1}$ at noon; at midnight the escape flux is several orders of magnitude smaller, due to the low nightside temperatures and the resulting large value of λ. These fluxes are insignificant compared to the actual escape fluxes that have been inferred from models of the hot H corona.

Hunten (1973a) was the first to recognize that the escape rate of a light species from a planetary atmosphere may be controlled by diffusion of the species to the exobase, rather than by the escape process itself. The escape flux of H from Venus is limited by the rate of transport of H through the middle atmosphere to the upper atmosphere; the limiting upward flux, ϕ_i of a species i with mixing ratio f_i can be estimated as

$$\phi_i \approx \frac{b_i f_i}{H_a},$$
(49)

where H_a is the average scale height of the atmosphere and b_i is the binary collision parameter (Hunten, 1973a, b; Hunten and Donahue, 1976). b_i is defined by $b_i = D_i n_T$, where D_i is the molecular diffusion coefficient, evaluated as an appropriate average of the binary diffusion coefficients D_{ij} of the species i diffusing through the major atmospheric constituents j. D_i is usually computed as

$$\frac{1}{D_i} = \sum_{j \neq i} \frac{n_i/n_T}{D_{ij}}.$$
(50)

The expression (49) above is usually evaluated at the homopause, with the mixing ratio taken from a suitable altitude in the middle atmosphere, but above the cold trap. The limiting flux obtains if and only if the mixing ratio is constant with altitude. The effect of photochemistry can be eliminated if all chemical forms of the species are counted in the calculation of f_i. H is found in the mesosphere in the form of HCl, H_2O, and H_2 an din the thermosphere mostly as H. In order to evaluate the limiting flux of H we must first determine the mixing ratios of H-containing compounds in the middle atmosphere and at the homopause. The abundances of H, H_2, and H_2O will be discussed below.

4.2. H AND H_2 DENSITIES

No *in situ* measurements of H densities in the thermosphere are available, but H^+ densities were reported from PV ion mass spectrometer data (e.g., Taylor *et al.*, 1980). Brinton *et al.* (1980) showed that, in the altitude regin where H^+ is in photochemical equilibrium, the major source of H^+ is the nearly thermoneutral charge transfer of O^+ to H

$$O^+ + H \rightarrow H^+ + O,$$
(51a)

while loss is via the reverse reaction

$$H^+ + O \rightarrow H + O^+$$
(51b)

and by reaction with CO_2

$$H^+ + CO_2 \rightarrow HCO^+ + O.$$

(52)

Thus the steady-state density of H can be computed from ONMS and OIMS data using the expression

$$[H] = \frac{[H^+]}{[O^+]}\left([O]\,\frac{k_{51b}}{k_{51a}} + \frac{k_{52}}{k_{51a}}\,[CO_2]\right).$$

Brinton et al. found that photochemical equilibrium is a valid approximation below 200 km on the dayside and below 170 km on the nightside. A large variation with solar hour angle was found, with maximum densities occurring in the pre-dawn sector near 04 : 00 hr local time. Figure 25 shows the H densities derived by Brinton et al. at 165 km
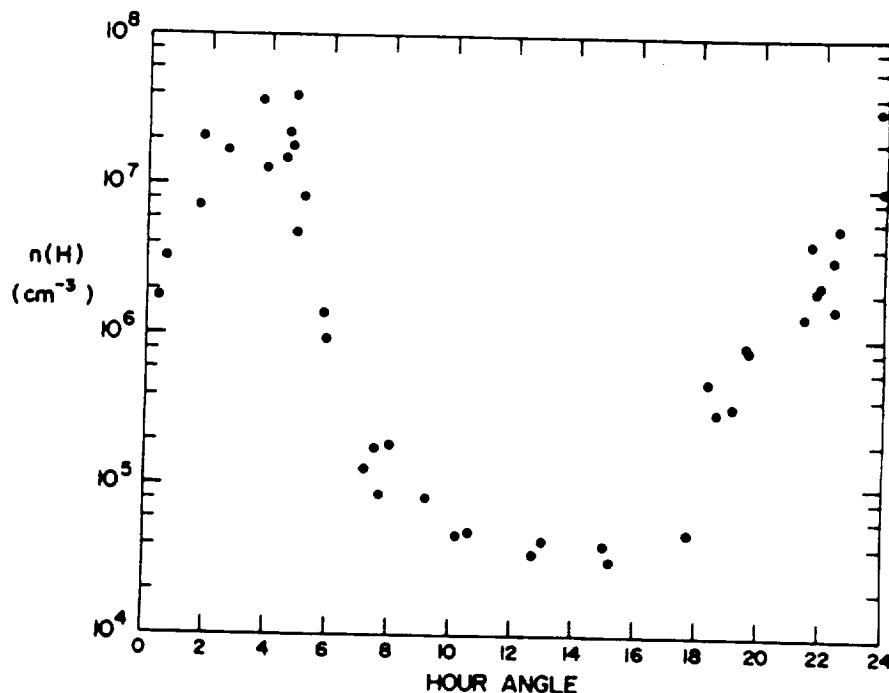
Fig. 25. Diurnal variation of atomic hydrogen concentration in the Venus thermosphere, derived from *in situ* measurements of ion and neutral composition. Data were obtained near 165 km altitude on 25 orbits of The Pioneer Venus spacecraft between December 1978 and July 1979. These values are based on non-normalized ONMS data and should be increased by a factor of about 1.63 (see text). Taken from Brinton et al. (1980).

as a function of hour angle. Since this study was done, a renormalization of the ONMS data by a factor of 1.63 has been suggested (Hedin et al., 1983) (see Section 2), so values of [H] presented by Brinton et al. should be multiplied by this factor also. Taylor et al. (1984, 1985), obtained similar results in a later analysis of three years of PV data. The

peak densities at 165 km were in the range $2-5 \times 10^7$ cm^{-3}, with a night-day ratio of about 400. No evidence for a long-term variation in the H densities was observed, as would be expected for the time period of the observations, when solar fluxes declined by less than 10%. The large scale height of H near 200 km on Venus, about 270 km for a temperature near 275 K, suggests that the densities of H do not change much with altitude over the altitude range from 150 to 250 km. In actuality, H is not in diffusive equilibrium above the homopause. Its density distribution deviates slightly from diffusive equilibrium because of the large flux through the exobase; the apparent scale height will be somewhat smaller than the diffusive equilibrium scale height.

The strongest resonance feature of atomic hydrogen is the Lα line at 1216 Å; it arises from the $2p \rightarrow 1s$ electronic transition. Radiation from Venus at Lα was detected by the ultraviolet spectrometers on Mariner 5 (Barth et al., 1967) and Venera 4 (Kurt et al., 1968). The Mariner 5 intensities were later reduced by a factor of 0.7 to account for a post-flight recalibration of the instrument (Broadfoot et al., 1974). A mean disk intensity of 40 kR has been derived for the Mariner 5 observations (Anderson, 1976). Rottman and Moos (1973) observed Lα with their moderate resolution rocket-borne spectrometer and reported an intensity of 27 kR. As discussed in the Introduction, Mariner 5 limb profiles showed a two-scale height distribution of H, the source of which was debated for several years (Barth et al., 1967). Stewart (1968) first suggested that the two components were due to H at two different temperatures. Barth (1968) proposed that the inner component was a mass-2 species, either H$_2$ or D, and the outer component H. Barth favored the H$_2$ interpretation, while other workers preferred the idea that the inner component was due to deuterium (Donahue, 1968; Wallace, 1969; McElroy and Hunten, 1969). Wallace et al. (1971) struck a fatal blow to the deuterium hypothesis when they measured Venusian Lα with a rocket-borne UV spectrometer capable of resolving the H and D Lα lines and failed to detect the deuterium line. In addition, other evidence suggested that the thermospheric temperatures were lower than the 700 K or more required for the scale height to be that of a species with a mass of 2. Kumar and Hunten (1974) advanced the two-temperature hypothesis by showing that the ion densities derived from the radio-occultation data were consistent with a neutral atmosphere model with a low exospheric temperature of 350 K; they further suggested that the hot H component could be produced by ion-neutral reactions such as

$$O^+ + H_2 \rightarrow OH^+ + H, \tag{54}$$
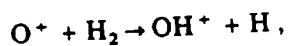
is sufficient H$_2$ were available.

The two-temperature interpretation was established by a re-analysis of the Mariner 5 bright limb and dark disk Lα data that employed a spherical radiative transport code (Anderson, 1976). Dayside temperatures of 275 ± 50 K and 1020 ± 100 K and critical level densities of 2×10^5 cm^{-3} and 1.3×10^3 cm^{-3} were determined for the cold and hot H components, respectively. For the nightside, temperatures of 150 ± 50 K and 1500 ± 200 K, and critical level densities of 2×10^5 cm^{-3} and 1×10^3 cm^{-3} for the cold and hot components, respectively, were reported. The temperatures derived by Anderson are in very good agreement with those later reported from Pioneer Venus data.

The dayside densities are significantly larger and the nightside densities are smaller than the values derived by Brinton *et al.* (1980) from Pioneer Venus data. The large diurnal variation in densities shows that the spherically-symmetric radiative transfer model used by Anderson is not valid, especially for the nightside. In addition, Anderson placed the critical level at 250 km, significantly higher than Pioneer Venus models indicate, although, as we have seen, the H densities do not vary rapidly with altitude.

The Mariner 10 spectrohotometer detected a strong signal at Lα but the intensity was less than at the time of the Mariner 5 encounter (Broadfoot *et al.*, 1974). Takacs *et al.* (1980) used a spherically-symmetric radiative transfer model to analyze the emissions on the bright limb. The derived values for the temperatures and densities were similar to those of Anderson (1976): 275 $\pm$ 50 K and 1.5 $\times$ 10^5 cm^{-3} for the temperature and density of the dayside cold component, respectively; and 1250 $\pm$ 100 K and 500 $\pm$ 100 for the temperatures and density of the dayside hot component, respectively. Takacs *et al.* found that a spherically-symmetric model was inadequate to analyze the dark disk data.

In addition to the visible spectrometers, Venera 9 and 10 were equipped with Lα photometers to measure the intensities at 1216 Å. Bertaux *et al.* (1978) analyzed the data obtained using a spherically-symmetric, isothermal radiative transfer model. They found that the data could be fit by a two-temperature model, but the fit was not better than that of a one-temperature model at 500 K with an exobase density of 1.5 $\times$ 10^4 cm^{-3}, values which are bracketed by those of the hot and cold components from the Mariner 5 and 10 analyses. The spacecraft also carried resonance-absorption cells filled with hydrogen and deuterium that were heated by tungsten filaments to produce H and D atoms, respectively. The reduction in the intensity of the planetary Lα line by the absorption cells would provide an indication of the line width and therefore of the temperature. No absorption was observed for the D$_2$ cell. The H$_2$ cell data showed that the temperature increases abruptly above about 3000 km, near the altitude above which the Mariner analyses showed the hot component to dominate.

The Venera 11 and 12 ten-channel UV photometers were also sensitive at Lα (Kurt *et al.*, 1979). Bertaux *et al.* (1981) reported sub-solar zenith intensities of 38–42 kR on the disk, similar to the values reported by Anderson (1976) from Mariner 5 data. Anderson showed, however, that the bright disk intensities are due mostly to Rayleigh scattering by CO$_2$. Since the Venera photometer aperture was not parallel to the limb, the altitude resolution in the limb scan was limited. Analysis showed that the data could be fit by a two-temperature model with temperatures of 400 and 700 K.

Reports of Pioneer Venus OUVS Lα limb scan observations have been presented by Paxton *et al.* (1985, 1988). Paxton *et al.* (1988) used a radiative transfer model that allowed for variations of temperature and density with altitude, latitude, and local time to analyze 20 orbits covering the first three years of operation of the PV orbiter. The inferred density of H at the exobase averaged 6 $\times$ 10^4 cm^{-3}; this compares favorably with the daytime average value of about 6.5 $\times$ 10^4 cm^{-3} determined from the analysis of Brinton *et al.* (1980). They attributed the factor of 2–3 discrepancy with the Mariner 5 and 10 analyses to the use of a more sophisticated radiative transfer model. The column

density of H above 110 km, the altitude below which CO_2 strongly absorbs Lα, averages $3.6 \pm 1 \times 10^{13}\,cm^{-2}$.

4.3. D/H RATIO

Interest in determining the D/H ratio in the Venus atmosphere began when the 2-scale height distribution of H was first measured by Mariner 5 (Barth *et al.*, 1967; see Section 4.2). The interpretation that the inner component was due to D at the same temperature as the outer H component required a D/H ratio of about 10% (McElroy and Hunten, 1969; Wallace, 1969). Although the derived ratio, which was enhanced over the terrestrial value by a factor of about 10^3, became meaningless after this hypothesis was shown to be invalid, the idea of some enrichment of D due to differential escape of H and D remained a possibility.

The PV OIMS detected an ion with a mass of 2, which could be either H_2^+ of D^+ (e.g., Taylor *et al.*, 1980). Originally this ion was believed to be H_2^+, with the H_2^+ produced mainly by direct photo- and electron-impact ionization of H_2. H_2 would be destroyed by reactions with O^+ (reaction 54) and with CO_2^+:

$$H_2 + CO_2^+ \rightarrow CO_2H^+ + H. \tag{55}$$

Kumar *et al.* (1981) derived an abundance of 10 ppm H_2 at the homopause from a model of the chemistry of H_2^+. McElroy *et al.* (1982), Cravens *et al.* (1983), and Rodriguez *et al.* (1984) have emphasized that a large mixing ratio of H_2 provides a significant source of H through the reactions (54) and (55) above, which cannot be balanced by the known loss mechanisms and is difficult to reconcile with the measured abundances of H.

McElroy *et al.* (1982) suggested that the mass-2 ion measured by the PV OIMS was D^+ rather than H_2^+, the atmosphere having become enriched in D relative to H by preferential escape of H. Donahue *et al.* (1982) were able to measure the D/H ratio in the lower atmosphere with the PV LNMS, by comparing the H_2O and HDO peaks during the time that the inlet to the mass spectrometer was clogged by sulfuric acid from cloud droplets. A value of 1.6×10^{-2} was reported.

Hartle and Taylor (1983) identified the mass-2 ion as D^+ by comparing the scale height of the mass-2 ion to that of H^+ in the photochemical equilibrium region and the diurnal variation of the mass-2 ion to that of H^+. They reasoned that the altitude profile of the ratio D^+/H^+ should vary as $\exp(\Delta z/H(1))$, where $H(1)$ is the scale height of a mass-1 species, but the ratio of H_2^+/H^+ should vary as $[O^+]^{-1}\exp(\Delta z/H(1))$. The observed altitude variation of the ratio supported the identification of the species as D^+, as did the observation that both the mass-2 ion and H^+ exhibit bulges in the pre-dawn sector, with densities an order of magnitude larger near 04 : 00 hr local time than during the day. From the measured ratio D^+/H^+ Hartle and Taylor derived a D/H ratio of 1.7×10^{-2} between 155 and 160 km, which, when projected down to the presumed homopause at 132 km yields a value of $2.2 \pm 0.6 \times 10^{-2}$, in fairly good agreement with the measured value of Donahue *et al.* (1982).

Kumar and Taylor (1985) modeled the pre-dawn bulge ionosphere, where the maxi-

mum densities of H^+ and D^+ (as well as those of light neutral species) are found. By analyzing two orbits of PV data, they obtained additional strong evidence that the mass-2 ion was D^+. The reaction of O^- with H_2 (reaction (54)) would strongly suppress the O^+ densities; a depletion in O^+ at times of enhanced mass-2 ion was not observed. Kumar and Taylor derived D/H ratios of 2.5 and 1.4% for PV orbits 117 and 120, respectively, and placed an upper limit on the H_2 abundance at the homopause of 0.1 ppm.

Using the high-resolution mode if the IUE satellite, Bertaux and Clarke (1989a) searched for the deuterium $L\alpha$ line, which is located 0.33 Å shortward of H $L\alpha$, but found no evidence for it. An upper limit was determined for its intensity of 300 R, compared to 21 kR measured for the H $L\alpha$ line. From the non-detection, they placed an upper limit on the D/H ratio at 100 km of $3.6 \pm 1.5 \times 10^{-3}$, a factor of more than 4 lower than the values estimated from the LNMS data by Donahue *et al.* (1982) and Hartle and Taylor (1983). Bertaux and Clarke suggested that the LNMS result for HDO may indicate a chemical fractionation process, and that the mass-2 ion may indeed be H_2^+, thus requiring the presence of 10 ppm H_2. They did not, however, account for the lack of suppression of O^+ in the bulge region, or for the large source of H atoms implied by such a large abundance of H_2. Donahue (1989) pointed out the inconsistency in their inference of 10 ppm H_2 a the homopause and the 0.7 ppm H required by the H $L\alpha$ data. He also challenged their conclusion that a D/H ratio of 1.6×10^{-2} would lead to 2.5 kR of D $L\alpha$, as ignoring the upward flux of D due to the global circulation, which will produce a different verticle distribution from diffusive equilibrium. Donahue found that a predicted intensity of 1.0 ± 0.4 kR is more appropriate and that the upper limit implied by 300 kR of D $L\alpha$ is about 5×10^{-3}. Bertaux and Clarke (1989b) suggest that the larger D/H ratio measured by Donahue *et al.* (1982) should produce observable limb brightening of the D $L\alpha$ emission and that a search of the data collected by the PV OUVS should reveal such a limb brightening.

According to Yung and DeMore (1982), the ratio of H_2 to H at the homopause is fixed by the photochemistry of H_2O in the mesosphere and should have a value of about 10%. For the VIRA standard noon model, an extrapolation of the H densities downward to 130 km, the approximate altitude of the H homopause, yields a mixing ratio of about 3 ppm, although this extrapolation, like that for He, is extremely sensitive to the assumed value of the eddy fissuion coefficient and should not be considered accurate to more than a factor of 2–3. The mixing ratio of H_2 at the homopause would, therefore, be about 0.3 ppm.

H_2 has been measured below the cloud tops by the PV large probe gas chromatograph (LGC). The mixing ratio appears to decrease toward the surface; the reported values at 52, 42, and 22 km are 200, 70, and 10 ppm. The gas chromatographs on Veneras 13 and 14 had a threshold sensitivity for detection of H_2 of 0.8 ppm. A value of 25 ppm was measured within the clouds for the altitude range 49–58 km (Mukhin *et al.*, 1983).

The mesospheric photochemical models of Yung and DeMore (1982) and Yatteau (1983) required much lower mixing ratios of H_2 above the cloud tops than were measured in or below the clouds or derived from the chemistry of H_2^+ at the homopause

by Kumar *et al.* (1981). The catalytic processes that recombine CO and O in the lower atmosphere of Venus are assumed to involve odd-chlorine compounds, rather than odd hydrogen as in the Martian atmosphere, where the abundance of water vapor is larger (see Section 3.11). H_2 renders Cl ineffective as a catalyst because the reaction

$$H_2 + Cl \rightarrow HCl + H \tag{56}$$
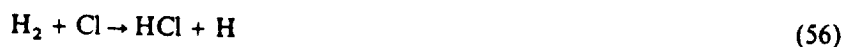
produces HCl, which is a relatively unreactive 'reservoir' species for odd chlorine. Yung and DeMore presented three models that differed mainly in the mixing ratio of H_2; values of 20 ppm, 0.5 ppm, and 1×10^{-7} ppm were tested. Only the extremely hydrogen-deficient model could account for the observed nighttime depletion of CO near the cloud tops reported by Schloerb *et al.* (1980), Wilson *et al.* (1981), and Clancy *et al.* (1981) from microwave observations.

Other problems with these models have, however, become apparent. First of all, as Krasnopol'sky and Parshev (1983) have noted, a constant mixing ratio of 1 ppm H_2O was used over the entire mesosphere, in contrast to the PV orbiter infrared radiometer (OIR) measurements, which show that, near the cloud tops at least, the mesosphere is not as dry as assumed. Second, some of the O_2 production reactions involving odd chlorine that were proposed to lead to production of $O_2(a^1\Delta_g)$, explaining the observed strong 1.27 μ emission have been shown, by Yung and coworkers, to produce $O_2(a^1\Delta_g)$ very inefficiently (see Section 3.11). It also appears that the diurnal variation of CO in the Venus mesosphere is more complicated than early microwave observations indicated. Clancy and Muhleman (1985a) showed that the CO mixing ratio in the altitude range 80–90 km is depleted by a factor of 2–4, but at 95 km is *enhanced* by a factor of 2–4 on the nightside relative to the dayside. The maximum in the 80–90 km region occurs in the early morning rather than at mid-day. Clancy and Muhleman (1985b) have, however, proposed that the midnight bulge above 90 km is a result of the sub-solar to anti-solar circulation rather than a photochemical effect. Nonetheless, it appears that the photochemical processes that voern the recombination of O and CO and the destruction of O_2 are not yet well understood.

4.4. H_2O DENSITIES

The abundance of water is unknown in the thermosphere of Venus and controversial in the lower atmosphere. Below the cloud tops, the Venera 9 and 10 narrow-band photometry measurements imply an H_2O mixing ratio of 300 ppm, accurate to within a factor of 2 in the altitude range 20–40 km (Ustinov and Moroz, 1978). The Venera 11 and 12 descent probes carried scanning infrared spectrophotometers that recorded the spectrum of the Venus daytime sky. Synthetic spectra constructed by Moroz *et al.* (1980) indicated that the H_2O abundance is about 20 ppm near the surface increasing to 200 ppm in the clouds. From measurements made by the net flux radiometers on the four PV probes, Revercomb *et al.* (1985) have reported that the water abundance below the clouds varies with latitude, with mixing ratio of 20 to 50 ppm at 60° increasing to about 500 ppm at the equator. The gas analyzers aboard the Soviet Vega 1 and 2 spacecraft indicated that the water vapor is concentrated in a 30 km layer centered at

40 km, with a maximum mixing ratio on the order of 1000 ppm at about 50 km, decreasing to about 20 ppm near the surface (Surkov *et al.*, 1987).

For the atmosphere above the cloud tops, ground-based infrared absorption measurements have indicated an H_2O mixing ratio of 1 ppm (Fink *et al.*, 1972; Barker, 1975). Subsequently space probes have yielded conflicitng results. In the cloud layer, from 49 to 58 km, the gas chromatography experiments on Veneras 13 and 14 yielded a value of 700 ± 300 ppm (Mukhin *et al.*, 1983). The mixing ratios measured by the Vega gas analyzers appear to decrease over the altitude range 60 to 75 km, with values in the range 1–100 ppm (Surkov *et al.*, 1987). The error bars, however, are more than a factor of 10 near 75 km. Above about 65 km the PV OIR showed a large diurnal variation in the water vapor abundance from about 100 ppm in the early afternoon to less than the detection threshold of 6 ppm at night (Schofield *et al.*, 1982). The abundance near the cloud tops is probably determined by the saturated vapor pressure of H_2O over sulfuric acid and should decrease with increasing altitude. Krasnopol'sky (1985) has computed a sulfuric acid 'trap function', which relates the water vapor and H mixing ratios at 90 km to that in the lower atmosphere. For an assumed lower atmosphere mixing ratio of 200 ppm, the mixng ratio of H_2O is about 0.5 ppm at 90 km and that of all H-containing compounds is about 3 ppm.

4.5. DIFFUSION LIMIT FOR ESCAPE OF H

On Venus, the atmosphere above the cloud tops, the mesosophere, has generally been chosen as the region in which to evaluate the ixing ratio of H-containing compounds, in order to calculate the diffusion limiting upward flux of H (Hunten and Donahue, 1976; Walker, 1977). The mixing ratio of HCl has been determined from ground-based infrared absorption measurements to be about 0.6 ppm (Connes *et al.*, 1967). In view of the influence of the clouds, care must be exercised in choosing the altitude range for determining the abundance of water vapor. Krasnopol'sky (1985) asserts that sulfuric acid affects the H_2O mixing ratio up to about 75 km, so the abundance at the cloud tops is not an appmropriate value to use in computing the diffusion limited flux. The abundance of H_2 in the clouds has been reported as 25 ppm by Mukhin *et al.* (1983) from Venera 13 and 14 gas chromatography, but mesospheric models cannot accommodate such large mixing ratios (Yung and DeMore, 1982; Yatteau, 1983). If it is assumed that the abundance of H_2 above the cloud tops is negligible, and that the abundance of H_2O above 75 km is 1 ppm, then the total abundance of H is 2.6 ppm. This is good agreement with the H-mixing ratio extrapolated to the H homopause at about 130 km of about 3 ppm, but the latter value is accurate to not better than a factor of 2.

In order to compute the flux through the homopause, the binary collision parameter $(b = Dn_T)$ must be evaluated. We assume here that the major form of H at the homopause is atomic hydrogen. The diffusion coefficient of H through the atmosphere can be computed as a suitable average of the binary diffusion coefficients for H through each of the major atmospheris constituents (cf. Chamberlain and Hunten, 1987). The values of the diffusion coefficents assumed are shown in Table IX. The diffusion coefficients of H through N_2 is taken from Banks and Kockarts (1973), and is taken

TABLE IX

Parameters A and s used to compute diffusion coefficients for H through the major gases in the Venus thermosphere. The diffusion coefficient in $cm^2 s^{-1}$ is given by $D = AT^s/n_T$, if the temperature T is in K and the total density n_T is in cm^{-3}.

System	A ($10^{17} cm^{-1} s^{-1} K^{-s}$)	s
H-O[a]	7.25	0.71
H-CO$_2$[b]	3.87	0.711
H-N$_2$[c]	4.87	0.698
H-CO[d]	4.87	0.698

[a] Cooper *et al.* (1984).
[b] Obtained by scaling the values for H-O$_2$ from Banks and Kockarts (1973) for the larger mass and radius of CO$_2$.
[c] Banks and Kockarts (1973).
[d] Assumed the same as for H-N$_2$.

to be the same as that for H–CO. The H–CO$_2$ diffusion coeficient was estimated by scaling D for H–O$_2$ for the larger mass and radius of CO$_2$ compared to O$_2$ (cf. Banks and Kockarts, 1973). The H–O diffusion coefficient is taken from the calculation of Cooper *et al.* (1984). The average value for b_H at 130 km in the VIRA dayside model is $1.8 \times 10^{19} cm^{-1} s^{-1}$, and the diffusion limited flux is $9.0 \times 10^7 cm^{-2} s^{-1}$. If the mixing ratio of H$_2$ is as large as 25 ppm in the mesosphere, and we consider this to be unlikely, the diffusion-limited flux could exceed $10^9 cm^{-2} s^{-1}$.

4.6. MODELS OF HOT AND ESCAPING HYDROGEN

McElroy and Hunten (1969) showed that the Mariner 5 Lα data implied a Jeans escape flux for H of only about $6 \times 10^5 cm^{-2} s^{-1}$, for assumed exospheric temperature of about 700 K. The exospheric temperature is now known to be less than 300 K and the magnitude of the thermal escape flux has been shown to be negligible (see Section 4.1); subsequently the bulk of the escape has been assumed to arise from non-thermal mechanisms. Kumar and Hunten (1974) evaluated several sources of hot hydrogen, H*, including momentum transfer from the solar wind to the atmospheric gases, resonant charge transfer from H$^+$ to H

$$H^+ + H \rightarrow H^* + H^+ ,\tag{57}$$

and the near-resonant process

$$H^+ + O \rightarrow H^* + O^+ .\tag{58}$$

Since ion temperatures are higher than neutral temperatures at high altitudes, the neutral H formed in these reactions will be hotter than thermal. For an H$_2$ abundance of 1–2 ppm at the homopause, the major source of energetic hydrogen atoms was reaction (54), which is followed by dissociative recombination

$$OH^+ + e \rightarrow O + H .\tag{59}$$

Chamberlain (1977) did the first detailed model calculations of the Venus exosphere, in which he attempted to reproduce the distribution of hot H inferred from Mariner 5 $L\alpha$ measurements, based on charge exchange of H^{+*} with thermal H (reaction (57)) as the source of H^*. Assuming a spherically-symmetric exosphere, he solved Liouville's equation (the collisionless Boltzmann equation) for the distribution of H and found that a higher ionopause than observed was necessary to reproduce the inferred densities. The ionopause has, however, been found from Pioneer Venus measurements to be highly variable (Taylor et al., 1979). An escape flux of 2×10^7 H atoms $cm^{-2} s^{-1}$ was derived.

The Venera 9 and 10 $L\alpha$ line shape measurements showed that the temperature increase abruptly near an altitude of 3000 km, from which Bertaux et al. (1978) inferred that the hot H is not generated near the exobase. They preferred charge exchange from solar wind protons as the source of hot H. Kumar et al. (1978), however, argued that the experiment could not distinguish an increase in temperature from a net Doppler shift.

Kumar et al. (1978) evaluated the proposed sources of non-thermal H atoms and concluded that reactions (54) and (59) were the most important sources. The production of CO_2H^+ in reaction (55) followed by dissociative recombination of the ion

$$CO_2H^+ + e \rightarrow CO_2 + H \tag{60}$$
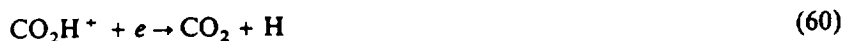
would also provide a significant, but lower altitude source of H atoms. In order to reconcile these large sources with the low thermospheric densities of H inferred from Mariner 5 and 10 data. Mayr et al. (1978) proposed that the H atoms created in this process are swept to the nightside by thermospheric winds. Kumar et al. found that the dayside densities could be reduced by a factor of 1000 by this process. An evaluation of the escape rates due to the various processes led to the conclusion that the largest source of escaping H atoms was charge exchange with solar wind protons followed by reacceleration of the newly formed low-energy protons. An escape flux of 10^7 H atoms $cm^{-2} s^{-1}$ was derived.

Cravens et al. (1980) presented the first model of the Mariner 5 hot hydrogen distribution based on atmospheric and ionospheric structure information from Pioneer Venus. Using a two-stream approach to evaluate the fluxes and densities of hot H at the exobase, they showed that the unexpectedly hot and dense nightside corona results from the high ion temperatures and densities observed by the PV orbiter (e.g., Taylor et al., 1980; Miller et al., 1980; Knudsen et al., 1979). They found that half the source of hot H was due to charge exchange from H^+ and O^+ (reactions (57) and (58)), and, for the H_2 densities adopted, half was due to the reaction of O^+ with H_2 (reaction (54)). Only preliminary data about the pre-dawn H bulge was available, so the importance of reaction (57) was underestimated for the nightside; the H_2 densities in their model were taken from Kumar and Hunten (1974), so the importance of reaction (45) was overestimated. Hodges and Tinsley (1981), however, found that charge exchange alone was sufficient to explain the Mariner 5 and 10 $L\alpha$ profiles. They constructed a 3-D (non-spherically symmetric) Monte-Carlo model of the Venus densities and temperatures, and found that the most important source is the charge exchange from O^+ contributing only near the exobase. They criticized the hot H source proposed by Bertaux et al.

(1978), charge exchange from solar wind protons, as requiring the deceleration of solar wind neutralized protons from 400 km s^{-1} to sub-escape speeds and concluded that the magnitude of this source of hot H was negligible. The charge exchange sources adequately reproduced the day/night ratios of the hot H concentrations and scale heights. A factor of 2 uncertainty in the hot hydrogen measurements did not, however, exclude the presence of another source, such as reaction (54). The computed global average escape rate from charge exchange was about 1.8×10^7 cm^{-2} s^{-1}. Kumar *et al.* (1981) predicted an escape rate of 1×10^8 cm^{-2} s^{-1} from reaction (54) based on the H_2 densities they derived from the assumption that the mass-2 ion was H_2^+.

The D/H ratio measured by Donahue *et al.* (1982), and inferred from the D^+/H^+ ratio, an enhancement of a factor of 100 over the terrestrial value, was interpreted as implying at least a hundred-fold depletion of the initial H inventory of the planet over the age of the solar system. Donahue *et al.* argued that most non-thermal escape mechanisms discriminate against D, but when the abundance of H_2 was enhanced by a factor of 100, hydrodynamic escape would take over, so the initial abundance of water vapor may be much larger than required by the D/H ratio. Hydrodynamic or transonic escape, also called *blow-off*, is a thermal loss process in which the atmosphere expands rapidly outward. The high frequency of collisions renders the process describable by the macroscopic theory of fluid dynamics, rather than by the microscopic kinetic theory. The dynamics of atmospheres undergoing hydrodynamic blow-off of hydrogen have been discussed by Watson *et al.* (1981) and the salient features of hydrodynamic escape have been reviewed by Hunten (1973b, 1982). Mass fractionation in hydrodynamic escape may be large, but the process is not as mass-selective as Jeans escape (Zahnle and Kasting, 1986; Hunten *et al.*, 1987). Blow-off becomes an appropriate description of the escape process above the altitude where λ, the reduced gravitational potential energy, is about 2. At this altitude, the rate of expansion of the atmosphere reaches the speed of sound; alternatively, the average thermal velocity of a molecule is approximately equal to the escape velocity. Hydrodynamic escape thus becomes the major escape mechanism if and when the $\lambda = 2$ level moves below the exobase (Walker, 1982).

McElroy *et al.* (1982) suggested another non-thermal mechanism for the escape of hydrogen that discriminates almost completely against deuterium: reaction with hot O produced in dissociative recombination of O_2^+ at the exobase. This process, which was first suggested for He and H escape from Mars by Knudsen (1973), can be represented by

$$O_2^+ + e \rightarrow O^* + O^* \tag{61}$$

followed by

$$O^* + H \rightarrow O + H^*. \tag{62}$$
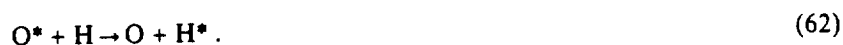
Using a Monte-Carlo method and assuming isotropic scattering, McElroy *et al.* computed the fraction of collisions (reaction (62)) leading to H atoms with energies greater than the escape energy as 15% for an O^* with initial velocity of 5.6 km s^{-1} (2.6 eV) colliding with a 300 K H-atom. A planetary average H atom escape rate due to
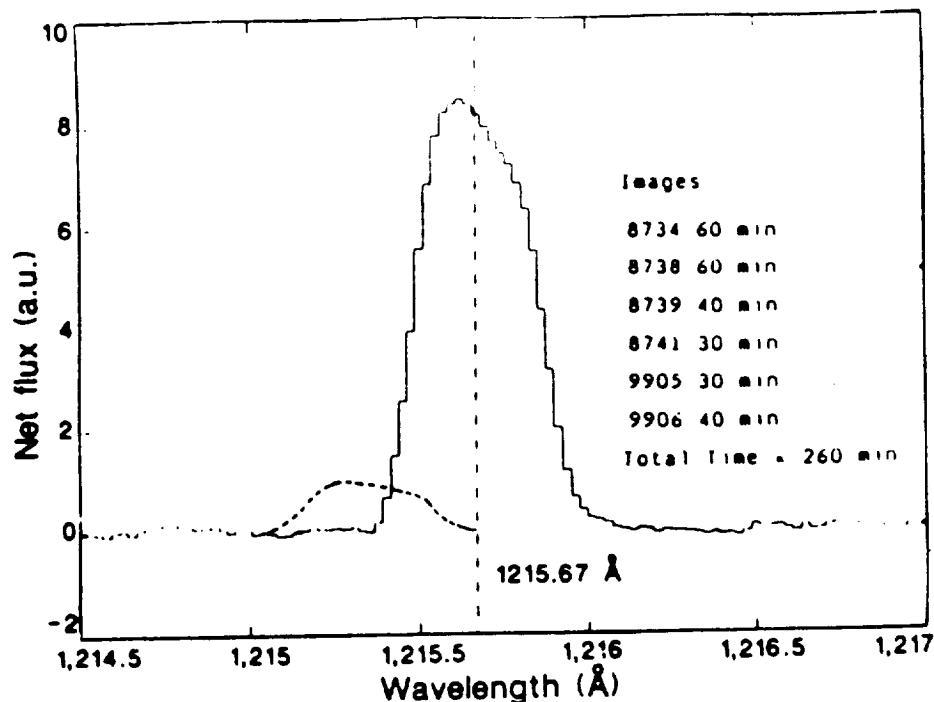
Fig. 26. Hydrogen Lα spectra of bright disk emission from Venus obtained with the IUE large aperture and summing the six best images (solid line). The line intensity corresponds to 21 x 10^3 R; the long-dashed line shows the line center. The short-dashed line shows the profile calculated for deuterium Lyman alpha emissions of 2.5 x 10^3 R (corresponding to a D/H ratio of 1.6 x 10^{-2}). The numbers refer to spectra reference numbers and exposure times. AU denotes 10^5 IUE flux units. Taken from Bertaux and Clarke (1989).

reaction (62) of 8 x 10^6 cm^{-2} s^{-1} was obtained. Much smaller escape rates due to charge transfer from H$^+$ (reactions (57) and (58)) were obtained, due partly to the assumption of a low (2000 K) ion temperature, compared to PV values, especially on the nioghtside, where ion temperatures have been shown to exceed 5000 K (Miller et al., 1980).

The escape fraction in reaction (62) computed by McElroy et al. (1982) was shown to be overestimated by Cooper et al. (1984), who derived a general formula for the rate coefficient for the production of a particle with a specific energy colliding with the atoms of a thermal gas. The cross sections for O–H elastic scattering were computed using semi-empirical and theoretical interaction potentials, and the effect of the anisotropy of the scattering was included. Figure 27 shows their calculated frequency of production of a hydrogen atoms with various kinetic energies upon collision with an O-atom traveling at 5.6 km s^{-1}. The computed fractions of escaping H-atoms were 5.1, 6.9, and 8.5% for temperatures of 100, 200, and 300 K, respectively, about half the values computed by McElroy et al. (1982). In addition, the O-atom velocity of 5.6 km s^{-1} used in the calculations of McElroy et al. was computed assuming that the dissociative
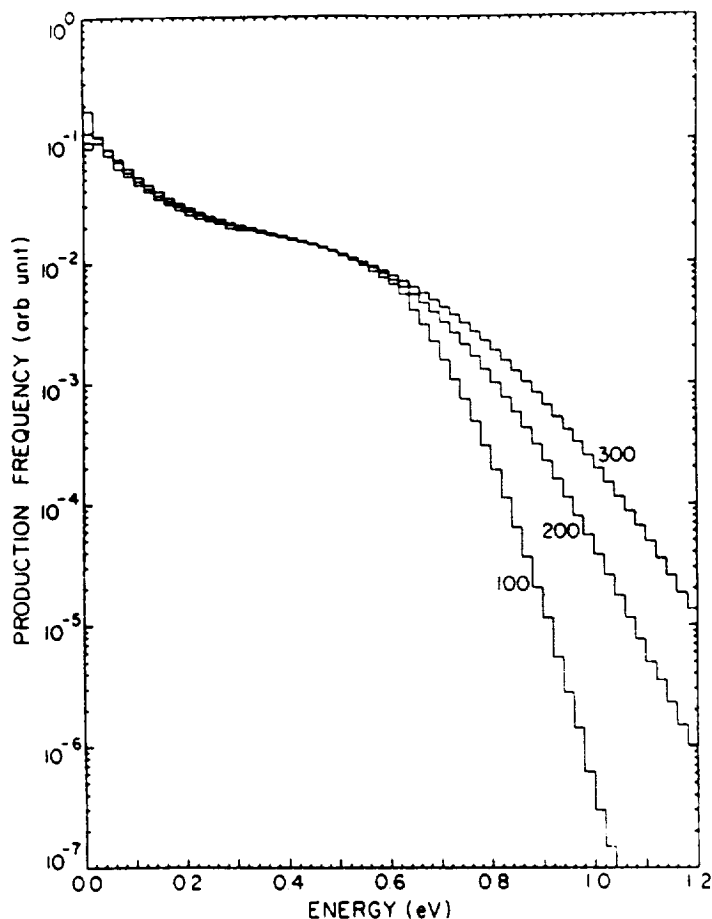
Fig. 27.   The frequency with which a hydrogen atom with energy E is produced in collision with a 2.5 eV oxygen atom at temperatures of 100, 200, and 300 K. Taken from Cooper *et al.* (1984).

recombination of O_2^+ produces one $O(^1D)$ and one $O(^3P)$ atom. As pointed out in Section 3.2, it has become clear from calculations and measurements that the yields of excited stated in DR of O_2^+ (v) depend on the vibrational level, v (e.g., Guberman, 1987, 1988; Bates and Zipf, 1980). Further discussion will be deferred to the discussion of the hot O corona in Section 4.7.

Rodriguez *et al.* (1984) computed the exospheric distribution and escape rates of H by an approximate numerical solution to the time-independent Boltzmann equation. The model parameters were based on PV data, including the pre-dawn bulge in the H densities inferred by Brinton *et al.* (1980), and the high ion temperatures measured by the ORPA (Miller *et al.*, 1980). Alternative O_2^+ densities were taken from the PV OIMS measurements (Taylor *et al.*, 1980) and the PV orbiter radio occultation (ORO) profiles (Kliore *et al.*, 1979). The H_2 abundance was assumed to be less than 0.5 ppm, in accord with the mesospheric photochemical models (Yatteau, 1983; Yung and DeMore, 1982).

A more realistic cross section for O^*-H elastic scattering was employed, similar to that computed by Cooper *et al.* (1984). The assumed exobase altitudes, 190 km and 150 km on the day- and nightsides, respectively, are somewhat lower than those used by other workers and computed here (see Section 4.1). Rodriguez *et al.* found that collisions with hot O (reaction (62)) and H^+-H charge transfer (reaction (57)) were comparable sources of hot hydrogen, with the latter contributing more to escape. On the nightside, if the OIMS measurements were used for the densities of O_2^+, reaction (62) was found to produce adequate hot hydrogen; if the ORO densities, which are significantly smaller than the OIMS values, were used, it was necessary to include reaction (57). An average escape flux of about 10^7 cm^{-2} s^{-1} was computed.

Hodges and Tinsley (1986) investigated the effect of $H-H^+$ charge exchange on the velocity distribution and escape of exospheric H in an update of their previous three-dimensional Monte-Carlo model of the Venus exosphere (Hodges and Tinsley, 1981). Their computed exospheric H-atom densities, presented as a function of solar hour angle, show that, due to lateral transport, at increasing planeto-centric distances, the pre-dawn bulge becomes less pronounced; outward of 8000 km, the distribution becomes nearly spherically symmetric. Hodges and Tinsley (1986) suggest that a measurement of the line profiles of Lα due to resonance scattering of solar photons should carry a signature of their source; they have computed the Lα line profiles for the charge exchange source of hot H. The profiles are essentially a superposition of a narrow and a broad Gaussian, corresponding to the thermal and hot hydrogen components, with asymmetries due to escape and lateral flow. An average planetary escape rate due to charge exchange of 2.8×10^7 cm^{-2} s^{-1} was computed.

Bishop (1989) has discussed modifications to the exospheric distribution and escape that result from radiation pressure due to resonance scattering of solar Lα. The effects on the distribution of H are largely confined to distances from the center of Venus greater than two Venus radii, where densities are small. A small increase in the hydrogen escape flux of 2×10^6 cm s^{-1} was computed.

The most comprehensive global model of non-thermal escape mechanisms and their evolution through the history of the planet is that of Kumar *et al.* (1983). The sources of ht H that they considered included charge-exchange of H^+ with H and impact of hot O with H. Their calculations for the production rates due to the reaction of O^+ with H_2 were contingent upon the identification of the mass-2 ion as H_2^+ rather than D^+, the currently accepted identification. The pre-dawn bulge region of the atmosphere was used as an indication of the structure of the thermosphere-ionosphere at earlier times, when the hydrogen abundance was larger. At present, the most important source of hot H is charge exchange of H^+-H (reaction (57)), with a global average escape rate of 1.2×10^7 cm^{-2} s^{-1}, and most of the flux occurs over the nightside hemisphere. Impact of hot O with H is slightly less important; the global average escape rate is 8×10^6 cm^{-2} s^{-1}. At earlier times, the importance of this source declines as the H abundances increases and the exobase rises above the O_2^+ peak. Figure 28 shows the evolution of the H escape flux due to various mechanisms as a function of the atomic hydrogen mixing ratio. The calculations of Kumar *et al.* show that when the M mixing
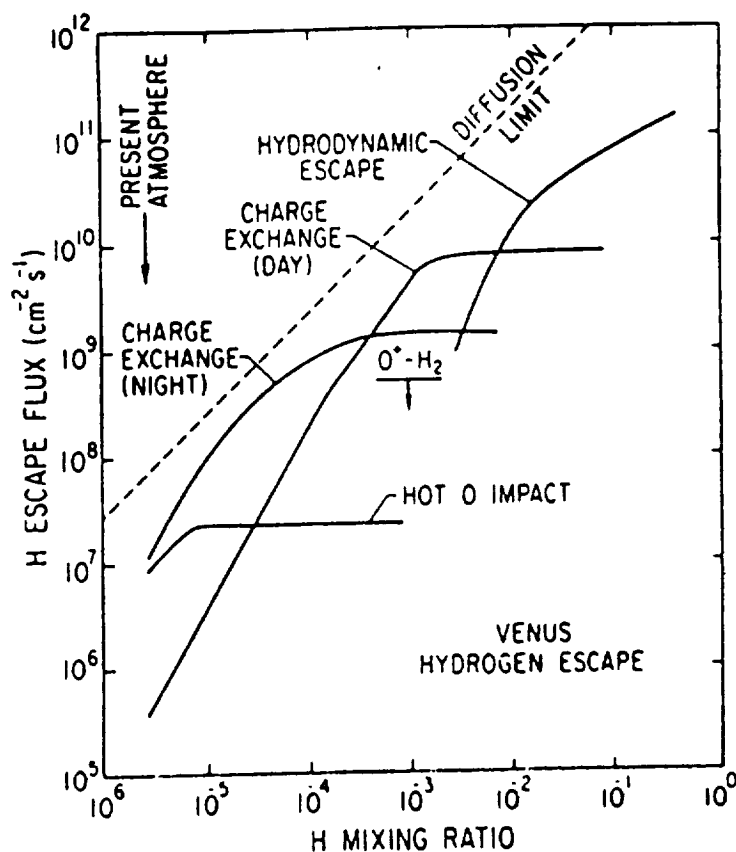
Fig. 28. Hydrogen atom escape flux on Venus as a function of H mixing ratio at the homopause is shown for various escape mechanisms. This H mixing ratio is equivalent to twice the H_2O vapor mixing ratio at the cold trap. The H mixing ratio at the homopause for the present atmosphere is 2.5×10^{-6}. Taken from Kumar et al. (1983).

ratio reaches 2×10^{-3}, the H density determines the exobase level and the escape rate of H levels off at a maximum value of $7.5 \times 10^9 \, cm^{-2} \, s^{-1}$. When the mixing ratio of H exceeds a value near 8×10^{-3}, a transition from non-thermal escape to hydrodynamic escape takes place.

Escape fluxes of H may be derived if the density profile of H below the exobase is known, because the actual scale height is slightly smaller than the diffusive equilibrium value. From $L\alpha$ profiles recorded by the PV OUVS, Paxton et al. (1988) deduced a value of $7.5 \pm 1.5 \times 10^7 \, cm^{-2} \, s^{-1}$ for the flux of H through the exobase near the sub-solar point. The model calculations discussed above show that the escape flux is a quarter to a third of this value. The remainder of this flux could be accounted for by the sub-solar to anti-solar circulation, and it would be balanced by a downward flux on the nightside.

Detailed models for the evolution of the Venus atmosphere have been presented by Watson et al. (1981), Kasting and Pollack (1983), and Watson et al. (1984). These

models assume that the ultimate source of the escaping hydrogen is water vapor, the predicted initial abundance of which is, therefore, much greater than at present. Toward earlier times, the larger amount of water vapor in the atmosphere increases the infrared opacity and causes the tropospheric temperature to rise. A critical value of the insolation exists for which liquid water cannot exist on the surface and the evaporation of the water produces a run-away greenhouse (Ingersoll, 1969). The insolation at Venus is proposed to be above the critical value. Kasting et al. (1984) showed that an increase in the water vapor mixing ratio also causes a decrease in the tropospheric lapse rate, causing the cold-trap to move to higher altitudes and lower pressures. The resulting increase in the mixing ratio of water vapor at high altitudes, the parameter that determines the atomic hydrogen escape rate, is dramatic. The predicted initial water abundance varies greatlyn from one model to another, depending on such factors as the mixing ratio of onset of hydrodynamic escape, the H/D fractionation factor during such escape, the magnitude of the hydrodynamic escape fl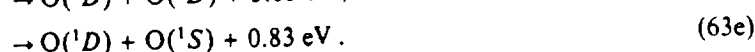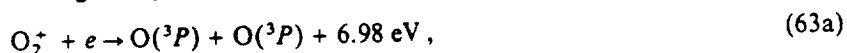ux (which depends on assumptions made about the magnitude of the solar flux in the past), and the outgassing rate of volatiles from the interior (e.g., Watson et al., 1981, 1984; Donahue et al., 1982; Kasting and Pollack, 1983; Kumar et al., 1983).

An alternative scenario has been proposed by Grinspoon and Lewis (1988). The current abundance of water vapor in the atmosphere could be in steady state as a result of a balance between loss by escape of H and a cometary source. As in the case of continuous slow outgassing, an enhanced D/H ratio could result from this exogenous source, but the value depends on the assumed rate of impact of large comets, which is somewhat stochastic and difficut to estimate. Nevertheless, a large initial abundance of water may not be necessary to explain the enhanced D/H ratio.

A detailed discussion of atmospheric evolution is beyond the scope of this review. The interested reader is referred to a review of the evolution of the atmosphere of Venus presented by Donahue and Pollack (1983) and to a book on the origin and evolution of planetary atmospheres (Atreya et al., 1989), especially to the articles by Hunten et al. (1989) and Kasting and Toon (1989) contained therein.

4.7. HOT OXYGEN CORONA

Dissociative recombination of molecular ions produces energetic fragments that are important to the thermal structure, coronas and escape from planetary atmospheres. A short review of the importance of dissociative recombination in aeronomy has been presented by Fox (1989a). Dissociative recombination of O_2^+ can proceed according to a number of energetically allowed channels, with exothermicities as:

$$O_2^+ + e \rightarrow O(^3P) + O(^3P) + 6.98\,\text{eV}, \tag{63a}$$

$$\rightarrow O(^1D) + O(^3P) + 5.02\,\text{eV}, \tag{63b}$$

$$\rightarrow O(^1S) + O(^3P) + 2.79\,\text{eV}, \tag{63c}$$

$$\rightarrow O(^1D) + O(^1D) + 3.05\,\text{eV}, \tag{63d}$$

$$\rightarrow O(^1D) + O(^1S) + 0.83\,\text{eV}. \tag{63e}$$

Since the escape energy per unit mass for Venus is 0.54 eV amu^{-1}, none of the channels produce oxygen atoms with enough energy to escape the gravitational field of the planet. Oxygen atoms produced above the exobase will, however, travel along ballistic trajectories in the exosphere, producing a corona of hot oxygen atoms, similar to the hot hydrogen corona. A hot oxygen corona has been observed to surround the Earth (Yee et al., 1980; Yee and Hays, 1980) and the density distribution has been modeled by Yee et al. (1980). The existence of hot oxygen coronas around Venus and Mars were predicted by Wallis (1978). The corona has a significant effect on the interaction of the planet with the solar wind (e.g., Biermann et al., 1967; Wallis, 1972, 1978, 1982). A review of hydrogen and oxygen coronas of Venus and Mars has been presented by Nagy (1989).

Bertaux et al. (1981) reported the existence of 'a strange feature' in the intensity profile recorded at 1304 Å by the spectrophotometer on Venera 11. Over a range of about 5000 km beyond the bright limb, a nearly constant intensity of about 500 R was measured. Because this feature was not observed by Venera 12, it was tentatively interpreted as being due to the presence of 'a sporadic hot component of exospheric oxygen', and an average density of 1.6×10^3 cm^{-3} was inferred.

Limb scans of the PV OUVS also showed the existence of an exospheric signal at 1304 Å (Nagy et al., 1981). The oxygen atom density profiles derived from the intensities exhibit two scale heights, corresponding to an inner thermal component and an outer hot component. The hot component, shown in Figure 29, dominates beyond an altitude of about 350 km, where the O density is about 5×10^4 cm^{-3}. The scale height of the
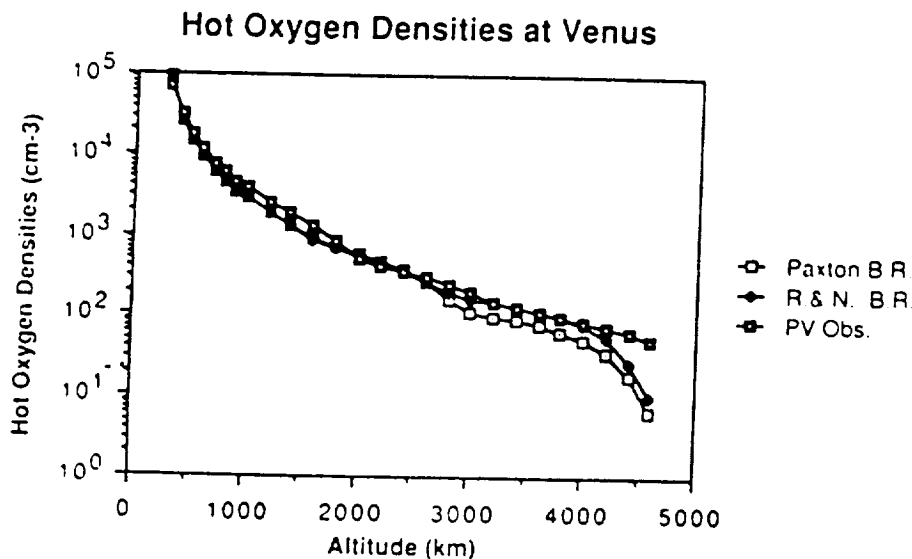

Fig. 29. Measured and calculated hot oxygen densities at Venus for different branching ratios in the dissociative recombination of O_2^+ (reactions 63). 'Paxton B.R.' denotes branching ratios from Paxton (1983). 'R & N B.R.' denotes branching ratios from Rohrbaugh and Nisbet (1973). The experimental values are derived from PV OUVS 1304 Å data. From Nagy and Cravens (1989).

hot component is approximately 400 km, indicating a 'temperature' of 6300 K. Nagy *et al.* (1981) constructed the first models of the hot O corona on both the dayside and the nightside using PV data. In addition to dissociative recombination of O_2^+, they considered the charge exchange processes

$$O^+ + O \rightarrow O^* + O^+ \tag{64}$$

and

$$O^+ + H \rightarrow O^* + H^+ , \tag{65}$$

as sources for the energetic oxygen, but found these reactions to be relatively unimportant. A modified two-stream approach, similar to that used in the hot hydrogen model (Cravens *et al.*, 1980) was used to compute the flux of O at the exobase; the exospheric distribution was then determined by solving Liouville's equation. Nagy *et al.* obtained hot O densities a factor of 4–5 larger than the densities derived from the PV measurements. The discrepancy was later attributed to the use of preliminary ion densities that were too high, and was resolved with the use of appropriate O_2^+ densities (Nagy and Cravens, 1988). The corrected calculated hot O density profile is shown also in Figure 29. In addition, the earlier paper (Nagy *et al.*, 1981) assumed very low exobase altitudes of 172 and 143 km on the day- and nightsides, respectively, compared to the values computed here, which would also tend to exaggerate the magnitude of the O source.

Reasonably successful models of the hot O corona were also presented by McElroy *et al.* (1982b) and by Paxton (1983). McElroy *et al.* (1982b) presented the first calculations of the hot O column density as a function of solar zenith angle from 0 to 90°. The results, presented here in Figure 30, show that the column density varies from about $3 \times 10^{12} \, \text{cm}^{-2}$ at the subsolar point to $1 \times 10^{12} \, \text{cm}^{-2}$ at the terminator.

Models of the hot oxygen corona depend on assumptions made about the relative importance of the channels (63a–e) in dissociative recombination of O_2^+. No definitive measurements of the yields of $O(^3P)$, $O(^1D)$, and $O(^1S)$ in dissociative recombination of the lower vibrational levels of $O_2^+(v)$ are available. It has become clear that the channel by which the dissociative recombination proceeds depends greatly on the vibrational state of the ion (Guberman, 1983, 1987, 1988; Bates and Zipf, 1980; Queffelec *et al.*, 1989). Zipf (1970) determined yields of 0.1 and 0.9 for $O(^1S)$ and $O(^1D)$, respectively, but these values were later withdrawn because the vibrational distribution of O_2^+ in the experiment was unknown. Guberman (1987, 1988) carried out *ab initio* calculations of the rate coefficients for production of $O(^1S)$ and $O(^1D)$ in dissociative recombination of O_2^+ in various vibrational levels. Some of the rate coefficients he obtained for a temperature of 300 K are shown in Table X. Specifically, he showed that the rate coefficient for production of $O(^1S)$ increases nearly two orders of magnitude from $v = 0$ to $v = 2$! Unfortunately, Guberman did not calculate the rate coefficient for the channel that leads to two ground state atoms (reaction (63a)), so the yields of excited states cannot be derived from his calculations alone. Recently, Queffelec *et al.* (1989) have studied the yields of ground and excited O atoms for $O_2^+(v)$ in vibrational levels
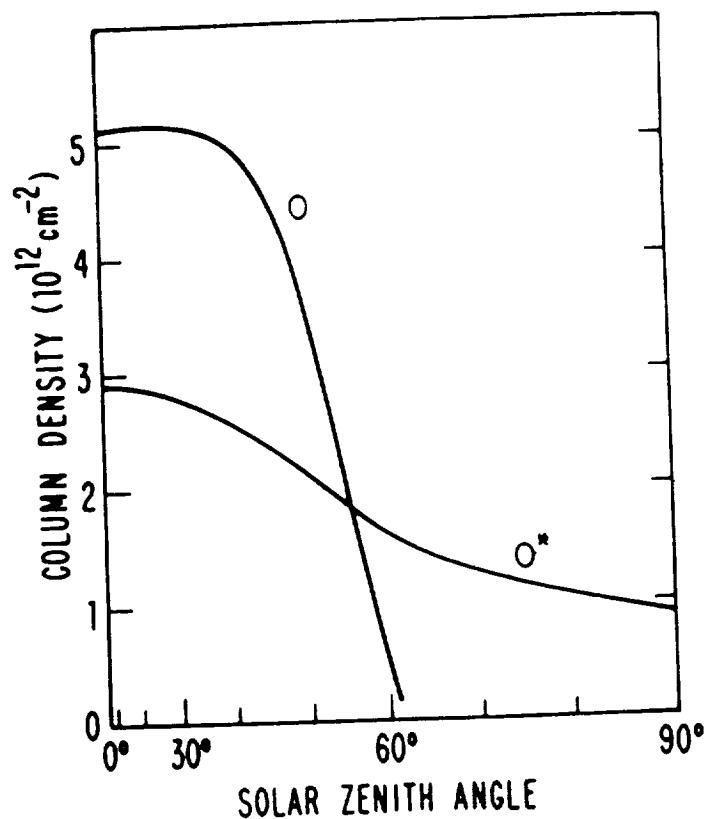
Fig. 30.   Column densities of neutral oxygen above Venus plasmapause as a function of solar zenith angle. The abscissa has been scaled in accord with fractional surface area. Thermal oxygen (O) and hot oxygen atoms (O*) contributed equally to the total amount of neutral O above the plasmapause, approximately 8×10^{30} atoms. Taken from McElroy *et al.* (1982b).

around $v = 9$ using a plasma flow tube experiment. The reported yields were 0.44, 1.0, and 0.56 for $O(^1S)$, $O(^1D)$ and $O(^3P)$, respectively. An average yield of about 0.1 was obtained for the yield of $O(^1S)$ in dissociative recombination of O_2^+ in an unknown distribution of vibrational levels 0, 1, and 2, in disagreement with Guberman's calcu-

TABLE X

Dissociative recombination coefficient ($cm^3 s^{-1}$) α for production of $O(^1D)$ and $O(^1S)$ from $O_2^+(v)$ in different vibrational levels at 300 K. From the *ab initio* calculations of Guberman (1987, 1988).

v	$\alpha(^1S)$	$\alpha(^1D)$
0	3.0×10^{-10}	2.2×10^{-7}
1	7.3×10^{-9}	1.8×10^{-7}
2	2.4×10^{-8}	1.2×10^{-7}

lations. The calculations of Guberman and the experimental study of Queffelec *et al.* (1989) do show, however, that the vibrational distribution of O_2^+ needs to be known in order to compute the production rates of excited states or the energy distribution of the O atoms.

Fox (1985) has modeled the vibrational distribution of O_2^+ in the thermosphere of Venus; at the exobase 55% of the O_2^+ ions are predicted to be vibrationally excited. Using the rate coefficients of Guberman and measured values for the total dissociative recombination rate, Fox (1990b) has computed the yields of the channels above and the fractions of O atoms with various energies produced at the exobase on Venus. The major uncertainty in this calculation is the yield of channel (63a), which is obtained as a difference between the measured total rate and the rates of the channels computed by Guberman. The total rate for dissociative recombination almost certainly depends on the vibrational level of O_2^+; that effect was only accounted for only by the choice of the rate coefficient of Mul and McGowan (1978) over that of Alge *et al.* (1983), since the merged beam experiments are expected to contain a larger fraction of vibrationally excited ions, and are therefore more appropriate to exobase altitudes, than flowing afterglow values, which pertain to thermalized conditions for temperatures of 200 to 600 K. The branching ratios for the channels (63a–e) derived from the model of Fox (1990b) are shown in Table XI, where they are compared to those assumed in other

TABLE XI

Yields of various channels in dissociative recombination of O_2^+ computed or assumed in calculations of the hot oxygen coronas

Channel	Energy (eV)	Yield			
		a	b	c	d
$^3P + {}^3P$	6.98	0.325	0.22	0.0	0.334
$^3P + {}^1D$	5.01	0.30	0.55	1.0	0.393
$^3P + {}^1S$	2.79	0.05	0.0	0.0	0.0
$^1D + {}^1D$	3.04	0.275	0.13	0.0	0.233
$^1D + {}^1S$	0.82	0.05	0.10	0.0	0.038

(a) Derived by Rohrbaugh and Nisbet (1973) from data of Zipf (1970). Used by Nagy *et al.* (1981) and Nagy and Cravens (1988).
(b) Determined by Paxton (1983) from a best fit to the PV OUVS hot oxygen data.
(c) Assumed by McElroy *et al.* (1982a).
(d) Derived by Fox (1990b) from calculations of Guberman (1987, 1988) and the measurements of Mul and McGowan (1979).

models. The branching ratios agree surprisingly well with those derived by Rohrbaugh and Nisbet (1973) from the measurements of Zipf (1970), that were used in the models of Nagy *et al.* (1981) and Nagy and Cravens (1988). The agreement is poorer with the values obtained by Paxton (1983), who varied the branching ratios to obtain agreement with the PV hot oxygen data. McElroy *et al.* (1982) assumed that all the dissociative

recombinations proceed by channel (63b). While this choice of branching ratios disagrees with those of other workers, the average energy of the O atoms is approximately correct, so fairly good agreement with experiment was obtained.

4.8. Escape of O

The large escape flux of H, the source of which is a putative large initial inventory of water or a continuous endogenous or exogenous source (see Section 4.6), raises the issue of the fate of the O atoms remaining behind, given the dearth of O_2 in the Venus atmosphere. The O atoms produced in dissociative recombination of O_2^+ are not energetic enough to escape on Venus, as they do above the Martian exobase. Most workers have assumed that the O atoms 'disappear' by oxidizing either crustal iron, Fe or Fe^{2+} to Fe^{3+}, or atomic carbon or CO rom the planet's initial endowment of volatiles to produce some of the CO_2 that is in the atmosphere today (McElroy *et al.*, 1982; Donahue *et al.*, 1982; Lewis and Prinn, 1984). Prinn (1985) has described some of the problems with these scenarios, which include the requirement that a fair fraction (1–3%) of the interior of Venus be exposed to the atmosphere over the first 0.3 billion years or so of its existence. Models of the evolution of the atmosphere indicate that the weathering process may be accelerated by the presence of liquid water on the surface (Kasting *et al.*, 1984) or by the presence of a molten surface due to a runaway greenhouse (Watson *et al.*, 1984).

McElroy *et al.* (1982b) and Wallis (1982) proposed that O escapes from the Venus atmosphere by photoionization and electron impact ionization of thermal and hot O above the plasmapause, and subsequent pick-up of O^+ by the solar wind. McElroy *et al.* estimated the total quantity of O atoms as 8×10^{30} and the loss rate about 6×10^6 cm^{-2} s^{-1}. They asserted that this escape flux was about half the escape flux of H, and that the escape rates of H and O are regulated by the oxidation state of the lower atmosphere. This analysis was, however, based on the H escape flux of 1.2×10^7 cm^{-2} s^{-1} computed by McElroy *et al.* (1982a), which is smaller by a factor of two or more than subsequent models indicate (see Section 4.6).

Recently, Luhmann and Kozyra (1990) have shown that approximately 90% of the O^+ ions created by photoionization above the plasmapause and picked up by the solar wind reimpact the planet, rather than being swept away. Significant and perhaps even enhanced escape still occurs due to sputtering of O atoms by the precipitating O. They computed a global loss rate of 2×10^{25} O atoms s^{-1} or an escape flux of 6×10^6 cm^{-2} s^{-1}, which is comparable to the escape flux computed by McElroy *et al.* (1982a).

4.10. C and N hot atom coronas

Paxton (1983) modeled the production rate of hot carbon due to knock-on from the hot O produced in dissociative recombination of O_2^+ near the exobase (reactions 63(a–e)):

$$O^* + C \rightarrow C^* + O . \qquad (66)$$

A smaller contribution, about 10% of that from reaction (66) was determined to arise

from dissociative recombination of CO^+:

$$CO^+ + e \rightarrow C^* + O^*. \tag{67}$$

The altitude distribution of C^* was derived from PV OUVS limb scans of the high altitude optically thin intensity at 1657 Å, assumed to arise from resonance scattering of solar radiation by atomic carbon. A C/O ratio of about 1% at the exobase was determined and the scale height of the altitude profile indicates a temperature that is approximately twice thermal.

Limb profiles of the signal at 1493 Å, a feature produced by resonance scattering of solar radiation by $N(^2D)$, were modeled by Paxton to determine the density distribution of hot $N(^2D)$ (Keating et al., 1985). The major source was determined to be dissociative recombination of N_2^+, with lesser contributions from dissociative recombination of NO^+ and knock-on from hot O.

4.10. He ESCAPE

Thermal escape of He from the atmosphere of Venus is negligibly small, but escape is possible by photoionization and electron impact ionization of He atoms above the ionopause, followed by pick-up of the resulting He^+ ions by the solar wind. Kumar and Broadfoot (1975) used Mariner 10 data to estimate an escape rate of 2×10^5 He atoms $cm^{-2} s^{-1}$ due to this source. This estimate was based on limited observations of the ionopause altitude, which has been found to be quite variable by PV observations (Taylor et al., 1979). Prather and McElroy (1983) have estimated the total escape rate as $1 \times 10^6 cm^{-2} s^{-1}$, with an accuracy of about $\pm 30\%$. It is interesting that they find that about 20% of the He above the ionopause is produced by knock-on from hot O, the process suggested by Knudsen (1973) for escape of He from Mars. Chassefiere et al. (1986) found, from Venera 11 and 12 observations of the He emission at 584 Å, that the abundance of He is a factor of two smaller than the value derived from PV data and, therefore, the estimated escape rate, $5 \times 10^5 cm^{-2} s^{-1}$, is also therefore smaller by a factor of 2.

In the terrestrial atmosphere, escape of ^{4}He is balanced by production in radioactive decay of uranium and thorium in the crust. The terrestrial escape flux is about $2 \times 10^6 cm^{-2} s^{-1}$ (MacDonald, 1963). Prather and McElroy conclude that the comparable magnitude of the sources of ^{4}He on Earth and Venus suggests comparable abundances of uranium and thorium and, along with independent data about other volatiles, indicates that Venus and Earth had similar origins.

5. Thermal Structure

5.1. GLOBAL MEAN HEAT BALANCE AND THERMAL STRUCTURE

The calculation of a reasonable dayside Venus mesosphere/thermosphere heat budget yielding observed temperatures has been an ongoing problem for nearly two decades. The difficulty is illustrated in Figure 31 (Keating and Bougher, 1987), which compares
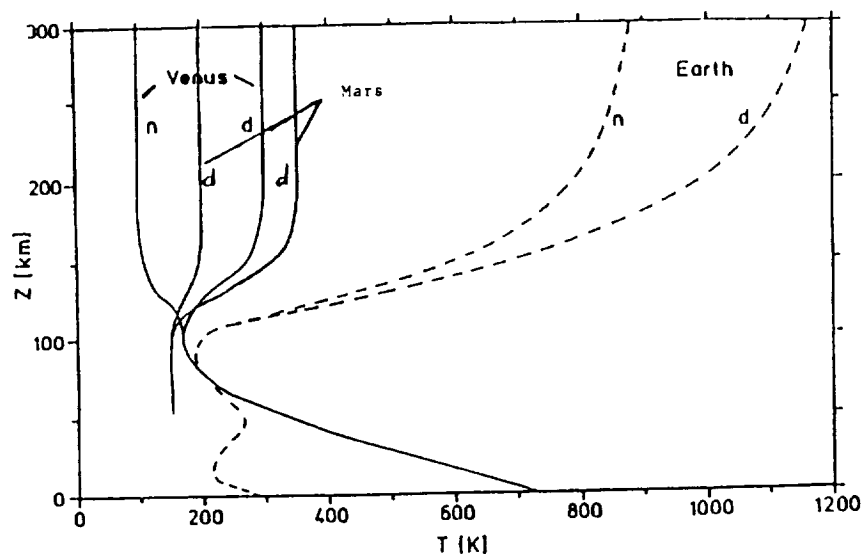
Fig. 31.   Temperatures of the neutral atmospheres of Earth, Venus, and Mars. Adapted from Schubert *et al.* (1983).

Venus, Earth, and Mars dayside thermospheric temperature profiles; Venus, although closest to the Sun, has the coldest temperatures above 100 km. This implies that, unlike the terrestrial thermosphere, a simple balance of EUV heat and molecular conduction may not be sufficient to maintain the observed relatively cold (≤ 300 K) temperatures. Several modeling efforts have attempted to determine what additional cooling mechanisms might be responsible. Uncertainties in the role of eddy conduction, the $O-CO_2$ collisional excitation rate, the EUV heating efficiencies, and the EUV solar fluxes themselves make the job very difficult. Recently additional constraints have been provided by the Pioneer Venus neutral thermospheric data, new laboratory measurements, and terrestrial modeling and observational efforts. Model simulations can be made in which EUV heating efficiency, CO_2 15-μm cooling, and eddy conduction are considered to be free model parameters. However, the range of realistic heating efficiencies reduces the possibilities considerably (see below).

5.2. EUV HEATING EFFICIENCIES

Heating due to the absorption of solar ultraviolet radiation occurs by photoionization and photodissociation. In photodissociation, the energy in excess of the dissociation threshold may be converted to internal or kinetic energy of the neutral fragments. Kinetic energy can be converted directly to heat through elastic collisions, or to internal energy through inelastic processes, such as collisional excitation of rotational or vibrational modes of molecules. Excited vibrational or electronic states may radiate, which results in cooling if the radiation escapes from the atmosphere, or they may be quenched, releasing their internal energies as heat; rotational energy is usually rapidly thermalized. In photoionization, the excess energy is carried away by the ejected electron, which can

produce further ionization, dissociation or excitation. Some of the chemical energy of the ions is released as heat in exothermic charge transfer reactions and ultimately in neutralization through dissociative recombination.

It is traditional and convenient to define the heating efficiency, ε, as the fraction of solar energy absorbed at an altitude that is converted locally to heat. Heating efficiencies for Venus were first computed by Henry and McElroy (1968). Their computed mean heating efficiency, about 60%, was based on the (incorrect) assumption that CO_2^+ was the major ion in the ionosphere. The predicted global mean exospheric temperature was about 700 K (McElroy, 1969). Stewart and Hogan (1969) estimated heating efficiencies about half that value from studies of the Martian thermosphere in which the heating efficiency was varied to reproduce the available data. They reasoned that the long Venus day would allow radiative equilibrium to be established on the dayside, so the computed (dayside) exospheric tempedrature was the same as McElroy's mean value (Hogan and Stewart, 1969). This contention was criticized by McElroy (1970), who pointed out that the Venus atmosphere could not sustain the large day–night density and temperature gradients.

In the years that followed, the exospheric temperature was determined to be much lower (≤ 300 K) than these early models indicated. Dickinson (1976) and Dickinson and Ridley (1977) computed 1-D and 2-D models of the thermal structure in the Venus thermosphere; they found that the low exospheric temperatures required very small values of the heating efficiency. They proposed that much of the energy involved in solar energy absorption would be taken up as vibrational and rotational excitation of CO_2, which has a larger number of degrees of freedom than the diatomic molecules that dominate the terrestrial atmosphere. Fox and Dalgarno (1981) computed heating efficiencies in the thermosphere for three models with different assumptions about the fraction of the excess energy that is converted to vibrational excitration in photodissociation and chemical reactions. In the standard model, for the assumption that 50% of the excess energy was converted to vibrational excitation, the heating efficiencies varied from about 18 to 22% over the altitude range from 115 to 235 km. Studies of the thermal structure of the Venus thermosphere in light of the knowledge gained from Pioneer Venus indicated that even heating efficiencies of that magnitude could not be accommodated and suggested that the heating efficiencies were on the order of 10% (Dickinson and Bougher, 1986; Hollenbach et al., 1985).

Fox (1988) considered the likelihood that 10% heating efficiencies could be justified from a molecular viewpoint. Both Hollenbach et al. and Dickinson and Bougher partially justified the low heating efficiencies by the assumption that 90% or more of the exothermicity of the quenching reaction

$$O(^1D) + CO_2 \rightarrow O(^3P) + CO_2 \tag{68}$$

is converted to vibrational excitation of CO_2. Fox adduced evidence that reaction (68) proceeds via a collision complex, which should produce statistical energy partitioning if the lifetime of the complex is long enough. The vibrational distribution that would be produced for statistical energy partitioning was computed by applying information

theory (e.g., Levine and Bernstein, 1974; Bernstein and Levine, 1975). It was found that only 55% of the excess energy appears as vibrational energy. An upper limit was determined from a survey of the literature, which indicated that a value of 75% would be high, but not unreasonable. After a consideration of the probable values and upper limits for energy deposited as vibrational excitation in photodissociation (about 25%, with an upper limit of about 35%) and chemical reactions (50–60%), and energy released in dissociative recombination of O_2^+, including a model of its vibrational distribution, altitude profiles of the heating rates, shown here in Figure 32, were
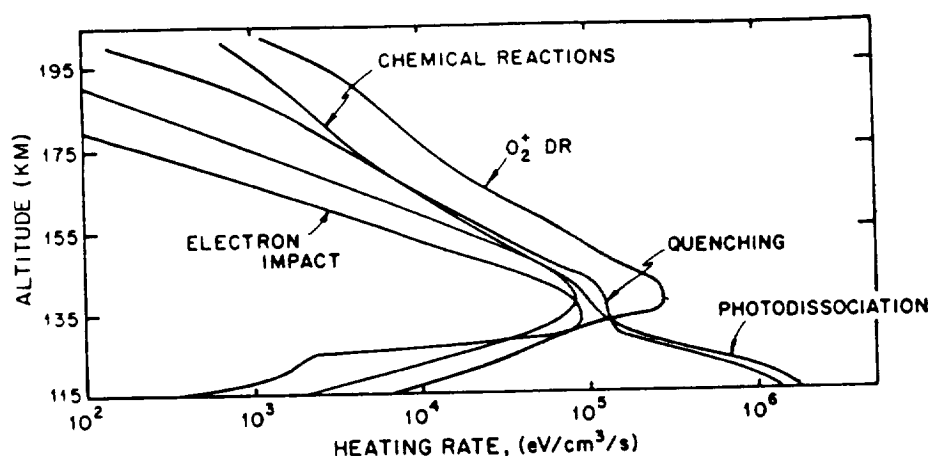
Fig. 32. Altitude profiles of heating rates due to the major source of neutral heating in the Venusian thermosphere from 115 to 200 km from the standard model, in which most probable values for the fraction of energy deposited as vibrational excitation in various elementary processes were employed (see text). Taken from Fox (1988).

computed. The major source of heating above about 130 km is dissociative recombination of O_2^+ (reaction (63)). Below that altitude, photodissociation and quenching of metastable electronic states are about equally important. Heating efficiencies for standard and lower limit models were computed and the results are shown in Figure 33. The standard model employs the probable values for the fraction of energy deposited as vibrational excitation in the processes discussed above and the lower limit model uses the upper limits for fraction of energy deposited as vibration excitation. Below 125 km, the heating efficiencies for the lower limit and standard models are about 16 and 22%, respectively, and above 130 km, they are 22 and 25%, respectively. The heating efficiencies are slightly higher and the difference between the standard and lower limit models is smaller than the calculations of Fox and Dalgarno (1981) indicate. Fox (1988) found that heating efficiencies on the order of 10% or less were difficult to justify with reasonable assumptions about molecular processes in the Venus thermosphere.

The F1 ion density peak at 140 km ($\tau = 1$ for EUV), composed mostly of O_2^+, should correspond closely to the maximum in per volume (eV cm^{-3} s^{-1}) heating if O_2^+ dissociative recombination and related ion-neutral chemical reactions dominate other heating
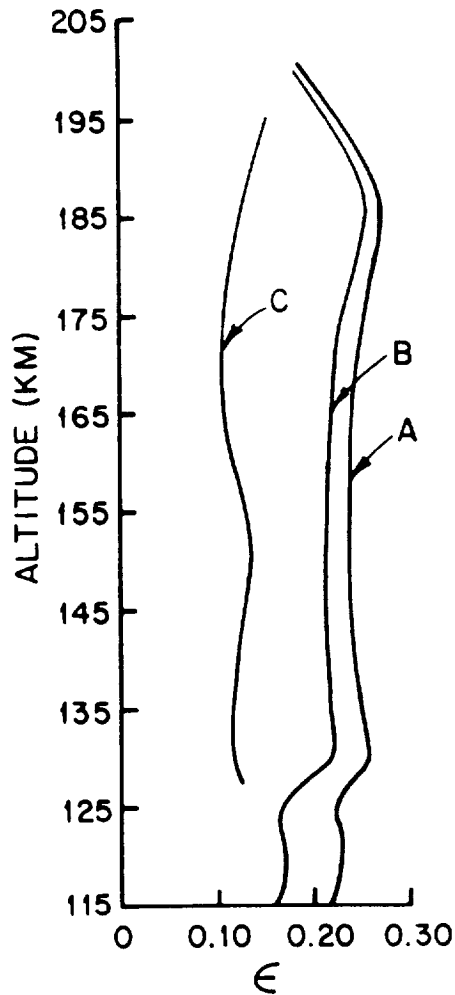
Fig. 33. Computed heating efficiencies for the altitude range 115–200 km. The curve labeled A is the standard model and B is the lower limit model. The curve labeled C is taken from Hollenbach *et al.* (1985). Taken from Fox (1988).

mechanisms (see Figure 32). But the magnitude of the heating at $\tau = 1$ is a function of the specific EUV fluxes and the heating efficiency used. The height of this level depends on the column of absorber and thus on the neutral atmosphere chosen. Some of the discrepancies that arise in the temperature calculations and the heating efficiencies may be due to the use of different inputs. An effort by the authors is underway to compute heating efficiencies and model thermal structure using common background atmospheric models and solar fluxes.

5.3. THE DAYSIDE HEAT BUDGET

One-dimensional modeling efforts for global mean conditions data back to those of McElroy (1968, 1969) and Dickinson (1972), for a nearly pure CO_2 atmosphere, before the advent of Venus general circulation models. In retrospect, it appears that the approach of calculating temperatures based upon a balance of radiative sources and sinks and thermal conduction is adequate to address the Venus dayside heat balance problem. Large-scale upwelling winds appear to provide little adiabatic cooling affecting the dayside thermospheric heat budget (see Section 6.3). Therefore, circulation models are not required to explain the observed dayside temperatures. As a result, 1-D model simulations for various combinations of input parameters provide a useful and relatively efficient method for examining heating and cooling processes on the Venus dayside.

Dickinson (1972) chose to address both the Venus mesosphere and thermosphere (65 to 200 km), where, as for the Earth, a non-LTE (NLTE) treatment is required. In particular, his 1-D radiative transfer calculation utilized a two-level NLTE formulation for the CO_2 vibrationally excited states. The primary radiative transfer was assumed to occur only in the 15-μm and 4.3-μm band systems, for which relative populations of the v_2 bending mode and v_3 asymmetric stretch vibrational levels were painstakingly calculated. Near-IR heating was realized through the collisional relaxation of the 15-μm fundamental band. Several isotopic and hot bands yielding 15-μm emission were also considered. Dickinson (1972) calculated a global mean temperature profile assuming an altitude independent EUV efficiency of 30%, as suggested by early arguments of Stewart (1972). This large efficiency was determined with the assumption that all the $O(^1D)$ energy is transformed to heat. Below 115 km, IR processes by themselves are in balance, with heating and cooling rates decreasing from 300 K day^{-1} at 115 km to 1 K day^{-1} at 65 km. The EUV absorbed above 160 km (≤ 2500 K day^{-1}) was almost entirely offset by downward molecular conduction. This conducted heat was deposited between 120 and 140 km, and was balanced by 15-μm cooling. Temperatures ranged from a minimum of 180 K at 122 km (the mesopause) to 475 K at the top. Dickinson found that the mesopause occurs at essentially the lowest pressure at which CO_2 15-μm cooling is balanced by EUV heating.

The relative uncertainty in the EUV heating efficiency, as well as other parameterizations, lead Dickinson (1976) to conduct several sensitivity studies in which the EUV efficiency, eddy mixing, and CO_2 collisional excitation by atomic-O (enhancing 15-μm emission, see below) were varied. Studies of Dickinson (1976) and Fox and Dalgarno (1981) both indicated that 30% is probably an upper limit heating efficiency. Dickinson (1976) suggested that the very rapid collisional quenching of $O(^1D)$ by CO_2 is consistent with the concomitant excitation of upper CO_2 vibrational-rotational states. Vibrationally excited states at the low pressures of the Venus thermosphere lose their energy to IR airglow, rather than by being quenched. Assuming that a significant fraction of the kinetic energy of hot atoms, ions, and molecules is also transferred to CO_2 vibrations, increased cooling (or a reduced heating efficiency) is obtained. Efficiencies of 3 to 30% were examined, yielding global mean exospheric temperatures of 250 to 475 K

(compared with later Pioneer Venus values of ~ 215 K). Thermospheric temperatures can be further reduced in the presence of O-atoms, for which the collisional excitation of the CO_2 v_2 bending mode:

$$CO_2(v_1, v_2, v_3C + O^* \rightarrow CO_2(v_1, v_2 + 1, v_3) + O \tag{69}$$
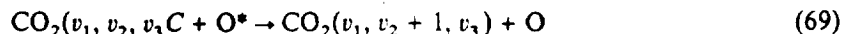
is more efficient. Dickinson argued tha tO excites the CO_2 15-μm level possibly ten times as rapidly per collision as do self-collisions (corresponding to a de-excitation rate of $k_{CO_2-O} = 5 \times 10^{-14}$ cm^3 s^{-1}) (see Section 5.4). This assumption resulted in a further reduction of model exospheric temperatures by 25–50 K. Dickinson considered the introduction of eddy cooling to be the least satisfactory method for modifying themrospheric temperatures (see Section 5.5). Calculations showed that eddy cooling using eddy diffusion coefficients $\leq 10^6$ cm^2 s^{-1} does not significantly alter thermospheric temperatures. However, values as large as 10^7 cm^2 s^{-1} have a substantial impact on the dayside heat budget. Temperatures near the mesopause are particularly sensitive to the amount of eddy heat conduction prescribed. Dickinson made the common assumption that the same eddy coefficient applies to eddy diffusion and eddy conduction; that is, mass and heat were assumed to be transported with the same efficiency.

Post-Pioneer Venus heat budget studies were first carried out by Hollenbach *et al.* (1985), who stressed the role of eddy cooling in reproducing the observed thermospheric temperature structure using a one-dimensional model. They suggested that the changing Venus circulation, as simulated by an effective eddy coefficient, adjusts to maintain a nearly constant thermospheric temperature, yielding exospheric values over the solar cycle that depart little from 300 K. Heating efficiencies of 12–15% were internally calculated and used for all simulations. The large $O + CO_2$ de-excitation rate (the inverse of reaction (69)) suggested by Sharma and Nadile (1980, 981) and Gordiets *et al.* (1982) ($\sim 1 \times 10^{-12}$ cm^3 s^{-1}) was found to be incompatible with their model calculations. Later circulation model studies of Bougher *et al.* (1986) showed that Venus dynamics has little impact on the dayside thermospheric heat budget; i.e., the circulation is not an effective thermostat regulating dayside temperatures (see Section 6.3).

Venus heat budget studies were also carried out by Gougher (1985) and Dickinson and Bougher (1986) using an updated version of the previous NTLE mesosphere/thermosphere code (Dickinson, 1972, 1976). They stressed the role played by CO_2 15-μm cooling in maintaining observed temperatures. Several modifications were made that affected the calculated exospheric temperatures significantly. Solar EUV and FUV fluxes were taken from the Torr *et al.* (1979) and Torr *et al.* (1980) tabulations for day 78348, corresponding to near solar maximum conditions ($F_{10.7} = 200$) of the early *in situ* Pioneer Venus observations (1978–1981). These changes essentially doubled the UV heating rates from those previously calculated, making the problem of obtaining low exospheric temperatures that much more difficult. In addition, Pioneer Venus measurements indicated that dayside atomic-O densities are about 3 times larger than previously thought (von Zahn *et al.*, 1983). This meant that the O/CO_2 ratio at the dayside ionospheric peak (~ 140 km) was 17–20% rather than 5.6%, as calculated earlier by Dickinson and Ridley (1977). This improvement increased the efficiency of excitation

of the CO_2 vibrational $v_2 = 1$ state by O collisions, thereby enhancing 15-μm emission and cooling where NLTE conditions prevail. Finally, the $O + CO_2$ energy transfer rate itself was increased from that previously used, based in part on recent studies of the Earth's lower thermosphere as reviewed by Dickinson (1984), and observational estimates for this rate coefficient provided by terrestrial rocket measurements (Sharma and Nadile, 1981; Stair et al., 1985). A value of $5-8 \times 10^{-13}$ cm^{-3} s^{-1} at 300 K was adopted for this rate (Dickinson and Bougher, 1986; Bougher et al., 1986), in contrast to 2×10^{-13} used in Dickinson (1984) for Earth, and about 5×10^{-14} used in previous Venus studies (e.g., Dickinson, 1976). This amounts to a ~ 150-fold increase over CO_2 self-collisions.

It was found that the observed Pioneer Venus global mean temperatures above 140 km could be simulated using strong 15-μm cooling alone for balancing $\sim 10\%$-efficient EUV heating. The maximum EUV heating rate (~ 1100 K earth day^{-1}) was offset by a combination of molecular conduction and 15-μm cooling. The region above 160 km, where molecular conduction removes most of the heat, is nearly isothermal. Thus, the exospheric temperature of Venus was shown to be rather insensitive to the precise details of molecular thermal conduction, if CO_2 cooling is indeed so strong. The near IR heating rate was nearly doubled from that of Dickinson (1972), with its peak altitude rising from 115 to 130 km. The global mean model was also decomposed into a dayside and nightside model, with solar IR heating partitioned between the two in order to simulate hydrodynamical effects. An improved 15-μm cooling rate was obtained by averaging these day and night profiles, yielding a reduced global mean exospheric temperature of 220 K. This is consistent with a dayside mean value of 300 K, and a corresponding nightside value of 130 K. Very efficient eddy cooling was shown to be required to yield observed temperatures in the face of larger EUV heating efficiencies (10-18%). However, such a possibility was generally ruled out since Venus circulation model studies (Bougher et al., 1986) require that eddy diffusion must be less than half that proposed by previous one-dimensional eddy diffusion models (e.g., von Zahn et al., 1980). Hydrodynamic model large-scale winds appear to be very important in maintaining the observed dayside density profiles (see Section 6.6). Therefore, the requirement that the eddy coefficient for diffusion and conduction be the same constrains the cooling to be rather small ($K \leq 2 \times 10^7$ cm^2 s^{-1}).

The low thermospheric heating efficiencies of 10-15% used by Hollenbach et al. (1985) as well as by Dickinson and Bougher (1986) have recently been shown to be improbable (Fox, 1988) (see Section 5.2). The narrow range of permissible EUV heating efficiencies (22-25% above 135 km) requires a re-examination of th Venus dayside heat budget. The NLTE model of Dickinson and Bougher (1986) has recently been updated to determine what reasonable combination of cooling parameters and EUV fluxes might enable observed temperatures to be simulated using EUV heating efficiencies consistent with the calculations of Fox (1988) (cf. Bougher et al., 1988a). The model EUV fluxes used have been revised according to Torr and Torr (1985), where solar maximum values are reduced as a result of a rocket calibration. The effect on the heating rates permits an increased EUV efficiency of 12% to be adopted. If dayside solar maximum tempera-

tures as large as 310 K are permitted, in accord with the Hedin *et al.* (1983) empirical model, then an additional 1% increase of the EUV efficiency to 13% is possible. Finally, recent terrestrial low thermosphere heat balance studies of Roble *et al.* (1987, 1989) suggest that an O + CO_2 de-excitation rate similar to that initially proposed by Sharma and Nadile (1980) ($\sim 1 \times 10^{-12}$) is not unreasonable. Its incorporation into the Venus NLTE code enhances the CO_2 cooling further, so that an EUV efficiency of 14% can be used. Figure 34 illustrates the cooling requirements for observed dayside tempera-
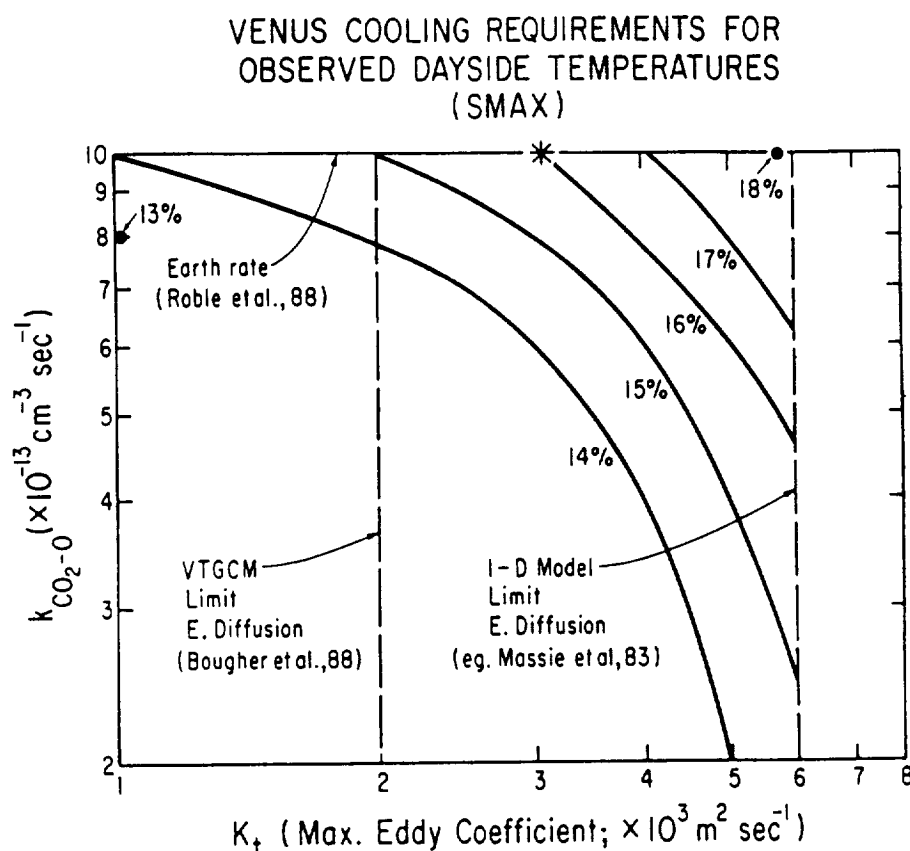
Fig. 34. Venus cooling requirements for observed dayside temperatures. Solar maximum conditions (F10.7 = 200). Based on the NCAR NLTE energy balance code.

tures; values along the ordinate correspond to the case of no eddy cooling. A further increase of EUV efficiencies seems to require cooling by eddy conduction. This, in fact, appears valid for moderate eddy coefficients with $K \leq 2 \times 10^7$ cm^2 s^{-1}, which is consistent with an upper limit for eddy diffusion incorporated in Venus odd-nitrogen studies (Bougher *et al.*, 1989) (see Section 3.10). The use of EUV efficiencies larger than 15%, as Fox (1988) has suggested they are, seems impossible at the present time, unless the

requirement that eddy diffusion and conduction coefficients be equal is relaxed. The low efficiencies required may, however, also be a due to the uncertainty of the solar EUV fluxes and the $O-CO_2$ energy exchange rate being used in model simulations.

5.4. IR HEATING AND 15-μm COOLING

Both IR heating and CO_2 15-μm cooling appear to be quite important in the Venus upper atmosphere. Dickinson and Bougher (1986) showed that IR heating and cooling offset one another below 130 km. Between 130 and 160 km, where the temperature increase is greatest, EUV heat is balanced by CO_2 15-μm cooling and molecular thermal conduction. Only above 160 km does molecular conduction balance EUV heating to maintain the observed thermospheric temperatures (see Figure 35).

The 15-μm cooling arises mostly from transfer of atomic-O kinetic energy to CO_2 vibrational energy; the magnitude of the cooling rate depends upon the $O-CO_2$ energy exchange rate and the relative amount of atomic-O in the Venus dayside thermosphere.
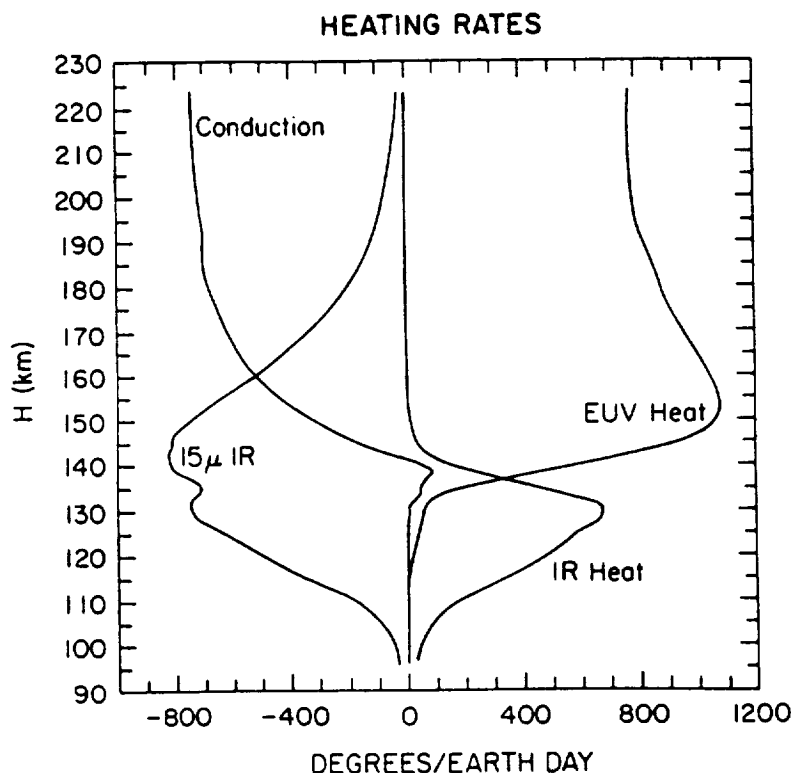
HEATING RATES

Fig. 35. Global average heating/cooling rates (K day^{-1}) for the Venus thermosphere. EUV heating efficiency = 10%. CO_2-O de-excitation rate = 8 × 10^{-13} cm^3 s^{-1} at 300 K. Taken from Dickinson and Bougher (1986). Later NCAR NLTE model calculations (Figure 34) make use of revised EUV fluxes, stronger CO_2 15-μm cooling, and larger heating efficiencies (~14%), yielding the same basic thermal balances shown here.

A pedagogical discussion of translation-vibration energy transfer can be found in Yardley (1980). The $O-CO_2$ excitation rate has not been measured at low temperatures, but may be large. In general the measured quantity that is commonly quoted is the rate coefficient for quenching or de-excitation (the reverse of reaction (69)). The rate coefficient for collisional excitation, k_{69}, is related to that for quenching, k_{-69}, by expression

$$_{69} = k_{-69} \times g \exp(-\Delta E/kT), \tag{70}$$

where ΔE is the vibrational spacing and g is the degeneracy of the upper state, equal to $v_2 + 1$ for the doubly-degenerate CO_2 bending mode. In the high temperature regime, the temperature dependence of the probability, P, of de-excitation in a collision, to which the rate coefficient is proportional, is given by the Landau-Teller expression (Landau and Teller, 1936)

$$P \sim \exp(-T^{-1/3}). \tag{71}$$

In the Landau-Teller model and its later refinement and extension to polyatomics, the SSH model (Schwarz et al., 1952), energy transfer results from a 'direct' interaction involving the exponential repulsive potential between the species. This strong temperature dependence is characteristic of models involving 'impulsive' energy transfer of all types (e.g., McClelland et al., 1979). At low temperatures, the energy transfer probabilities are found to deviate substantially from the Landau-Teller values. The deviation is small for noble gases; the probabilities are found to decrease with decreasing temperature over a large range of temperature, but level off at very low (150 K) temperatures (Inoue and Tsuchiya, 1975; Simpson et al., 1977). For some species, usually efficient quenchers, the deviation from the Landau-Teller model can be several orders of magnitude at low temperatures and, below a certain temperature, the probability of quenching can increase with decreasing temperature. For example, the rate coefficient for quenching of the v_3 mode of CO_2 by N_2 is large and exhibits a minimum at about 1500 K (Moore et al., 1967; Rosser et al., 1969). This behavior for a near-resonant $V - V$ transfer was successfully explained by Sharma and Brau (1969), who incorporated the effect of long-range attractive multipole forces into the model for vibrational relaxation. Large rates and negative temperature dependence were also observed for de-activation of CO_2, H_2O, and D_2O at temperatures below 1000 K (Buchwald and Bauer, 1972). Significant departures from the Landau-Teller temperature dependence are also oibserved in de-activation of the asymmetric stretch mode of CO_2 by several molecular species at temperatures below about 400 K (Bauer et al., 1987). Quenching of the bend-stretch manifold of CO_2 by H_2 is rapid, even though the vibrational modes have dissimilar energies. Allen et al. (1980) have reported a rate coefficient of 5×10^{-12} cm^3 s^{-1} at 295 K; the rate coefficient increases with decreasing energy to 7.5×10^{-12} cm^3 s^{-1} at 170 K. The corresponding quenching probabilities are 7.4×10^{-3} and 1.4×10^{-2}. $V - T$, R transfer in other systems such as NO-NO has been reported to be rapid, with quenching probabilities on the order of 10^{-3} and increasing with decreasing temperature below 400 K (Yardley, 1980).

Quenching of small molecules by atoms can be anomalously fast if the atom has an open shell (Chu et al., 1983). H, Cl, and F quench CO_2 rapidly compared to noble gases, such as He, Ne, and Xe (Chu et al., 1983; Flynn and Weston, 1986). The large cross sections and the negative temperature dependences at low collision energies for such systems have been ascribed to the formation of long-lived collision complexes in the presence of strong attractive chemical, hydrogen bonding or Van der Waals forces (Ewing, 1978; Lin et al., 1979; Parmenter and Seaver, 1979; Gordon, 1981; McClelland et al., 1979). The lifetime of a collision complex is longer at low collision energies, and the longer-lived the collision complex, the greater the probability that the energy in the vibrational mode may flow into the weak bond of the complex and cause its dissociation. The $V - T, R$ transfer probability for $HF-HF$, a system with strong hydrogen bonding, is about 1% at room temperature and increases with decreasing temperature (cf. Poulson et al., 1978). For CO_2-H, the large rates even at high energies have been ascribed to the presence of a chemically reactive channel, $CO + OH \rightarrow CO_2 + H$, and to the formation of a stable intermediate radical, HCO_2 (Flynn and Weston, 1986).

Atomic oxygen is a very efficient quencher of vibrational excitation, probably due to its reactivity, especially where de-activation can take place by atom exchange. The de-excitation rate coefficients for $CO^{\dagger\dagger}$ (the double dagger denotes vibrational excitation) and $O_2^{\dagger\dagger}$ by O are about 9×10^{-13} cm^3 s^{-1}; these rates are about 25 times faster than that for quenching of $N_2^{\dagger\dagger}$, where atom exchange is not possible (McNeal et al., 1974; Fernando and Smith, 1969; Eckstrom, 1973). Isotope exchange studies of NO with ^{18}O showed that the rate coefficient for O atom exchange at 298 K is 3.7×10^{-11} cm^3 s^{-1}; if the complex is assumed to break-up statistically, the implied rate of complex formation is 7.4×10^{-11} cm^3 s^{-1} (Anderson et al., 1986). The rate coefficient for vibrational relaxation of NO by O is of the same order of magnitude, 6.5×10^{-11} cm^3 s^{-1} (Fernando and Smith, 1979). Isotope exchange of ^{18}O with O_2 proceeds with a rate coefficient of 2.9×10^{-12} cm^3 s^{-1} and vibrational relaxation with a rate coefficient of 5.4×10^{-12} cm^3 s^{-1} (Anderson et al., 1986; Quack and Troe, 1977).

All of the measurements or calculations of the $O-CO_2$ quenching rate have been at high temperatures where the Landau-Teller model might be expected to be valid. Center (1973) found O atoms an order of magnitude more efficient at relaxing the bending mode than Ar atoms; a probability of about 1% was measured at 3000 K. Bass (1974) computed the probabilities assuming classical scattering with a hard sphere interaction and quasi-diatomic model for CO_2 for energies from 1 to 10 eV and found that when the C atom was struck by the impinging O atom, the average fraction of energy transferred to the ν_2 mode was 0.447. Schatz and Redmon (1981) used quasi-classical trajectory theory to compute the cross sections for excitation of the beznding mode and found a value of 1.9×10^{-15} cm^2 at 2.2 eV, whereas the excitation of the symmetric and asymmetric stretch modes were 2 and 4-5 orders of magnitude smaller, respectively. Harvey (1982) obtained cross sections 50% smaller than Schatz and Redmon (1981) with a quantum mechanical vibrational close-coupling calculation using the same potential surface. Extrapolation of these results to low temperatures using the Landau-Teller

expression would give very small quenching probabilities, but is not justified. The potential used by Schatz and Redmon (1981) and Harvey (1982) is a sum of pairwise exponential repulsion terms; no portion of the potential was attractive. At center-of-mass energies larger than 1 eV, the repulsive core of the potential dominates (Bass, 1974), but at low energies, attractive forces are expected to become important.

A value for the $O-CO^{2\dagger\dagger}$ quenching rate at low energies was derived by Sharma and Nadile (1980) from measurements of the 15 μm radiation in the terrestrial atmosphere. They recommended a de-excitation rate coefficient of $6.67 \times 10^{-10-14}T^{0.5}$ cm^3 s^{-1}. This rate has been refined by Wintersteiner et al. (1988) to

$$1.5 \times 10^{-13}T^{0.5} + 2.32 \times 10^{-9}\exp(-76.75/T^{1/3})\,\text{cm}^3\,\text{s}^{-1}, \qquad (72)$$

valid in the approximate temperature range 200–700 K. The first term in expression (72) is due to attractive forces, which dominate at low temperatures and the second is the Landau–Teller expression that accounts for the short-range repulsive forces. The potential error in this expression, about a factor of 2, are mostly due to uncertainties in the atomic O density (Wintersteiner, private communication). At 200 K, the temperature which prevails in the lower part of the Venus thermosphere, the rate coefficient would be 2×10^{-12} cm^3 s^{-1}, about 1% of gas kinetic. The rate adopted by Dickinson (1984) is less than 40% of the value in expression (72) and other recent models have assumed quenching coefficients less than 1% of the Wintersteiner et al. value. Rates on the order of 1×10^{-12} cm^3 s^{-1} appear to be consistent with the terrestrial and martian heat budgets (Dickinson et al., 1987; Roble et al., 1987, 1989; Bougher and Dickinson, 1988; Bougher et al., 1990b). The reluctance to adopt the rate derived from terrestrial 15 μm observations is not justified. Certainly, however, a low temperature laboratory measurement of this rate coefficient is badly needed, not only for models of the Venus thermosphere, but for the Earth and Mars as well.

The strong nonlinear (exponential) temperature dependence of the CO_2 15-μm cooling insures that the Venus exospheric temperature does not vary by more than ~ 65 K over the solar cycle (300–235 K) (Dickinson and Bougher, 1986) (see Section 7). In addition, the O densities themselves increase with increasing solar activity. Calculations show that the production rate of O above 100 km on Venus increases from 2.2×10^{12} to 3.3×10^{12} cm^{-2} s^{-1} from low to high solar activity (Fox, 1989b). The VTS3 model predicts an increase of O from 2.7 to 7.3% at 135 km from $F_{10.7} = 74$ to $F_{10.7} = 200$. This change in the O abundance will act to dampen the response of the thermospheric temperature to changing solar activity, increasing the cooling at higher solar fluxes. The combination of the effects of the exponential temperature dependence of the $O-CO_2$ collisional excitation rte and the change in the atomic O mixing ratio with solar activity provide the Venus thermosphere with an 'atomic oxygen thermostat', regulating CO_2 cooling, that is less effective at Mars where the O abundance is lower (Dickinson and Bougher, 1986; Bougher and Dickinson, 1988; Fox, 1989b).

The nonlinear temperature dependence of the 15 μm cooling also means that it cannot be adequately addressed by simple linear perturbation (Newtonian cooling) schemes

(Dickinson, 1973). Instead, a nonlinear temperature-dependent cooling parameterization was developed by Bougher *et al.* (1986) for use in multi-dimensional model simulations. It first requires an exact 1-D NLTE calculation of a representative reference 15-μm cooling and corresponding temperature profile. For Venus, since the day-to-night temperature variation is so large (~ 200 K), separate dayside and nightside mean reference cooling rate profiles were generated. These were later used to drive a nonlinear NLTE cool-to-space formulation for deviations from these references. The deviations depend on departures of total temperature and atomic-O concentrations from the 1-D model values. The separate reference cooling for dayside and nightside mean conditions is matched across the terminator by interpolation so that discontinuities are minimized. Such an interactive scheme is fast, yet it allows the accurate calculation of total 15-μm cooling at other temperatures at any local time over the globe. The expression for the cooling rate derived by Bougher (Equation (A.5) of Bougher *et al.* (1986)) gives approximately the correct dependence of the IR cooling on temperature, pressure, and O concentration, and reduces to reference model cooling for composition and temperature profiles of either the day- or nightside reference models. Recent Mars TGCM model studies also confirm the usefulness of this NTLE cool-to-space formulation (Bougher *et al.*, 1988c, 1990b).

The one-dimensional model results of Dickinson and Bougher (1986) showed that dayside CO_2 cooling is dominated by the 15-μm fundamental above 130 km. Near-IR heating peaks at 130 km, with 2.7-μm bands important above 120 km, and ≤ 2.0-μm bands strongly contributing over 100 to 120 km. A calculation of the dayside $v_2 = 1$ populations relative to LTE confirms that complete NLTE conditions hold above about 140 km, while LTE is a good assumption only below 110 km.

5.5. MOLECULAR AND EDDY CONDUCTION

Molecular conduction serves to transfer EUV heat deposited in the thermosphere downward to a lower level, the mesopause, where it can be radiated to space by IR active gases. On Venus, CO_2 15-μm emission dominates all others in providing this cooling near the bottom of the thermosphere. Temperatures are also affected by the amount of cooling eddy processes are assumed to produce (Hunten, 1974; Izakov, 1978). The turbulence responsible can heat the thermosphere through the dissipation of its energy; conversely, cooling can take place by eddy heat conduction in a process analogous to molecular conduction. The relative importance of turbulent heating or cooling in a given planetary thermosphere is still the subject of much debate (e.g., Hunten, 1974).

Izakov (1978) argued theoretically that conditions exist when cooling of a planetary thermosphere by turbulence predominates, and conditions when heating prevails. For Venus, eddy mixing is estimated to provide cooling (upper limit) or a compensation of heating and cooling (lower limit). Hollenbach *et al.* (1985) approached the problem from a more empirical point of view, whereby the relative roles of heating and cooling were varied to match the observed temperatures over the solar cycle. The 1-D model calculations of Dickinson (1972, 1976) and Dickinson and Bougher (1986) have all addressed the case where vertical eddy mixing gives rise only to cooling. This establishes an upper

limit to the role of eddy mixing in contributing to the overall thermospheric heat budget (see Section 5.3).

Questions still remain as to the complementary roles of eddy cooling and diffusion, particularly in the context of Venus circulation models. A few key points can be gleaned from recent modeling studies. The same eddy coefficient must be used for eddy diffusion and heat conduction in the absence of theoretical arguments to the contrary (Bougher et al., 1986, 1988b). However, the coefficient for eddy viscosity and diffusion may be different (Prandtl No. 1) (Mengel et al., 1989). This implies that a self-consistent calculation of winds, composition, and temperatures is required to address the impact of eddy mixing in the thermosphere. The practice of calculating temperatures using eddy heat conduction independent of the corresponding mixing effect on model densities is improper. Furthermore, observed densities appear to be influenced by a combination of global wind and eddy mixing processes; i.e., smaller eddy coefficients are needed in Venus circulation models than formerly implied by 1-D (non-dynamical) models (see Section 6.6). Thus, it appears that the introduction of eddy cooling is not generally a viable method for modeling thermospheric temperature profiles until all other dynamical, radiative cooling, and heating processes have been carefully examined. The effects of small-scale mixing, although difficult to model, need to be incorporated in a self-consistent fashion. No Venus model yet devised has this capability.

6. Thermospheric Circulation and Transport

6.1. INTRODUCTION

The dynamics of Venus's atmosphere can be separated into two distinct regimes in which very different flow patterns dominate: (1) a retrograde, zonal, superrotating flow from the surface up to ~70 km, and (2) a mean subsolar-to-antisolar (SS–AS) solar-driven flow above ~95–100 km. In between (70–95 km), zonal winds are generally decreasing with altitude while thermospheric-type SS–AS winds are increasing. This is a complicated transition region in which changing zonal and meridional flow patterns may be superimposed on a possible lower return branch of the SS–AS circulation (Clancy and Muhleman, 1985b; Goldstein, 1989). A summary of these basic dynamical regions and the relevant supporting data is given in Figure 36 (Goldstein, 1989).

Solar UV–IR heating clearly drives the SS–AS circulation. An eddy viscosity appears to be required to reduce pressure-driven winds toward acceptable values (see Section 6.4). A redistribution of angular momentum by a strong cloud-top Hadley circulation maintains the retrograde zonal jets observed at mid-latitudes (Hou, 1984; Hou and Goody, 1985; Walterscheid et al., 1985). Recent studies support the idea, originally proposed by Fels and Lindzen (1974), that the superrotation at cloud tops is maintained by the pumping action of thermally driven tides (Pechmann and Ingersoll, 1984; Hou, 1984; Hou and Goody, 1985). Baker and Leovy (1987) and Leovy (1987) suggest that the equatorial wind speed near Venus's cloud top is maintained by a balance between the pumping effect of the semidiurnal tide and vertical advection by the Hadley

Proposed Circulation Model for Venus

Evidence for Super-rotation

Altitude (km)

170
150
130
110
90
70
50
30
10
SS
NP
AS
10
30
50
70
90
110
130
150
170

* PV Orbiter Neutral Mass Spectrometry
  (Brinton et al. 1980; Niemann et al. 1980)
* PV Orbiter Atmospheric Drag (Keating et al. 1980)
* PV Orbiter UV Spectroscopy (Stewart and Barth 1979)

CO2 IR Heterodyne Spectroscopy (Goldstein, 1989)

* CO2 IR Heterodyne Spectroscopy (Betz et al. 1977, 1982)
* CO Microwave Spectroscopy (Clancy and Muhleman 1985a,b)
* PV Orbiter UV Photopolarimetry (Limaye 1984)
* Reinterpretation of Betz et al. data (Goldstein, 1989)
* Cyclostrophic Balance Models

In Situ Descent Probes
    Venera, Pioneer Venus, Vega
Orbital UV Imaging
    Mariner 10, Pioneer Venus
Ground-Based
    UV Imaging
    IR Imaging
    PEPSIOS Spectroscopy

Evidence for Subsolar-Antisolar Circulation

* Reinterpretation of Betz et al. data (Goldstein,1989)

* CO Microwave Spectroscopy (Clancy and Muhleman 1985a,b)

CO2 IR Heterodyne Spectroscopy
    * Betz et al. (1977, 1982)
      Goldstein et al. (1987, 1988)

Fig. 36. Dynamical regions of the Venus mesosphere-thermosphere. Taken from Goldstein (1989).

circulation in the thermal driving region. This rapid superrotation (at all latitudes) has not yet been adequately explained.

Zonal circulation seems to exist throughout the atmosphere, although it does not dominate SS–AS flow above 100 km (Goldstein, 1989). Venus cyclostrophic balance models predict maximum zonal winds of 130 m s^{-1} near 70 km. The observed poleward warming above this level implies decreasing zonal speeds with altitude (70–90 km), becoming negligible by 90–100 km. A concomitant increase in the mean meridional component with possible 120 m s^{-1} speeds near 90–100 km has also been predicted (Taylor et al., 1980). Infrared heterodyne observations detect a weak zonal retrograde component (20–30 m s^{-1}) (equatorial) at 110 ± 10 km, superimposed on strong 100–140 m s^{-1} (SS–AS) cross-terminator winds (Goldstein, 1989). Finally, a slightly larger component of retrograde zonal winds (~ 50–60 m s^{-1}) is implied above 150 km

from helium and night airglow observations (Mayr *et al.*, 1980; Stewart *et al.*, 1980). See Section 6.5 for details of superrotation mechanisms and sensitivity studies.

There are, however, no direct or indirect measurements of wind velocity in Venus's upper atmosphere above 110 km. The circulation of most of the thermosphere must, therefore, be inferred from observations of its temperature and density structure (Mayr *et al.*, 1980; Schubert *et al.*, 1983; von Zahn *et al.*, 1983) and subsequent modeling efforts (Bougher, 1985; Mayr *et al.*, 1985; Bougher *et al.*, 1986, 1988b, 1989; Mengel *et al.*, 1989).

6.2. THERMOSPHERIC CIRCULATION: SYMMETRIS VS ZONAL

The most prominant feature of the thermosphere which suggests a strong SS–AS wind system is the large contrast in temperatures and densities between day and night. Temperatures on the dayside of Venus increase from ~ 170–180 K at the 'mesopause' (100 km) level (Taylor *et al.*, 1979, 1980; Seiff *et al.*, 1980) to near 300–310 K above 150 km for solar maximum conditions (von Zahn *et al.*, 1979, 1980; Niemann *et al.*, 1979, 1980b; Hedin *et al.*, 1983; Keating *et al.*, 1980, 1985). The rise of temperatures above a 100 km mesopause is similar to that of the Earth's thermosphere, although the temperatures are much colder (see Figure 31). Nightside temperatures are shown to decrease from 170 K at the mesopause to values as low as 100–130 K above 150 km (Keating *et al.*, 1979, 1980; Niemann *et al.*, 1979, 1980b; Seiff *et al.*, 1980; Seiff, 1982). This vertical structure is remarkably unlike the terrestrial nightside thermosphere, and has been termed a 'cryosphere' (Schubert *et al.*, 1980). In addition, changes in temperature across the terminator are very abrupt, with the minimum value observed just beyond midnight at 02:00 LT (Mayr *et al.*, 1980; Keating *et al.*, 1980).

These thermospheric (above 150 km) kinetic temperatures are inferred primarily from the observed scale heights of the measured neutral densities. The diurnal variation of the heaviest species (CO_2, CO, N_2, and O) show a near symmetry about the subsolar-to-anti-solar axis (see Figure 37), with a density maximum at a fixed altitude at local noon and minimum at midnight (von Zahn *et al.*, 1983). The slow planetary rotation coupled with dayside solar heating results in this expansion of the dayside thermosphere; i.e., the height of a given pressure surface rises (falls) with increasing (decreasing) temperatures. Nightside densities are strongly depleted with respect to dayside values, suggesting a significant contraction of the nightside thermosphere with constant pressure surfaces decreasing abruptly in altitude across the terminators. Helium and hydrogen, the two lightest species, show a diurnal density reversal, with densities higher at night than during the day (Niemann *et al.*, 1980b; Brinton *et al.*, 1980). This signature is consistent with their small atomic weights and correspondingly large-scale heights. These properties increase the transport efficiencies by the large scale winds for these species, just as in the atmosphere of the Earth (Mayr *et al.*, 1978). The diurnal variation of helium at 165 km reveals a distinct (lasting) nightside bulge (see Figures 38(a) and 38(b)), with a maximum at 03:00 LT roughly 30–40 times that on the dayside (Taylor *et al.*, 1984). Results obtained from Brinton *et al.* (1980) suggest a similar night–day bulge of hydrogen peaking at 05:00 LT, with a diurnal ratio of nearly 400:1 at 165 km (see Figure 25).

Fig. 37. Measurements of CO_2 and O densities at 170 km altitude taken by the Pioneer Venus orbiter neutral mass spectrometer (ONMS) over nearly three diurnal cycles. Taken from von Zahn *et al.* (1983).

These bulges imply a 'wind-induced diffusion' in which light constituents are preferentially transported from day-to-night, with little returning to the dayside along the return branch of the circulation (Mayr *et al.*, 1978, 1980).

This temperature difference between day and night gives rise to horizontal pressure gradients, which to first order should drive a strong subsolar-to-anti-solar (SS-AS) circulation in Venus's upper atmosphere (Dickinson and Ridley, 1977; Mayr *et al.*, 1980; Seiff, 1982). A simplified flow pattern would be axisymmetric about the Sun-Venus line, with dayside upwelling centered on the subsolar point, strong cross-terminator flow, and subsidence centered on the antisolar point (Schubert *et al.*, 1983).
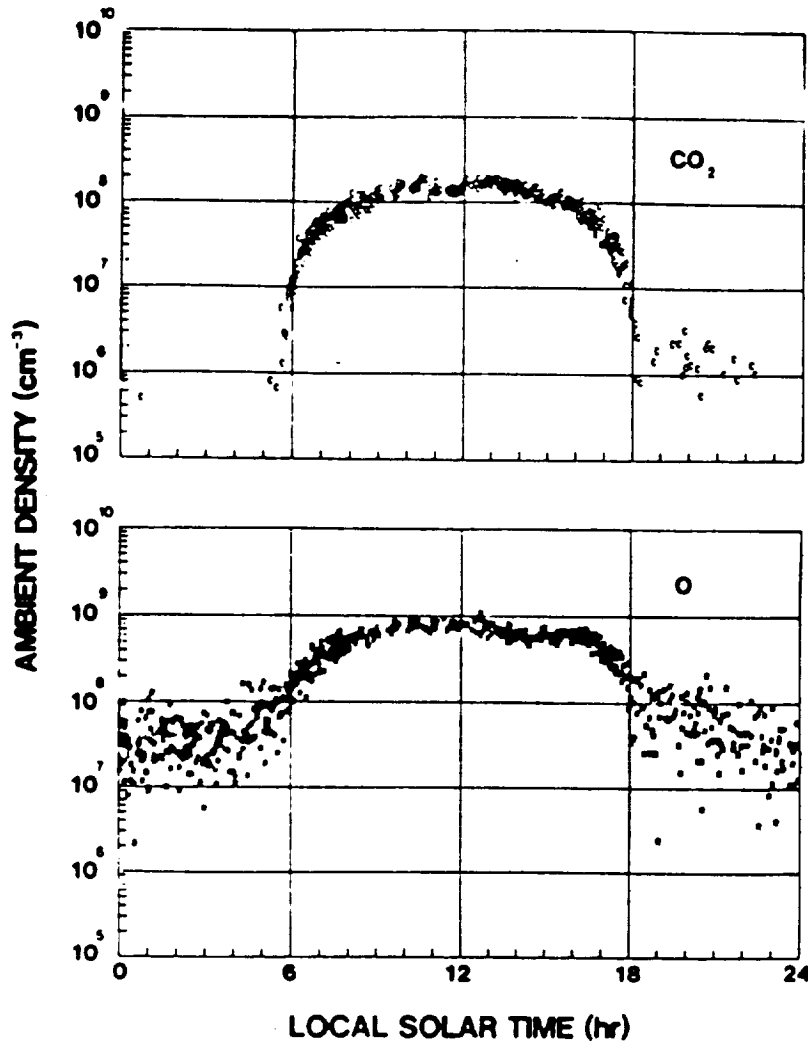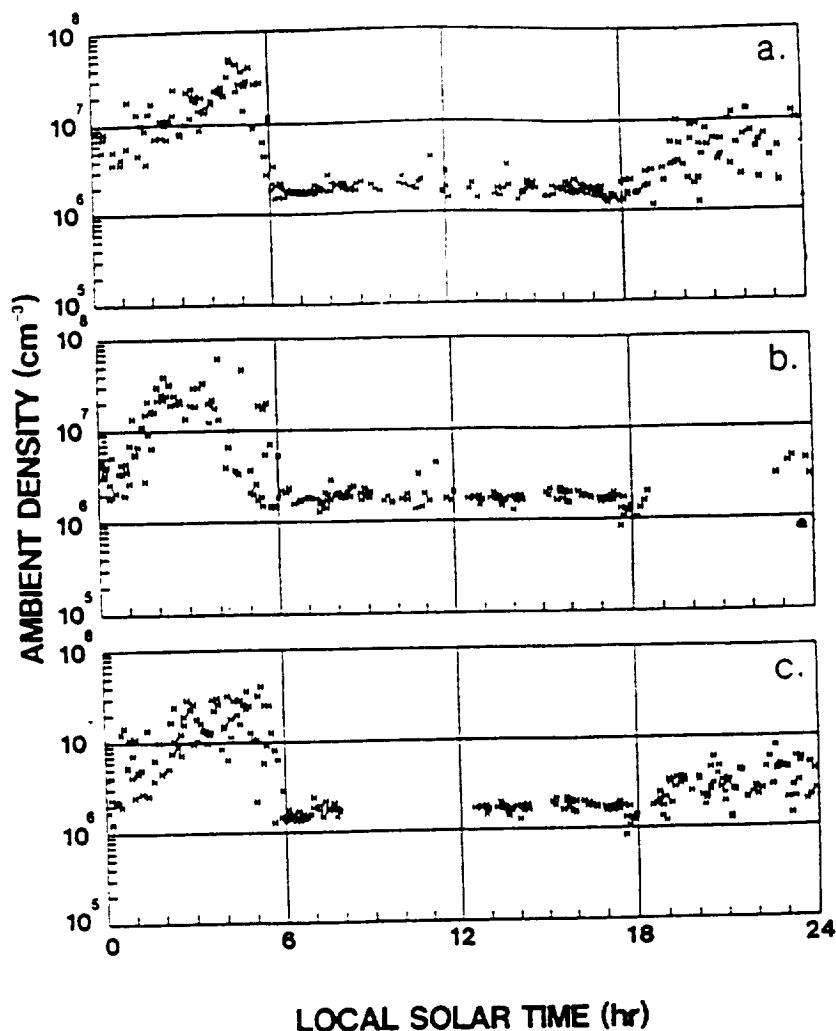
Fig. 38. Measurements of He densities at 170 km altitude taken by the Pioneer Venus orbiter neutral mass spectrometer (ONMS) over nearly three diurnal cycles. Helium has a dawn bulge analogous to that in hydrogen, with some differences in shape. Taken from von Zahn *et al.* (1983).

Return flow, possibly between 70–90 km (Goldstein, 1989), would complete the circuit. Streamlines for transported species approximately follow constant pressure surfaces, which descend in altitude from day to night (Seiff, 1982). Supersonic velocities are estimated across the terminators for laminar flow conditions; turbulent viscosity is likely important in modifying the pressure-driven wind speeds (Seiff, 1982; Bougher *et al.*, 1986). This basic day–night flow pattern was hypothesized and studied in a series of numerical models by Dickinson and Ridley (1972, 1975, 1977) prior to Pioneer Venus measurements, and by Bougher *et al.* (1986, 1988b, 1990a), Mayr *et al.* (1980, 1985), and Mengel *et al.* (1989) afterwards.

This single symmetric cell, driven by solar UV–IR heat, must occur. However, the actual motions in Venus's thermosphere are likely a superposition of this SS–AS flow and a retrograde zonal wind component. Post-midnight maxima in the helium and hydrogen densities (Niemann et al., 1979; Brinton et al., 1980; Taylor et al., 1984), displacement of the minimum diurnal temperature to 02:00 LT (Mayr et al., 1980; Keating et al., 1980), and the NO night airglow maxima at 02:00LT (Stewart et al., 1980; Bougher et al., 1990a) all suggest a westward superrotation of the upper atmosphere (≤ 150 km) with zonal winds speeds of 50–100 m s^{-1}. This corresponds to a rotational period of 4–8 Earth days. This modified flow pattern now includes upwelling (divergence) near the subsolar point, and subsidence (convergence) offset from midnight, yielding a nightside flow which stagnates near 02:00–03:00 LT (see Figure 39). The zonal winds add to the SS–AS flow across the evening terminator, giving stronger winds there than at dawn.
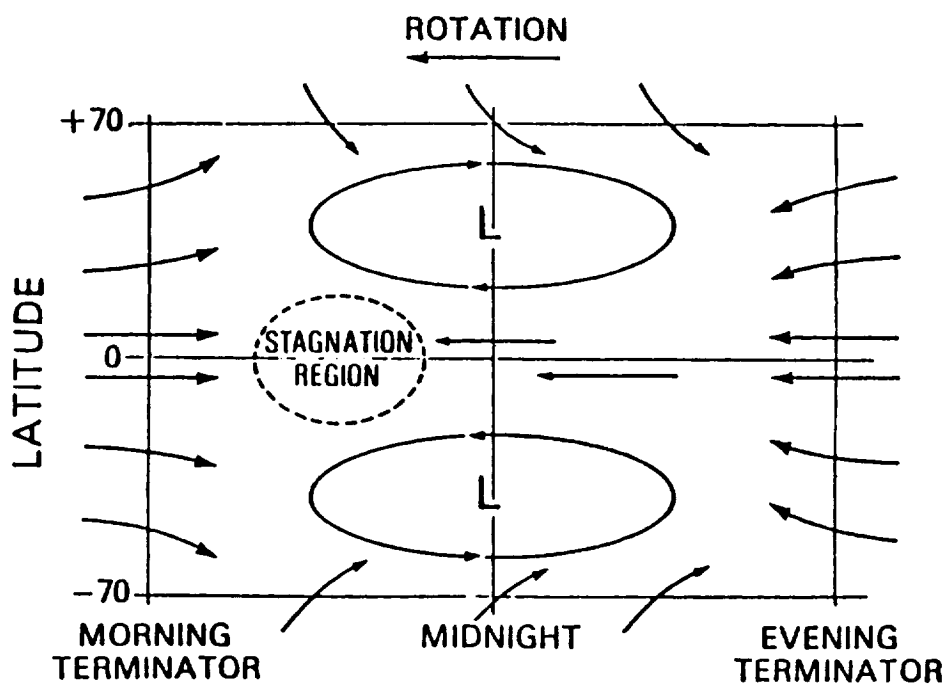
Fig. 39. A schematic flow pattern for the nightside thermosphere of Venus. Taken from Niemann et al. (1980).

Models of the Venus thermospheric circulation have been under development for nearly 18 years. Experience gained from Earth thermosphere studies initially guided the model processes and parameterizations considered. Prior to Pioneer Venus, only the SS–AS circulation pattern was generally thought to be operating in the Venus thermosphere. The Dickinson and Ridley (1972, 1975, 1977) two-dimensional model

(DRM) of the temperature, winds, and composition of the Venus thermosphere, correctly predicted the gross characteristics of this SS–AS mean circulation. Axial symmetry was assumed in choosing altitude and solar zenith angle (SZA) as the two model coordiantes, in accord with the dominant SS–AS flow. Later versions of this model were fully self-consistent and used linear perturbation theory to simultaneously calculate thermal structure, winds, and CO_2, CO, and O densities above 100 km. Detailed results of the model, however, differed considerably from the Pioneer Venus observations (Schubert et al., 1983; Dickinson and Bougher, 1986). Figure 40 shows

COMPARISON OF DRM(77) PREDICTIONS AND P.V. OBSERVATIONS
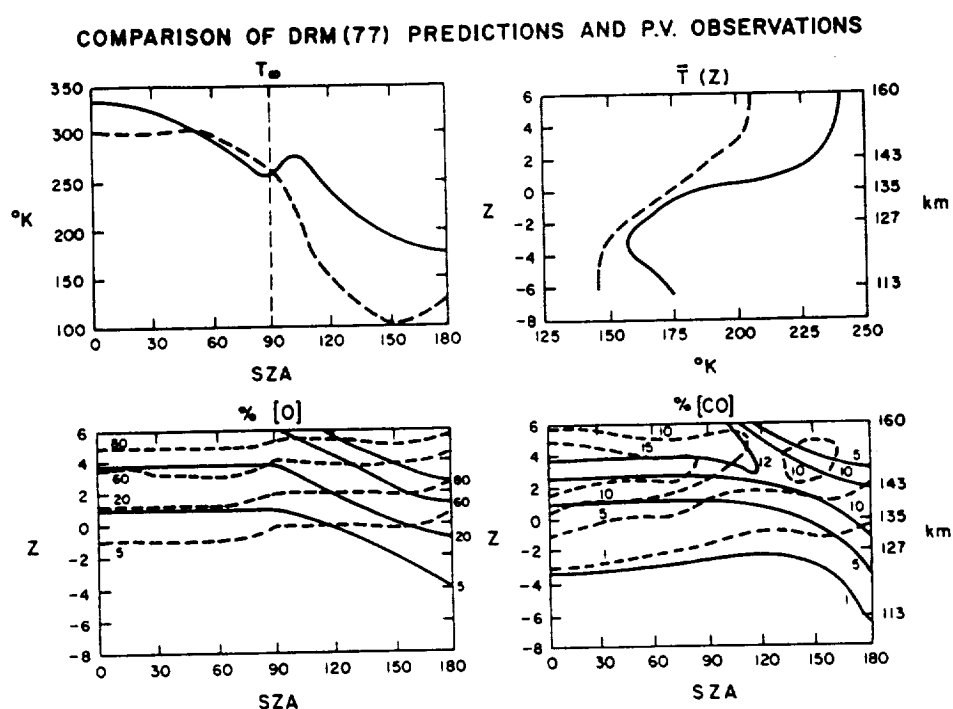
Fig. 40.   Comparisons of Dickinson and Ridley (1977) (DRM) model predictions and Pioneer Venus (PVO) observations. Solid lines are for the 2-D model simulations; dashed lines are from PVO observations as given by the empirical model of Hedin et al. (1983). Taken from Dickinson and Bougher (1986).

that the Dickinson–Ridley temperatures were somewhat too warm on the dayside and much too warm, by as much as 100 K, on the nightside. Their calculations failed to predict the nightside cryosphere entirely. Model atomic-O and CO bulges on the nightside were also predicted by the DRM, that were not observed. Correspondingly, the dayside O-mixing ratios at the F1-peak (140 km) were calculated to be 2.5–5.6%, much smaller than actually observed (17–20%) (von Zahn et al., 1983). No shift in the nighttime minimum temperatures from midnight is possible using the axially-symmetric framework assumed in the DRM. Effects of zonal flow require a three-dimensional model simulation (Mayr et al., 1980; Bougher, 1985; Bougher et al., 1988b).

Several explanations were initially forwarded to account for these discrepancies between DRM and the data. Two groups, in particular, focused their attention on the Pioneer Venus neutral data and its global modeling. The Goddard group (cf. Mayr *et al.*, 1980, 1985) used a 3-D spectral model to simulate the observed day–night distribution of composition and temperatures. Dynamical properties of the Venus theermosphere were initially inferred using a simplified linear spectral model and Pioneer Venus ONMS measurements (Niemann *et al.*, 1979, 1980; Mayr *et al.*, 1980). A combination of parametrically prescribed strong vertical eddy diffusion ($K \leq 3 \times 10^7 \, cm^2 \, s^{-1}$) and retrograde zonal winds (5–10 day period) seemed to modify the fundamental diurnal tide sufficiently to yield a reasonable match between observed and modeled phases and magnitudes of global temperatures and densities. Strong vertical eddy diffusion was required to counteract the mass-transport effects of the large-scale winds. Non-linear processes (i.e., wind-induced diffusion), important for helium and hydrogen, were estimated to steepen the nighttime density maxima and shift them significantly toward dawn (0200–0400 LT). Maximum horizontal winds of $\sim 200 \, m \, s^{-1}$ were inferred from the day–night density (temperature) variations observed by the ONMS. Strong vertical eddy diffusion, retrograde zonal winds, and reasonable day–night winds were all suggested to improve the DRM simulations.

Further work was described by Mayr *et al.* (1985), whose spectral model is more realistic in that it accounts for nonlinear processes, includes higher order tidal components, and describes the major gases in self-consistent form. Eddy diffusion and conduction were modified to vary inversely as the square root of the number density (after von Zahn *et al.*, 1980), with a maximum eddy coefficient of $6 \times 10^7 \, cm^2 \, s^{-1}$. The EUV heating efficiency was taken to be 30%. The basic diurnal contrasts in heavy (CO_2, CO, and O) and light (He) species and temperatures observed by PV were reproduced. Also, superrotating zonal winds (6-day period) were found to have little impact on the diurnal distributions of the heavy species and temperatures. However, a significant dayside depletion and nightside enhancement in O and CO densities (with respect to Hedin *et al.* (1983) values) was obtained. This occurs because the calculated solar-driven thermospheric wind system, with maximum horizontal wind speed of about $300 \, m \, s^{-1}$, is too strong. The Mayr *et al.* (1985) lower thermosphere wind speeds ($\sim 110 \, km \, s^{-1}$) are not consistent with ground-based measurements (Goldstein, 1989).

The group at NCAR updated and improved the DRM code, and subsequently adopted the finite-difference approach of the terrestrial Thermospheric General Circulation Model (TGCM) (cf. Dickinson *et al.*, 1984) modified for Venus. Bougher (1985) and Bougher *et al.* (1986) proposed that a global circulation system weaker than the DRM originally predicted would enable increased dayside O and CO densities to be maintained, while simultaneously reducing the buildup on the nightside. Furthermore, since nightside heating is maintained primarily from the circulation (i.e., adiabatic compressional heating), slower winds would also result in cooler nightside temperatures more indicative of a cryosphere. Suggestions along this line were also made by von Zahn *et al.* (1983) who noted that dayside O/CO_2 ratios increased for the series of Dickinson and Ridley (1972, 1975, 1977) models, due to progressively weaker day-to-night winds.

Schubert *et al.* (1983) also noted that dynamical processes may be required to explain the very low nightside thermospheric temperatures. Specifically, low temperatures must be maintained in the face of (1) advection and convection of dayside heat across the terminator, (2) compressional heating due to nightside subsidence, and (3) upward molecular heat conduction from the relatively warm 100 km level.

This weakened circulation hypothesis seems to give the most self-consistent explanation for all the available Pioneer Venus composition, temperature, and airglow data. An updated version of the DRM model was constructed by Bougher *et al.* (1986) to examine how SS–AS winds, eddy diffusion/conduction, and strong CO_2 15-μm cooling affect the day–night contrasts in Venus densities and temperatures. It was learned that symmetrized empirical model fields of Hedin *et al.* (1983) could be simulated largely by adding a wave-drag mechanism, resulting from turbulent dissipation effects on the horizontal winds, which weakened the day-to-night flow. Eddy viscosity and Rayleigh friction were parameterized within the horizontal momentum equation to mimic the wave-mean-flow interaction responsible (see Section 6.4). Maximum terminator winds of ≤ 230 m s^{-1} were found to be consistent with observed global composition and temperature fields. Such a reduction of winds by nearly a factor of two (from those of DRM) permitted less O and CO to be carried to the nightside. The dayside F1-peak O-mixing ratios were calculated to be $\sim 15\%$. The increased isolation of the day and nightside thermospheres also serves to enhance the diurnal temperature contrast, giving midnight exospheric temperatures of about 115 K, characteristic of the cold temperatures inferred from density data. This occurs because slower winds support less adiabatic compressional heating, the dominant source of nightside heating (Dickinson and Ridley, 1977). It was also shown that drag could not be used simultaneously with strong eddy conduction to derive the cold nightside temperatures. Slower winds are sufficient to maintain cold nightside temperatures, and are also consistent with the observed diurnal density contrasts. Winds calculated near 110 km match Earth-based measured values (100–140 m s^{-1}) quite well (Goldstein, 1989). Figures 41(a–d) illustrate contour plots from the standard NCAR 2-D model simulamtion (Bougher *et al.*, 1988) for solar maximum conditions ($F_{10.7} = 200$). Notice that constant pressure surfaces decrease in altitude from the day to the nightside, in agreement with the 'collapsed' nightside cryosphere observed.

Superrotation effects on thermospheric densities and temperatures can only be examined in a three-dimensional coupled chemical-dynamical model. A fully self-consistent code coupling large-scale and sub-grid scale effects, including wave-drag and superrotation, is very difficult to formulate. A prelude to such a code was developed by Bougher *et al.* (1988b), based on the NCAR terrestrial TGCM. The general framework of this Earth code (Dickinson *et al.*, 1984) was used in concert with new inputs and physical parameterizations to examine Venus thermospheric processes. The Venus TGCM (VTGCM) is internally self-consistent in that it calculates global distributions of CO_2, CO, and O that are consistent with the three-dimensional day–night temperature contrasts and corresponding large-scale winds. The model covers a 5° by 5° latitude-longitude grid, with 24 constant log-pressure levels in the vertical, extending
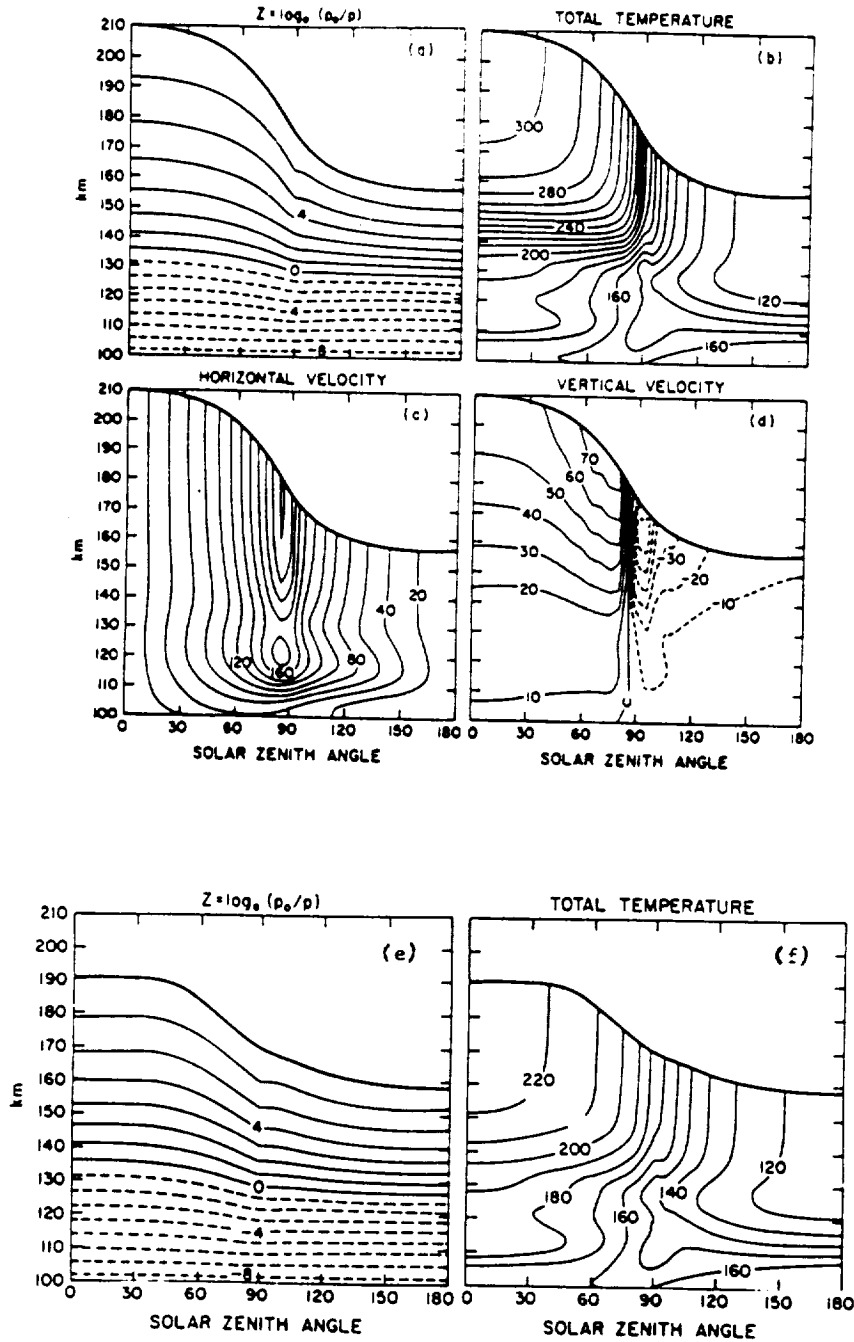
Fig. 41. NCAR 2-D model contour plots. All frames are presented on an altitude scale for convenience. The sharp upper level cutoff ($z = 7$) corresponds to the top boundary of the model. Solar maximum simulation: (a) $z = \log_e(p_0/p)$, (b) total temperature (K), (c) horizontal velocity in m s^{-1}, (d) vertical velocity in cm s^{-1}. Solar minimum simulation: (e) $z = \log_e(p_0/p)$, (f) total temperature (K). Taken from Bougher et al. (1986).

from approximately 105 to 200 km at local noon. Dayside O and CO sources arise from CO_2 net dissociation; sinks are provided primarily by advection and convection of the large-scale winds. Total temperature is derived as the sum of an adopted global mean reference temperature profile (Dickinson and Bougher, 1986) and calculated perturbation temperatures. Sub-grid scale processes (i.e., eddy diffusion, viscosity, conduction, and wave-drag) are not self-consistently incorporated, but rather parameterized using standard aeronomical formulations (cf. Hunten, 1974; von Zahn et al., 1980). Rayleigh friction is used to mimic wave-drag effects on the mean flow (see Section 6.4); its incorporation is analogous to early terrestrial mesopause studies which sought to define an approximate time-scale for the required wave-breaking process (Schoeberl and Strobel, 1978).

A symmetric form of the VTGCM was first used to examine the SS–AS circulation on Venus for solar maximum conditions (Bougher et al., 1988b). Inputs and parameters comparable to the NCAR 2-D model of Bougher et al. (1986) were incorporated, including a low 10% EUV heating efficiency, an O–CO_2 de-excitation rate coefficient of 8×10^{-13} cm^3 s^{-1} at 300 K, a maximum nightside eddy coefficient of 1×10^7 cm^2 s^{-1}, and minimal dayside eddy diffusion and cooling ($K \leq 5 \times 10^6$ cm^2 s^{-1}). Prescribed wave-drag (Raleigh friction coefficient $\leq 10^{-4}$ s^{-1}) was primarily responsible for the relatively weak winds calculated (≤ 230 m s^{-1}), which is consistent with the observed day–night contrast in calculated densities and temperatures. Model exospheric temperatures ranged from 309 K (day) to 136 K (night), simulating the nightside cryosphere seen by Pioneer Venus instruments.

Once the VTGCM was validated (in its symmetric form) by comparison with the NCAR 2-D code, further tests were conducted to examine the asymmetric character of the circulation by incorporating prescribed superrotating retrograde zonal winds. The adopted zonal wind profile was specified to increase from zero to 60 m s^{-1} over 105 to 140 km. Such a profile is consistent with recent suggestions that zonal flow near 100–110 km is quite weak (Clancy and Muhlemann, 1985; Goldstein, 1989), while zonal flow above 140 km is significant (Mayr et al., 1980, 1985). Results show that the major (heavy) species and temperatures are not greatly affected by this superrotation. However, the exospheric temperature minimum shifts to 02:00 LT, which is consistent with data and with the convergence of the horizontal winds after midnight. Figures 42(a) and 42(b) show pressure levels slices (at an average of 162 km) of VTGCM total temperatures, horizontal winds, and vertical winds. Also, the VTGCM nightside temperatures appear to be larger in the exosphere than in the lower thermosphere (see Figure 43); the NCAR 2-D model, formulated explicity for total temperatures, does not show this behavior. This discrepancy may be due to the difficulty of generating a representative global mean temperature profile for use with VTGCM perturbation values to give total temperatures (Bougher et al., 1988b).

A more sensitive tracer of the thermospheric winds is required to further constrain the circulation. The incorporation of minor (light) species, such as helium, can provide such a tracer of the SS–AS winds and the superimposed zonal wind component (Bougher et al., 1988b; Mengel et al., 1989). The magnitude of the nightside helium bulge
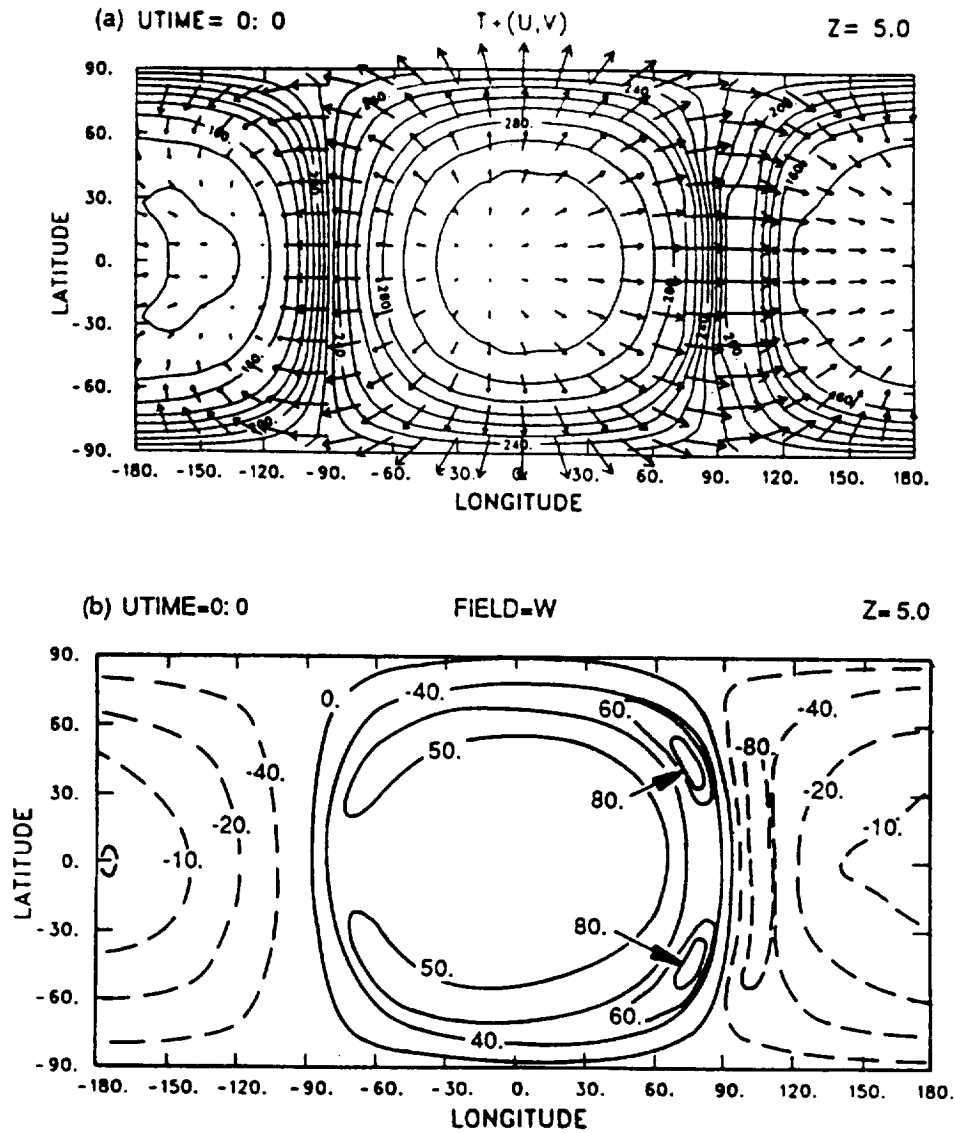
Fig. 42. VTGCM superrotating model pressure level slices (local time vs latitude) at $z = 5$ (or roughly 162 km average altitude): (a) $T + (u, v)$ – superimposed total temperature and horizontal wind vectors, (b) w – vertical velocity in cm s^{-1}. The maximum horizontal wind vector in (a) corresponds to 230 m s^{-1}. Taken from Bougher et al. (1988b).

should be very sensitive to the overall strength of the circulation and the amount of global eddy diffusion. Likewise, the local-time position of the bulge is a measure of the degree of asymmetry of the otherwise symmetric SS–AS flow. Mengel et al. (1989) presented calculations of helium that were used to fine tune the Mayr et al. (1985) 3-D spectral model circulation and eddy diffusion formulation. This improved model

VIRA — —
VTS3 ————
VTGCM —■—
BOUGHER et al., 1986 —●—
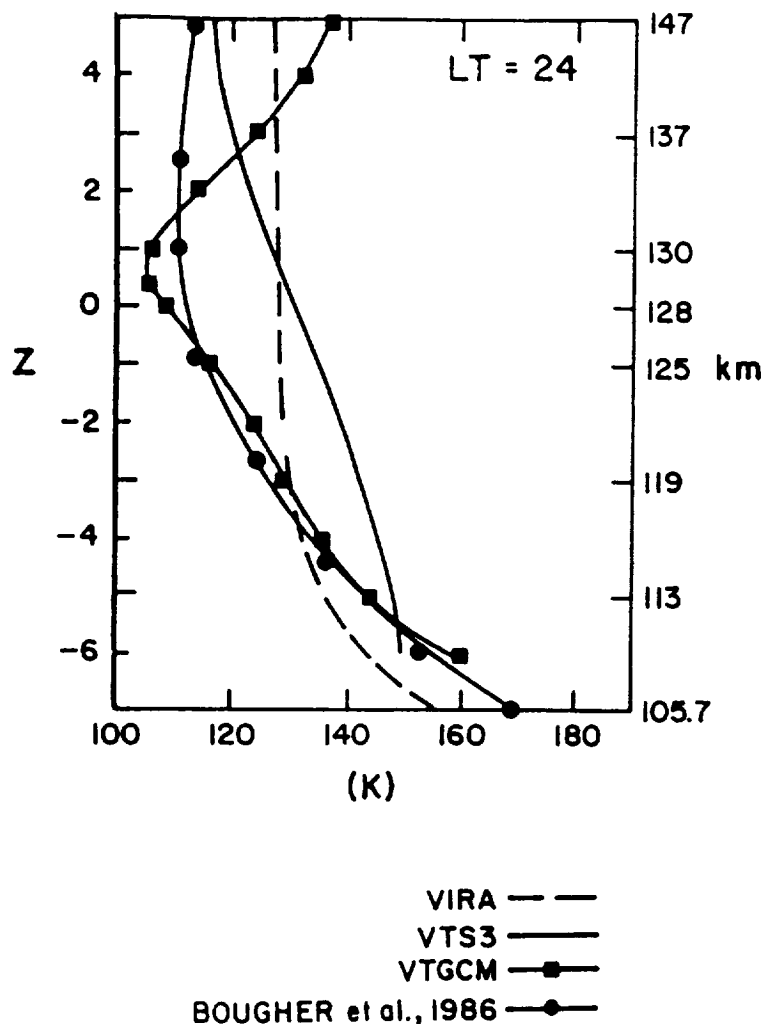
Fig. 43. VTGCM symmetric model (a) noon and (b) midnight temperature profiles above 100 km. Calculated profiles are compared to the corresponding empirical model profiles of Hedin *et al.* (1983)(VTS3) and Keating *et al.* (1985) (VIRA). The NCAR 2-D model profiles of Bougher *et al.* (1986) are also shown. Taken from Bougher *et al.* (1988b).

accounted for nonlinear processes and superrotation through a solid-shell approximation. They assumed a 6-day superrotation period and used the EUV heating rates of Fox (1988) with an efficiency close to 20%. An altitude dependent Rayleigh friction scheme (see Section 6.4) was also adopted to weaken the pressure driven winds.

Standard spectral-model profiles for noon, midnight, and global mean temperatures are illustrated in Figure 44. The global mean exospheric temperature of 220 K is consistent with data, and lies between 325 K (noon) and 155 K (midnight) model values for extreme solar maximum conditions. Superrotation was found to have relatively little

TEMPERATURE PROFILE
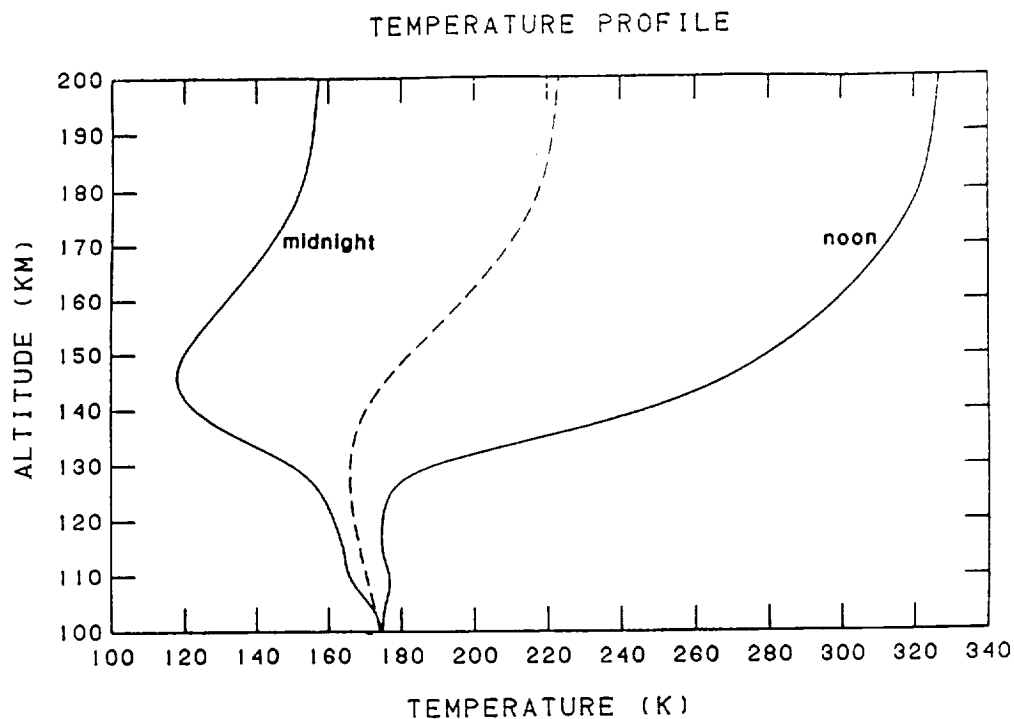
Fig. 44. Equatorial temperature:height profiles for the standard GSFC spectral model case. The solid lines are the noon and midnight temperatures. The dashed line is the globally averaged model profile. Extreme solar maximum conditions ($F10.7 = 238$). Taken from Mengel *et al.* (1989).

effect on the temperature contrast between day and night (see Figure 45(a)); however, it did produce a shift in the temperature minimum to 02 : 00 LT, in accord with observations. This dawn-dusk asymmetry in the flow also enabled the nightside helium bulge to peak at 05 : 00 LT (see Figure 45(b)). Its night–day ratio at 170 km was calculated to be 45 : 1, in good agreement with the 30 : 1 value seen at 165 km over the three diurnal periods analyzed by Taylor *et al.* (1984). Results show that the longer the superrotation period, the larger is the day-to-night buildup in the helium density, and the shorter is the time delay in the peak density after midnight. Figure 46 schematically shows the combined effects of the SS–AS flow plus the superrotating winds on the diurnal He density distribution. Both the horizontal and the vertical He distributions are also strongly dependent on the eddy diffusion coefficient. The data are best fitted by a SS–AS circulation of ~ 100 m s^{-1}, a moderate height-dependent global mean eddy diffusion ($K \leq 3 \times 10^7$ cm^2 s^{-1}), and a superrotation period of 6 Earth days. In this model, the Prandtl number, which is defined as the ratio of the kinematic viscosity to the thermal diffusivity, and indicates the relative efficiency of mass and heat transport by turbulence, was assumed to be unity. Strong superrotating zonal winds appear to reduce (smear out) the magnitude of the nightside helium bulge from what SS–AS wind-induced diffusion would otherwise produce.

EQUATORIAL CROSS-SECTION
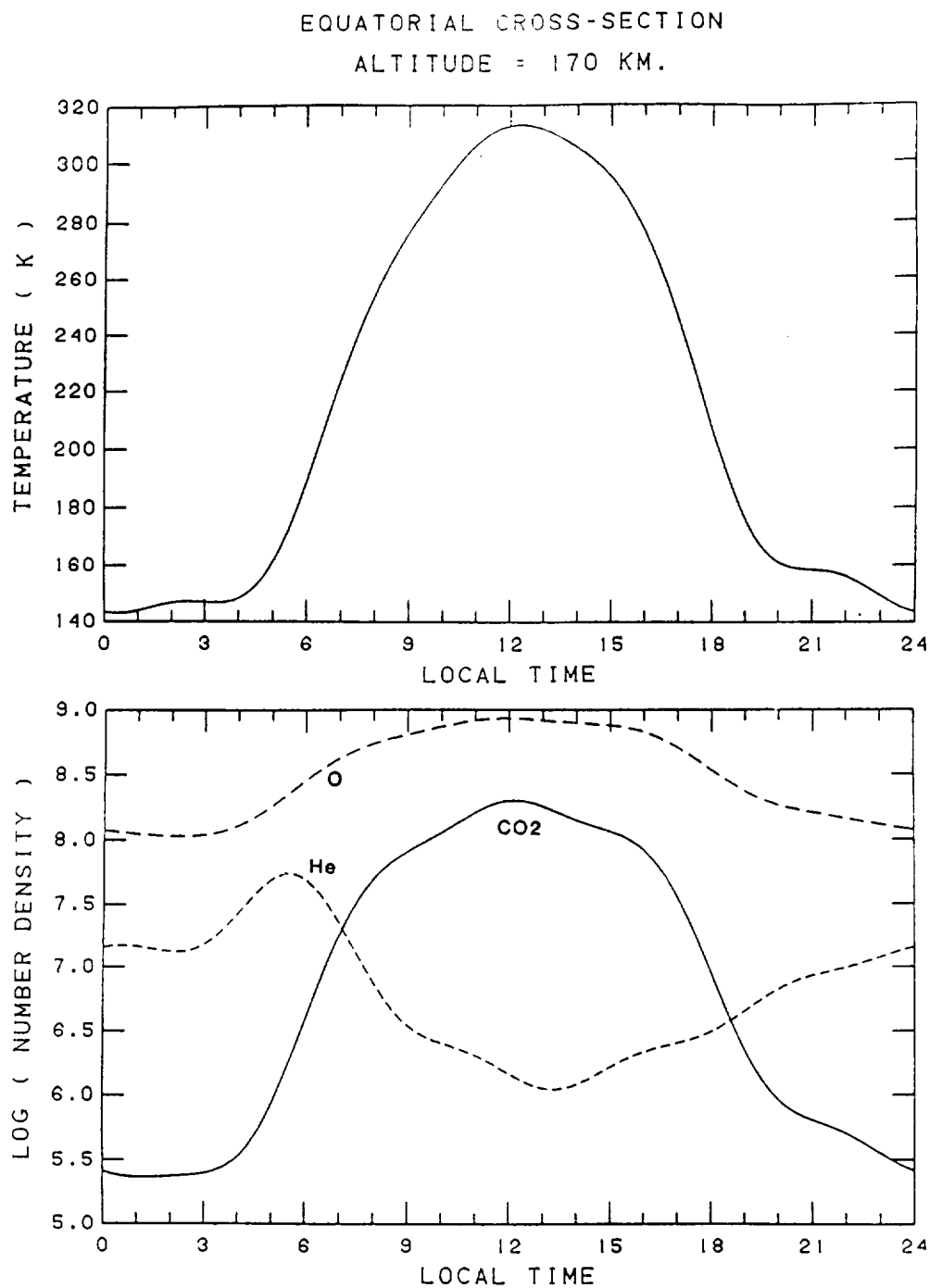
ALTITUDE = 170 KM.

Fig. 45.   Equatorial output fields vs local time at an altitude of 170 km for the standard GSFC spectral model. (a) Temperature; and (b) CO_2, O, and He number densities. Extreme solar maximum conditions ($F10.7 = 238$). Taken from Mengel et al. (1989).
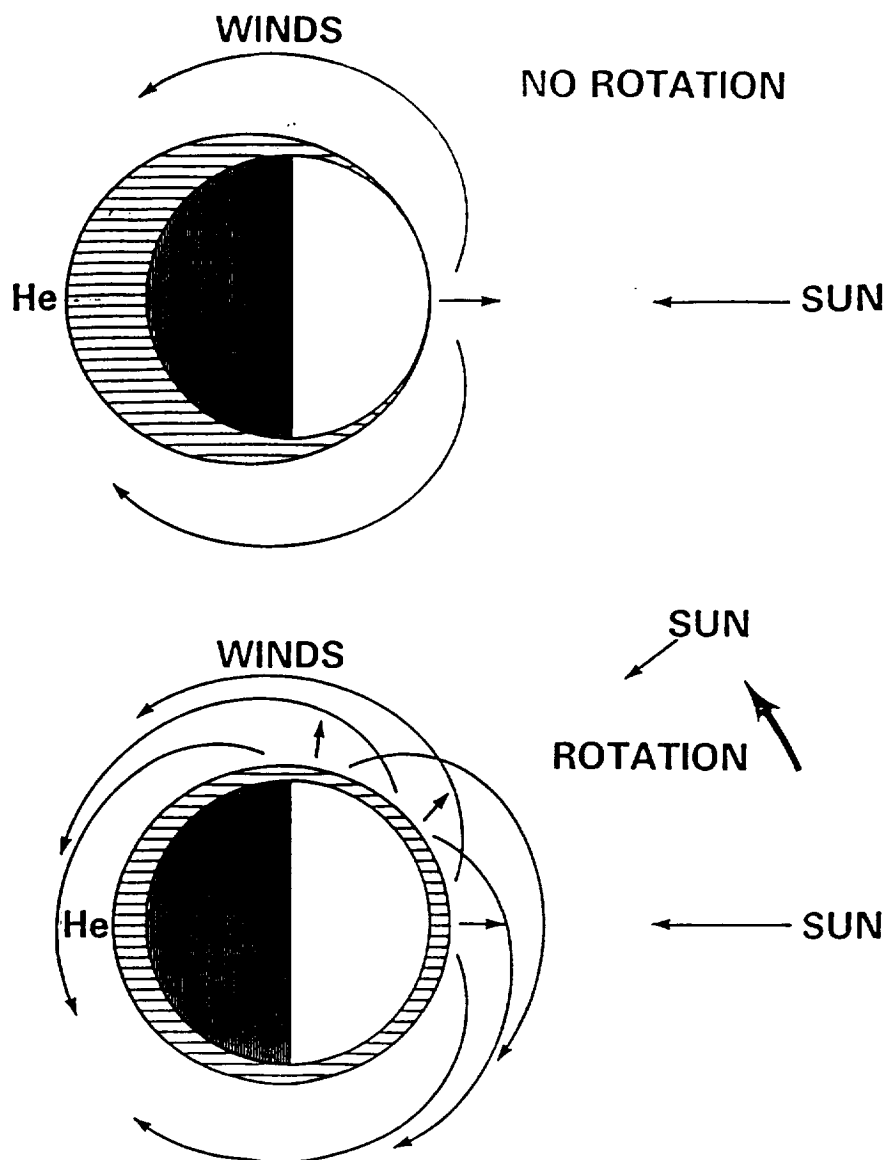
Fig. 46. Schematic illustrating the effect of atmospheric superrotation on the magnitude and phase of the diurnal variations of helium in the Venus thermosphere. Taken from Mengel *et al.* (1989).

An additional tracer of the thermospheric circulation is given by the observed NO nightglow, which is shown to be produced by radiative recombination of N and O atoms transported from their source on the dayside to the nightside (Bougher *et al.*, 1990a). This work, described in Section 3.10, shows how the maintenance of this nightglow constrains the magnitude of the SS–AS winds (≤ 150 m s^{-1}) and global mean eddy diffusion ($K \leq 2 \times 10^7$ cm^2 s^{-1}) in the face of moderate zonal winds (~ 55 m s^{-1})

having a period of 8 days. This nightglow provides a means to fine tune the VTGCM circulation presented by Bougher *et al.* (1988b).

It is apparent that differences in the mean state of the solar maximum Venus thermospheric circulation (and small-scale processes) still exist in the most recent model simulations (Bougher *et al.*, 1990a; Mengel *et al.*, 1989). However, the major tunable parameters have been identified: (1) zonal superrotation period, (2) the magnitude of the maximum global mean eddy diffusion coefficient, and (3) the magnitude of the peak Rayleigh friction coefficient (see Section 6.4) which is used to modify SS–AS wind speeds. A reasonable range of peak SS–AS wind speeds is ~ 100–200 m s^{-1}, yielding a close match of model fields to available temperature, density, and airglow data.

6.3. DEPARTURES FROM RADIATIVE EQUILIBRIUM: ADIABATIC EFFECTS

Radiative heating and cooling processes can be augmented by dynamical effects in planetary atmospheres, thereby maintaining temperatures that depart from radiative equilibrium values. This is particularly the case for Venus's nightside, in which a given planet-fixed meridian experiences darkness for as much as 117 Earth days. The nightside temperatures would be expected to be extremely cold without some sort of day-to-night heat redistribution. The NCAR dynamical models of Dickinson and Ridley (1977) and Bougher *et al.* (1986, 1988b) have all presented heat budgets thought to maintain day and night temperatures. Little difference in mean dayside heat balances is estimated between 1-D and 3-D models; i.e., adiabatic cooling (due to upwelling/divergent flow) is negligible (Bougher *et al.*, 1986).

Thermospheric winds, however, have a controlling effect on the maintenance of nightside temperatures. Weakened SS–AS winds have produced a significant change in the nightside heat budget that has enabled nightside cryospheric temperatures to be explained (Bougher *et al.*, 1986, 1988b). Figure 47 shows heating and cooling rates at 120 SZA for both the NCAR 2-D and VTGCM model calculations. Notice that adiabatic heating (from subsiding/convergent winds) largely balances CO_2 15-μm cooling below 140 km. Above, molecular conduction is offset by this same compressional heating. The magnitude of this heating is reduced by about a factor of three from the Dickinson and Ridley (1977) model, permitting the observed cold nightside temperatures (Niemann *et al.*, 1979, 1980b; Keating *et al.*, 1980) to be reproduced. Early ideas that invoked nightside eddy heat conduction to give cold nightside temperatures (cf. Niemann *et al.*, 1980b; Schubert *et al.*, 1983; Gordiets and Kulikov, 1985) appear to be inappropriate. Observed nightside temperatures (and the diurnal density contrasts) can be maintained by weakened thermospheric winds alone (Bougher *et al.*, 1986).

6.4. DRAG PROCESSES

It is evident by the observed day–night density and temperature contrasts that some type of deceleration mechanism is necessary to slow the otherwise pressure-driven neutral winds (Seiff, 1982; Bougher *et al.*, 1986). Early in the Pioneer Venus mission, thought was given to ion-drag and its possible influence on neutral winds (Mayr *et al.*, 1980).
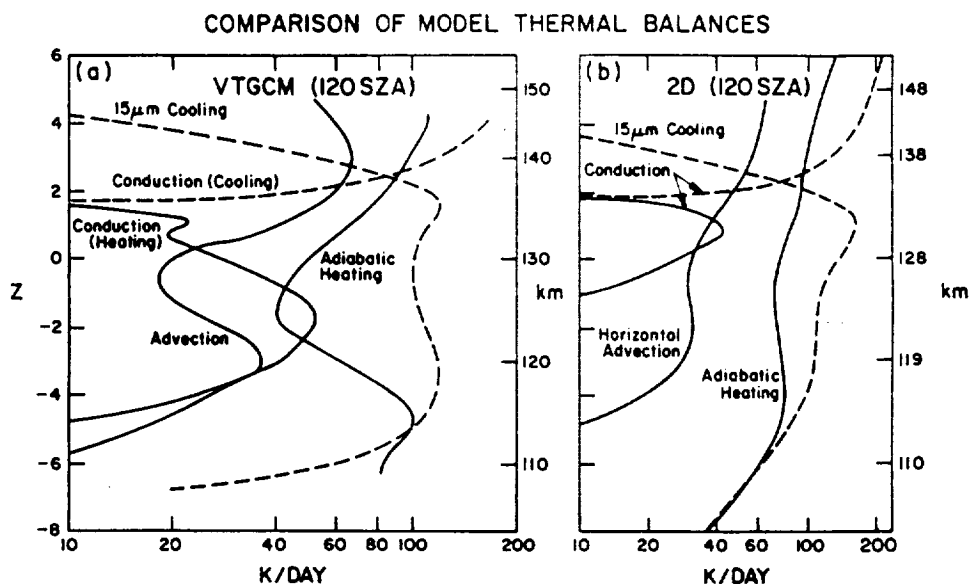
COMPARISON OF MODEL THERMAL BALANCES

Fig. 47. A comparison of nightside mean heat balances for the NCAR VTGCM and 2-D models at 120 SZA. Units in K Earth day^{-1}. (a) VTGCM symmetric model heat balances at the equator, and (b) 2-D model heat balances. Taken from Bougher et al. (1988b).

Since Venus does not have a significant intrinsic magnetic field (Russell et al., 1979), ions are not generally confined to field lines, thereby eliminating a 'grid' for neutrals to encounter. Rather, large horizontal ion-drift velocities, measured by the PV ion mass spectrometer (Taylor et al., 1980) and the retarding potential analyzer (Knudsen et al., 1980) (on the order of ≤ 1 km s^{-1} below 200 km), may carry along neutrals to the nightside. This effect was estimated to be negligible since ion-neutral collision frequencies below 200 km are small (Mayr et al., 1980). The situation may be different during times of high solar wind dynamic pressure, when the region below the minimum ionopause (∼ 220 km) may be penetrated by interplanetary magnetic fields (Luhmann et al., 1987). Under these conditions, temporary fields may generate a possible ion-neutral drag for ion velocities in excess of neutral velocities. A definitive analysis awaits a 3-D coupled ionosphere/thermosphere calculation of global winds.

Alternatively, there is ample evidence for turbulence or wave perturbations in the upper atmosphere of Venus (Seiff et al., 1980; Seiff, 1982; von Zahn et al., 1983; Kasprzak et al., 1988; Mayr et al., 1988). All available observations, however, are snapshots of wave structure; horizontal (vertical) wavelengths in the range of 100–600 km (5–15 km) have been observed in the major neutral densities. There seems to be more wave activity during nighttime than during the day, with considerable activity occurring in the vicinity of the predawn and postdusk terminators. Comparison with the model of Mayr et al. (1988) shows that the observed perturbations can be interpreted as being due to gravity waves propagating upward from source regions in the lower

thermosphere (130 km), or below 80 km. Most important, the data imply that significant wave energy arrives in the thermosphere from lower altitudes on a continuing basis. The effect of such waves on the thermospheric densities, temperatures, and winds is significant. Specifically, nightside neutral densities vary by as much as $\pm 50\%$ from day-to-day, likely due to upward propagating waves (Hedin et al., 1983; Kasprzak et al., 1988).

Eddy conduction, eddy or wave drag, and eddy diffusion are typically parameterized in planetary models to mimic turbulent effects on temperatures, densities, and winds. For the Earth, it has been shown that the heat and momentum budgets near the mesopause cannot both be simultaneously satisfied without a strong zonal drag force (Lindzen, 1981; Holton, 1982, 1983). Such a frictional force is required to simulate the reversal of the latitudinal temperature gradient observed at the mesopause, with the lowest temperatures at the summer pole (due to adiabatic cooling from upwelling) and the warmest at the winter pole (due to adiabatic heating from subsidence). A modified meridional circulation is responsible. The underlying mechanism has long been thought to result from the unstable breakdown of tides or gravity waves near the terrestrial mesopause. Waves generated in the troposphere are assumed to attain sufficient amplitudes in the mesosphere to produce superadiabatic lapse rates, giving rise to convective overturning and turbulence. This causes attenuation of further growth and a convergence of the vertical momentum flux, resulting in a net zonal drag force (Lindzen, 1981; Holton, 1982, 1983).

Rayleigh friction is an *ad hoc* scheme commonly used to mimic this 'wave-drag' force *in-lieu* of self-consistently calculating momentum stress terms based on wave properties and the large-scale flow. Specifically, Rayleigh friction is formulated as a damping term added to the horizontal equation of motion which is proportional to the horizontal velocity. The constant of proportionality is assigned a fixed peak value (s^{-1}) at some reference level, and prescribed to vary as a function of altitude (or pressure) below. The shape of the profile is usually chosen to be that of the corresponding eddy coefficient used in the model study.

Models of this terrestrial wave drag progressed from crude Rayleigh friction schemes (Schoeberl and Strobel, 1978), to current wave drag models patterned after Lindzen (1981) and Holton (1982), which describe self-consistent methods for parameterizing the stress and diffusion due to gravity wave breaking in terms of the mean zonal wind, static stability, and specific wave parameters. A height-dependent Rayleigh friction is a first choice when little is known about wave parameters and their source. The initial approach for Venus has been guided by these terrestrial mesopause wave-drag schemes and the underlying wave-breaking mechanism as well. Bougher et al. (1986) assumed that small-scale gravity waves are responsible for the observed wavelike features in the altitude profiles of temperature and density (Seiff et al., 1980; Schubert, 1983). A deceleration of the SS–AS winds is proposed to become important at a level where wave-breaking maximizes; i.e., also where eddy diffusion peaks on the dayside (135–140 km). A profile for drag is prescribed that increases with height up to this level, consistent with a vertical propagating spectrum of waves each of which breaks at a different level. A Rayleigh friction time-scale of $\leq 1 \times 10^{-4}\ s^{-1}$ is specified. This leaves

SS–AS winds below 110 km largely unaffected, while those near 150 km are reduced from Dickinson and Ridley (1977) values by a factor to two.

The day–night contrasts in observed Venus thermospheric temperatures and densities are closely matched by Bougher et al. (1986) using this wave-drag mechanism (see Section 6.2). It is, however, somewhat unsatisfying that an ad hoc formulation, rather than a self-consistent scheme, for wave-induced drag was used. Nevertheless, Rayleigh friction is the best that can be used until further wave parameters (and measured thermospheric winds) are available. The Bougher et al. (1986, 1988b) and Mengel et al. (1989) benchmark models, all of which rely on Rayleigh friction, serve as starting points for later studies.

6.5. THERMOSPHERIC SUPERROTATION

The observed asymmetries in the helium (and hydrogen) densities, as well as the observed NO nightglow intensity (Niemann et al., 1980b; Brinton et al., 1980; Stewart et al., 1980), suggest that the Venus thermosphere superrotates (above 150 km) with a period of 5 to 10 days (Mayr et al., 1980, 1985). The origin of this superrotation is not known. Thermospheric superrotation could be a remnant of the cloud-top 4-day zonal winds observed in the lower atmosphere (cf. Schubert and Walterscheid, 1984). A decrease in the superrotation rate between the cloud tops (4-day period) and the thermosphere is related to the temperature reversal observed above 70 km (where it increases toward the poles). In principle, thermospheric superrotation could also be generated in situ, presumably through zonally symmetric pressure gradients producing a geostrophic or cyclostrophic balance or by nonlinear interactions involving the diurnal tides (Mengel et al., 1989).

All circulation model studies to date have chosen to circumvent this question of the origin of this zonal flow, in order to examine its effects on the thermospheric structure (Mayr et al., 1985; Bougher et al., 1988b; Mengel et al., 1989). Mayr et al. (1985) and Mengel et al. (1989) both specify a solid-body rotation in which SS–AS winds are calculated with respect to a rotating reference frame. This has the effect of adding zonal wind speeds of ~ 75 m s^{-1} at the equator. A considerable shift in the nightside helium bulge (to 05:00 LT) is produced. However, any altitude dependence of a zonal wind profile cannot be given by assuming solid-body rotation. Bougher et al. (1988b) prescribed an altitude dependent zonal wind profile increasing from zero to 60 m s^{-1} over 105 to 140 km. This vertical variation is consistent with weak zonal winds at 100–110 km (Clancy and Muhlemann, 1985b; Goldstein, 1989) and strong zonal winds above 150 km (Mayr et al., 1980). Since tracer species are thought to generally follow constant pressure surfaces (streamlines) in their path from the day to the nightside, zonal wind shear could be important in modifying the nightside distribution of helium densities and NO nightglow intensities. A self-consistent model formulation (and mechanism) needs to be developed to explain Venus thermospheric superrotation. These initial sensitivity studies serve as useful starting points for future work.

6.6. CONCEPT OF HOMOPAUSE REVISITED

One-dimensional coupled continuity-diffusion models are a reasonable first step in modeling the vertical density profiles observed in the Venus dayside thermosphere. Von Zahn et al. (1980) developed a morningside model at 60 SZA for examination of BNMS densities above 130 km. The success of the model fit to observations is in large part due to the chosen estimate of the altitude dependance of the eddy coefficient profile used for eddy diffusion. The analytical representation of the eddy coefficient profile was taken from Lindzen (1971) as $K = A/\sqrt{N}$, where N is total number density, and A is a tuning factor chosen to be 1.4×10^{13} cm$^{0.5}$ s^{-1}. The helium data taken by the BNMS were used to constrain the eddy profile and provide this specific factor. The upper level cutoff was set at $K = 5 \times 10^{8}$ cm^{2} s^{-1}, despite the fact that unique values above the homopause (where eddy and molecular diffusion are equal) are not easily determined or meaningful. Homopause altitudes were established at 136, 130, and 134 km for N_2, He, and mean composition, respectively. A similar approach was taken by Massie et al. (1983), who incorporated detailed chemistry and von Zahn et al. (1980) eddy diffusion coefficients ($K \leq 5 \times 10^{7}$ cm^{2} s^{-1}) in an improved dayside model extending down to 100 km. A nightside mean model was also constructed assuming dayside fluxes of O- and N-atoms as upper boundary conditions for the nightside equations. One dimensional models of this type are subject to several limitations, the principal one of which concerns the neglected or improperly parameterized effects of large-scale winds on the calculated densities (Bougher, 1985).

By contrast, Venus circulation model studies of Bougher et al. (1990a) and Mengel et al. (1989) suggest that vertical small-scale eddy diffusion is only a partial contributor to the maintenance of observed day and nightside thermospheric densities. Eddy coefficients required are about 2–3 times smaller than values used by previous one-dimensional composition models (von Zahn et al., 1980; Stewart et al., 1980; Massie et al., 1983). This implies that the vertical eddy coefficient dependence derived by von Zahn et al. (1980) within a one-dimensional model is not solely a signature of small-scale vertical mixing. Rather, it provides a reasonable description of compositional variations brought about by a combination of large-scale horizontal and vertical winds and small-scale mixing. The conventional homopause, a well-defined level where molecular diffusion and eddy mixing processes balance, might better be described as a statistically average level where gravitational separation is offset by global wind plus small-scale mixing effects. The changing Venus thermospheric circulation has a modest influence on this level at any time. In general, one-dimensional eddy mixing models are valuable since they quantify the magnitude of the total dynamical effect expected; however, no information on the relative contribution of winds or turbulence can be obtained (von Zahn et al., 1980; Bougher et al., 1986, 1990a).

Current Venus modeling efforts (Bougher et al., 1990a; Mengel et al., 1989) disagree as to the magnitude of this residual eddy diffusion required to supplement global circulation in maintaining observed vertical and diurnal density distributions at solar maximum. The bougher et al. (1989) VTGCM cannot tolerate global eddy diffusion

exceeding $2 \times 10^7 \, cm^2 \, s^{-1}$ and still yield atomic-N and O densities that reasonably match Hedin et al. (1983) empirical model values. Furthermore, the altitude of the NO nightglow peak volume emission rate (115 ± 2 km) is a very sensitive indicator of the nightside eddy diffusion possible within this global circulation model. Global winds for this code reach a maximum of ~ 100–$200 \, m \, s^{-1}$ across the terminators for a super-position of SS–AS and prescribed zonal winds having a period of 8 days. Conversely, the Mengel et al. (1989) spectral model uses eddy diffusion reaching $3 \times 10^7 \, cm^2 \, s^{-1}$, in concert with maximum horizontal winds of $\sim 100 \, m \, s^{-1}$, to obtain observed diurnal helium distributions. Superrotating winds are included with a 6-day period.

The discrepancies in eddy, wind (wave-drag), and superrotation parameters in these two models reflect the difficulty in obtaining a unique solution without further observations, namely measurements of thermospheric winds. The effectiveness of the circulation in building up the nightside densities of atomic-O (and lighter species) decreases as the eddy coefficient increases. Likewise, the magnitude of the circulation regulates the amount that can be transported from day to night. Furthermore, superrotating winds not only shift the local time position of the nightside helium, hydrogen and NO airglow bulges, but they also serve to 'smear out' the magnitudes of these bulges. Therefore, future progress in Venus thermospheric modeling will likely require either remote or in situ wind measurements for convergence on a unique combination of wind, eddy, and superrotation parameters.

7. Solar Cycle Variation

Very little thermospheric data exists for Venus at solar minimum. A range of exospheric temperatures (275 ± 50 K) was obtained from Mariner 5 and 10 Lα data (Anderson, 1976; Takacs et al., 1980) taken in October 1967 and February 1974, respectively. The latter corresponds to a near minimum in the solar cycle ($F_{10.7} = 68$). The Venera 9 and 10 orbiters also visited the planet in October 1975 through February 1976. Remote Lα (Bertaux et al., 1978) and visible airglow (Krasnopolsky et al., 1976) observations were made ($F_{10.7} = 75$). No definitive estimate of neutral temperatures could, however, be derived. Lastly, the Pioneer Venus orbiter took in situ neutral data for nearly three diurnal periods (1978–1980). Periapsis altitude was actively controlled to remain within an altitude range of about 145–160 km until June, 1980. Afterward, this altitude was allowed to rise to a maximum mean value of about 2200 km in 1986. Presently, periapsis is moving downward toward an entry and burn-up in 1992. The only in situ neutral/ion observations available are for near solar maximum conditions ($F_{10.7} = 150$–240).

Nevertheless, remote information regarding the ionosphere/thermosphere at solar minimum was obtained from various radio occultation measurements (Kliore and Mullen, 1988). Most of this data in fact comes from the Pioneer Venus Orbiter, although a few profiles come from Venera 9/10 and Mariner 10 (Kliore and Mullen, 1987; Kim et al., 1989). Photochemical equilibrium conditions hold for the major dayside ion densities below ~ 180 km (Cravens et al., 1981; Kim et al., 1989). Therefore, the most useful electron density measurements for inferring neutral temperatures are just above

the ion peak (≥ 140 km). A simple model (Kliore and Mullen, 1987) suggests that neutral temperatures during 1984–1986 at 150 km (55–75 SZA) are about 215 K, nearly 60 K lower than values at solar maximum (275 K). Mars derived neutral temperatures near its dayside ionospheric peak, also based on radio occultation electron density data, similarly show a rather weak dependence on $F_{10.7}$ (Bauer and Hantsch, 1989). Solar cycle exospheric temperatures, however, vary by a larger amount than ionospheric peak values, especially for Mars (Bougher and Dickinson, 1988; Bougher et al., 1988a).

Bauer and Taylor (1981) sought to explain the weak solar cycle response of the Venus thermosphere compared to that of the Earth as arising from the stronger temperature dependence of the conductivity of CO_2 ($K \sim T^{1.23}$) compared to that of O ($K \sim T^{0.71}$). Dickinson and Bougher (1986) showed, however, that conduction is the dominant cooling mechanism only above 160 km on Venus, where O is the dominant constituent.

The Venus electron/ion density calculations of Kim et al. (1989) indicate that the Hedin et al. (1983) model predicts the neutral densities reasonably well for dayside solar minimum conditions; i.e., the resulting ion peak is given at the observed altitude (139–140 km). The empirical models of Hedin et al. (1983) and Keating et al. (1985), based primarily on in situ solar maximum data, predict a solar cycle exospheric temperature variation ($F_{10.7} = 200$ to 70) of about 55 to 70 K (310 to 255 K and 310 to 240 K, respectively). The well monitored 27-day exospheric temperature variation of ± 11 K (cf. Keating and Bougher, 1987) also suggests that a larger, non-negligible, solar cycle variation exists. However, without additional Venus in situ density (or temperature) measurements, a firm confirmation of this rather weak thermospheric response to the solar cycle is still lacking! Figure 48 illustrates a collection of possible dayside Venus solar minimum neutral temperature profiles. The only data on the plot comes from the PV–ORO radio occultation measurements of Kliore and Mullen (1987).

The true test of a useful predictive model is its ability to reliably simulate the observed fields under a wide range of conditions. The NCAR 1-D (Dickinson and Bougher, 1986), 2-D (Bougher et al., 1986) and VTGCM (Bougher et al., 1990a) models have been modified to predict the Venus solar minimum thermospheric circulation (dynamical models) and structure. The primary solar cycle change occurs in the EUV fluxes shortward of 105 nm; i.e., a reduction of peak EUV heating and net CO_2 dissociation is given of approximately a factor of 3. This is consistent with a 21% smaller peak ion density (55–75 SZA) for solar minimum than solar maximum (Kliore and Mullen, 1987). Indirectly, through cooler temperatures, CO_2 15-μm cooling is also reduced, since it is strongly nonlinearly temperature dependent. The EUV fluxes of Heroux and Hinteregger (1978) were chosen, corresponding to an $F_{10.7} = 74$.

Dickinson and Bougher (1986) confirmed that the Venus exospheric temperatures should be relatively insensitive to changes in the solar flux; dayside values were shown to change by less than ~ 65 K over the solar cycle (300 to 235 K). The strong nonlinear temperature dependence of the CO_2 cooling and the variation of atomic oxygen densities with solar activity ('the atomic O thermostat') effectively buffer against solar perturbations, thereby reducing the temperature variation from that which would occur if a balance were present between peak EUV heating and molecular conduction. Corre-
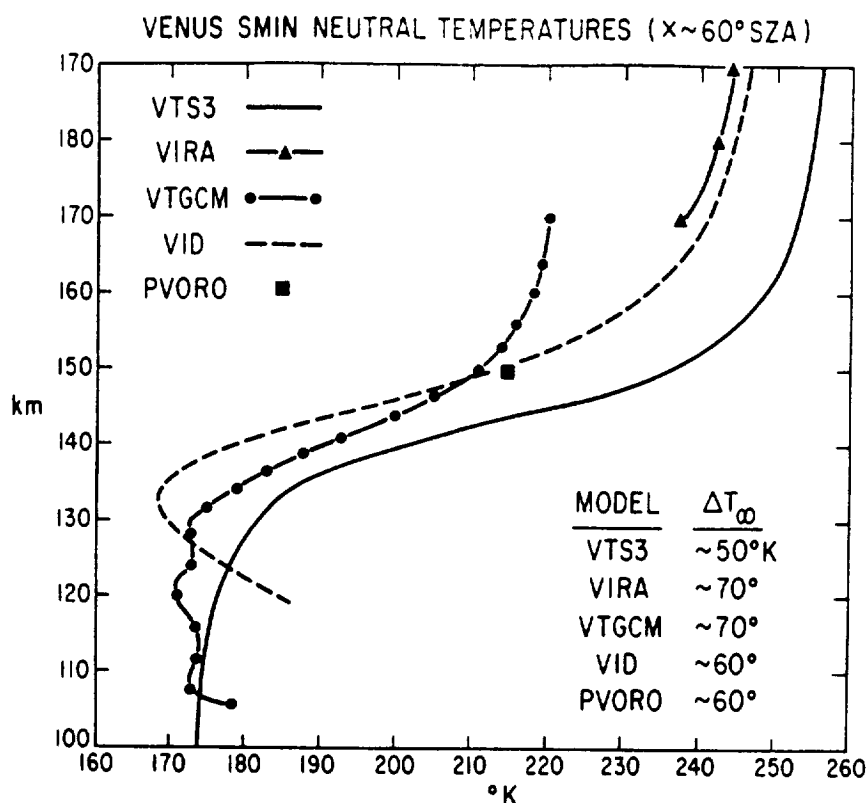
VENUS SMIN NEUTRAL TEMPERATURES (x~60°SZA)

Fig. 48. Venus dayside solar minimum neutral temperature profiles (60 SZA). VTS3 and VIRA profiles are only reasonable extrapolations from near solar maximum data. The one true data point is inferred from ORO measured electron density profiles just above the ion peak (150 km). The NCAR 1-D (VID) and VTGCM model predictions are also shown for comparison.

sponding nightside mean calculations suggested that little change in temperatures with solar activity should be expected, so that global mean values drop by only 30 K from solar maximum.

Hydrodynamic effects were carefully examined in subsequent Venus circulation models for an improved description of solar cycle response. Figures 41(e–f) illustrate NCAR 2-D solar minimum contour plots, for comparison to corresponding solar maximum fields of Figures 41(a) and 41(b). The dayside exospheric temperatures are reduced from 300 K to ~230 K, giving a dayside solar cycle temperature variation of at most 70 K. These newly calculated dayside solar minimum temperatures are somewhat low, yet the values fall within the range of exospheric temperatures estimated from Mariner 5 and 10 Lα data (Anderson, 1976; Takacs et al., 1980). Also, values at 150 km (over 55–75 SZA) are close to 215 K, quite similar to those inferred from 1984–1986 radio occultation data (Kliore and Mullen, 1987). Adiabatic cooling serves to reduce dayside temperatures slightly below previous radiative equilibrium model values (Dickinson and Bougher, 1986). The solar driven winds are also 20–30 m s^{-1} weaker; this slight change

causes the nightside thermospheric major densities and temperatures to remain largely the same. Both the NCAR 2-D and VTGCM solar minimum models suggest that the Venus thermospheric major densities and temperatures are relatively insensitive to the factor of 3 reduction in EUV inputs over the solar cycle (Bougher et al., 1986, 1990a).

This does not appear to be the case for tracer species and the UV nightglow. Odd-nitrogen studies using the VTGCM (see Section 3.10) predict a variation of nearly a factor of 3 in the $NO(0, 1)$ δ-band intensities over the solar cycle (see Figures 20(a) and 20(b)). This sensitivity is due to the net change in dayside production of N-atoms, which varies strongly with solar cycle. A detailed analysis of recently obtained PV–OUVS data taken from 1984–1986 will provide an opportunity to validate this VTGCM solar cycle nightglow variation. A reasonable match of the model and OUVS imaged dark-disk intensity variation over the solar cycle would be a substantial validation of the odd-nitrogen chemistry adopted and the solar cycle response predicted by the VTGCM thermospheric winds. Also, since the NO nightglow is a good tracer of the Venus thermospheric circulation, its monitoring over the solar cycle should provide a remote means to study the variation of the winds once the dayside N-production is calculated.

Acknowledgements

References

Abreu, V. J., Eastes, R. W., Yee, J. H., Solomon, S. C., and Chakrabarti, S.: 1986, 'Ultraviolet Nightglow Production Near the Magnetic Equator by Neutral Particle Precipitation', J. Geophys. Res. 91, 11365.
Adams, W. S. and Dunham, T.: 1932, 'Absorption Bands in the Infrared Spectrum of Venus', Publ. Astron. Soc. Pacific 44, 243.
Ajello, J. M.: 1971, 'Emission Cross Section of CO_2 by Electron Impact in the Interval 1260–4500 Å', J. Chem. Phys. 55, 3169.
Alge, E., Adams, N. G., and Smith, D.: 1987, 'Measurements of the Dissociative Recombination Coefficients of O_2^+, NO^+, and NH_4^+ in the Temperature Range 200–600 K', J. Phys. B16, 1433.
Allen, D. C., Scragg, T., and Simpson, C. J. S. M.: 1980, 'Low Temperature Fluorescence Studies of the Deactivation of the Bend-Stretch Manifold of CO_2', Chemical Phys. 51, 279.
Ali, A. A., Ogryzlo, E. A., Shen, Y. Q., and Wassel, P. T.: 1986, 'The Formation of $O_2(a^1\Delta_g)$ in Homogeneous and Heterogeneous Atom Recombination', Can. J. Phys. 64, 1614.
Anderson, D. E.: 1975, 'The Mariner 5 Ultraviolet Photometer Experiment: Analysis of Rayleigh-Scattering and 1304-Å Radiation from Venus', J. Geophys. Res. 80, 3063.
Anderson, D. E.: 1976, 'The Mariner 5 Ultraviolet Spectrometer Experiment: Analysis of Hydrogen Lyman-α Data', J. Geophys. Res. 81, 1213.
Anderson, D. E., Klein, F. S., and Kaufman, F.: 1986, 'Kinetics of the Isotope Exchange Reaction of ^{18}O with NO and O_2 at 298 K', J. Chem. Phys. 1648.
Atkinson, R. and Welge, K. H.: 1972, 'Temperature Dependence of $O(^1S)$ Deactivation by CO_2, O_2, N_2, and Ar', J. Chem. Phys. 57, 3689.

Atreya, S. K., Pollack, J. B., and Matthews, M. S.: 1989, *Origin and Evolution of Planetary and Satellite Atmospheres*, Univ. of Arizona Press, Tucson.

Baker, N. L. and Leovy, C. B.: 1987, 'Zonal Winds Near Venus' Cloud Top Level: A Model Study of the Interaction between the Zonal Mean Circulation and the Semidiurnal Tide', *Icarus* 69, 202.

Banks, P. M. and Kockarts, G.: 1973, *Aeronomy*, Academic Press, New York.

Barker, E. S.: 1975, 'Observations of Venus Water Vapour over the Disc of Venus', *Icarus* 25, 268.

Varth, C. A.: 1964, 'Three-Body Reactions', *Ann. Geophys.* 20, 183.

Barth, C. A.: 1968, 'Interpretation of Mariner 5 Lyman Alpha Measurements', *J. Atmospheric Sci.* 25, 564.

Barth, C. A.: 1969, 'Planetary Ultraviolet Spectroscopy', *Appl. Optics* 8, 1295.

Barth, C. A., Pierce, J. B., Kelly, K. K., Wallace, L., and Fastie, W. G.: 1967, 'Ultraviolet Emission Observed Near Venus from Mariner V', *Science* 158, 1675.

Barth, C. A., Wallace, L., and Pearce, J. B.: 1968, 'Mariner 5 Measurement of Lyman-alpha Radiation Near Venus', *J. Geophys. Res.* 73, 2541.

Barth, C. A., Hord, C. W., Pearce, J. B., Kelly, K. K., Anderson, G. P., and Stewart, A. I.: 1971, 'Mariner 6 and 7 Ultraviolet Spectrometer Experiment: Upper Atmospheric Data', *J. Geophys. Res.* 76, 2213.

Barth, C. A., Hord, C. W., Stewart, A. I., and Lane, A. L.: 1972, 'Mariner 9 Ultraviolet Spectrometer Experiment: Initial Results', *Science* 175, 309.

Bass, J. N.: 1974, 'Translation to Vibration Energy Transfer in O + NH_3 and O + CO_2 Collisions', *J. Chem. Phys.* 60, 2913.

Bates, D. R.: 1981, 'The Green Light of the Night Sky', *Planetary Space Sci.* 29, 1061.

Bates, D. R.: 1988a, 'Transition Probabilities of the Bands of the Oxygen Systems of the Nightglow', *Planetary Space Sci.* 36, 869.

Bates, D. R.: 1988b, 'Excitation and Quenching of the Oxygen Bands in the Nightglow', *Planetary Space Sci.* 36, 875.

Bates, D. R.: 1988c, 'Excitation of 447.7 nm Line in Nightglow', *Planetary Space Sci.* 36, 883.

Bates, D. R.: 1989, 'Oxygen Band System Transition Arrays', *Planetary Space Sci.* 37, 881.

Bates, D. R. and Zipf, E. C.: 1980, 'The $O(^1S)$ Quantum Yield from O_2^+ Dissociative Recombination', *Planetary Space Sci.* 28, 1081.

Bauer, S. J. and Hantsch, M. H.: 1989, 'Solar Cycle Variation of the Upper Atmosphere Temperature of Mars', *Geophys. Res. Letters* 16, 373.

Bauer, S. J. and Taylor, H. A.: 1981, 'Modulation of Venus Ion Densities Associated with Solar Variations', *Geophys. Res. Letters* 8, 840.

Bauer, S. H., Caballero, J. F., Curtis, R., and Wiesenfeld, J. R.: 1987, 'Vibrational Relaxation Rates of $CO_2(001)$ with Various Collision Partners for $T < 300$ K', *J. Geophys. Chem.* 91, 1778.

Baulch, D. L., Cox, R. A., Hampson, R. F., Kerr, J. A., Troe, J., and Watson, R. T.: 1980, 'Evaluated inetic and Photochemical Data for Atmospheric Chemistry', *J. Phys. Chem. Ref. Data* 9, 295.

Belton, M. J. S., Hunten, D. M., and Goody, R. M.: 1968, in J. C. Brandt and M. C. McElroy (eds.), 'Quantitative Spectroscopy of Venus in the Region 8000–11000 Å', *The Atmospheres of Venus and ars*, Gordon and Breach, New York, pp. 69–98.

Bernstein, R. B. and Levine, R. D.: 1975, 'Role of Energy in Reactive Scattering: An Information-Theoretic Approach', *Adv. At. Mol. Phys.* 11, 215.

Bertaux, J. L. and Clarke, J. T.: 1989a, 'Deuterium Content of the Venus Atmosphere', *Nature* 338, 567.

Bertaux, J. L. and Clarke, J. T.: 1989b, 'Reply to Donahue, T. M., Deuterium on Venus', *Nature* 340, 514.

Bertaux, J. L., Blamont, J., Marcelin, M., Kurt, V. G., Romanova, N. N., Smirnov, A. S.: 1978, 'Lyman-alpha Observations of Venera 9 and 10. I. The Nonthermal Hydrogen Population in the Exosphere of Venus', *Planetary Space Sci.* 26, 817.

Bertaux, J. L., Blamont, J. E., Lupine, V. M., Kurt, V. G., Romanova, N. N., and Smirnov, A. S.: 1981, 'Venera 11 and Venera 12 Observations of EUV Emission from the Upper Atmosphere of Venus', *Planetary Space Sci.* 29, 149.

Bertaux, J. L., Lepine, V. M., Kurt, V. G., and Smirnov, A. S.: 1982, 'Altitude Profile of H in the Atmosphere of Venus from Lyman-α Observations of Venera 11 and Venera 12 and Origin of the Hot Exospheric Component', *Icarus* 52, 221.

Bertaux, J. L., Chassefiere, E., and Kurt, V. G.: 1985, 'Venus EUV Measurements of Hydrogen and Helium from Venera 11 and Venera 12', *Adv. Space Res.* 5, 119.

Biermann, L., Brosowski, B., and Schmidt, H. U.: 1967, 'Interaction of the Solar Wind with a Comet', *Solar Phys.* 1, 254.

Bougher, S. W.: 1980, 'The Ultraviolet Night Airglow of Venus – Morphology and Implications', MS Thesis, University of Colorado, Boulder.

Boucher, S. W.: 1989, 'Venus Thermospheric Circulation', PhD. Thesis, University of Michigan, Ann Arbor.

Bougher, S. W. and Dickinson, R. E.: 1988, 'Mars Mesosphere and Thermosphere. I. Global Mean Heat Budget and Thermal Structure', *J. Geophys. Res.* 93, 7325.

Bougher, S. W., Dickinson, R. E., Ridley, E. C., Roble, R. G., Nagy, A. F., and Cravens, T. E.: 1986, 'Venus Mesosphere and Thermoshere. II. Global Circulation, Temperature, and Density Variations', *Icarus* 68, 284.

Bougher, S. W., Roble, R. G., and Dickinson, R. E.: 1988a, 'The Thermospheres of Venus and Mars: A Comparison of Global Structure and Winds Using the NCAR-TGCM', *Bull. Am. Astron. Soc.* 20, 851.

Bougher, S. W., Dickinson, R. E., Ridley, E. C., and Roble, R. G.: 1988b, 'Venus Mesosphere and Thermosphere. III. Three-Dimensional General Circulation with Coupled Dynamics and Composition', *Icarus* 73, 545.

Bougher, S. W., Dickinson, R. E., Roble, R. G., and Ridley, E. C.: 1988c, 'Mars Thermospheric General Circulation Model: Calculations for the Arrival of Phobos at Mars', *Geophys. Res. Letters* 15, 1511.

Bougher, S. W., Gerard, J. C., Stewart, A. I. F., and Fesen, C. G.: 1990a, 'The Venus Nitric Oxide Night Airglow: Model Calculations Based on the Venus Thermospheric General Circulation Model', *J. Geophys. Res.* (in press).

Bougher, S. W., Roble, R. G., Ridley, E. C., and Dickinson, R. E.: 1990b, 'The Mars Thermosphere General Circulation with Coupled Dynamics and Composition', *J. Geophys. Res.* (in press).

Braun, W., Bass, A. M., Davis, D. D., and Simmons, J. J.: 1969, 'Flash Photolysis of Carbon Suboxide: Absolute Rate Constants for Reactions of $C(^3P)$ and $C(^1D)$ with H_2, N_2, CO, NO, O_2 and CH_4', *Proc. Roy. Soc. London Ser.* A312, 417.

Breus, T. K., Gringauz, K. I., and Verigin, M. I.: 1985, 'On the Properties and Origin of the Venus Ionosphere', *Adv. Space Res.* 5, 145.

Brinton, H. C., Taylor, H. A., Jr., Niemann, H. B., Mayr, H. G., Nagy, A. F., Cravens, T. E., and Strobel, D. F.: 1980, 'Venus Nighttime Hydrogen Bulge', *Geophys. Res. Letters* 7, 865.

Broadfoot, A. L., Kumar, S., Belton, M. J. S., and McElroy, M. B.: 1974, 'Ultraviolet Observations of Venus from Mariner 10: Preliminary Results', *Science* 183, 1315.

Broadfoot, A. L., Clapp, S. S., and Stuart, F. E.: 1977, 'Mariner 10 Ultraviolet Spectrometer: Airglow Experiment', *Space Sci. Instr.* 3, 199.

Buchwald, M. I. and Bauer, S. H.: 1972, 'Vibrational Relaxation in CO_2 with Selected Collision Partners', *J. Phys. Chem.* 76, 3108.

Burnett, T. and Rountree, S. P.: 1979, 'Differential and Total Cross Sections for Electron Impact Ionization of Atomic Oxygen', *Phys. Rev.* A20, 1468.

Carlson, R. W. and Judge, D. L.: 1973, 'Rocket Observations of the Extreme Ultraviolet Dayglow', *Planetary Space Sci.* 21, 879.

Center, R. E.: 1973, 'Vibrational Relaxation of CO_2 by O Atoms', *J. Chem. Phys.* 59, 3523.

Chamberlain, J. W.: 1963, 'Planetary Coronae and Atmospheric Evaporation', *Planetary Space Sci.* 11, 901.

Chamberlain, J. W.: 1977, 'Charge Exchange in a Planetary Corona: Its Effect on the Distribution and Escape of Hydrogen', *J. Geophys. Res.* 82, 1.

Chamberlain, J. W. and Hunten, D. M.: 1987, *Theory of Planetary Atmospheres: An Introduction to Their Physics and Chemistry*, Academic Press, New York, pp. 45–48.

Chapman, S.: 1931, 'Some Phenomena of the Upper Atmosphere', *Proc. Roy. Soc. London* A132, 353.

Chassefiere, E., Bertaux, J. L., Kurt, V. G., and Smirnov, A. S.: 1986, 'Venus EUV Measurements of Helium at 58.4 nm from Venera 11 and Venera 12 and Implications for the Outgassing History', *Planetary Space Sci.* 24, 585.

Choo, Y. C. and Ming-Tuan Leu: 1985, 'Determination of $O_2(^1\Sigma_g^+)$ and $O_2(^1\Delta_g)$ yields in Cl + O_2 and Cl + O_3 Reactions', *J. Phys. Chem.* 89, 4832.

Chu, J. O., Flynn, G. W., and Weston, R. E.: 1983, 'Spectral Distribution of Vibrational States Produced by Collisions with Fast Hydrogen Atoms from Laser Photolysis of HBr', *J. Chem. Phys.* 78, 2990.

Clancy, R. T. and Muhleman, D. O.: 1985a, 'Diurnal CO Variations in the Venus Mesosphere from CO Microwave Spectra', *Icarus* 64, 157.

Clancy, R. T. and Muhleman, D. O.: 1985b, 'Chemical-Dynamical Models of the Venus Mesosphere Based Upon Diurnal Microwave CO Variations', *Icarus* 64, 183.

Cleary, D. D.: 1986, 'Daytime High Latitude Rocket Observations of the NO γ, δ, and ε Bands', *J. Geophys. Res.* **91**, 11337.

Connes, P., Connes, J., Benedict, W. S., and Kaplan, L. D.: 1967, 'Traces of HCL and HF in the Atmosphere of Venus', *Astrophys. J.* **152**, 731.

Connes, P., Connes, J., Kaplan, L. D., and Benedict, W. S.: 1968, 'Carbon Monoxide in the Venus Atmosphere', *Astrophys. J.* **152**, 731.

Connes, J., Connes, P., and aillard, J. P.: 1969, *Atlas des spectres dans le proche infrarouge de Venus, Mars, Jupiter et Saturn*, Centre National de a Recherche Scientific, Paris.

Connes, P., Noxon, J. F., Traub, W. A., and Carleton, N. P.: 1979, '$O_2(^1\Delta)$ Emission in the Day and Night Airglow of Venus', *Astrophys. J.* **233**, L29.

Conway, R. R.: 1981, 'Spectroscopy of the Cameron Bands in the Mars Airglow', *J. Geophys. Res.* **86**, 4767.

Cook, G. R., Metzger, P. H., and Ogawa, M.: 1965, 'Photoionization and Absorption Coefficients of CO in the 600 to 1000 Å Region', *Can. J. Phys.* **43**, 1706.

Cooper, D. L., Yee, J. H., and Dalgarno, A.: 1984, 'Energy Transfer in Oxygen-Hydrogen Collisions', *Planetary Space Sci.* **32**, 825.

Cravens, T. E., Gombosi, T. I., and Nagy, A. F.: 1980, 'Hot Hydrogen in the Exosphere of Venus', *Nature (London)* **283**, 178.

Cravens, T. E., Kliore, A. J., Kozyra, J. U., and Nagy, A. F.: 1981, 'The Ionospheric Peak on the Venus Dayside', *J. Geophys. Res.* **86**, 11323.

Cravens, T. E., Brace, L. H., Taylor, H. A., Russell, C. T., Knudsen, W. L., Miller, K. L., Barnes, A., Mihalov, J. D., Scarf, F. L., Quenon, S. J., and Nagy, A. F.: 1982, 'Disappearing Ionospheres on the Nightside of Venus', *Icarus* **51**, 271.

Cravens, T. E, Crawford, S. L., Nay, A. F., and Gombosi, T. I.: 1983, 'A Two-Dimensional Model of the Ionosphere of Venus', *J. Geophys. Res.* **88**, 5595.

Dalgarno, A. and Degges, T. C.: 1971, in C. Sagan, T. Owen, and H. J. Smith (eds.), 'CO_2^+ Dayglow on Mars and Venus', *Planetary Atmospheres*, D. Reidel Publ. Co., Dordrecht, Holland, pp. 337–345.

Degen, V.: 1981, 'Vibrational Enhancement and the Excitation of N_2^+ and the First Negative System in the High Altitude Red Aurora and the Dayside Cusp', *J. Geophys. Res.* **86**, 11, 372.

DeMore, W. B. and Yung, Y. L.: 1982, 'Catalytic Processes in the Atmospheres of the Earth and Venus', *Science* **217**, 12099.

DeMore, W. B., Leu, M.-T., Smith, R. H., and Yung, Y. L.: 1985, 'Laboratory Studies on the Reactions between Chlorine, Sulfur Dioxide and Oxygen: Implications for the Venus Stratosphere', *Icarus* **63**, 347.

Del Genio, A. D., Schubert, G., and Strauss, J. M.: 1979, 'Acoustic Gravity Waves in the Thermosphere of Venus', *Icarus* **39**, 401.

Dickinson, R. E.: 1972, 'Infrared Radiative Heating and Cooling in the Venusian Mesosphere. I. Global Mean Radiative Equilibrium', *J. Atmospheric Sci.* **29**, 1531.

Dickinson, R. E.: 1973, 'Method for Parameterization for Infrared Cooling between Altitudes of 30 and 70 Kilometers', *J. Geophys. Res.* **78**, 4451.

Dickinson, R. E.: 1976, 'Venus Mesosphere and Thermosphere Temperature Structure: Global Mean Radiative and Conductive Equilibrium', *Icarus* **27**, 479.

Dickinson, R. E.: 1984, 'Infrared Radiative Cooling in the Mesosphere and Lower Thermosphere', *J. Atmospheric Terrest. Phys.* **46**, 995.

Dickinson, R. E. and Bougher, S. W.: 1986, 'Venus Mesosphere and Thermosphere. I. Heat Budget and Thermal Structure', *J. Geophys. Res.* **91**, 70.

Dickinson, R. E. and Ridley, E. C.: 1972, 'A Numerical Solution for the Composition of a Steady Subsolar-to-Antisolar Circulation with Application to Venus', *J. Atmospheric Sci.* **29**, 1557.

Dickinson, R. E. and Ridley, E. C.: 1975, 'A Numerical Model for the Dynamics and Composition of the Venusian Thermosphere', *J. Atmospheric Sci.* **32**, 1219.

Dickinson, R. E. and Ridley, E. C.: 1977, 'Venus Mesosphere and Thermosphere Temperature Structures. II. Day-Night Variations', *Icarus* **30**, 163.

Dickinson, R. E., Ridley, E. C., and Roble, R. G.: 1984, 'Thermospheric General Circulation with Coupled Dynamics and Composition', *J. Atmospheric Sci.* **41**, 205.

Dickinson, R. E., Roble, R. G., and Bougher, S. W.: 1987, 'Radiative Cooling in the NLTE Region of the Mesosphere and Lower Thermosphere – Global Energy Balance', *Adv. Space Res.* **7**, 10, 5.

Doering, J. P. and Gulcicek, E. E.: 1988, 'Absolute Differential and Integral Electron Excitation Cross

Sections for Atomic Oxygen: 7. The $^3P \rightarrow {}^1D$ and $^3P \rightarrow {}^1S$ Transitions from 4.0 to 30 eV', *J. Geophys. Res.* (in press).

Doering, J. P. and Gulcicek, E. E.: 1989, 'Absolute Differential and Integral Electron Excitation Cross Sections for Atomic Oxygen', *J. Geophys. Res.* **94**, 2733.

Doering, J. P. and Vaughan, S. O.: 1986, 'Absolute Experimental Differential and Integral Cross Sections for Atomic Oxygen. 1. The $(^3P \rightarrow {}^3S^o)$ Transition (1304 Å) at 100 eV', *J. Geophys. Res.* **91**, 3279.

Doering, J. P., Gulcicek, E. E., and Vaughan, S. O.: 1985, 'Electron Impact Measurements of Oscillator Strengths for Dipole-Allowed Transitions of Atomic Oxygen', *J. Geophys. Res.* **90**, 5279.

Donahue, T. M.: 1968, 'The Upper Atmosphere of Venus: A Review', *J. Atmospheric Sci.* **25**, 568.

Donahue, T. M.: 1989, 'Dueterium on Venus', *Nature* **340**, 513.

Donahue, T. M. and Pollack, J. B.: 1989, in D. M. Hunten, L. Colin, T. M. Donahue, and V. I. Moroz (eds.), 'Origin and Evolution of Venus's Atmospheric Structure', *Venus*, Univ. of Arizona Press, Tucson.

Donahue, T. M., Hoffman, J. H., Hodges, R. R., and Watson, A. J.: 1982, 'Venus was Wet: A Measurement of the Ratio of Deuterium to Hydrogen', *Science* **216**, 630.

Doschek, G. A., Behring, W. E., and Feldman, U.: 1974, 'The Widths of the Solar He I and He II Lines at 584, 538, and 304 Å', *Astrophys. J.* **190**, L141.

Durrance, S. T.: 1981, 'The Carbon Monoxide Fourth Positive Bands in the Venus Dayglow. 1. Synthetic Spectra', *J. Geophys. Res.* **86**, 9115.

Durrance, S. T., Barth, C. A., and Stewart, A. I. F.: 1988, 'Pioneer Venus Observations of the Venus Dayglow Spectrum 1250–1430 Å', *Geophys. Res. Letters* **7**, 222.

Durrance, S. T., Conway, R. R., Barth, C. A., and Lane, A. L.: 1981, 'IUE High Resolution Observation of the Venus Dayglow Spectrum 1280–1380 Å', *Geophys. Res. Letters* **8**, 111.

Eckstrom, D. J.: 1973, 'Vibrational Relaxation of Shock-Related N_2 by Atomic Oxygen Using the IR Tracer Method', *J. Chem. Phys.* **59**, 2787.

Erdman, P. W. and Zipf, E. C.: 1983, 'Electron-Impact Excitation of the Cameron System $(a^3\Pi \rightarrow X^1\Sigma)$ of CO', *Planetary Space Sci.* **31**, 317.

Ewing, G.: 1978, 'The Role of van der Waals Molecules in Vibrational Relaxation Processes', *Chem. Phys.* **29**, 253.

Fehsenfeld, F. C., Dunkin, D. B., and Ferguson, E. E.: 1970, 'Rate Constants for the Reaction of CO_2^+ with O, O_2, and NO; N_2^+ with O and NO; and O_2^+ with NO', *Planetary Space Sci.* **18**, 1267.

Feldman, P. D., Moos, H. W., Clarke, J. T., and Lane, A. L.: 1979, 'Identification of the UV Nightglow from Venus', *Nature* **279**, 221.

Feldman, P. D., Anderson, D. E., Meier, R. R., and Gentieu, E. P.: 1981, 'The Ultraviolet Dayglow. 4. The Spectrum and Excitation of Singly Ionized Oxygen', *J. Geophys. Res.* **86**, 3583.

Fels, S. B. and Lindzen, R. S.: 1974, 'The Interaction of Thermally Driven Excited Gravity Waves with Mean Flows', *Geophys. Fluid Dyn.* **6**, 149.

Fernando, R. P. and Smith, I. W. M.: 1979, 'Vibrational Relaxation of NO by Atoic Oxygen', *Chem. Phys. Letters* **66**, 218.

Fesen, C. G., Gerard, J. C., and Rusch, D. W.: 1989, 'Rapid Deactivation of $N(^2D)$ by O: Impact and Thermospheric and Mesospheric Odd Nitrogen', *J. Geophys. Res.* **94**, 5419.

Fink, U., Larson, H. P., Kuiper, G. P., and Poppen, R. F.: 1972, 'Water Vapor in the Atmosphere of Venus', *Icarus* **17**, 617.

Flynn, G. W. and Weston R. E.: 1986, 'Hot Atoms Revisited: Laser Photolysis and Product Detection', *Ann. Rev. Phys. Chem.* **37**, 551.

Fox, J. L.: 1978, 'The Upper Atmospheres of Mars and Venus', Ph.D. Thesis, Harvard University.

Fox, J. L.: 1982a, 'The Chemistry of Metastable Species in the Venusian Ionosphere', *Icarus* **51**, 248. Erratum: 1985, *J. Geophys. Res.* **90**, 11106.

Fox, J. L.: 1985, 'Atomic Carbon in the Atmosphere of Venus', *J. Geophys. Res.* **87**, 9211.

Fox, J. L.: 1986a, 'The O_2^+ Vibrational Distribution in the Venusian Ionosphere', *Adv. Space Res.* **5**, 165.

Fox, J. L.: 1986b, 'The O_2^+ Vibrational Distribution in the Dayside Ionosphere', *Planetary Space Sci.* **34**, 1252.

Fox, J. L.: 1986c, 'Models for Aurora and Airglow Emissions from Other Planetary Atmospheres', *Can. J. Phys.* **64**, 1631.

Fox, J. L.: 1988, 'Heating Efficiencies in the Thermosphere of Venus Reconsidered', *Planetary Space Sci.* **36**, 37.

Fox, J. L.: 1989a, in J. B. A. Mitchell and S. L. Guberman (eds.), 'Dissociative Recombination in Aeronomy', *Dissociative Recombination: Theory, Experiment and Applications*, World Scientific, Singapore.

Fox, J. L.: 1989b, 'The Neutral Thermospheres of Mars and Venus', *EOS (Trans. Am. Geophys. Union)* **70**, 387.

Fox, J. L.: 1990a, 'The Red and Green Lines of Atomic Oxygen in the Nightglow of Venus', *Adv. Space Res.* **10**(5), 31.

Fox, J. L.: 1990b, *The Production of Hot Oxygen at the Exobases of the Terrestrial Planets* (in preparation).

Fox, J. L. and Black, J. H.: 1989, 'Photodissociation of CO in the Thermosphere of Venus', *Geophys. Res. Letters* **16**, 291.

Fox, J. L. and Dalgarno, A.: 1979, 'Ionization, Luminosity and Heating of the pper Atmosphere of Mars', *J. Geophys. Res.* **84**, 7315.

Fox, J. L. and Dalgarno, A.: 1981, 'Ionization, Luminosity, and Heating of the Upper Atmosphere of Venus', *J. Geophys. Res.* **86**, 629.

Fox, J. L. and Dalgarno, A.: 1983, 'Nitrogen Escape from Mars', *J. Geophys. Res.* **88**, 9027.

Fox, J. L. and Dalgarno, A.: 1985, 'The ibrational Distribution of N_2^+ in the Terrestrial Ionosphere', *J. Geophys. Res.* **90**, 7557.

Fox, J. L. and Stewart, A. I. F.: 1990, 'The Venus Ultraviolet Aurora: a Soft Electron Source', *J. Geophys. Res.* (submitted).

Frederick, J. E. and Rusch, D. W.: 1977, 'On the Chemistry of Metastable Atomic Nitrogen in the F Region Deduced frm Simultaneous Measurements of the 5200 Å Airglow and Atmospheric Composition', *J. Geophys. Res.* **82**, 3509.

Freund, R. S.: 1971, 'Dissociation of CO_2 by Electron Impact with the Formation of Metastable $CO(a^3\Pi)$ and $O(^5S)$', *J. Chem. Phys.* **55**, 3569.

Gel'man, B. G., Zolotukhin, V. G., Lamonov, N. I., Levchuk, B. V., Lipatov, A. N., Mukhin, L. M., Nenarokov, D. F., Rotin, V. A., and Okhotnikov, B. P.: 1979, 'Analysis of Chemical Composition of Venus Atmosphere by Gas Chromatography', *Kossm. Issled.* **17**, 708; 1980, *Cosmic Res.* (Engl. transl.) **17**, 585.

Gerard, J. C., Stewart, A. I. F., and Bougher, S. W.: 1981, 'The Altitude Distribution of the Venus Ultraviolet Nightglow and Implication on Vertical Transport', *Geophys. Res. Letters* **8**, 633.

Gerard, J. C., Denye, E. J., and Lerho, H.: 1988, 'Sources and Distribution of Odd Nitrogen in the Venus Daytime Thermosphere', *Icarus* **75**, 171.

Goldstein, J.: 1989, 'Absolute Wind Speed Measurements in the Lower Thermosphere of Venus Using Infrared Heterodyne Spectroscopy', Ph.D. Thesis, University of Pennsylvania, Philadelphia.

Gordiets, B. F. and Kulikov, Y. N.: 1985, 'On the Mechanisms of Cooling of the Nightside Thermosphere of Venus', *Adv. Space Res.* **5**(9), 113.

Gordiets, B. F., Kulikov, Yu. N., Markov, M. N., and Marov, M. Ya.: 1982, 'Numerical Modelling of the Thermospheric Heat Budget', *J. Geophys. Res.* **87**, 4504.

Gordon, R. J.: 1981, 'A Metastable Complex Model for Vibrational Relaxation', *J. Chem. Phys.* **74**, 1676.

Grechnev, K. V., Istomin, V. G., Ozerov, L. N., and Klimovitskii, V. G.: 1979, 'The Mass Spectrometer from Venera 111 and 12', *Kossm. Issled.* **17**, 697; 1980, *Cosmic Res.* (Engl. transl.) **17**, 575.

Greer, R. G. H. Murtagh, D. P., McDade, I. C., Dickinson, P. H. G., Thomas, L., Jenkins, D. B., Stegman, J., Llewellyn, E. J., Witt, G., MacKinnon, D. J., and Williams, E. R.: 1986, 'ETON 1: A Data Base Pertinent to the Study of Energy Transfer in the Oxygen Nightglow', *Planetary Space Sci.* **34**, 771.

Gringauz, K. I., Verigin, M. I., Breus, T. K., and Gombosi, T.: 1979, 'The Interaction of Electrons in the Optical Umbra of Venus with the Planetary Atmosphere – The Origin of the Nighttime Ionosphere', *J. Geophys. Res.* **84**, 2123.

Grinspoon, D. H. and Lewis, J. S.: 1988, 'Cometary Water on Venus: Imlplications of Stochastic Impacts', *Icarus* **74**, 21.

Guberman, S. L.: 1987, 'The Production of $O(^1S)$ in Dissociative Recombination of O_2^+', *Nature* **327**, 408.

Guberman, S. L.: 1988, 'The Production of $O(^1D)$ from Dissociative Recombination of O_2^+', *Planetary Space Sci.* **36**, 47.

Gulcicek, E. E. and Doering, J. P.: 1988, 'Absolute Differential and Integral Cross Sections for Atomic Oxygen. 5. Revised Values for the $^3P \rightarrow {}^3S^0$ (1304 Å) and $^3P \rightarrow {}^3D^0$ (989 Å) Transitions Below 30 eV', *J. Geophys. Res.* **93**, 5879.

Gulcicek, E. E., Doering, J. P., and Vaughan, S. O.: 1988, 'Absolute Differential and Integral Electron Excitation Cross Sections for Atomic Oxygen. 6. The $^3P \rightarrow {}^3P$ and $^3P \rightarrow {}^5P$ Transitions from 13.87 eV to 100 eV', *J. Geophys. Res.* **93**, 5885.

Gutcheck, R. A. and Zipf, E. C.: 1973, 'Excitation of the CO Fourth Positive System by the Dissociative Recombination of CO$_2^+$ Ions', *J. Geophys. Res.* **78**, 5429.

Hartle, R. E. and Taylor, H. Z.: 1983, 'Identification of Deuterium Ions in the Ionosphere of Venus', *Geophys. Res. Letters* **10**, 965.

Harvey, N. M.: 1982, 'A Quantum Mechanical Investigation of Vibrational Energy Transfer in O(^3P) + CO$_2$ Collisions', *Chem. Phys. Letters* **88**, 553.

Hedin, A. E., Niemann, H. B., Kasprzak, W. T., and Seiff, A.: 1983, 'Global Empirical Model of the Venus Thermosphere', *J. Geophys. Res.* **88**, 73. Erratum: 1983, *J. Geophys. Res.* **88**, 6352.

Henry, R. J. W. and McElroy, M. B.: 1968, in J. C. Brandt and M. B. McElroy (eds.), 'Photoelectrons in Planetary Atmospheres', *The Atmospheres of Venus and Mars*, Gordon and Breach Publishers, New York.

Heroux, L. and Hinteregger, H. E.: 1978, 'Aeronomical Reference Spectrum for Solar UV Below 2000 Å', *J. Geophys. Res.* **83**, 5305.

Herzberg, G.: 1950, *Spectra of Diatomic Molecules*, Van Nostrand Reinhold Co., New York.

Hodges, R. R. and Tinsley, B. A.: 1981, 'Charge Exchange in the Venus Thermosphere as a Source of Hot Exospheric Hydrogen', *J. Geophys. Res.* **86**, 7649.

Hodges, R. R. and Tinsley, B. A.: 1986, 'The Influence of Charge Exchange on the Velocity Distribution of Hydrogen in the Venus Exosphere', *J. Geophys. Res.* **91**, 13, 649.

Hoffman, J. H., Hodges, R. R., Donahue, T. M., and McElroy, M. B.: 1980a, 'Composition of the Venus Lower Atmosphere from the Pioneer Venus Mass Spectrometer', *J. Geophys. Res.* **85**, 7882.

Hoffman, J. H., Oyama, V. I., and von Zahn, U.: 1980b, 'Measurements of the Venus Lower Atmosphere Composition: a Comparison of Results', *J. Geophys. Res.* **85**, 7871.

Hogan, J. S. and Stewart, R. W.: 1969, 'Exospheric Temperatures on Mars and Venus', *J. Atmospheric Sci.* **26**, 332.

Hollenbach, D. J., Prasad, S. S., and Whitten, R. C.: 1985, 'The Thermal Structure of the Dayside Upper Atmosphere of Venus Above 125 km', *Icarus* **64**, 205.

Holton, J. R.: 1982, 'The Role of Gravity Wave Induced Drag and Diffusion in the Momentum Budget of the Mesosphere', *J. Atmospheric Sci.* **39**, 791.

Holton, J. R.: 1983, 'The Influence of Wave Breaking on the General Circulation of the Middle Atmosphere', *J. Atmospheric Sci.* **40**, 2497.

Hou, A.: 1984, 'Axisymmetric Circulations Forces by Heat and Momentum Sources: A Simple Model Applicable to the Venus Atmosphere', *J. Atmospheric Sci.* **41**, 3437.

Hou, A. and Goody, R. M.: 1985, 'Diagnostic Requirements for the Superrotation of Venus', *J. Atmospheric Sci.* **42**, 413.

Hunten, D. M.: 1973, 'The Escape of H$_2$ from Titan', *J. Atmospheric Sci.* **30**, 726.

Hunten, D. M.: 1973, 'The Escape of Light Gases from Planetary Atmospheres', *J. Atmospheric Sci.* **30**, 1481.

Hunten, D. M.: 1974, 'Energetics of Thermospheric Eddy Transport', *J. Geophys. Res.* **79**, 2533.

Hunten, D. M.: 1982, 'Thermal and Nonthermal Escape Mechanisms for Terrestrial Bodies', *Planetary Space Sci.* **30**, 773.

Hunten, D. M. and Donue, T. M.: 1976, 'Hydrogen Loss from the Terrestrial Planets', *Ann. Rev. Earth Planetary Sci.* **4**, 265.

Hunten, D. M. and McElroy, M. B.: 1970, 'Production and Escape of Hydrogen on Mars', *J. Geophys. Res.* **75**, 5989.

Hunten, D. M., Pepin, O., and Walker, J. C. G.: 1987, 'Mass Fractionation in Hydrodynamic Escape', *Icarus* **69**, 532.

Hunten, D. M., Donhue, T. M., Walker, J. C. G., and Kasting, J. F.: 1989, in S. Atreya, J. Pollack, and M. Matthews (eds.), 'Escape of Atmospheres and Loss of Water', *Origin and Evolution of Planetary and Satellite Atmospheres*, Univ. of Arizona Press, Tucson, pp. 396–422.

Ingersoll, A. P.: 1969, 'The Runaway Greenhouse: A History of Water on Venus', *J. Atmospheric Sci.* **26**, 1191, 1969.

Inoue, G. and Tsuchiya, S.: 1975, 'Vibrational Relaxation of CO$_2$(00^{0}1) in CO$_2$, He, Ne, and Ar in the Temperature Range of 300–140 K', *J. Phys. Soc. Japan* **38**, 870.

Istomin, V. G., Grechnev, K. V., Kochnev, V. A., and Ozerov, L. N.: 1979, 'Composition of Venus Lower Atmosphere from Mass-Spectrometer Data', *Kossm. Issled.* **17**, 703; 1980, *Cosmic Res.* (Engl. transl.) **17**, 581.

Izakov, M. N.: 1978, 'Effect of Turbulence on the Thermal Regime of Planetary Thermospheres', *Kossm. Issled.* **16**, 401 (in Russian).

James, T. C.: 1971, 'Transition Moments, Franck–Condon Factors, and Lifetimes of Forbidden Transitions. Calculation of the Intensity of the Cameron System of CO', *J. Chem. Phys.* **55**, 4118.

Jeans, J. H.: 1925, *The Dynamical Theory of Gases*, Cambridge Univ. Press, Cambridge.

Johnson, C. E.: 1972, 'Lifetime of $CO(a^3\Pi)$ Following Electron Impact Dissociation of CO_2', *J. Chem. Phys.* **57**, 576.

Julienne, P. S., Davis, J., and Oran, E.: 1974, 'Oxygen Recombination in the Tropical Nightglow', *J. Geophys. Res.* **79**, 2540.

Jusinski, L. E. and Slanger, T. G.: 1987, 'Determination of the Rate Coefficient for Quenching $N(^2D)$ by $O(^3P)$', *EOS Trans. AGU* **68**, 1389.

Jusinski, L. E. and Slanger, T. G.: 1988, 'Resonance-Enhanced Multi-Photon Ionization Measurement of $N(^2D)$ Quenching by $O(^2P)$', *J. Phys. Chem.* **92**, 5977.

Kakar, R. K., Waters, J. W., and Wilson, W. J.: 1976, 1976, 'Venus: Microwave Detection of Carbon Monoxide', *Science* **191**, 379.

Kasprzak, W. T., Hedin, A. E., Niemann, H. B., and Spencer, N. W.: 1980, 'Atomic Nitrogen in the Upper Atmosphere of Venus', *Geophys. Res. Letters* **7**, 106.

Kasprzak, W. T., Hedin, A. E., Mayr, H. G., and Niemann, H. B.: 1988, 'Wavelike Perturbatinos Observed in the Neutral Thermosphere of Venus', *J. Geophys. Res.* **93**, 11237.

Kassel, T.: 1976, 'Scattering of Solar Lyman Alpha by the (14, 0) Fourth Positive System of CO', *J. Geophys. Res.* **81**, 1411.

Kasting, J. F. and Pollack, J. B.: 1983, 'Loss of Water from Venus. I. Hydrodynamic Escape of Hydrogen', *Icarus* **53**, 479.

Kasting, J. F. and Toon, O. B.: 1989, in S. Atreya, J. Pollack, and M. Matthews (eds.), 'Climate Evolution on the Terrestrial Planets', *Origin and Evolution of Planetary and Satellite Atmospheres*, Univ. of Arizona Press, Tucson, pp. 423–449.

Kasting, J. F., Pollack, J. B., and Ackerman, T. P.: 1984, 'Response of the Earth's Atmosphere to Increases in Solar Flux and Implications for Loss of Water from Venus', *Icarus* **57**, 335.

Keating, G. M.: 1977, 'Pioneer Venus Experiment Descriptions', *Space Sci. Rev.* **20**, 520.

Keating, G. M. and Bougher, S. W.: 1987, 'Neutral Upper Atmospheres of Venus and Mars', *Adv. Space Res.* **7**, 12, 57.

Keating, G. M., Taylor, F. W., Nicholson, J. Y., and Hinson, E. W.: 1979, 'Short-Term Cyclic Variations and Diurnal Variations of the Venus Upper Atmosphere', *Science* **205**, 62.

Keating, G. M., Nicholson, J. Y., and Lake, L. R.: 1980, 'Venus Upper Atmosphere Structure', *J. Geophys. Res.* **85**, 7941.

Keating, G. M., Bertaux, J. L., Bougher, S. W., Cravens, T. E., Dickinson, R. E., Hedin, A. E., Krasnopol'sky, V. A., Nagy, A. F., Nicholson, J. Y., III, Paxton, L. J., and von Zahn, U.: 1985, 'Models of Venus Neutral Upper Atmosphere: Structure and Composition', *Adv. Space Res.* **5**, 117.

Keldysh, M. V.: 1977, 'Venus Exploration with the Venera 9 and Venera 10 Spacecraft', *Icarus* **30**, 605.

Kenner, R. D. and Ogryzlo, E. A.: 1983, 'Quenching of $O_2(c^1\Sigma_u^-)v = 0$ by $O(^3P)$, $O_2(a^1\Delta_g)$, and Other Gases', *Can. J. Chem.* **61**, 921.

Kenner, R. D., Ogryzlo, E. A., and Turley, S.: 1979, 'On the Excitation of the Night Airglow on Earth', Venus and Mars', *J. Photochem.* **10**, 199.

Kim, J., Nagy, A. F., Cravens, T. E., and Kliore, A. J.: 1988, 'Solar Cycle Variations of the Electron Densities Near the Ionospheric Peak of Venus', *J. Geophys. Res.* **94**, 11997.

Kirby, K., Constantinides, E. R., Babeu, S., Oppenheimer, M., and Victor, G. A.: 1979, 'Photoionization and Photoabsorption Cross Sections of He, O, N_2, and O_2 for Aeronomic Calculations', *At. Data Nucl. Data Tables* **23**, 68.

Kley, D., Lawrence, G. M., and Stone, E. C.: 1977, 'The Yield of $N(^2D)$ atoms in the Dissociative Recombination of NO^+', *J. Chem. Phys.* **66**, 4157.

Kliore, A., Levy, G. S., Cain, D. L., Fjeldbo, G., and Rasool, S. I.: 1967, 'Atmosphere and Ionosphere of Venus from the Mariner V S-Band Radio Occultatin Measurement', *Science* **158**, 1683.

Kliore, A., Patel, I. R., Nagy, A. F., Cravens, T. E., and Gombosi, T.: 1979, 'Initial Observations of the Nightside Ionosphere of Venus from Pioneer Venus Orbiter Radio Occultations', *Science* **205**, 99.

Kliore, A. J. and Mullen, L.: 1987, 'Solar Cycle Influence on the Topside Plasma Scale Height of the Venus Dayside Ionosphere', *Bull. Am. Astron. Soc.* **19**, 846.

Kliore, A. J. and Mullen, L.: 1988, 'The Long-Term Behavior of the Main Peak of the Dayside Ionosphere

of Venus During Solar Cycle 21 and Its Implications on the Effect of the Solar Cycle Upon the Electron Temperature in the Main Peak Region', *J. Geophys. Res.* 94, 13339.

Knudsen, W. C.: 1973, 'Escape of ⁴He and Fast O Atoms from Mars and Inferences on the ⁴He Mixing Ratio', *J. Geophys. Res.* 78, 8049.

Knudsen, W. C.: 1988, 'Solar Cycle Changes in the Morphology of the Venus Ionosphere', *J. Geophys. Res.* 93, 8756.

Knudsen, W. C. and Miller, K. L.: 1985, 'Pioneer Venus Superthermal Electron Flux Measurements in the Venus Umbra', *J. Geophys. Res.* 90, 2695.

Knudsen, W. C., Spenner, K., Whitten, R. C., Spreiter, J. R., Miller, K. L., and Novak, V.: 1979, 'Thermal Structure and Energy Influx into the Nightside Ionosphere', *Science* 205, 105.

Knudsen, W. C., Spenner, K., Miller, K. L., and Novak, V.: 1980a, 'Transport of Ionospheric O⁺ Ions Across the Venus Terminator and Implications', *J. Geophys. Res.* 85, 7803.

Knudsen, W. C., Spenner, K., Miller, K. L., and Novak, V.: 1980b, 'Transport of Ionospheric O⁺ Ions Across the Venus Terminator and Implications', *J. Geophys. Res.* 85, 7803.

Knudsen, W. C., Miller, K. L., and Spenner, K.: 1986, *J. Geophys. Res.* 91, 11, 936.

Krasnopol'sky, V. A.: 1979, 'Threshold Estimates of the Content of Some Substances in the Atmosphere of Mars and Venus from the Results of Spectroscopy of the Twilight Glow on the Mars 5, Venera 9 and Venera 10 Satellites', *Kosm. Issled.* 16, 895; 1979, *Cosmic Res.* 16, 713.

Krasnopol'sky, V. A.: 1979, 'Nightside Ionosphere of Venus', *Planetary Space Sci.* 27, 1403.

Krasnopol'sky, V. A.: 1981, 'Excitation of Oxygen Emission in the Night Airglow of the Terrestrial Planets', *Planetary Space Sci.* 29, 925.

Krasnopol'sky, V. A.: 1983, '5577-Å Airglow and Electron Fluxes in the Nighttime Atmosphere of Venus', *Kosm. Issled.* 20, 742; 1983, *Cosmic Res.* (Engl. transl) 20, 530.

Krasnopol'sky, V. A.: 1982b, 'Atomic Carbon in the Atmospheres of Mars and Venus', *Kosm. Issled* 20, 595; 1983, *Cosmic Res.* (Engl. transl.) 20, 430.

Krasnopol'sky, V. A.: 1983a, in D. M. Hunten, L. Colin, T. M. Donahue, and V. I. Moroz (eds.), 'Venus Spectroscopy in the 3000–8000 Å Region by Veneras 9 and 10', *Venus.* Univ. of Arizona Press, Tucson, pp. 459–483.

Krasnopol'sky, V. A.: 1983b, 'Lightning and Nitric Oxide on Venus', *Planetary Space Sci.* 31, 1363.

Krasnopol'sky, V. A.: 1985, 'Total Injection of Water Vapor Into the Venus Atmosphere', *Icarus* 62, 221.

Krasnopol'sky, V. A.: 1986a, *Photochemistry of the Atmospheres of Mars and Venus*, Springer-Verlag, New York.

Krasnopol'sky, V. A.: 1986b, 'Oxygen Emission in the Night Airglow of the Earth, Venus and Mars', *Planetary Spoace Sci.* 34, 511.

Krasnopol'sky, V. A. and Parshev, V. A.: 1981, 'Chemical Composition of the Atmosphere of Venus', *Nature* 282, 610.

Krasnopol'sky, V. A. and Parshev, V. A.: 1983, in D. M. Hunten, L. Colin, T. M. Donahue, and V. I. Moroz (eds.), 'Photochemistry of the Venus Atmosphere', *Venus*, Univ. of Arizona Press, Tucson, p. 431.

Krasnopol'sky, V. A. and Tomashova, G. V.: 1980, 'Venus Nightglow Variations', *Cosmic Res.* 18, 766.

Krasnopol'sky, V. A., Krus'ko, A. A., Rogachev, V. N., and Parshev, V. A.: 1976, 'Spectroscopy of the Night-Sky Luminescence of Venus from the Interplanetary Spacecraft Venera 9 and Venera 10', *Kossm. Issled.* 14, 789; 1977, *Cosmic Res.* (Engl. transl.) 14, 687.

Kumar, S. and Broadfoot, A. L.: 1975, 'Helium 584 Å Airglow Emissin from Venus: Mariner 10 Observations', *Geophys. Res. Letters* 2, 357.

Kumar, S. and Hunten, D. M.: 1974, 'Venus: An Ionospheric Model with an Exospheric Temperature of 350 K', *J. Geophys. Res.* 79, 2529.

Kumar, S. and Taylor, H. A.: 1985, 'Deuterium on Venus: Model Comparisons with Pioneer Venus Observations of the Predawn Bulge Ionosphere', *Icarus* 62, 494.

Kumar, S., Hunten, D. M., and Broadfoot, A. L.: 1978, 'Non-Thermal Hydrogen in the Venus Exosphere: the Ionospheric Source and the Hydrogen Budget', *Planetary Space Sci.* 26, 1063.

Kumar, S., Hunten, D. M., and Taylor, H. A.: 1981, 'H₂ Abundance in the Atmosphere of Venus', *Geophys. Res. Letters* 8, 237.

Kumar, S., Hunten, D. M., and Pollack, J. P.: 1983a, 'Nonthermal Escape of Hydrogen and Deuterium from Venus and Implications for Loss of Water', *Icarus* 55, 369.

Kumar, S., Chakrabarti, S., Paresce, F., and Bowyer, S.: 1983b, 'The O⁺ 834-Å Dayglow: Satellite Observations and Interpretation with a Radiation Transfer Model', *J. Geophys. Res.* 88, 9271.

Kurt, V. G., Dostovalow, S. B., and Sheffer, E. K.: 1968, 'The Venus Far Ultraviolet Observations with Venera 4', *J. Atmospheric Sci.* **25**, 668.

Kurt, V. G., Romanova, N. N., Smirnov, A. S., Bertaux, J. L., and Blamont, J. L.: 1979, 'Venus Ultraviolet Radiation in the Wavelength Region from 300 Å to 1657 Å from Venera 11 and Venera 12 Data (Preliminary Results)', *Kossm. Issled.* **17**, 772; 1980, *Cosmic Res.* (Engl. transl.) **17**, 638.

Kufg, V. G., Smirnov, A. S., Titarchuk, L. G., Bertaux, J. L., and Lepine, V. M.: 1983, 'Scattering of Resonance Lines in the Upper Atmosphere of Venus According to Venera 11 and Venera 12 Ultraviolet Data', *Kossm. Issled.* **21**, 545; 1984, *Cosmic Res.* (Engl. transl.) **21**, 443.

Kuz'min, A. D.: 1970, 'The Atmosphere of the Planet Venus', *Radio Sci.* **5**, 339.

Kuz'min, A. D., Nanmov, A. P., Smirnova, T. V., and Vetekhnooskaya, N.: 1971, 'Lower Atmosphere of Venus from Radio Astronomical and Space Measurements', *Space Res.* **11**, 141.

Landau, L. and Teller, E.: 1936, *Physik. Z. Sowjetunion* **10**, 34.

Lawrence, G. M.: 1971, 'Quenching and Radiation Rates of $CO(a^3\Pi)$', *Chem. Phys. Letters* **9**, 575.

Lawrence, G. M., Barth, C. A., and Argabright, V.: 1977, 'Excitation of the Venus Night Airglow', *Science* **195**, 573.

Leach, S., Devoret, M., and Eland, J. H. D.: 1978a, 'Fluorescence Quantum Yields of Isotope CO_2^+ Ions', *Chem. Phys.* **33**, 113.

Leach, S., Stannard, P. R., and Gelbart, W. M.: 1978b, 'Interelectronic-State Perturbation Effects on Photoelectron Spectra and Emission Quantum Yields: Application to CO_2^+', *Mol. Phys.* **36**, 1119.

LeCompte, M. A., Paxton, L. J., and Stewart, A. I. F.: 1989, 'Analysis and Interpretation of Observations of Airglow at 297 nm in the Venus Thermosphere', *J. Geophys. Res.* **94**, 208.

Lee, L. C. and Judge, D. L.: 1972, 'Cross Sectins for Production of CO_2^+ $[A^2\Pi_u; B^2\Sigma_u^+ \rightarrow X^2\Pi_g]$, Fluorescence by Vacuum Ultraviolet Radiation', *J. Chem. Phys.* **57**, 4433.

Leovy, C. B.: 1987, 'Zonal Winds Near Venus' Cloud Top Level: An Analytic Model of the Equatorial Wind Speed', *Icarus* **69**, 193.

Letzelter, C. et al.: 1987, 'Photoabsorption and Photodissociation Cross Sections of CO Between 88.5 and 115 nm', *Chem. Phys.* **114**, 273.

Leu, M.-T. and Yung, Y. L.: 1987, 'Determination of $O_2(a^1\Delta_g)$ and $O_2(b^1\Sigma_g^+)$ Yields in the Reaction $O + ClO \rightarrow Cl + O_2$: Implications for Photochemistry in the Atmosphere of Venus', *Geophys. Res. Letters* **14**, 949.

Levine, R. D. and Bernstein, R. B.: 1974, 'Energy Disposal and Energy Consumption in Elementary Chemical Reactions: An Information Theoretic Approach', *Accts. Chem. Res.* **7**, 393.

Lewis, J. S. and Prinn, R. G.: 1984, *Planets and Their Atmospheres: Origin and Evolution*, Academic Press, New York.

Lin, H.-M., Seaver, M., Tang, K. Y., Knight, A. E. W., and Parmenter, C. S.: 1979, 'The Role of Intermolecular Potential Well Depths in Collision-Induced State Changes', *J. Chem. Phys.* **70**, 5442.

Lindzen, R. S.: 1981, 'Turbulence and Stress Owing to Gravity Wave and Tidal Breakdown', *J. Geophys. Res.* **86**, 9707.

Link, R., Gladstone, G. R., Chakrabarti, S., and McConnell, J. C.: 1988, 'A Reanalysis of Rocket Measurements of the Ultraviolet Dayglow', *J. Geophys. Res.* **93**, 14, 631.

Liu, S. C. and Donahue, T. M.: 1974a, 'The Aeronomy of Hydrogen in the Atmosphere of Earth', *J. Atmospheric Sci.* **31**, 1118.

Liu, S. C. and Donahue, T. M.: 1974b, 'Mesospheric Hydrogen Related to Exospheric Escape Mechanisms', *J. Atmospheric Sci.* **31**, 1466.

Llewellyn, E. J., Solheim, B. H., Witt, G., Stegman, J., and Greer, R. G. H.: 1980, 'On the Excitation of Oxygen Emissions in the Night Airglow of the Terrestrial Planets', *J. Photochem.* **12**, 179.

Lopez-Gonzales, J., Lopez-Moreno, J., Lopez-Valverde, M. A., and Rodrigo, R.: 1989, 'Behaviour of the O_2 Infrared Atmospheric (0–0) Band in the Middle Atmosphere During Evening Twilight and at Night', *Planetary Space Sci.* **37**, 61.

Lopez-Moreno, J. J., Rodrigo, R., Moreno, F., Lopez-Puertas, M., and Molina, A.: 1988, 'Roket Measurements of O_2 Infrared Atmospheric System in the Nightglow', *Planetary Space Sci.* **36**, 459.

Lowell, P.: 1984, 'Mars', *Pop. Astron.* **2**, 154.

Luhmann, J. G. and Kozrya, J. U.: 1990, 'Dayside Pick-Up Oxygen Ion Precipitation at Venus and Mars: Spatial Distribution, Energy Deposition and Consequences', *J. Geophys. Res.* (in press).

Marmo, F. and Engelman, A.: 1970, 'Carbon Atoms in the Upper Atmosphere of Venus', *Icarus* **12**, 128.

McDonald, G. J. G.: 1963, 'The Escape of Helium from the Earth's Atmosphere', *Rev. Geophys.* **1**, 305.

Massie, S. T., Hunten, D. M., and Sowell, D. T.: 1983, 'Day and Night Models of the Venus Thermosphere', *J. Geophys. Res.* **88**, 3955.

Mayr, H. G., Harris, I., and Spencer, N. W.: 1978, 'Some Properties of the Upper Atmosphere Dynamics', *Rev. Geophys. Space Phys.* **16**, 539.

Mayr, H. G., Harris, I., Niemann, H. B., Brinton, H. C., Spencer, N. W., Taylor, H. A., Jr., Hartle, R. E., Hoegy, W. R., and Hunten, D. M.: 1980, 'Dynamic Properties of the Thermosphere Inferred from Pioneer Venus Mass Spectrometer Measurements', *J. Geophys. Res.* **85**, 7841.

Mayr, H. G., Harris, I., Stevens-Rayburn, D. R., Niemann, H. B., Taylor, H. A., Jr., and Hartle, R. E.: 1985, 'On the Diurnal Variations in the Temperature and Composition: A Three-Dimensional Model with Superrotation', *Adv. Space Res.* **5**, 9, 109.

Mayr, H. G., Harris, I., Kasprzak, W. T., Dube, M., and Varosi, F.: 1988, 'Gravity Waves in the Upper Atmosphere of Venus', *J. Geophys. Res.* **93**, 11247.

McClelland, G. M., Saenger, K. L., Valentini, J. J., and Herschbach, D. R.: 1979, 'Vibratinal and Rotational Relaxation of Iodine in Seeded Supersonic Beams', *J. Phys. Chem.* **83**, 947.

McCoy, R. P.: 1983, 'Thermospheric Odd Nitrogen, 1. NO, N(^4S), and O(^3P) Densities from Rocket Measurements of NO δ and γ Bands, the O$_2$ Herzberg I Bands', *J. Geophys. Res.* **88**, 3197.

McDade, I. C., Llewellyn, E. J., Greer, R. G. H., and Murtagh, D. P.: 1987, 'ETON 6: A Rocket Measurement of the O$_2$ Infrared Atmospheric (0–0) Band in the Nightglow', *Planetary Space Sci.* **35**, 1541.

McElroy, M. B.: 1968, 'The Upper Atmosphere of Venus', *J. Geophys. Res.* **73**, 1513.

McElroy, M. B.: 1969, 'Structure of the Venus and Mars Atmospheres', *J. Geophys. Res.* **74**, 29.

McElroy, M. B.: 1970, 'Ionization Processes in the Atmospheres of Venus and Mars', *Ann. Geophys.* **26**, 643.

McElroy, M. B. and McConnell, J. C.: 1971, 'Atomic Carbon in the Atmospheres of Mars and Venus', *J. Geophys. Res.* **76**, 6674.

McElroy, M. B. and Hunten, D. M.: 1969, 'The Ratio of Deuterium to Hydrogen in the Venus Atmosphere', *J. Geophys. Res.* **74**, 115.

McElroy, M. B., Prather, M. J., and Rodriguez, J. M.: 1982a, 'Escape of Hydrogen from Venus', *Science* **215**, 1614.

McElroy, M. B., Prather, M. J., and Rodriguez, J. M.: 1982b, 'Loff of Oxygen from Venus', *Geophys. Res. Letters* **9**, 649.

McNeal, R. J., Whitson, M. E., and Cook, G. R.: 1974, 'Temperature Dependence of the Quenching of Vibrationally Excited Nitrogen by Atomic Oxygen', *J. Geophys. Res.* **79**, 1527.

Meier, R. R. and Anderson, D. E.: 1983, 'Determination of Atmospheric Composition and Temperature from the UV Airglow', *Planetary Space Sci.* **31**, 967.

Meier, R. R., Anderson, D. E., and Stewart, A. I. F.: 1983, 'Atomic Oxygen Emissions Observed from Pioneer Venus', *Geophys. Res. Letters* **10**, 214.

Meier, R. R., Conway, R. R., Anderson, D. E., Feldman, P. D., Eastes, R. W., Gentieu, E. P., and Christensen, A. B.: 1985, 'The Ultraviolet Dayglow at Solar Maximum. 3. Photoelectron Excited Emissions of N$_2$ and O', *J. Geophys. Res.* **90**, 6608.

Mengel, J. G., Mayr, H. G., Harris, I., and Stevens-Rayburn, D. R.: 1988, 'Non-Linear Three-Dimensional Spectral Model of the Venusian Thermosphere with Superrotation. II. Temperature, Composition, and Winds', *Planetary Space Sci.* (submitted).

Miller, K. L., Knudsen, W. C., Spenner, K., Whitten, R. C., and Novak, V.: 1980, 'Solar Zenith Angle Dependence of Ionospheric Ion and Electron Temperatures and Density on Venus', *J. Geophys. Res.* **85**, 7759.

Miller, S. M., Fell, C. P., and Steinfeld, J. I.: 1988, 'Rate Constants for Quenching of N* by O(^3P)', *EOS (Trans. Am. Geophys. Union)* **69**, 1347.

Moore, C. B., Wood, R. E., Hu, B. L., and Yardley, J. T.: 1967, 'Vibrational Energy Transfer in CO$_2$ Lasers', *J. Chem. Phys.* **46**, 4222.

Moos, H. W. and Rottman, G. J.: 1971, 'O I and H I emissions from the Upper Atmosphere of Venus', *Astrophys. J.* **169**, L127.

Moos, H. W., Fastie, W. G., and Bottema, M.: 1969, 'Rocket Measurement of Ultraviolet Spectra of Venus and Jupiter Between 1200 and 1800 Å', *Astrophys. J.* **155**, 887.

Moroz, V. I.: 1963, 'The Infrared Spectrum of Venus (1–2.5 μ)', *Soviet Astron.–AJ* **7**, 109.

Moroz, V. I.: 1968, 'The CO$_2$ Bands and Some Optical Properties of the Atmosphere over Venus', *Soviet Astron.–AJ* **11**, 653.

Moroz, V. I., Golovin, Yu. M., Ekhonomov, A. P., Moshkin, B. E., Parfent'ev, N. A., and San'ko, N. F.: 1980, *Nature* **284**, 243.

Mukhin, L. M., Gel'man, B. G., Lamonov, N. I., Mel'nikov, V. V., Nenarokov, D. F., Okhotnikov, B. P., Rotin, V. A., and Khoklov, V. N.: 1983, 'Gas-Chromatograph Analysis of the Chemical Composition of the Atmosphere of Venus by the Landers of Venera 13 and Venera 14 Spacecraft', *Kossm. Issled.* **21**, 225; 1983, *Cosmic Res.* **21**, 168.

Mul, P. M. and McGowan, J. W.: 1979, 'Temperature Dependence of Dissociative Recombination for Atmospheric Ions NO$^+$, O$_2^+$, N$_2^+$', *J. Phys.* **B12**, 1591.

Nagy, A. F.: 1989, 'Hot Hydrogen and Oxygen Atoms in the Upper Atmospheres of Venus and Mars', *Ann. Geophys.* (in press).

Nagy, A. F. and Cravens, T. E.: 1988, 'Hot Oxygen Atoms in the Upper Atmosphere of Venus and Mars', *Geophys. Res. Letters* **15**, 433.

Nagy, A. F., Cravens, T. E., Yee, J.-H., and Stewart, A. I. F.: 1981, 'Hot Oxygen Atoms in the Upper Atmosphere of Venus', *Geophys. Res. Letters* **8**, 629.

Nakata, R. S., Watanabe, K., and Matsunaga, F. M.: 1965, 'Absorption and Photoionization Coefficients of CO$_2$ in the Region 580–1970 Å', *Sci. Light* **14**, 54.

Niemann, H. B., Hartle, R. E., Hedin, A. E., Kasprzak, W. T., Spencer, N. W., Hunten, D. M., and Carrigan, G. R.: 1979, 'Venus Upper Atmosphere Neutral Gas Composition: First Observations of the Diurnal Variations', *Science* **205**, 54.

Niemann, H. B., Booth, J. R., Cooley, J. E., Hartle, R. E., Kasprzak, W. T., Spencer, N. W., and Way, S. H.: 1980a, 'Pioneer Venus Orbiter Neutral Mass Spectrometer Experiment', *IEEE Trans. Geosci. Remote Sensing* **GE-18**, 60.

Niemann, H. B., Kasprzak, W. T., Hedin, A. E., Hunten, D. M., and Spencer, N. W.: 1980b, 'Mass Spectrometer Measurements of the Neutral Gas Composition of the Thermosphere and Exosphere of Venus', *J. Geophys. Res.* **85**, 7817.

Ogawa, H. S. and Judge, D. L.: 1986, 'Absolute Solar Flux Measurement Shortward of 575 Å', *J. Geophys. Res.* **91**, 7089.

Ogawa, H. S., Phillips, E., and Judge, D. L.: 1984, 'Line Width of the Solar EUV HeI Resonance Emissions at 584 and 537 Å', *J. Geophys. Res.* **89**, 7537.

Oyama, V. I., Carle, G. C., Woeller, F., Pollack, J. B., Reynolds, R. T., and Craig, R. A.: 1980, 'Pioneer Venus Gas Chromatography of the Lower Atmosphere of Venus', *J. Geophys. Res.* **85**, 7891.

Parmenter, C. S. and Seaver, M.: 1979, 'The Temperature Dependence of Collision-Induced State Changes', *Chem. Phys. Letters* **67**, 279.

Partridge, H., Bauschlicher, and Langhoff, S. R.: 1990, *J. Chem. Phys.*, quoted in Bates, 1988c (in press).

Paxton, L. J.: 1983, 'Atomic Carbon in the Venus Thermosphere: Observatins and Theory', Ph.D. Thesis, University of Colorado, Boulder.

Paxton, L. J.: 1985, 'Pioneer Venus Orbiter Ultraviolet Spectrometer Limb Observations: Analysis and Interpretation of the 166- and 165-nm Data', *J. Geophys. Res.* **90**, 5089.

Paxton, L. J.: 1988, 'CO$_2^+$ and N$_2^+$ in the Venus Ionosphere', *J. Geophys. Res.* **93**, 8473.

Paxton, L. J. and Meier, R. R.: 1986, 'Reanalysis of Pioneer Venus Orbiter Ultraviolet Spectrometer Data: OI 1304 Intensities and Atomic Oxygen Densities', *Geophys. Res. Letters* **13**, 229.

Paxton, L. J., Anderson, D. E., and Stewart, A. I. F.: 1985, 'The Pioneer Venus Orbiter Ultraviolet Spectrometer: Analysis of Hydrogen Lyman Alpha Data', *Adv. Space Res.* **5**, 129.

Paxton, L. J., Anderson, D. E., and Stewart, A. I. F.: 1988, 'Analysis of Pioneer Venus Orbiter Ultraviolet Spectrometer Lyman α Data from Near the Subsolar Region', *J. Geophys. Res.* **93**, 1766; 1988, erratum in *J. Geophys. Res.* **93**, 11, 551.

Pechmann, J. B. and Ingersoll, A. P.: 1984, 'Thermal Tides in the Atmosphere of Venus: Comparison of Model Results with Observations', *J. Atmospheric Sci.* **41**, 3290.

Phillips, J. L., Stewart, A. I. F., and Luhmann, J. G.: 1986, 'The Venus Ultraviolet Aurora: Observations at 130.4 nm', *Geophys. Res. Letters* **13**, 1047.

Piper, L. G.: 1989, 'The Rate Coefficients for Quenching N(^2D) by O(^3P)', *J. Chem. Phys.* **91**, 3516.

Piper, L. G., Donahue, M. E., and Rawlins, W. T.: 1987, 'Rate Coefficients for N(^2D) Reactions', *J. Phys. Chem.* **91**, 3883.

Porter, H. S., Silverman, S. M., and Tuan, T. F.: 1974, 'On the Behavior of Airglow Under the Influence of Gravity Waves', *J. Geophys. Res.* **79**, 3827.

Poulson, L. L., Billing, G. D., and Steinfeld, J. I.: 1978, 'Temperature Dependence of HF Vibrational Relaxation', *J. Chem. Phys.* **68**, 5121.

Prather, M. J. and McElroy, M. B.: 1983, 'Helium on Venus: Implications for Uranium and Thorium', *Science* **228**, 410.

Prinn, R. G.: 1985, in J. S. Levine (ed.), 'The Photochemistry of the Atmosphere of Venus', *The Photochemistry of Atmospheres: Earth the Ptlher Planets and Comets*, Academic Press, New York, 1985.

Quack, M. and Troe, T.: 1977, 'Vibrational Relaxation of Diatomic Molecules in Complex Forming Collisions with Reactive Atoms', *Ber. Bunsenges. Physik. Chem.* **81**, 160.

Queffelec, J. L., Rowe, B. R., Vallee, F., Gomet, J. C., and Morlais, M.: 1989, 'The Yield of Metastable Atoms Through Dissociative Recombination of O_2^+ Ions with Electrons', *J. Chem. Phys.* **91**, 5335.

Revercomb, H. E., Sromovsky, L. A., Suomi, V. E., and Boese, R. W.: 1985, 'Thermal Net Flux Measurements on the Pioneer Venus Entry Probes', *Adv. Space Res.* **5**, 81.

Roble, R. G., Dickinson, R. E., and Ridley, E. C.: 1982, 'Global Circulation and Temperature Structure of the Thermosphere with High Latitude Plasma Convection', *J. Geophys. Res.* **87**, 1599.

Roble, R. G., Ridley, E. C., and Dickinson, R. E.: 1987, 'On the Global Mean Structure of the Thermosphere', *J. Geophys. Res.* **92**, 8745.

Rodriguez, M., Prather, J., and McElroy, M. B.: 1984, 'Hydrogen on Venus: Exospheric Distribution and Escape', *Planetary Space Sci.* **32**, 1235.

Rohrbaugh, R. P. and Nisbet, J. S.: 1973, 'Effect of Energetic Oxygen Atoms on Neutral Density Models', *J. Geophys. Res.* **78**, 6768.

Rosser, W. A., Wood, A. D., and Gerry, E. T.: 1969, 'Deactivation of Vibrationally Excited Carbon Dioxide (v_2) by Collisions with Carbon Dioxide or with Nitrogen', *J. Chem. Phys.* **50**, 4996.

Rottman, G. J.: 1981, 'Rocket Measurements of the Solar Spectral Irradiance During Solar Minimum, 1972–1977', *J. Geophys. Res.* **86**, 6697.

Rottman, G. J. and Moos, H. W.: 1973, 'The Ultraviolet (1200–1900 Å) Spectrum of Venus', *J. Geophys. Res.* **78**, 8033.

Rusch, D. W. and Cravens, T. E.: 1979, 'A Model of the Neutral and Ion Nitrogen Chemistry in the Daytime Thermosphere of Venus', *Geophys. Res. Letters* **6**, 791.

Russell, C. T., Elphic, R. C., and Slavin, J. A.: 1979, 'Initial Pioneer Venus Magnetic Field Results: Dayside Observations', *Science* **203**, 745.

Samson, J. A. R. and Gardner, J. L.: 1973, 'Fluorescence Excitatin and Photoelectrons Spectra of CO_2 Induced by Vacuum Ultraviolet Radiation Between 185 and 716 Å', *J. Geophys. Res.* **78**, 3663.

Saxon, R. P. and Liu, B.: 1977, '*Ab Initio* Configuration Interaction Study of the Valence States of O_2^+', *J. Chem. Phys.* **67**, 5432.

Schatz, G. C. and Redmon, M. J.: 1981, 'A Quasi-Classical Trajectory Study of Collisional Excitation in $O(^3P) + CO_2$', *Chem. Phys.* **58**, 195.

Schloerb, F. P., Robinson, S. E., and Irvine, W. M.: 1980, 'Observations of CO in the Stratosphere of Venus via Its $J = 0 \rightarrow 1$ Rotational Transition', *Icarus* **43**, 121.

Schoeberl, M. R. and Strobel, D. F.: 1978, 'The Zonally Averaged Circulation of the Middle Atmosphere', *J. Atmospheric Sci.* **35**, 577.

Schofield, J. T., Taylor, F. W., and McClee, D. J.: 1982, 'The Global Distribution of Water Vapor in the Middle Atmosphere of Venus', *Icarus* **52**, 263.

Schubert, G.: 1983, in D. M. Hunten, L. Colin, T. M. Donahue, and V. I. Moroz (eds.), 'General Circulation and the Dynamical State of the Venus Atmosphere', *Venus*, Univ. of Arizona Press, Tucson.

Schubert, G. and Walterscheid, R. L.: 1984, 'Propagation of Small-Scale Acoustic-Gravity Waves in the Venus Atmosphere', *J. Atmospheric Sci.* **41**, 1202.

Schubert, G. et al.: 1980, 'Structure and Circulation of the Venus Atmosphere', *J. Geophys. Res.* **85**, 8007.

Schwartz, R. N., Slawsky, Z. I., and Herzfeld, K. F.: 1952, 'Calculation of Vibrational Relaxation Times in Gases', *J. Chem. Phys.* **20**, 1591.

Seaton, M. J. and Osterbrock, D. E.: 1957, 'Relative O II Intensities in Gaseous Nebulae', *Astrophys. J.* **66**, 125.

Seiff, A.: 1982, 'Dynamical Implications of the Observed Thermal Contrasts in Venus's Uupper Atmosphere', *Icarus* **51**, 574.

Seiff, A., Kirk, D. B., Young, R. E., Blanchard, R. C., Findlay, J. T., Kelly, G. M., and Sommer, S. C.: 1980, 'Measurements of Thermal Structure and Thermal Contrasts in the Atmosphere of Venus and Related Dynamical Observations: Results from the Four Pioneer Venus Probes', *J. Geophys. Res.* **85**, 7903.

Sharma, R. D. and Brau, C. A.: 1969, 'Energy Transfer in Near-Resonant Molecular Collisions Due to Long-Range Forces with Applicatin to Transfer of Vibrational Energy from v_3 Mode of CO_2 to N_2', *J. Chem. Phys.* **50**, 924.

Sharma, R. D. and Nadile, R. M.: 1980, 'Carbon Dioxide (v_2) Radiance Results Using a New Non-Equilibrium Model', *EOS* **61**, 17, 322.

Sharma, R. D. and Nadile, R. M.: 1981, *Carbon Dioxide (v_2) Radiance Results Using a New Non-Equilibrium Model*. AFGL Tech. Rep. 81-0064, Air Force Geophys. Lab., Hanscom Air Force Base, Bedford, Mass.

Simpson, C. J. S. M., Gait, P. D., and Simmie, J. M.: 1977, 'The Vibrational Deactivation of the Bending Mode of CO_2 and by N_2', *Chem. Phys. Letters* **47**, 133.

Sinton, W. M.: 1963, 'Infrared Observations of Venus', *Mem. Soc. Roy. Sci. Liège* **7**, 300.

Slanger, T. G.: 1978, 'Generation of $O_2(c^1\Sigma_r^-, C^3\Delta_u, A^3\Sigma_g^-)$ Emissin in the Terrestrial Nightglow', *J. Chem. Phys.* **69**, 4779.

Slanger, T. G. and Black, G.: 1976, 'O(^1S) Production from Oxygen Atom Recombination', *J. Chem. Phys.* **64**, 3767.

Slanger, T. G. and Heustis, D. L.: 1981, '$O_2(c^1\Sigma_u^- \rightarrow X^3\Sigma_g^+)$ Emission in the Terrestrial Nightglow', *J. Geophys. Res.* **86**, 3551.

Smith, I. W. M.: 1984, 'The Role of Electronically Excited States in Recombination Reactions', *Int. J. Chem. Kinet.* **16**, 423.

Spenner, K., Knudsen, W. C., Whitten, R. C., Michelson, P. F., Miller, K. L., and Novak, V.: 1981, 'On the Maintenance of the Venus Nightside Ionosphere: Electron Precipitation and Plasma Transport', *J. Geophys.* **86**, 9170.

Stair, A. T., Jr., Sharma, R. D., Nadile, R. M., Baker, D. J., and Grieder, W. F.: 1985, 'Observations of Limb Radiance with Cryogenic Spectral Infrared Rocket Experiment', *J. Geophys. Res.* **90**, 9763.

Stewart, A. I.: 1969, paper presented at *The Tucson Conference on the Atmosphere of Venus*. Quoted in McElroy and Hunten (1969).

Stewart, A. I. F.: 1980, 'Design and Operation of the Pioneer Venus Orbiter Ultraviolet Spectrometer', *IEEE Trans. Geosci. Remote Sensing* **GE-18**, 65.

Stewart, A. I.: 1972, 'Mariner 6 and 7 Ultraviolet Spectrometer Experiment: Implications of CO_2^+, CO, and O Airglow', *J. Geophys. Res.* **77**, 54.

Stewart, A. I. and Barth, C. A.: 1979, 'Ultraviolet Night Airglow of Venus', *Science* **205**, 59.

Stewart, A. I., Anderson, D. E., Esposito, L. W., and Barth, C. A.: 1979, 'Ultraviolet Spectroscopy of Venus: Initial Results from the Pioneer Venus Orbiter', *Science* **203**, 777.

Stewart, A. I. F., Gerard, J. C., Rusch, D. W., and Bougher, S. W.: 1980, 'Morphology of the Venus Ultraviolet Night Airglow', *J. Geophys. Res.* **85**, 7861.

Stewart, R. W.: 1968, 'Interpretation of Mariner 5 and Venera 4 Data on the Upper Atmosphere of Venus', *J. Atmospheric Sci.* **25**, 578.

Stewart, R. W. and Hogan, J. S.: 1969, 'Empirical Determination of Heating Efficiencies in the Mars and Venus Atmospheres', *J. Atmospheric Sci.* **26**, 330.

Stone, E. J. and Zipf, E. C.: 1974, 'Electron Impact Excitatin of the $^3S^o$ and $^5S^o$ States of Atomic Oxygen', *J. Chem. POhys.* **60**, 4237.

Stoney, G. J.: 1968, 'On the Physical Constitution of the Sun and Stars', *Proc. Roy. Soc. London* **17**, 1.

Stoney, G. J.: 1898, 'Of Atmospheres Upon Planets and Satellites', *Trans. Roy. Soc. Dublin* **6**, 305; reprinted in 1898: *Astrophys. J.* **7**, 25.

Strickland, D. J.: 1973, 'The O I 1304- and 1356-Å Emissions fro mthe Atmospheres of Venus', *J. Geophys. Res.* **78**, 2827.

Strickland, D. J., Thomas, G. E., and Sparks, P. R.: 1972, 'Mariner 6 and 7 Ultraviolet Spectrometer Experiment: Analysis of the O I 1304- and 1356-Å Emissions', *J. Geophys. Res.* **77**, 4052.

Surkov, Yu. A., Shchelgov, O. P., Ryvkin, M. L., Sheinin, D. M., and Davydov, N. A.: 1988, 'Water Vapor Distribution in the Middle and Lower Venusian Atmosphere', *Kossm. Issled.* **25**, 678; 1988: *Cosmic Res.* **25**, 517.

Sze, N. F. and McElroy, M. B.: 1975, 'Some Problems in Venus Aeronomy', *Planetary Space Sci.* **23**, 763.

Takacs, P. Z., Broadfoot, A. L., Smith, G. R., and Kumar, S.: 1980, 'Mariner 10 Observations of Hydrogen Lyman-α Emission from the Venus Exosphere: Evidence of Complex Structure', *Planetary Space Sci.* **28**, 687.

Taylor, F. W. *et al.*: 1979, 'Infrared Remote Sounding of the Middle Atmosphere of Venus from Pioneer Venus Orbiter', *Science* **203**, 779.

Taylor, F. W. *et al.*: 1980, 'Structure and Meteorology of the Middle Atmosphere of Venus: Infrared Remote Sensing from the Pioneer Orbiter', *J. Geophys. Res.* **85**, 7963.

Taylor, H. A., Jr., Brinton, H. C., Bauer, S. J., Hartle. R. E., Cloutier, P. A., and Daniell, R. E., Jr.: 1980, 'Global Observations of the Composition and Dynamics of the Ionosphere of Venus: Implications for Solar Wind Interaction', *J. Geophys. Res.* **85**, 7765.

Taylor, H. A., Jr., Brinton, H. C., Niemann, H. B., Mayr, H. G., Hartle, R. E., Barnes, A., and Larson, J.: 1984, 'Interannual and Short-Term Variations of the Venus Nighttime Hydrogen Bulge', *J. Geophys. Res.* **89**, 10669.

Taylor, H. A., Brinton, H., Niemann, H. B., Mayr, H. G., Hartle, R., Barnes, A., and Larson, J.: 1985, 'In Situ Results on the Variation of Neutral Atmospheric Hydrogen at Venus', *Adv. Space Res.* **5**, 125.

Taylor, M. J., Hapgood, M. A., and Rothwell, P.: 1987, 'Observations of Gravity Wave Propagation in the O I (555.7 nm), Na (589.2 nm) and the Near Infrared OH Nightglow Emissions', *Planetary Space Sci.* **35**, 413.

Thomas, R. J.: 1981, 'Analysis of Atomic Oxygen Emissions in the Airglow of the Terrestrial Planets', *J. Geophys. Res.* **86**, 206.

Tobiska, W. K., Barth, C. A., and Culp, R. D.: 1988, 'Use of Solar Lyman-α and 1–8 Å X-Rays as EUV Flux Indices', *A.I.A.A.* (preprint).

Torr, M. R. and Torr, D. G.: 1985, 'Ionizatin Frequencies for Solar Cycle 21: Revised', *J. Geophys. Res.* **90**, 6675.

Torr, M. R., Torr, D. G., Ong, R. A., and Hinteregger, H. E.: 1979, 'Ionization Frequencies for Major Thermospheric Constituents as a Function of Solar Cycle 21', *Geophys. Res. Letters* **6**, 771.

Torr, M. R., Torr, D. G., and Hinteregger, H. E.: 1980, 'Solar Flux Variability in the Schumann–Runge Continuum as a Functin of Solar Cycle 21', *J. Geophys. Res.* **85**, 6063.

Traub, W. A. and Carleton, N. P.: 1974, in A. Woszczyk and C. Iwaniszewska (eds.), 'Observations of O_2, H_2O, and HD in Planetary Atmospheres', *Exploration of Planetary Atmospheres*. D. Reidel Publ. Co., Dordrecht, Holland, p. 223.

Trauger, J. T. and Lunine, J. I.: 1983, 'Spectroscopy of Molecular Oxygen in the Atmospheres of Venus and Mars', *Icarus* **55**, 272.

Ustinov, E. A. and Moroz, V. I.: 1978, 'Refinement of the H_2O Content Value in the Atmosphere of Venus ith Narrow-Band Photometry Data from Venera 9 and Venera 10', *Kosm. Issled.* **16**, 127; 1978: *Cosmic Res.* (Engl. transl.) **16**, 98.

van Dishoeck, E. F. and Black, J. H.: 1988, 'The Photodissociatin and Chemistry of Interstellar CO', *Astrophys. J.* **334**, 771.

Vaughan, S. O. Doering, J. P.: 1986, 'Absolute Experimental Differential and Integral Electron Excitation Cross Sections for Atomic Oxygen. 2. The $(^3P \rightarrow {}^3S^0)$ Transition (1304 Å) from 16.5 to 200 eV with Comparison to Atomic Hydrogen', *J. Geophys. Res.* **91**, 13755.

Vinogradov, A. P., Surkov, U. A., and Florensky, C. P.: 1968, 'The Chemical Composition of the Venus Atmosphere Based on the Data of the Interplanetary Station Venera 4', *J. Atmospheric Sci.* **25**, 535.

Vinogradov, A. P., Surkov, Yu. A., Andreichikov, B. M., Kalinkina, O. M., and Grechischeva, I. M.: 1971, in C. Sagan, T. C. Owen, and H. J. Smith (eds.), 'The Chemical Composition of the Atmosphere of Venus', *Planetary Atmospheres*, D. Reidel Publ. Co., Dordrecht, Holland.

von Zahn, U.: 1977, 'Bus Neutral Mass Spectrometer (BNMS)', *Space Sci. Rev.* **20**, 451.

von Zahn, U. and Moroz, V. I.: 1986, 'Compositino of the Venus Atmosphere Below 100 km Altitude', *Adv. Space Res.* **5**, 173.

von Zahn, U., Krankowsky, D., Mauersberger, K., Nier, A. O., and Hunten, D. M.: 1979, 'Venus Thermosphere: *In Situ* Composition Measurements, the Temperature Profile, and the Homopause Altitude', *Science* **203**, 768.

von Zahn, U., Fricke, K. H., Hunten, D. M., Krankowsky, D., Mauersberger, K., and Nier, A. O.: 1980, 'The Upper Atmosphere of Venus During Morning Conditions', *J. Geophys. Res.* **85**, 7892.

von Zahn, U., Kumar, S., Niemann, H., and Prinn, R.: 1983, in D. M. Hunten, L. Colin, T. M. Donahue, and V. I. Moroz (eds.), 'Composition of the Venus Atmosphere', *Venus*, Univ. of Arizona Press, Tucson.

Walker, J. C. G.: 1977, *Evolution of the Atmosphere*, MacMillan, New York.

Walker, J. C. G.: 1982, 'The Earliest Atmosphere of the Earth', *Precambrian Res.* **17**, 147.

Wallace, L.: 1969, 'Analysis of the Lyman-Alpha Observations of Venus Made from Mariner 5', *J. Geophys. Res.* **74**, 115.

Wallace, L., Stuart, F. E., Nagel, R. H., and Larson, D. M.: 1971, 'A Search for Deuterium on Venus', *Astrophys. J.* **168**, L29.

Wallis, M. K.: 1972, 'Comet-Like Interaction of Venus with the Solar Wind. I', *Cosmic Electrodyn.* **3**, 45.

Wallis, M. K.: 1978, 'Exospheric Density and Escape Fluxes of Atomic Isotopes on Venus and Mars', *Planetary Space Sci.* **26**, 949.

Wallis, M. K.: 1982, 'Comet-Like Interaction of Venus with the Solar Wind. III. The Atomic Oxygen Corona', *Geophys. Res. Letters* **9**, 427.

Walterscheid, R. L., Schubert, G., Newman, M., and Kliore, A. J.: 1985, 'Zonal Winds and the Angular Momentum Balance of Venus' Atmosphere Within and Above the Clouds', *J. Atmospheric Sci.* **42**, 1982.

Waterston: 1846, *Proc. Roy. Soc. London* **5**, 604.

Waterston: 1892, *Phil. Trans. Roy. Soc. (London)* A183, 1892.

Watson, A. J., Donahue, T. M., and Walker, J. C. G.: 1981, 'The Dynamics of Rapidly Escaping Atmosphere: Applications to the Evolution of Earth and Venus', *Icarus* **48**, 150.

Watson, A. J., Donahue, T. M., and Kuhn, W. R.: 1984, 'Temperatures in a Runaway Greenhouse on the Evolving Venus: Implications for Water Loss', *Earth Planetary Sci. Letters* **68**, 1.

Wauchop, T. S. and Broida, H. P.: 1972, 'Lifetime and Quenching of $CO(a^2\Pi)$, Produced by Recombination of CO_2 Ions in a Helium Afterglow', *J. Chem. Phys.* **56**, 330.

Wells, W. C., Borst, W. L., and Zipf, E. C.: 1972, 'Production of $CO(a^3\Pi)$ and Other Metastable Fragments by Electron Impact Dissociation of CO_2', *Planetary Space Sci.* **31**, 317.

Wilson, W. J., Klein, M. J., Kakar, R. K., Gulkis, S., Olsen, E. T., and Ho, P. T. P.: 1981, 'Venus. I. Carbon Monoxide Distribution and Molecular-Line Searches', *Icarus* **45**, 624.

Wintersteiner, P. P., Sharma, R. D., Winick, J. R., and Picard, R.: 1988, 'Determination of $CO_2(v_2)$ Vibrational Temperature Using a New Line-by-Line Radiative Transfer Algorithm', *EOS (Trans. Am. Geophys. Union)* **69**, 1346.

Wraight, P. C.: 1982, 'Association of Atomic Oxygen and Airglow Excitation Mechanisms', *Planetary Space Sci.* **30**, 251.

Yardley, J. T.: 1980, *Introduction to Molecular Energy Transfer*, Academic Press, New York.

Yatteau, J. H.: 1983, 'Some Issues Related to the Evolution of Planetary Atmospheres', Ph.D. Thesis, Harvard University, Cambridge, MA.

Yee, J.-H. and Hays, P. B.: 1980, 'The Oxygen Polar Corona', *J. Geophys. Res.* **85**, 1795.

Yee, J.-H. and Killeen, T. L.: 1986, 'Thermospheric Production of $O(^1S)$ by Dissociative Recombination of Vibrationally Excited O_2^+', *Planetary Space Sci.* **34**, 1101.

Yee, J.-H., Meriwether, J. W., and Hays, P. B.: 1980, 'Detection of a Corona of Fast Oxygen Atoms During Solar Maximum', *J. Geophys. Res.* **85**, 3396.

Yoshino, K. *et al.*: 1988, 'High Resolution Spectra and Photoabsorption Coefficients for Carbon Monoxide Absorption Bands Between 94.0 and 100.4 nm', *J. Physique* (in press).

Young, L. D. G.: 1972, 'High Resolution Spectra of Venus', *Icarus* **17**, 632.

Yung, Y. L. and DeMore, W. B.: 1982, 'Photochemistry of the Stratosphere of Venus: Implications for Atmospheric Evolution', *Icarus* **51**, 199.

Zahnle, K. L. and Kasting, J. F.: 1986, 'Mass Fractionation During Transonic Escape and Implictions for Loss of Water from Mars and Venus', *Icarus* **68**, 462.

Zipf, E. C.: 1970, 'The Dissociative Recombination of O_2^+ Ions into Specifically Identified States', *Bull. Am. Phys. Soc.* **15**, 498.

Zipf, E. C.: 1986, 'On the Direct and Dissociative Excitation of the $O(3s^3S^0)$ State by Electron Impact on Atomic and Molecular Oxygen', *J. Phys.* **B19**, 2199.

Zipf, E. C. and Erdman, P. W.: 1985, 'Electron Impact Excitation of Atomic Oxygen: Revised Cross Sections', *J. Geophys. Res.* **90**, 11087.

Zipf, E. C. and Stone, E. J.: 1971, 'Photoelectron Excitation of Atomic-Oxygen Resonance Radiation in the Terrestrial Nightglow', *J. Geophys. Res.* **26**, 6865.